Nanostructure and Engineering Properties of 1.4 nm Tobermorite, Jennite and Other Layered Calcium Silicate Hydrates

Pouya Pourbeik

Thesis submitted
to the
Faculty of Graduate and Postdoctoral Studies
in partial fulfillment of the requirements
for the Doctorate in Philosophy degree in
Civil Engineering

Department of Civil Engineering
Faculty of Engineering
University of Ottawa

Abstract

The nature of the calcium-silicate-hydrate phase in hydrated Portland cement has been the subject of considerable debate for decades. Various nanostructural models have been proposed including those constructed from colloidal-based particulate systems and those formulated on the basis of layered calcium-silicate-hydrates. These are examined in detail in the literature review section of the thesis. Relatively recent composition-based models have been proposed by Taylor and Richardson-Groves. These models contain structural elements comprised of 1.4 nm tobermorite and jennite. Details are also provided in the literature review. There is however a paucity of data on the engineering properties of pure calcium-silicate-hydrate phases and virtually none on the mechanical performance of 1.4 nm tobermorite and jennite. The global objective of this thesis was to examine the compatibility of the composition-based models with the engineering behaviour of the pure tobermorite and jennite phases. Pure phases of a variety of layered calcium-silicate-hydrates were synthesized and novel techniques developed to determine their engineering characteristics in a variety of test environments. The silicate phases investigated included high temperature silicates e.g. gyrolite as these layered structures are known to be cross-linked. Investigation of the role of 'structural' water in layered silicates was also a part of these studies.

The thesis is based on a series of twelve refereed journal papers by the candidate (eight are published or accepted and four have been submitted for publication). The research is reported in four parts with each part comprised of three papers. Each part provides insight into the nanostructure of C-S-H in hydrated cement. The arguments developed evolve from an assessment of various factors including aging and the state of water in the layered silicates.

The first part of the thesis focuses on the development and application of dynamic mechanical thermo-analysis methods that are sensitive to phase changes and are useful for assessing the compatibility of engineering behaviour with model composition based on 1.4 nm tobermorite and jennite. The second part represents a study of volume stability and mechanical property-porosity relationships for the pure silicate phases that are germane to these studies. The third part focuses on prolonged aging and role of structural water in cement paste hydrated for 45 years. The fourth and final part attempts to address the role of layer structure e.g. cross-linking of silicate sheets on engineering behaviour. The non-uniqueness of modulus of

elasticity with respect to equilibrium moisture content is demonstrated. Structurally related irreversible effects that are dependent on drying history are rationalized.

A summary chapter is provided wherein the evidence for a composition-based model with tobermorite and jennite structural units is rationalized in terms of the experimental evidence provided in this study and suggestions for future research are discussed.

To my beloved parents and brother

Acknowledgements

I would like to first express my sincere appreciation to my supervisor, Dr. James J. Beaudoin (Researcher Emeritus at the National Research Council, Canada (NRC) and Adjunct Professor at the University of Ottawa) for his continuous support. The completion of this thesis would not have been possible without his encouragement, constant support, invaluable suggestions, and continuous assistance throughout this research program. I am grateful I had the opportunity to work with him.

A big thank you goes to Dr. Rouhollah (Aali) Alizadeh (CEO at Giatec Scientific) for his willingness to share his experiences regarding the application of engineering techniques and nanotechnology in the study of cement-based materials.

My deep gratitude goes to Dr. Laila Raki for her guidance in PhD Research project. She introduced me to different aspects of chemistry and its application in studying cement-based materials and for her insightful comments and suggestions on various parts of my research.

I thank my kind colleagues for their support: Mses. Rahil Khoshnazar and Dan-Tam Nguyen. Considerable thanks go to Mr. Gordon Chan as well for his invaluable help with lab equipments at National Research Council Canada. (NRC)

The experimental work of this thesis was conducted at the National Research Council of Canada including the laboratories at the Institute for Research in Construction, Steacie Institute for Molecular Sciences and Institute for Chemical Process and Environmental Technology. I would also like to acknowledge the financial support provided through an NSERC discovery grant on "Nanostructural tailoring of cement systems for sustainability". I was also partially supported by assistantships at the University of Ottawa.

A special thank you to my examination committee members Drs. Arezki Tagnit-Hamou, Pouria Ghods, Beatriz Martin-Pérez, and Mamadou Fall for their suggestions on the current work.

This doctoral research also benefited from scientific discussions with researchers at NRC: Drs. Jon Makar, Taijiro Sato, Patrick Grattan-Bellew, Jean-Francois Masson and Pierre-Claver Nkinamubanzi.

I am truly thankful to Messrs. Jim Margeson, Ken Trischuk, Dave Edwards, Bruce Baldock, Omran Madani and Peter Collins, and Mses. Ana Delgado, Sladana Bundalo-Perc and Helen Yew for their training on various experimental methods and equipment.

I thank my friends for all their support and encouragement.

Finally, special appreciation goes to my beloved parents and brother, Pedram, for their endless support, encouragement, and understanding during this long journey.

Contents

Chapter 1

Introduction

1.1 Statement of Global Objective

The sustainability of concrete infrastructure continues to be an enormous engineering challenge. Solutions lie in developing a comprehensive understanding of the mechanisms that are responsible for the deleterious processes that can occur on exposure of concrete to aggressive environments. It is argued that basic phenomena at the nano and micro-level control behavior at the macro-level. Concrete is a heterogeneous material produced for application at the macro or real world level. Chemical and physical interactions occur at the nano and micro level. Control of these is paramount to enhanced performance. The ability to tailor the nanostructure of C-S-H through the application of 'seeds', for example, offers engineers the possibility of designing durable concrete structures through manipulation of C/S ratio of the binding phase. The tobermorite-jennite models for C-S-H investigated in this thesis provide an improved knowledge base for assessing how engineers can control the nanostructure of the concrete binder. A next step would be to investigate the use of tobermorite and jennite seeds to modify C-S-H nanostructure in a systematic manner. It is a clear demonstration of how fundamental work on cement mineral behavior can be potentially be applied to real concrete.

Hydrated Portland cement paste is the principal binder of conventional cement-based materials. The behavior of the binder phase in concrete has a significant effect on its performance. In this context the dependence of the latter on paste microstructure and nanostructure is of great importance. Mechanical strength and volume stability are key descriptors of sustainability that are influenced by the physico-mechanical and physico-chemical characteristics of the paste. Further understanding of the nature of the

nanostructural components of the calcium-silicate-hydrate phases in hydrated cement paste underlies the ability to enhance its engineering properties. This constitutes the global objective of this thesis.

1.2 Historical Background

Extensive research effort toward the resolution of the structure of hydrated cement paste has been on-going since 1934 [1]. This work was initiated at the Portland Cement Association in the USA. The work of Powers and Brownyard led to the development of a colloidal model from which many inferences regarding behavior were drawn. The evolution of layered silicate models first suggested by Bernal [2] and later advanced in detail by Feldman and Sereda has been at the centre of debate that continues to the present day. The primary difficulty in resolving these issues has been the relatively amorphous nature (i.e. lack of a basal-spacing) of the C-S-H formed from the hydration of Portland cement. Chapter 4 of this thesis contains a focused discussion of various physico-chemical and compositional models for C-S-H –based systems as it is germane to the experimental program outlined in this document. A significant portion of the proposed research relates to investigation of the engineering behavior of three layered calcium-silicate-hydrate systems: synthetic C-S-H with variable C/S ratio; 1.4 nm tobermorite; jennite. There is a paucity of engineering data available for these materials. This data is vital in oreder to assess the relevance of the current composition-based models comprised of nanostructural units containing these minerals.

1.3 Program Description

The experimental program is outlined in detail in Chapter 7. Briefly, the program is comprised of four parts. Part 1 outlines the novel application of dynamic mechanical thermoanalysis to cement paste and the selected layered calcium silicate systems of interest. Part 2 is concerned with volume stability and factors that influence mechanical properties of layered silicate minerals. Part 3 involves extensive use of instrumented microindentation testing and its application toward understanding the engineering behavior of 45 year old hydrated cement paste. Part 4 involves the synthesis and study of

the engineering behavior of high temperature C-S-H phases e.g. gyrolite with a view to understanding the structural role of water in layered silicates. This part included experiments utilized to evaluate nanostructural factors affecting the engineering performance of layered calcium silicate hydrates. All of the parts are designed to provide information and insight on the role of 'structural' water on the performance of cement-based materials.

The main body of the thesis contains the following components: discussion of the structural characteristics of the key minerals investigated; a comprehensive description of C-S-H structural models; details of the synthesis methods for the various layered silicate systems studied; a description of experimental techniques used in the study of layered silicates; four chapters comprised of twelve papers (eight published, four under review) ; a concluding chapter containing a summary of the major findings and an outline of plans for future research; a list of publications based on this research.

References

1. Powers T. C. and Brownyard T.L., "Studies of the physical properties of hardened Portland cement paste", Portland Cement Association USA, Bulletin 22, Part 9, 971-992 ,1948.

2. Bernal J.D., "The structure of cement hydration compounds", Third Int. Symp. Chem. Cement, Cem. And Concr. Assoc., London, 216-236, 1952.

Chapter 2

Pure Calcium-Silicate-Hydrates Phases Investigated- General Description

A brief description of the calcium-silicate-hydrate phases synthesized and investigated in this study is as follows. A description of the C-A-S-H phases (not investigated) also is included. Synthesis procedures are described in Chapter 6 of the thesis. The research papers themselves also contain descriptions of the synthesis procedures.

1.4nm tobermorite

The structure of 1.4 nm tobermorite has only recently been solved (Bonaccorsi et. al., [1]). It is built up of complex layers formed by sheets of sevenfold coordinated calcium cations flanked on both sides by wollastonite-like chains. The Si-O chains are kinked so as to repeat at intervals of three tetrahedra. The space between two complex layers contains additional calcium cations and H_2O molecules. The crystal chemical formula indicated by the structural results is $Ca_5Si_6O_{16}(OH)_2.7H_2O$. On heating to 55-60°C it loses interlayer water and undergoes uni-dimensional lattice shrinkage giving 1.1nm tobermorite (Taylor [2]). A model for the unit cell of 1.1nm tobermorite is shown in Figure 2.1. Other transformations at higher temperatures (to for example the 0.90nm form) have been identified by Kirkpatrick et. al.[3].

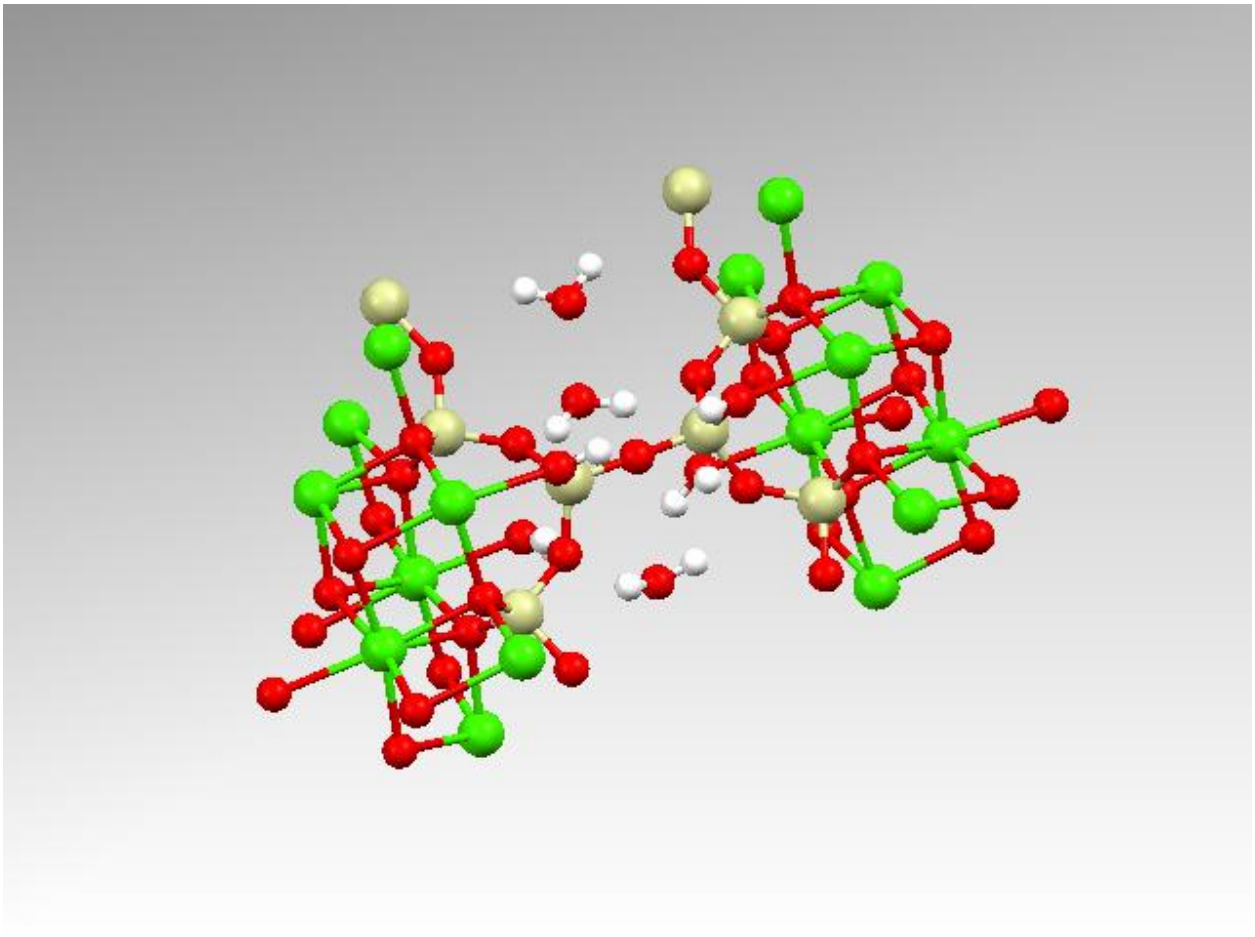

Figure 2.1. Unit cell of 1.1nm tobermorite. Color assignments are: Green (calcium); Red (oxygen); Tan (Silicon); White (hydrogen).

Jennite

The crystal structure of jennite, $Ca_9Si_6O_{18}(OH)_6.8H_2O$, was solved by Bonaccorsi et. al. in 2004 [4]. A model for the unit cell of jennite is shown in Figure 2.2. Like tobermorite it has a layer structure.The structure of jennite is built up by three distinct modules: ribbons of edge sharing calcium octahedra, wollastonite-type silicate chains and additional calcium octahedra. All the hydroxyl groups are bonded to three calcium ions. SiOH groups are not found. Jennite loses water at 70-90°C with a unidimensional lattice shrinkage giving metajennite, $C_9S_6H_7$. The layer thickness for jennite is 1.05nm and for metajennite 0.87nm. The structure resembles that of 1.4nm tobermorite but with two important differences. There

are only half as many silicate chains for a given number of calcium atoms in the central part of the layer, the other half being replaced by hydroxyl ions. The other difference is that the central, Ca-O part of the layer is distorted from that in CH in a way that differs from 1.4 nm tobermorite. This follows from the different repeat distance in the direction perpendicular to the chains, which is 1.0 nm compared with 0.56 nm for 1.4nm tobermorite. It is suggested that the Ca-O part of the layer in jennite is corrugated. The structure of metajennite is presumably derived from that of jennite by omission of some of the interlayer water molecules.

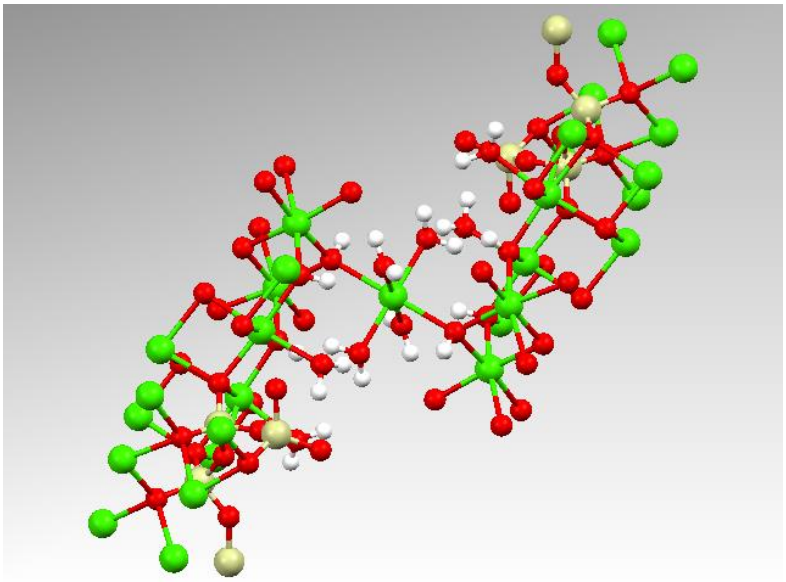

Figure 2.2. Unit cell of jennite. Color assignments are: Green (calcium); Red (oxygen);Tan (Silicon); White (hydrogen).

C-S-H (I)

Reaction between colloidal silica and CH in aqueous suspension at ordinary temperature gives a product referred to as C-S-H (I). This material has been fully described by Taylor [2]. C-S-H (I) is considerably more ordered than the C-S-H gel formed in Portland cement pastes at ordinary temperature. C-S-H (I) is generally prepared with Ca/Si ratios varying from

0.8 to about 1.5. The degree of crystallinity tends to decrease with an increase in C/S ratio and the basal spacing also decreases (1.4nm at Ca/Si = 0.8 to about 1.1nm at Ca/Si = 1.5. C-S-H (I) generally consists of crumpled foils a few nanometers thick with a tendency to a fibrous character at higher Ca/Si ratios. Data shows that C-S-H is a structurally imperfect form of 1.4nm tobermorite with little or no more than two-dimensional order.

C-S-H (II)

C-S-H (II) has a Ca/Si ratio somewhat below 2.0 and gives a characteristic X-Ray pattern which is different from that of C-S-H (I). The pattern shows similarities to that of jennite and the unit-cell parameters are near those of jennite. C-S-H (II) appears to be a structurally imperfect form of jennite. The Ca/Si ratio of the C-S-H gel of calcium silicate or cement pastes which is approximately 1.75 is higher than that of jennite and much higher than that of 1.4nm tobermorite.

C-A-S-H

It was concluded (Kalousek et. al. [5] and Copeland et.al. [6]) that ions could be taken up by the C-S-H and that up to about one silicon atom in six could be replaced by aluminum, iron or sulfur, and that aluminum and iron could also replace calcium. Subsequent work by Richardson and Groves [7] indicates that substitution of silicon by aluminum does occur and that it is confined to the bridging tetrahedra but that it is less extensive in normal pastes of Portland cements than was suggested by Copeland et. al. They demonstrated that the Al/Ca ratio increased linearly with the Si/Ca ratio. The general conclusion from the evidence presently available is that, in hydration products of Portland cement pastes, Al^{3+} can occur as a substituent in C-S-H and in AF_m or AF_t phases sufficiently crystalline to be detectable by XRD or thermal methods.

High Temperature Silicate Phases

(1) Gyrolite

Gyrolite can form under autoclave conditions at 200°C if the SiO_2 is supplied in a highly reactive form. The mineral is a hydrated calcium silicate with an approximate composition of $2CaO.3SiO_2.3H_2O$. The basal spacing is 2.21nm.It reverts to 1.91nm after heating to 400°C. The basal spacing can be recovered simply by wetting with water. Gyrolite loses water in two distinct stages. Heating up to 450°C results in a water loss of about 75%.The second dehydration stage is observed between 550°C and 850°C where the rest of the water is lost. This is accompanied by complete destruction of the structure. The gyrolite structure is transformed in an ordered way to pseudowollastonite and to amorphous silica.

(2) Xonotlite

Xonotlite ($Ca_6Si_6O_{17}(OH_2)$ occurs widely as a natural mineral and is formed from any sufficiently reactive starting materials of 1:1 CaO/SiO_2 ratio when treated hydrothermally in the range 150-400°C. Kalousek determined that xonotlite can be deficient in calcium with respect to the ideal 1:1 ratio. A calcium deficiency is balanced by the presence of Si-OH groups and thus explains, in part, the observation that samples made at low temperatures contain more water than indicated by the formula $Ca_6Si_6O_{17}(OH)_2$. Xonotlite has a medium-weak basal spacing at 0.0705nm.

(3) Hillebrandite

Hillebrandite ($Ca_2SiO_3(OH)_2$) is one of the main strength-forming phases in steam-cured cement mortar. The Ca/Si ratio is 2.0. The hillebrandite structure consists of a three-dimensional network of Ca polyhedral connected to form tunnels parallel to (100) that accommodate isolated wollastonite-type SiO_4 tetrahedral chains [2]. Powder X-ray diffraction studies have shown that hillebrandite resembles a synthetic β-$Ca_2SiO_4.H_2O$ phase and the C-S-H (II) phases described by Taylor [4]. The basal spacing is 1.183 nm.

References

1. Bonaccorsi E. and Merlino S., "The crystal structure of tobermorite 14 Å (Plombierite), a C-S-H phase," J American Ceramic Society, 88(3), 505-512, 2005.
2. Taylor H. F. W., "Cement Chemistry", 2nd Edition, Thomas Telford Pub., pp. 459, 1997.
3. Yu P., Kirkpatrick R. J. "Thermal dehydration of tobermorite and jennite," Concrete Science and Engineering, 1, 185-191, 1999.
4. Bonaccorsi E., Merlino S., and Taylor H.F.W., "The crystal structure of jennite, $Ca_9Si_6O_{18}(OH)_6.H_2O$, 34(9), 1481-1488, 2004.
5. Kalousek G. L. , Crystal chemistry of hydrous calcium silicates: I. Substitution of aluminum in lattice of tobermorite". J. Amer. Ceram. Soc., 40(3), 74-80, 1957.
6. Copeland L. E., Bodor E., Chung T.N. and Weise C.H., "Reactions of tobermorite gel with aluminates, ferrites and sulfates", J. Res. Dev. Labs., Portland Cem. Assoc., 9, 61-74, 1967.
7. Richardson I. G. and Groves G. W., "The incorporation of minor and trace elements into calcium silicate hydrate (C-S-H) gel in hardened cement pastes", Cem. Concr. Res., 23, 131-138, 1993.
8. Dai Y. and Post J. E., "Crystal structure of hillebrandite: A natural analogue of calcium silicate hydrate (CSH) phases in Portland cement", Amer. Miner., 80, 841-844, 1995.

Chapter 3

Calcium-Silicate-Hydrate Phases in Cement-Based Materials

It is advantageous and strategic to review relevant information pertaining to the nature of the cement-water reaction and the important characteristics of the C-S-H binding phase in cement-based materials. This underscores the rationale and arguments presented in the thesis proposal.

3.1 The Portland cement-water reaction

Portland cement contains four main compounds; silicate phases: C_3S and C_2S, and aluminate phases: C_3A and C_4AF. In cement chemistry, mineralogical notation e.g. C, S, A, F and H is often used in the chemical formulas for CaO, SiO_2, Al_2O_3, Fe_2O_3 and H_2O, respectively. The chemical reaction between the silicate phases of Portland cement and water results in the formation of two important components; crystalline calcium hydroxide and a nearly amorphous calcium silicate hydrate referred to as C-S-H [1]. The hyphens indicate that the stoichiometry is variable. C-S-H forms up to about 60% of the hydration products in hardened cement paste and is primarily responsible for some of its principal properties such as strength, shrinkage, and for its durability. An electron micrograph of the products formed in hydrated Portland cement is shown in Figure 3.1.

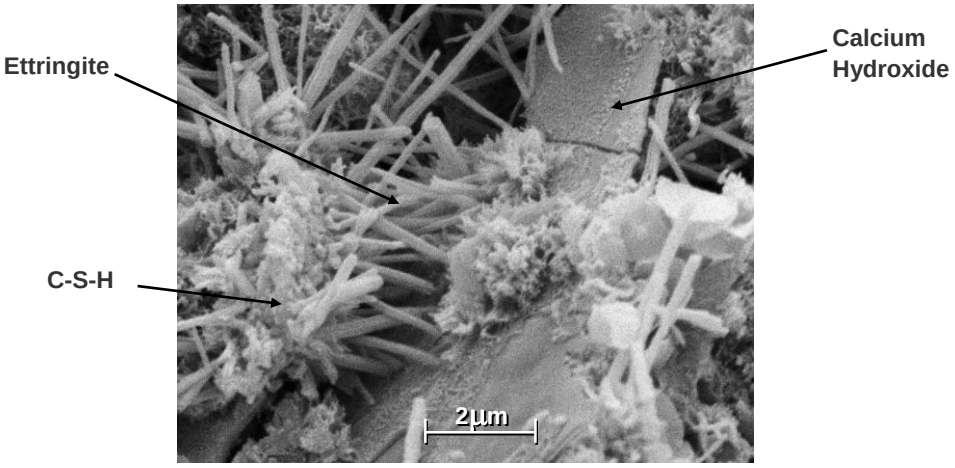

Figure 3.1. An electron microscope image of Portland cement hydration products

The ill-defined and variable crystalline nature of C-S-H in cement binders and incorporation of other elements such as aluminum into its structure are some of the barriers in the physical and chemical characterization of C-S-H. These have often been the main causes of the discrepancies in the research results and a major source of discussions.

3.2 *Relation of C-S-H with more ordered phases*

There are more than 45 known calcium (alumino) silicate hydrates of interest to cement chemists [2]. It was in the early 1950's when it became apparent that the short-range order structure of C-S-H can be related to the structure of crystalline compounds with a silicate-chain repeat distance of 0.73 nm in one direction [3]. An important advance occurred when the crystal structure of Maddrell's salt (isostructural with β-wollastonite) was determined [4]. It was found that β-wollastonite contains infinite chains of SiO_3^{2-} repeating at the intervals of three tetrahedra termed dreierketten. The Ca-O polyhedra repeats at a distance of 0.365 nm (half of that of silicate chain) considering the type of the silicate dreierkette's linkage to the Ca-O layer. Water molecules and calcium ions fill the space between these layers.

Among various calcium silicates, tobermorite and jennite appear to provide more structural clues about the C-S-H gel in hydrated Portland cement. Both of these minerals have a layered

structure and can be synthesized. Jennite is a rare mineral and is difficult to synthesize, but various forms of the tobermorite are available and can be easily prepared; 0.93, 1.1 and 1.4 nm tobermorite (the prefix denotes the distance between the layers (d_{002} basal spacing). The structure of tobermorite (from Northern Ireland) was first described by Megaw and Kelsey [5]. They showed that this substance was closely related to the C-S-H (I) [6]. Although their work did not clarify to what extent the hydrogen atoms in the interlayer region are from OH groups or H_2O, they verified that its removal results in the shrinkage of 002 basal spacing and allows two adjacent layers to pack together.

The crystal structure of 1.1 nm tobermorite was resolved by Hamid [7]. More recently the crystal structure of 1.4 nm tobermorite was also resolved [8]. A tobermorite layer is formed from a sheet of calcium oxide flanked on both sides by silicate tetrahedra (Schematic shown in Figure 3.2).

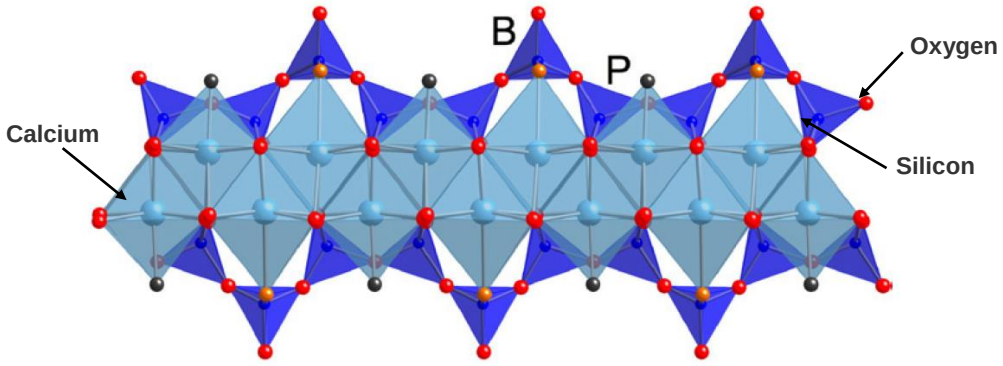

Figure 3.2. A schematic of a tobermorite layer showing a main Ca-O layer with silicate tetrahedra attached on both sides. The directly connected silicate tetrahedron is called *paired* and the silicate tetrahedron connecting two paired tetrahedra is called a *bridging* tetrahedron.

C-S-H that is akin to tobermorite is lacking some of the bridging tetrahedra and is referred to as the defect tobermorite structure [9]. A stacking of these layers with mainly water molecules and calcium ions in between forms a typical C-S-H material.

3.3 *Characteristics of C-S-H*

C-S-H systems can be studied from various aspects as a *material*. The scope of the literature in this field is broad and the following sections provide only a brief review of some of the research work relevant to the current project.

3.3.1 *C/S ratio*

An important stoichiometric parameter that defines C-S-H is the molar ratio of CaO to SiO2 in its structure (C/S ratio). It is possible to calculate the C/S ratio of the C-S-H by determining the content of calcium hydroxide [10] and unreacted materials using analytical methods such as thermo-gravimetric analysis or quantitative X-ray diffraction,. The C/S ratio in calcium silicate hydrates usually covers a range from 0.7 to 2.0 with an average value of 1.75 for that in hydrated Portland cement [11].

Taylor categorized C-S-H systems into C-S-H (I) and C-S-H (II) for C/S ratios below and above the dividing value of 1.5 [1, 12, 13]. However, not many researchers were able to reproduce the C-S-H (II). It had been shown that a C/S ratio of 1.5 is maximum in the hydrate unless extreme unless extreme reaction conditions applied [14]. Other studies distinguished various differences for the phase transition that occurs at the C/S ratio of 1.0 within the composition range of C-S-H (I) [15-19]. Nonat, therefore, suggested a categorization of three kinds of of C-S-H systems: C-S-H(I) for C/S<1.0, C-S-H(II) for 1<C/S<1.5 and C-S-H(III) for C/S>1.5 [20, 21]. The most significant changes in the structure of C-S-H with decreasing the C/S ratio are the longer silicate chains and the increase in the distance between the layers of C-S-H. The BET surface area of the C-S-H increases noticeably when the C/S ratio is decreased below 1.0. These characteristics have been shown to affect the physico-chemical behavior of C-S-H.

The mean C/S ratio of C-S-H varies with age and degree of hydration in hardened C_3S paste [22]. By means of TEM analysis, the C/S ratio of 1 month, 3 month, 3.5 year and 26 year old C_3S paste was measured to be 1.71±0.05, 1.77±0.20, 1.74±0.13 and 1.75±0.05, respectively.

3.3.2 *State of water in C-S-H*

A minimum amount of water is required for the hydration reaction of Portland cement to go to completion and provide a reasonable workability of concrete. Further, moist conditions after the setting of the cement paste maintain the stability of the microstructure of cementitious materials. The presence of water in the pore structure also facilitates the ionic movement and transport of aggressive chemicals into the concrete. Water and concrete truly form a combination of 'love' and 'hate' [23]. The role of water in hydrated cement paste is very complex and has been always controversial. Water, as a part of the microstructure of cement paste, plays an important role in controlling some of the major characteristics such as shrinkage and mechanical properties [24].

The classification of the state of water in cement paste is generally based on the location where it is held and, the nature of its bonding with the solid structure. The latter is a function of energy required to remove that water [25]. Although several investigations have attempted to separate the various forms of water in the cement paste and even in the more crystalline forms of C-S-H systems, the dividing line between the various states of water in not very clear [26, 27]. Various techniques such as NMR and DMA have been used to differentiate the role water in various structural locations. The dynamic mechanical response of the hydrated Portland cement in the temperature range of –140 to +25 °C revealed two transitions that were attributed to the water adsorbed on the internal surface of the microporous substance and capillary condensed water [28].

The study of the state of water using NMR requires the application of transient techniques. In an NMR test, the sample continues to emit resonance radiation for a measurable time after the incident radiation is removed. The rate of the decrease in this radiation is detected as well as a variety of "induction decay" signals. Application of this method on the protons can provide information on their mobility or the state of binding [29]. The tightly bound proton to the structure is relaxed faster than free protons in the liquid as manifested by the spin-spin relaxation time (T_2). This time is of several ms for loosely bound water, ~100μs for tightly bound water and about 10μs for protons in the crystalline structure [30].

It has been suggested that the C-S-H lamellae are held together by an electrostatic force. In this configuration, the interlamellar space is filled with quasi-immobile water molecules and calcium ions that are bonded to the C-S-H layer by partially covalent bonds [31].

It is suggested that water can exist in various forms e.g. capillary water (in voids larger than 5 nm), adsorbed water (held by hydrogen bonds on the surface of the hydrated particles) and interlayer water [32]. The debate about the latter i.e. water that is associated with the nanostructure of C-S-H and is strongly held, still continues [33-35]. Implications of the state of water in the structural models for C-S-H will be discussed in a following section.

An understanding of the composition and physico-mechanical and physico-chemical behavior of pure C-S-H systems is at the heart of resolving concrete durability issues. The scope of the literature in this field is broad and the following sections provide only a brief review of some of the research work relevant to the current project.

3.4 *Silicate polymerization*

The silicate tetrahedra that is flanked on both sides of the Ca-O layer, can be present in the form of dimers, dreierketten or a chain of dreierketten. Polymerization of silicates is defined by the mean length of these chains and is usually determined from the spectroscopic data from a ^{29}Si NMR experiment.

Polymerization of C-S-H is crucially affected by its compositional C/S ratio. The mean silicate chain length (number of silicate tetrahedra in a chain) is normally calculated form the Q^2/Q^1 intensity ratio obtained from a ^{29}Si NMR experiment:

Mean Chain Length = $2(1+Q^2/Q^1)$

The chain length increases significantly from 2.6 to 9.2 as the C/S ratio decreases from about 1.44 to 0.92 in synthetic C-S-H materials (double decomposition) [36].

Incorporation of supplementary cementitious materials in hydrated cement paste results in the formation of *secondary* C-S-H, which has a relatively lower C/S ratio of about 1.0 [1, 37]. It has been shown that this type of C-S-H is more polymerized and thus has different

characteristics [38]. It may also account for some of the enhanced durability aspects of the concrete using pozzolanic materials.

Polymerization of silicates is also affected by the curing humidity and temperature. The C-S-H in moist cured cement paste samples virtually contains all dimers, whereas pastes cured at the low relative humidity conditions (below 10% RH) have a greater degree of polymerization [39]. This effect is not that pronounced in aged samples. C-S-H samples prepared hydrothermally at temperatures above 120 ºC are highly polymerized at all C/S ratios ranging from 0.3 to 2.0 [40, 41]. The degree of hydration also affects the mean chain length in addition to the volume fraction of the C-S-H produced [22]. A 10%-hydrated sample (C_3S paste) has a silicate mean chain length of about 2. This value increases linearly to about 2.5 at 85% and 5 at 100% hydration.

Young hydrated C_3S at various temperatures and dried the sample at 105 °C before ^{29}Si NMR tests [42]. The results indicated an increase in the degree of polymerization due to the high temperature curing conditions (65 °C compared to 25 °C). Silica fume addition also resulted in an increase of the Q^2/Q^1 ratio. He did not suggest any cross-linking as no Q^3 was observed. Drying at 105 °C as evidenced by our results can increase the degree of polymerization and affect any assessment of the effect of curing temperature.

Yu and Kirkpatrick studied the effect of elevated temperatures up to 1000 °C on synthetic low C/S ratio C-S-H (referred to as tobermorite and jennite in their paper) [43]. XRD, ^1H NMR and ^{29}Si NMR results were interpreted to be an indication of the formation of meta-stable and stable phases with lower basal spacing. Q^3 and even Q^4 chemical shifts were observed in various samples after heat treatment at 250 °C. Cross-linking was concluded from the charge balance requirement after the removal of H from Si-OH groups. It was suggested that these linkages between the layers restrict the dynamical behavior of interlayer water that is now in “cages”.

The crystallization of tobermorite from the C-S-H precursor was studied by Sato and Grutzeck [44]. C-S-H was prepared in digestion bombs at 130 °C and 180 °C. The charge was removed at various times and dried at 80 °C for 24h before conducting low-angle XRD,

^{29}Si NMR and ^{29}Si CP NMR tests. C-S-H forms after two hours with the appearance of the XRD peak at low angles (~7°, 2θ) after 4 hours. They identified higher field Q^2 peaks in some samples prepared from quartz that were attributed to the bridging tetrahedra connected between the layers by hydrogen bonds. An interesting observation was that the C-S-H samples prepared from the quartz or amorphous silica even with the same C/S ratio are different in the polymerization degree. The sample made from quartz is less polymerized and it was suggested that the initial C/S ratio of the C-S-H that is formed on the surface of quartz particles is high. They concluded that the C-S-H, C/S ratio > 1, can be crystallized into tobermorite, while the silica rich samples do not seem to have this potential.

In their study, Wieker et al., for the first time applied ^{29}Si NMR to study the structure of various tobermorites [45]. Most of the samples were prepared at high temperatures and by the dehydration of other forms of tobermorite. Their results, indicated a high degree of polymerization with the presence of Q^3 site even at the C/S ratio of 1.0. These observations that led to the suggestion of double chain structures for tobermorites, are not unexpected as the heat treatment can increase the polymerization. The decrease in the Q^1 (end groups) intensity contributed to the condensation of the single chains upon dehydration. It was also observed that the low C/S ratio sample keeps the basal spacing on drying possibly due to the cross-linked sites preventing the collapse of the layers (anomalous behavior). The importance of the preparation method in the properties of tobermorite was emphasized and it was suggested that the thermal dehydration causes lengthening the chains.

References

1. Taylor H. F. W., “Cement Chemistry”, 2nd Edition, Thomas Telford Pub., pp. 459, 1997.
2. Richardson I. G., “The calcium silicate hydrates,” Cement and Concrete Research, 38, 137-158, 2008.
3. Taylor H. F. W., “Tobermorite, jennite and cement gel,” Zeitschrift für Kristallograohie, 202, 41-50, 1992.

4. Dornberger-Schiff, K.; Liebau, F.; Thilo, E., "Über die Kristallstruktur des (NaAsO3)x, des Maddrellschen Salzes und des β-Wollastonits," Die Naturwissenschaften, 41 (23), 551, 1954.
5. Megaw H.D. and C.H. Kelsey, "Crystal structure of tobermorite," Nature, 177, 390–391, 1956.
6. Taylor H. F. W., "Cement Chemistry", 2nd Edition, Thomas Telford Pub., pp. 459, 1997.
7. Hamid S.A., "The crystal structure of the 11 Å natural tobermorite Ca2.25[Si3O7.5(OH)1.5].1H2O," Zeitschrift fur Kristallographie, 154, 189-198, 1981.
8. Bonaccorsi E. and Merlino S., "The crystal structure of tobermorite 14 Å (Plombierite), a C-S-H phase," J American Ceramic Society, 88(3), 505-512, 2005.
9. Cong X. and Kirkpatrick R. J., "29Si MAS NMR Study of the Structure of Calcium Silicate Hydrate," Adv. Cem. Based Mat., 3, 144-156, 1996.
10. Ramachandran V.S., "Differential thermal method of estimating calcium hydroxide in calcium silicate and cement pastes," Cement and Concrete Research, 9(6) 677-684, 1979.
11. Richardson I. G., "The nature of C-S-H in hardened cements," Cement and Concrete Research, 29, 1131-1147, 1999.
12. Taylor H.F.W., "Hydrated calcium silicates: part I. Compound formation at ordinary temperatures," J. Chem. Soc. 3682-3690, 1950.
13. Gard J. A., Taylor H. F. W., "Calcium Silicate Hydrate (II)," Cement and Concrete Research, 6, 667-678, 1976.
14. Greenberg S. A., "Calcium Silicate Hydrate (I)," J. Phys. Chem., 58(4) 362-367, 1954.
15. H. Stade and W. Wieker, ''Zum aufbau schlecht geordneter alciumhydrogensilicate. I. Bildung und eigenschaften einer schlecht geordneten calciumhydrogendisilicatphase,'' Zeit. Anorg. Allg. Chemie., 466, 55-70, 1980.
16. M. Grutzeck, A. Benesi, and B. Fanning, ''Silicon-29 magic-angle spinning nuclear magnetic resonance study of calcium silicate hydrates,'' J. Am. Ceram. Soc., 72, 665-668, 1989.

17. Klur I., Pollet B., Virlet J., Nonat A., "C-S-H structure evolution with calcium content by multinuclear NMR," 2nd International conference on NMR spectroscopy of cement based materials, 119-141, 1998.
18. Nonat A., "The structure and stoichiometry of C-S-H," Cement and Concrete Research, 34, 1521–1528, 2004.
19. Garbev K., Stemmermann P., Black L., Breen C., Yarwood J., Gasharova B., "Structural features of C–S–H(I) and its carbonation in air- A Raman spectroscopic study. Part I: Fresh phases," J. Am. Ceram. Soc., 90(3), 900-907, 2007.
20. Nonat A., "Interactions between chemical evolution (hydration) and physical evolution (setting) in the case of tricalcium silicate," Materials and Structures, 27(4),187-195, 1994.
21. Nonat A., Lecoq X., The structure, stoichiometry and properties of C-S-H prepared by C3S hydration under controlled condition, NMR Spectroscopy of Cement Based Materials, edt. Colombet, A. R. Grimmer, H. Zanni, P. Sozzani, Springer-Verlag, Berlin Heidelberg, 197-207, 1998.
22. Richardson I.G., Groves G.W., "Models for the composition and structure of calcium silicate hydrate (C-S-H) gel in hardened tricalcium silicate pastes," Cem. Concr. Res., 22, 1001-1010, 1992.
23. Neville A., "Water and Concrete: A Love-Hate Relationship," Concrete International, 22(12), 34-38, 2000.
24. Wittmann F. H., "Interaction of hardened cement paste and water," J American fCeramic Society, 70(5), 323-328, 1987.
25. Mehta P. K. and Monteiro P. J. M., Concrete; Microstructure, Properties and Materials, 3rd edition, McGraw-Hill, 2006.
26. Feldman R.F. and Ramachandran V.S., "Differentiation of interlayer and adsorbed water in hydrated Portland cement by thermal analysis," Cement and Concrete Research, 16, 607–620, 1971.
27. Feldman R.F., Sereda P.J., "A datum point for estimating the adsorbed water in hydrated Portland cement," Journal of Applied Chemistry, 13, 375-382, 1963.
28. Radjy F., Sellevold E. J. "Internal friction peaks due to adsorbed and capillary water in microporous substances," Nature Physical Science, 241, 133-135, 1973.

29. Bohris A.J., Goerke U., McDonald P.J., Mulheron M., Newling B. and Le Page B., "A broad line NMR and MRI study of water and water transport in Portland cement pastes," Magnetic Resonance Imaging, 16(5/6), 455-461, 1998.
30. Miljkovic L., Lasic D., MacTavish J. C., Pintar M. M., Blinc R. and, Lahajnar G., "NMR studies of hydrating cement: A spin-spin relaxation study of the early hydration stage," Cement and Concrete Research, 18(6), 951-956, 1988.
31. Pellenq R.J.-M., Lequeux N., Van Damme H., "Engineering the bonding scheme in C–S–H: The iono-covalent framework," Cement and Concrete Research, 38, 159-174, 2008.
32. Ramachandran V. S., Feldman R. F., Beaudoin J. J., Concrete Science, Heyden, 1981.
33. Jennings H. M., "Refinements to colloid model of C-S-H in cement: CM-II," Cement and Concrete Research, 38, 275–289, 2008.
34. Beaudoin J. J. and Alizadeh R., "Discussion of the paper 'Refinements to colloid model of C-S-H in cement: CM-II,' by Jennings H. M.," Cement and Concrete Research, 38(7), 1026-1027, 2008.
35. Jennings H. M., "Reply to the discussion by J.J. Beaudoin and R. Alizeadab of the paper "Refinements to colloid model of C–S–H in cement: CM-II" by H.M. Jennings," Cement and Concrete Research, 38(7), 1028-1030, 2008.
36. Chen J.J., Thomas J.J., Taylor H.F.W., Jennings H.M., "Solubility and Structure of Calcium Silicate Hydrate," Cement and Concrete Research, 34(9) 1499-1599, 2004.
37. Taylor H.F.W., "Proposed structure for calcium silicate hydrate gel," J. Am. Ceram. Soc., 69(6) 464-467, 1986.
38. Wu Z., Young J. F., "The hydration of tricalcium silicate in the presence of colloidal silica," J. Mater. Sci., 19, 3477-86, 1984.
39. Luke K., "Phase studies of pozzolanic stabilized calcium silicate hydrates at 180 °C," Cement and Concrete Research, 39, 1725-1732, 2004.
40. Macphee D. E., Lachowski E. E., Glasser F. P., "Polymerization effects in C-S-H: implications for Portland cement hydration," Advances in cement research, 1(3), 131-137, 1998.
41. Okada Y., Ishida H., Mitsuda T., "29Si NMR spectroscopy of silicate anions in hydrothermally formed C-S-H," J. Am. Ceram. Soc., 77(3), 765-768, 1994.

42. Young J. F., "Investigations of Calcium Silicate Hydrate Structure Using Silicon-29 Nuclear Magnetic Resonance Spectroscopy," J. Am. Ceram. Soc., 71(3) C118-C120, 1988.
43. Yu P., Kirkpatrick R. J. "Thermal dehydration of tobermorite and jennite," Concrete Science and Engineering, 1, 185-191, 1999.
44. Sato H., Grutzeck M. "Effect of starting materials on the synthesis of tobermorite," Mat. Res. Soc. Symp. Proc., vol. 245, 235-240, 1992.
45. Wieker W., Grimmer A.-R., Winkler A., Mägi M., Tarmak M. and Lippmaa E., "Solid-state high-resolution 29Si NMR spectroscopy of synthetic 14Å, 11and 9Å tobermorites," Cem. Concr. Res. 12, 333-339, 1982.

Chapter 4

Physico-chemical and Compositional Models of Cement Paste and C-S-H Nanostructure

4.1 Introduction

The strategic research plan presented in this thesis proposal focuses on improving understanding of the fundamental mechanisms and the role of water underlying the engineering behavior of cement-based binders with emphasis on layered calcium-silicate-hydrate systems. New techniques based on DMA and DMTA (dynamic and thermal dynamic analysis) methods have been developed by the candidate for this investigation. Microindentation methods have also been used to study these systems and to provide corroborating evidence in support of the conclusions drawn from thermal analysis. The candidate has synthesized a number of pure C-S-H phases including 1.4 nm tobermorite (T) and jennite (J) (details are presented elsewhere in the proposal) that are key components of modern compositional models in order to investigate the compatibility of their performance with these models. There appears to be no existing mechanical performance data for these minerals in the literature. A critical and chronological discussion of some of the prevailing physico-chemical models for hydrated cement paste follows. It is intended to draw attention to microstructural factors and nanostructural characteristics that influence mechanical behavior. The compositional models after Taylor and Richardson-Groves in large-part are 'nanostructural-mixtures' of T and J. The experimental work described in the proposal is designed to assess the correspondence and sensitivity of real performance data with these models.

The models discussed provide insight for understanding engineering performance of cement-based construction materials. Resolution of C-S-H nanostructure also forms the basis for structural modification and optimization –a focal point for sustainability. Several models of hydrated cement paste have been developed in attempts to explain the underlying

mechanisms responsible for the physico-mechanical and chemical properties of this material. The models have been effective drivers for many significant research investigations. They represent the diverse and disparate views of researchers covering a period of several decades of research. Nevertheless they have proven useful in enhancing our overall general understanding of important phenomena including concepts related to strength development and durability issues. This will be illustrated by the description and presentation of selected models that follow. A critical assessment of their merits and limitations is given.

4.2 Powers and Brownyard (P-B) Model

Cement paste is considered a microporous solid referred to as cement gel randomly distributed in a network containing capillary cavities that are orders of magnitude larger than the gel pores [1, 2]. The gel has a porosity of about 28 per cent with an average pore size estimated at 1.8nm or about 5 times the diameter of a water molecule. It is argued that any region where the porosity exceeds 28 percent is a region where new crystals could nucleate or existing crystals could continue to grow. Powers and Brownyard also introduced the concept of 'outward growth' and 'inward' growth of gel particles and suggested that the gel particles formed by 'inward' growth likely had a different morphology and stoichiometry from the particles formed by 'outward' growth. This idea was later elaborated on by Diamond and Bonen, Goto and Taylor [3-7]. More recent colloidal-based models also argue the presence of two types of C-S-H hydration products. This will be discussed later.

The origins of the P-B model are seated in the analysis of adsorption-desorption isotherm data obtained with water as the adsorbate. A fundamental assumption is that adsorption processes are thermodynamically reversible and the application of the B.E.T. theory is valid. This tenet has been challenged and will be discussed in detail as other models are introduced. A major factor is the ability of water to re-enter the structure following drying. The B.E.T. analysis was used to estimate the surface area (typically about 170 m^2/g for paste with w/c=0.45, hydrated 1year) and the size of the gel pores through calculation of the hydraulic radius (about 0.7 nm).The monolayer capacity, Vm (g/g dry paste), is also an output of the analysis. It represents the mass of adsorbed water that occupies one molecular layer on the surface of the adsorbent. It is also considered proportional to the internal surface area and amount of colloid material in the sample. A saturated paste with no capillary pore space

contains a quantity of evaporable water equal to approximately 4Vm. Water in pastes that exceeds this amount is considered to be capillary water. A schematic of the P-B model is given in Figure 4.1(A and B). The spherical gel particles contain microcrystalline hydrates and anhydrous cement. Capillary condensed water occupies the interstitial space (Figure 4.1A).A lower water/cement ratio paste is depicted in Figure 4.1B. There is an absence of capillary water as the capillary space has been filled with gel.

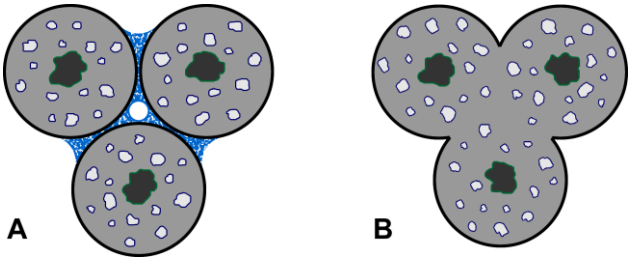

Figure 4.1. Model for hydrated cement: A. Spherical particles of cement gel with embedded non-colloidal particles (microcrystalline hydrates and unreacted cement); Capillary condensed water is depicted as lenses around the spherical contact points B.Paste with equivalent degree of hydration but lower w/c ratio depicting the elimination of all capillary water. [1]

The particles in the P-B model are not discrete. Instead they are described as forming a continuous solid body by virtue of a number of primary chemical bonds that are required to limit the swelling of the gel in water. The chemical nature of these bonds was not discussed by Powers and Brownyard. The solid body is therefore comprised of interconnected colloidal particles. Emphasis is placed on the minimum or least dimensions (a few nanometers) of many of the spaces that can be occupied by evaporable water. Estimates of the average surface to surface distance of the densest structure (low water/cement ratio paste) were about 1.5nm with minimum values of about 1 to 2nm. This was interpreted to mean that van der Waals forces of attraction are operative over a large proportion of the solid surfaces. Calculations indicated that in dry samples the forces were significant with estimates of about 280 MPa for a spacing of 0.6 nm. Utilizing data for the differential heat of adsorption and the amount of water adsorbed the adsorbate was estimated to be up to 5 molecular layers thick. It was concluded therefore that a distance of 3.0 nm between opposite surfaces was required for unhindered adsorption. It was also argued that pressure variations on the

adsorbed film were required for thermodynamic equilibrium. These pressure differences are maintained by tensile stresses in the primary bonds that impart structural integrity to the solid network and prevent dispersion of the particles. This phenomenon is at the heart of explanations for volume change.

The concept of disjoining pressure was invoked to account for forces produced in places where adsorption of water is hindered. Volume change in the adsorption region of the isotherm was attributed to both disjoining pressure and change in solid surface tension. Total volume change at higher humidities (nominally above 45% RH) included the effects of capillary condensation and hydrostatic tension. External loads are considered as transferring stress to water in regions of hindered adsorption; this water is referred to as load-bearing. It is noted here that many of these concepts are not compatible with models (to be discussed in detail later) that consider the solid material to behave as a layered silicate where interlayer water plays a significant role. The thermodynamics-based arguments inherent in the P-B model indicate that it is not possible for disjoining pressure to change without changing solid surface tension. The total volume change is considered to be the sum of these effects. The volume change is expressed as follows:

$$\Delta V/V = RT\ [\ 2/3\ \alpha \int w_a/V_s\ d(\ln h) + \beta'\ f(w_a) \int d(\ln h)]$$

where the definitions for the components for the first term in the brackets are: Vs = the volume of the solid; wa = mass of adsorbed water per unit mass of paste ;α = the coefficient of compressibility of the solid; h = humidity. The second term represents the volume change due to disjoining pressure where β' is the coefficient of compressibility of the specimen under sustained stress and f (wa) is the area fraction over which the disjoining pressure is operative. V is the overall volume. The contribution of the first term is considered uncertain, small and of opposite sign from the second term.

Shrinkage and creep during first drying of cement paste result in irreversible changes in volume and internal surface area. These are due to the formation of primary bonds where surfaces that were previously in close proximity are brought into contact by compression. The initial structural collapse may involve the fracture of some interparticle bonds.It is argued, however, that there is no apparent justification for the assumption that irreversible creep is due to viscous or plastic flow of the solid structure.

4.3 *Feldman-Sereda (F-S) model*

This model is much more complex than the P-B model [8-11]. The presence and role of interlayer water in physical phenomena is significant. This feature makes it quite distinct from the P-B model. Evidence for the layered nature of hydrated Portland cement is provided through several types of experiments: length and mass change scanning isotherms, mechanical property isotherms; helium inflow methods; similarities with the behavior of C-S-H (I) on the removal of water; dynamic mechanical analysis of C-S-H (I) and cement paste following removal of water; relaxation experiments of C-S-H (I) and cement paste on removal of water. The model is depicted in Figure 4.2 (A and B). The types of water (physically adsorbed and interlayer hydrate water) and the nature of the disordered layer structure are illustrated in Figure 4.2 (A). A more detailed illustration of a suggested C-S-H gel structure illustrating possible bonding arrangements between and along sheets and the polymerization of silicate chains is given in Figure 4.2 (B).

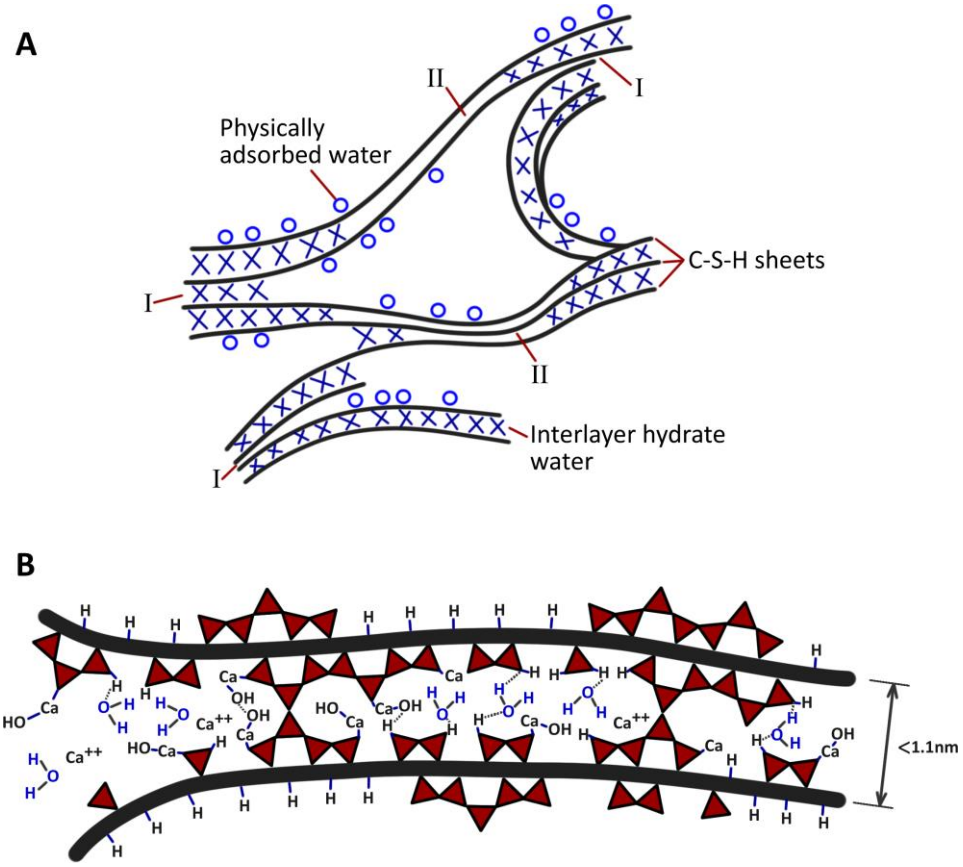

Figure 4.2 A: Schematic of the structure of C-S-H gel according to Feldman and Sereda, [8]. The Symbols I and II refer to intercrystallite bonds and faults giving disordered layers, respectively.
B: Suggested C-S-H gel structure illustrating bonds between and along sheets and polymerization of silicate chains. [12]

Validation of the model and its role in engineering behavior is discussed as follows:

4.3.1 Cement paste mass and length-change sorption isotherms.

Large primary and secondary hysteresis were observed in the water sorption isotherms of Feldman, Daimon et. al. and Helmuth [13-15] for both mass and length change, Figure 4.3 (A,B and C). All exhibited scanning loops over the entire humidity range. Feldman was able to reproduce these isotherms (Figure 4.3(A)) for a wide range of drying severity including D-drying (-78◦C at a vapor pressure of 5 x 10-4 mmHg) for many months and oven drying

at 100◦C for 3 hours. The isotherms of Daimon et. al. (Figure 4.3 (B)) were obtained for hydrated C3S from which the calcium hydroxide had been extracted i.e. C-S-H. The length change isotherm of Helmuth (Figure 4.3 (C)) for hydrated C_3S is similar to that obtained by Feldman. Note the similarity in the isotherms from all these authors-for cement paste, tricalcium silicate paste and C-S-H. It is clear from these experiments alone that the application of reversible thermodynamics and related theories for the determination of surface area and other sorption parameters cannot be directly applied to data from these isotherms. Feldman was able to overcome this through the use of scanning loops to separate the reversible and irreversible components of the isotherms enabling the construction of reversible and irreversible isotherms. The method of separation of interlayer and adsorbed water is illustrated in Figure 4.3 (D).

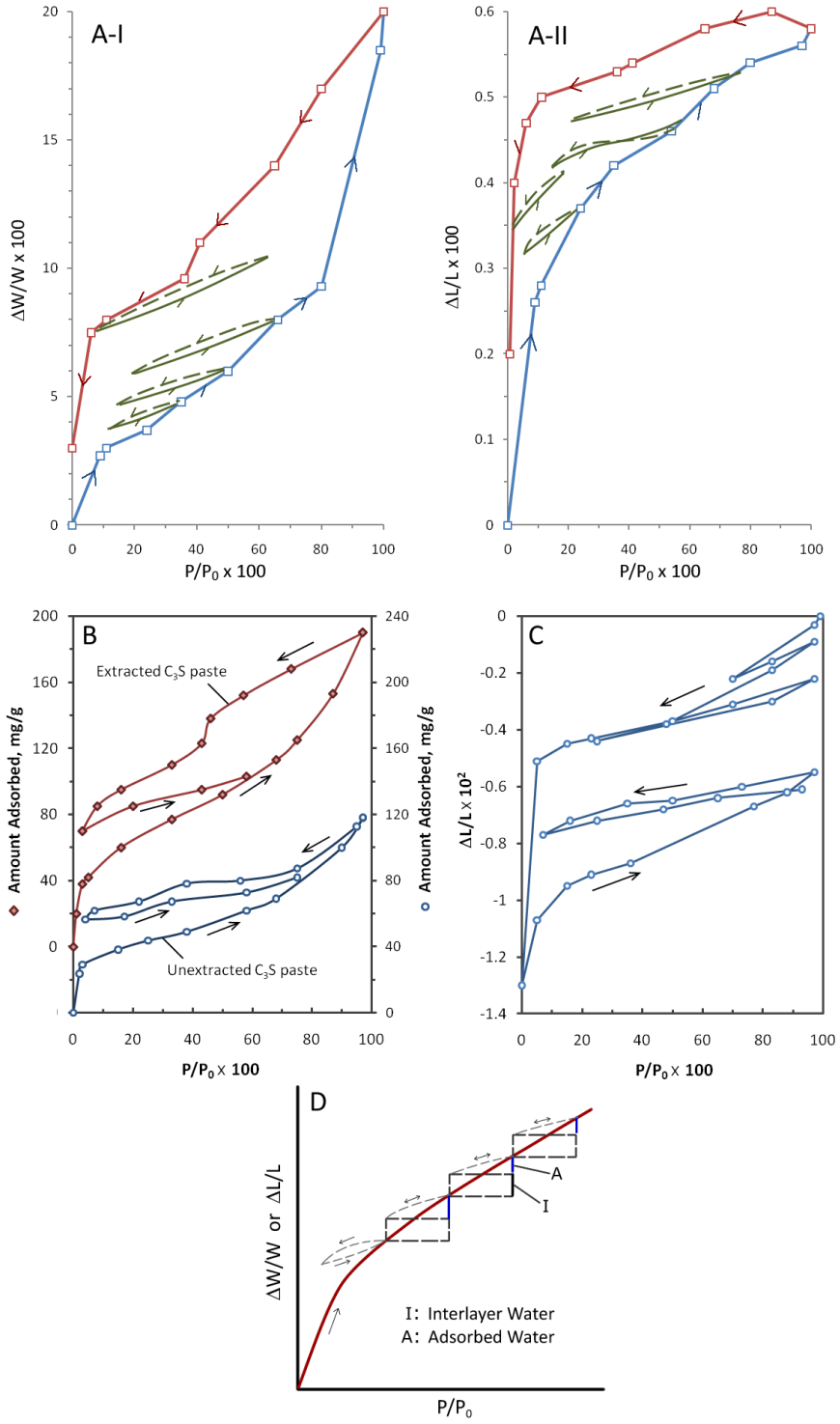

Figure 4.3 A: Mass-change (I) and length-change (II) isotherms of hydrated Portland cement paste (w/c=0.50) indicating the existence of scanning loops. [11] B: Mass-change isotherms for C_3S paste and C_3S paste from which calcium hydroxide has been extracted. [14] C: Length-change isotherm for C_3S paste (w/s ratio=0.61). [15] D: Method of separation of interlayer and adsorbed water applied to adsorption isotherms for cement paste. [8]

The adsorbed water was considered to go on and off reversibly over small increments on the isotherm. The interlayer water was considered not to come off over the small pressure increment. The irreversibility was attributed to intercalation and de-intercalation effects of water with respect to exit and entry from and into the C-S-H layers. A typical construct for the reversible isotherm is given in Figure 4.4

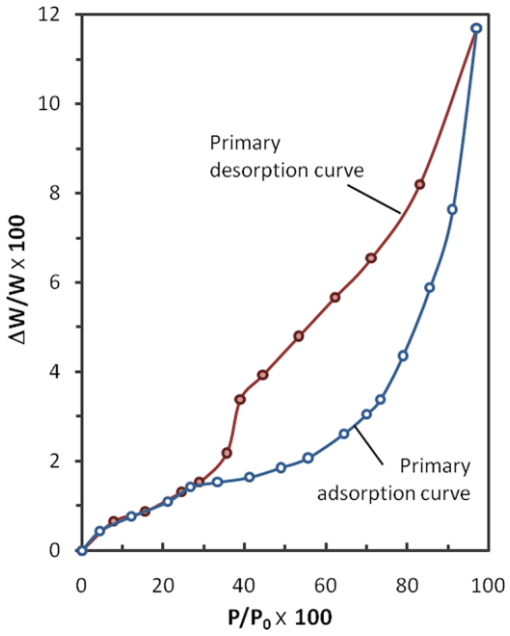

Figure 4.4. Constructed reversible water isotherm for cement paste (w/c=0.50). [13]

The B.E.T. theory for surface adsorption and classical thermodynamics can be applied to this isotherm to compute surface area and the elastic constants of the solid. The surface areas determined from N_2 and H_2O adsorption are very similar. A value of $40 m^2/g$ is typical. In addition the total volume of interlayer water found by calculation from scanning isotherms was equal to the difference between the total volume of water sorbed and the total volume of nitrogen or methanol sorbed i.e.

$$V_{H_2O} - V_{N_2} \text{ or methanol} = V_{\text{interlayer water}}$$

The elastic constants of the solid can be determined through application of the Gibbs' adsorption equation and the Bangham equation to the reversible isotherm data. The Gibbs' equation:

$$\Delta F = -RT \int_0^P n \, dP/P$$

represents the change in free energy of pure adsorbent provided that this integral represents a path of thermodynamic reversibility. n is the number of moles of adsorbate on a fixed mass of adsorbent. The solid with surface area, σ (m^2/g), undergoes a change in solid surface tension, Δγ, where:

$$\Delta F = \sigma \Delta \gamma$$

and

$$\boldsymbol{\Delta\gamma = RT/\sigma \int_0^P n\, dP/P}$$

Length change can be determined from the Bangham equation:

$$\Delta L/L = k1\ \Delta\gamma$$

The modulus of elasticity of the solid can now be calculated as:

$$E = \rho\sigma/k1$$

where E is the modulus of elasticity and ρ is the solid density.

The application of Gibbs' equation requires thermodynamic reversibility.

Capillary water in the high pressure region of the reversible isotherm is assumed to be 'bulk' as it is generally remote from the surface forces. Equilibrium with different vapor pressures is maintained by changing the radius of its meniscus. The water within the range of surface forces (assumed to be the first two molecular layers) will, however , also induce changes in surface free energy. The total length change is thus:

$$\Delta L/L = \{k_1 RT/\sigma\ .\ n + k_2 RT/\rho M\}\ \ln P_2/P_1$$

4.3.2 Mechanical Property Isotherms

The irreversible isotherm construct is particularly instructive with regard to the dependence of the elastic modulus on relative humidity and the role of interlayer water. The correspondence of the humidity dependence of length change, mass change and modulus of elasticity change is striking and is illustrated in Figure 4.5. In all cases there is a large hysteresis over the entire humidity range. The modulus of elasticity increases significantly on wetting after about 55% relative humidity up to saturation. It remains relatively constant on drying until a sharp decrease is observed below 11% relative humidity. The modulus returns to the original value in the dry state. Similar behavior on drying is observed for the length and mass change isotherm data.

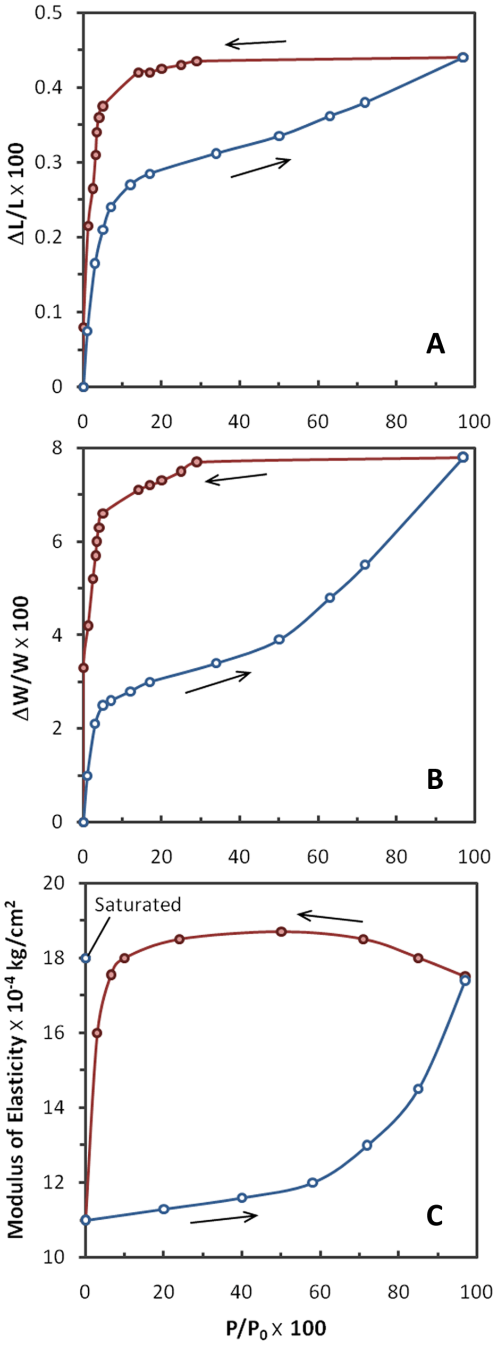

Figure 4.5 Irreversible isotherm construct for cement paste: A. Length-change; B. Mass-Change; C. Modulus of elasticity. [8]

The modulus values can be explained using a layered model for the exit and entry of interlayer water (Figure 4.6). Entry of water at low humidities begins from layer ends and has a minimal effect on stiffening. Above 55% humidity water penetrates further into the

layer structure and an increase in stiffening occurs as the central part of the system acquires rigidity. Maximum stiffness is achieved when all the interlayer positions are filled. The reverse process occurs on drying. Stiffness is maintained until the relative humidity is less than about 11%. Interlayer water, at this point, begins to be removed from central positions accounting for the sudden decrease in stiffness.

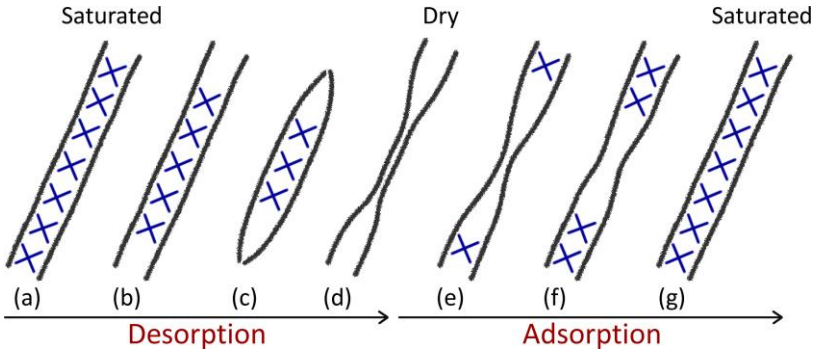

Figure 4.6 Simplified model for the exit and entry of water between C-S-H layers in cement paste.[13]

The effect of humidity on microhardness of porous glass and strength of cement paste differs from the modulus of elasticity isotherm. In both cases the values decrease significantly on wetting to 11% relative humidity. This is followed by a slight but gradual decrease to saturation. The decrease in strength is attributed to a change in the environment where the fracture process is occurring. Fracture is initiated at crack tips where there are stress concentrations. Si-O-Si bonds are strained and the strain energy facilitates the formation of hydroxyl groups {Si-OH HO-Si} in the presence of water vapor. No further decrease in strength occurs when the concentration of water molecules is sufficient to maintain a rate of diffusion that will deliver a minimum amount of water into a spreading crack.

4.3.3 Helium Inflow Methods

The space occupied by interlayer water in the C-S-H layer structure can be measured quantitatively using helium inflow methods [16]. This enables the systematic monitoring of the volume changes associated with water removal beginning with the equilibrium condition at 11% relative humidity. The surfaces are covered with a monolayer of water at this position.

The samples are exposed to helium gas (at 2 atmospheres) in a vacuum cell and measurements of instantaneous volume change (ΔV) and time dependent volume change (ΔD) are made at specific moisture contents as water is removed in steps by drying. The latter is due to the diffusion of helium gas into space vacated by water. The time dependent volume change is plotted against time for each incremental removal of water. A typical set of helium inflow curves for cement paste is shown in Figure 4.7.

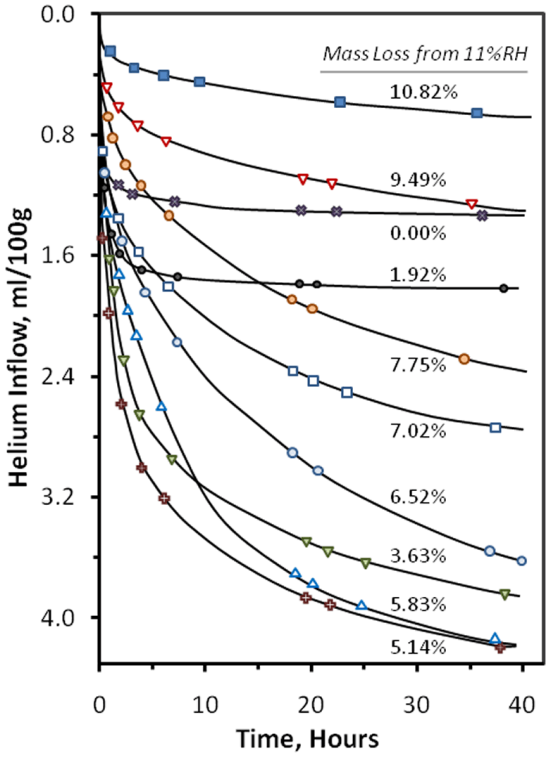

Figure 4.7 A typical set of helium inflow versus time curves for cement paste (w/c-0.40). [16]

The curves generally reach an asymptotic value after about 40-50 hours. The total inflow after this period increases to a maximum at a mass loss of about 5% and then decreases (Figure 4.8).

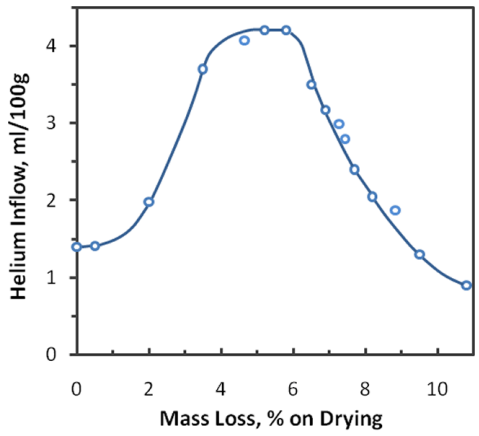

Figure 4.8 Total helium inflow versus mass-loss for cement paste at 40 h (w/c=0.40). [16]

This is interpreted as due to a structural collapse of the C-S-H layers. The quantity (ΔV-ΔD) provides an estimate of the space occupied by interlayer water before its removal. ΔV is negative and therefore the volume change terms are additive. A plot of (ΔV-ΔD) versus mass change (Figure 4.9) is linear up to about 5.5% mass loss.

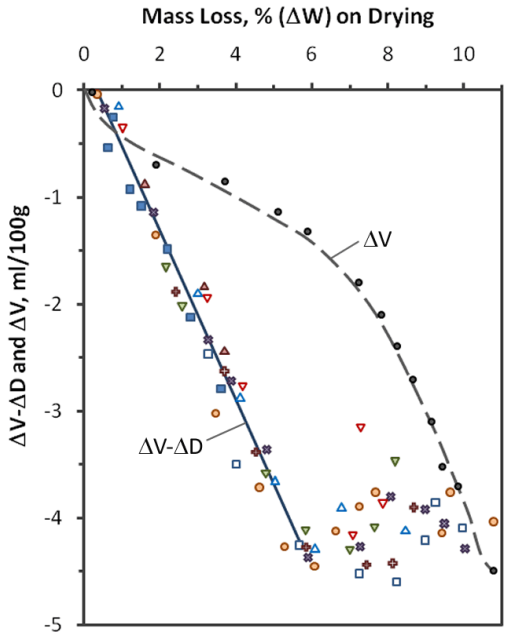

Figure 4.9 A plot of ΔV-ΔD and ΔV as a function of mass-loss for several cement pastes. [16]

The inverse of the slope (1.27± 0.08 g/cc) provides an estimate of the density of the interlayer water. This density value is greater than the 'bulk' density of water and corresponds with measurements made on expanding and non-expanding clays for water contents of less than one monolayer [16]. Results of density measurements for some adsorbates 30% above their bulk values have been reported [17, 18]. The scatter at greater mass losses is due to the structural collapse of the layers. A layered model is compatible with the (ΔV-ΔD) versus mass change plot. A 'gel pore' model is not compatible with the plot as a linear curve would be expected over the entire range of mass loss.

4.3.4 C-S-H (I) – A Nanostructural Model for the Removal of Water from Cement Paste

Synthetic C-S-H (I) has been studied extensively. It includes a family of calcium silicate hydrates with CaO/SiO_2 molar ratios varying from 0.6 to 1.5. It has a definite X-ray pattern with the strongest peaks at 1.250, 0.304 and 0.280 nm. The 002 basal spacing at 1.250 nm is sensitive to changes in relative humidity and moisture content. Helium inflow methods were used to probe the volume change sensitivity of C-S-H (I) (C/S = 1.2) nanostructure to moisture change on drying [19]. The helium inflow versus time curves followed a similar pattern to those obtained for cement paste (see Figure 4.7). The total helium inflow at 40 hours for the C-S-H (I) sample is plotted against mass loss in Figure 4.10.

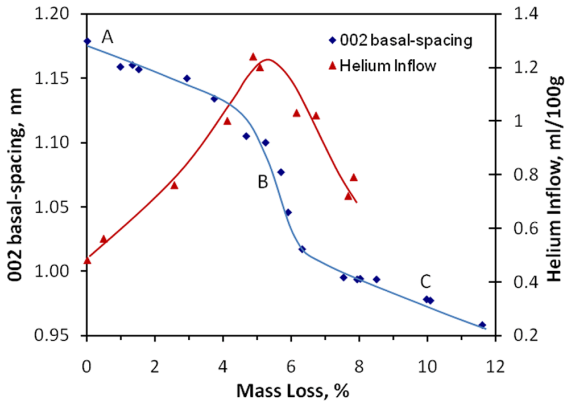

Figure 4.10. Total helium inflow at 40h and the 002 basal spacing as a function of mass-loss for C-S-H (I) - C/S=1.20.

The inflow reaches a maximum at about 5% mass loss and then decreases in a manner similar to that for cement paste. The basal spacing change with mass loss is also shown in the Figure 4.10. There is a sharp decrease in spacing between 4 and 6% mass loss coinciding with the region of maximum inflow. This supports the view that the maximum in the helium inflow curve is associated with a collapse of the layered structure. It is suggested then that the similar correspondence of the inflow curve for cement paste is indicative of behavior akin to that of a layered material.

Further evidence that C-S-H (I) is a valid model for C-S-H in cement paste is obtained from dynamic mechanical analysis data of C-S-H (I) and cement paste. The dynamic modulus ,E,obtained from the analysis, can be expressed by the following equation:

$$E = E' + E'' \tan\partial$$

where E' is the storage modulus, E'' is the loss modulus, ∂ is the phase lag angle and $\tan\partial$ is a damping factor or measure of internal friction. Curves of E' and $\tan\partial$ versus mass loss (from the 11% RH condition) are plotted in Figure 4.11 (A and B) for two C-S-H preparations-one with C/S ratio 1.20 and the other 1.50. The C-S-H present in cement paste typically has a C/S ratio in the range of 1.50-1.70.

The E'curves (Figure 4.11 (A)) will be discussed first. There is a plateau at the beginning of the curves followed by a rapid decrease in E' up to about 2% mass loss. This is followed by an increase in E' to a maximum at about 5-5.5% mass loss and a subsequent continuous decrease up to a mass loss of about 10% These effects are much less pronounced for the C/S ratio of 1.50. The plateau and initial decrease is attributed to the loss of adsorbed water and some interlayer water. The increase is explained as follows. Drying of C-S-H results in an increase in the degree of polymerization and possible cross- linking of the silicate chains [20-22]. Evidence for this is based on 29Si NMR observations of an increase in the Q^2/Q^1 ratio and some indication of the presence of a Q^3 peak. The increase may therefore be a result of the interaction of silicates between the layers (forming Q^3 sites). The increase may also be explained by the role of calcium ions in the interlayer region. Partially dehydrated calcium ions interact specifically with the ≡ Si-O- groups of the short silicate chains [23]. There is also the possibility of covalent bonding between C-S-H sheets and interlayer cations resulting in strong 'surface-cation-surface' ionic-covalent interactions [24]. The decrease in storage modulus at mass losses greater than 5.5% is the result of the removal of the final quantities

of interlayer water which provide structural stability to the layered nanostructure. The rapid decrease of the X-ray basal spacing of the C-S-H in this region of mass loss suggests a possible association of the decrease in E' with a collapse of structure mechanism. The results are also compatible with a collapse mechanism proposed to explain the decrease in the helium inflow (see discussion in previous section) at a similar mass loss. Removal of water molecules is critical to the structural integrity of the C-S-H framework.

It is now instructive to examine and discuss the tan∂ versus mass loss curves in Figure 4.11(B).

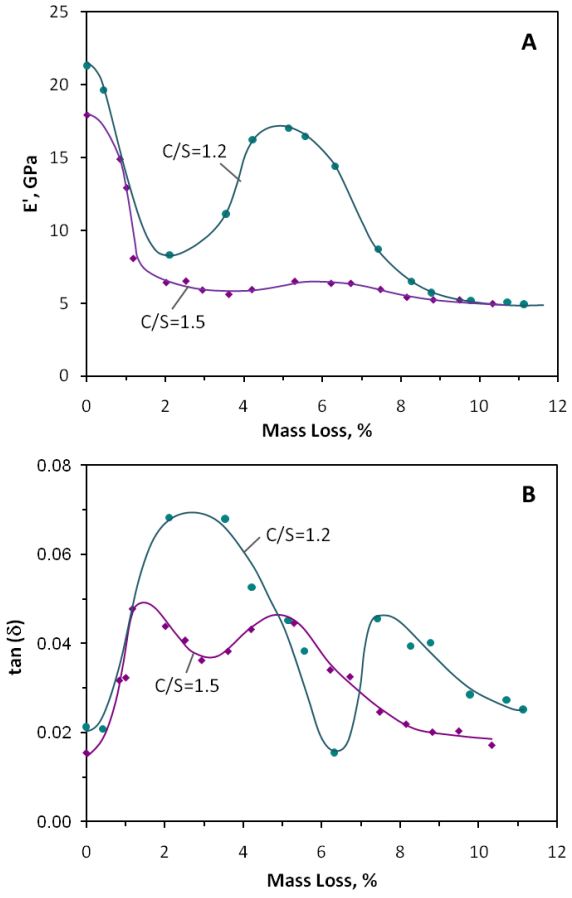

Figure 4.11 A: E' versus mass-loss for C-S-H-C/S= 1.20 and 1.50 (porosity=30%). B: tanð versus mass-loss for C-S-H-C/S= 1.20 and 1.50 (porosity=30%). [25]

The curves for both C/S ratio preparations are similar in that they both display two maxima. The curves can be separated into 4 stages of mass loss that represent different damping

behavior due to the removal of water from various nanostructural locations. In the initial region (stage I) leading up to the first maximum there is a significant increase in internal friction. This is attributed to the removal of adsorbed water corresponding to the plateau at the beginning and interlayer water on further drying. This may increase the flexibility of the layers since interlayer water molecules are considered as restraining the restraining the C-S-H sheets. More energy is therefore dissipated as observed by the increase in tan∂. The descending portion of the curve (stage II) following the first maximum is likely to be a result of the initial cross-linking between the silicate layers and the increase in polymerization. Increase in the interaction of calcium ions with the lamellae can also be responsible. Bridging of the C-S-H sheets and an increase in the number of strong bonds (either Si-O-Si or ≡–Si-O--Ca2+) reduces the damping behavior. Stage III in the curve shows an ascending behavior rising to a second maximum. This increase might be due to the sliding of silicate layers due to their closer proximity to each other as a consequence of the removal of additional interlayer water. The decline in damping (stage IV) after the second maximum is attributed to the removal of the remaining amount of interlayer water and possibly some constitutional water at higher mass losses. A schematic illustrating nanostructural changes to the C-S-H in the various stages as described is shown in Figure 4.12.

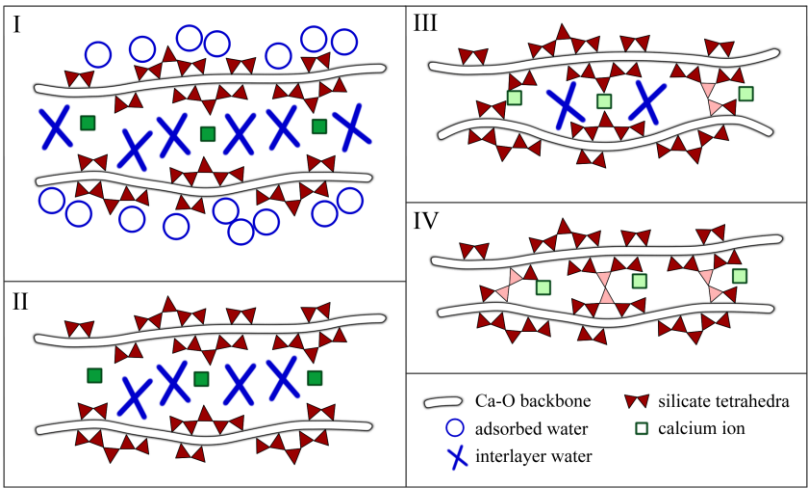

Figure 4.12. Schematic illustrating nanostructural changes to the C-S-H in various stages described in the text. [25]

The E' and tan∂ versus mass loss curves for cement paste (water/cement ratio = 0.40) show similar trends to the curves for C-S-H with C/S= 1.50. The transitions in the E' curve for cement paste are present but they are much more subtle. The C-S-H in cement paste is nearly amorphous and incorporates in its structure elements other than silicon e.g. aluminum. This may reduce the cross-linking potential and interaction of silicate sites in cement paste that are likely contributing mechanisms to stiffness increase. The tan∂-mass loss curve for cement paste (Figure 4.13) contains two distinct maxima and the similarities with curves for synthetic C-S-H (I) (C/S = 1.50) are evident. The maxima for the paste and C-S-H (I) curves respectively are only slightly displaced with respect to mass loss. The similarities in the curves for cement paste and C-S-H (I) add to the many supporting arguments for the layered nature of C-S-H in cement paste.

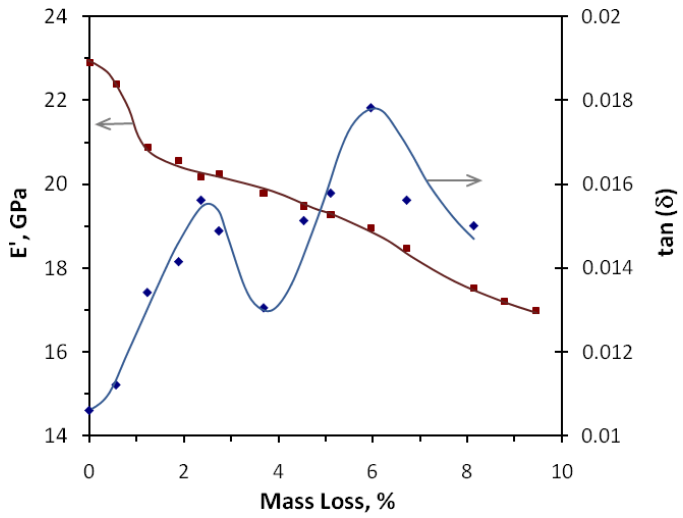

Figure 4.13 E′ and tan δ versus mass-loss curves for cement paste (w/c=0.40). [25]

4.3.5 Stress Relaxation of C-S-H

Relaxation phenomena can be studied by determining the time dependent change in applied load or stress on a sample while maintaining a constant strain or deformation. There are two components of stress relaxation in saturated porous solids [26]. The initially observed component is the hydrodynamic component due to the release of pore water pressure. The second component is the viscoelastic component separated from the first by an inflection point after a few seconds.

Stress relaxation curves obtained in the flexural mode for C-S-H (C/S = 1.50) beam specimens with rectangular cross- section conditioned at 100% relative humidity and 11% relative humidity or lower including the dry state are plotted in Figure 4.14. The vertical axis is the ratio of time dependent stress to the initial stress. Time since application of the initial load is plotted on the x-axis. The saturated specimen experiences a relatively higher relaxation at the initial times. The shape of the curve and the rate of decrease in the stress are different from those obtained at 11%RH and below. This is due to the hydrodynamic component that is active at the initial times. This component ceases after about 20 seconds at which time an inflection occurs in the stress relaxation curve. The remainder of the relaxation is attributed to the viscoelastic component of the C-S-H phase. There is no apparent hydrodynamic component in the curves for C-S-H conditioned at 11%RH and lower due to the absence of pore water at these humidity levels. A dominant viscoelastic response is observed in all these specimens. Some of the relaxation curves however display a subtle concave-up within the first 100 seconds. This may be associated with a small hydrodynamic component other than that related to 'bulk' pore water. This water may exist in entrapped spaces [14]. The drying of specimens conditioned at 11%RH changes the vicoelastic response of the C-S-H generally resulting in lower stress relaxation at initial times. The relaxation for specimens with water content lower than that for 11%RH is less. These samples contain essentially interlayer water. It is therefore suggested that interlayer water has a major role in the time-dependent viscoelastic deformation of the C-S-H. This conclusion is reinforced by relaxation measurements (not shown in Figure 18 on specimens resaturated from the 11% RH condition and dried back to the 11%RH position. The lower interlayer water content corresponds with a lower amount of relaxation suggesting a correlation. The viscoelastic behavior may be indicative of a creep mechanism associated with the sliding of the C-S-H sheets.

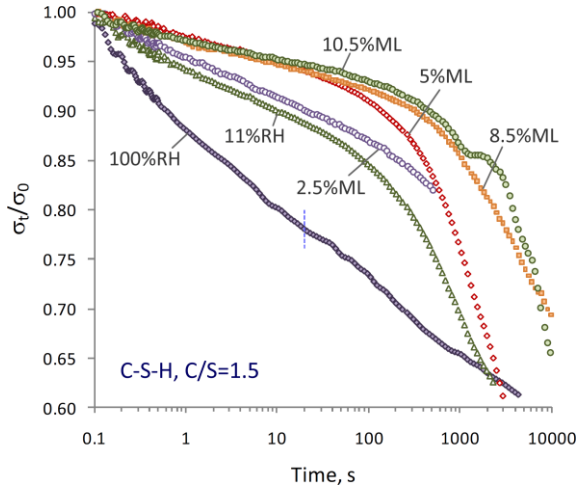

Figure 4.14 Stress relaxation curves for C-S-H samples (C/S=1.50) at various moisture contents. The compacted specimens were prepared from the C-S-H powder conditioned at 11%RH. [18] ML is mass- loss in % from the 11% RH condition.

Extensive work at Princeton has led to solutions for the stress relaxation equations for cement paste in the saturated state [27-29]. The analytical solution for the load as a function of time for a beam with rectangular cross-section can be expressed as:

$$W(t) = W(0)R(t)\Psi_{VE}(t)$$

where: W(0) is the theoretical load at zero time; R(t) is the hydrodynamic function and

$\Psi_{VE}(t)$ is the viscoelastic function.

A viscoelastic function for saturated C-S-H (C/S = 1.50) was computed using the above equation and the Princeton procedure. It was observed that the total viscoelastic relaxation of the saturated specimen is less than the stress relaxation for most of the specimens dried below 11%RH. This suggests that the removal of interlayer water modifies the viscoelatic nature of the C-S-H and results in an increase in the total stress relaxation. An increase in the creep compliance upon drying has been previously reported for Portland cement paste [30]. The viscoelastic component of porous glass appears to be independent of the moisture content on drying below 11%RH [31]. This supports the argument that variations in the viscoelastic properties of C-S-H are attributable to the role of interlayer water. Differences in the surface energy of the C-S-H in the saturated state and the C-S-H conditioned at 11%RH or lower might also contribute to changes in viscoelasticity.

The stress relaxation curves of cement paste (water/cement = 0.40) are plotted in Figure 4.15.The general trend in terms of the order of the curves for the samples in the saturated

state and those conditioned at 11%RH and below are similar to those for the synthetic C-S-H. In general cement paste exhibits a noticeably lower stress relaxation. The relatively well ordered and semi-crystalline structure of synthetic C-S-H may provide more sites (analogous to 'creep' sites) that contribute to stress relaxation. Further the poorly crystalline C-S-H in cement paste can contain substituted aluminum which may be responsible for variations in stress relaxation upon drying that differ from those of synthetic C-S-H. It is noted that there is a considerable stress relaxation in dry cement paste and C-S-H samples after the removal of the final increments of water. This implies that even the completely dry solid structure of the C-S-H undergoes time-dependent deformations under load. This is contradictory to some research that suggests that there is no creep behavior in cement paste if the evaporable water is removed [32].

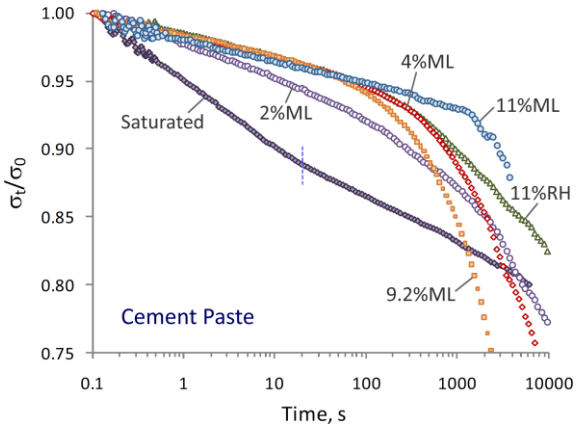

Figure 4.15. Stress relaxation curves for Portland cement paste (w/c=0.40) at various moisture contents obtained by drying from the 11%RH condition. Ref.69. ML is mass-loss in % from the 11% RH condition.

It appears that the similarity in relaxation behavior of cement paste and synthetic C-S-H provides additional validation for the argument that hydrated Portland cement behaves like a layered material.

4.3.6 Colloidal-based Particle Model (P-B) and Layered Silicate Model (F-S)-A Polemic

A brief discussion of the limitations of the colloidal-based model (P-B) for hydrated cement paste is presented here. The thermodynamic equations used to describe the behavior of the system were generally those derived for dilute solutions, e.g. the well-known osmotic pressure equation ($\Delta P = (RT/V) \ln p1/p2$). This approach is not applicable for the 'surface phase' which includes the perturbed layers of solid and the adsorbed water. The use of 'solution- phase' thermodynamics is based on the following assumptions: adsorbed water is a homogeneous phase; a fairly dilute solution; bulk properties-i.e. no interfacial or surface effects.

There are several areas of experimental evidence that cannot be adequately explained by the P-B model. These are: the variation of modulus of elasticity with relative humidity; the variation of flexural strength with relative humidity; the complete irreversibility of the sorption and length change scanning isotherms (see previous discussion of F-S model); differences between the surface area and porosity values determined using nitrogen/or methanol adsorbates and water; Nuclear Magnetic Resonance evidence [33] indicating the presence of primarily interlayer water with only a small amount of adsorbed water.

The correct application of thermodynamics (i.e. to the separated 'reversible' and 'irreversible' isotherms has shown that less than 20% of the total expansion of hydrated cement is due to physical adsorption. This water obeys the Gibbs-Bangham equations that results in a realistic estimate of the modulus of elasticity value for the solid material. The bulk of the expansion is due to irreversible interlayer rehydration. It is also apparent that a re-assessment of creep phenomena would be warranted.

Further discussion of the validity of applying the concept of 'disjoining pressure' to explain volume change behavior in the adsorption region is useful. It is very difficult to reconcile with the basic parameters governing physical adsorption. Consider the following argument. The adsorbed film is in a state of compression, normal to the surface. There is also a two dimensional spreading pressure tangential to the surface. Some rupture of the solid may take place due to the tangential spreading pressure force or by a shear force created by an isotropic expansion of the 'crystallites' or a decrease of their surface free energy. The movement of the solid will, however, involve other terms in the equation for the total free energy (i.e. $dG_{\text{surface phase}} = VdP - SdT - Sd\gamma + \mu 1 dn1 + \mu 2 dn2$). The terms $\mu 1$ and $\mu 2$ are the chemical

potentials of the adsorbate and adsorbent respectively. Also n1 and n2 are the molar quantities of the adsorbate and adsorbent respectively. The other terms are as previously defined. The Gibbs-Bangham equation fully account for the 'reversible' length change using a valid application of thermodynamic principles without the necessity of invoking the abstract concept of 'disjoining pressure'. It is noted here that, for example, the swelling of clays can involve the intercalation of several layers of water into the interlayer regions. This occurs at relatively high humidities and has been referred to as a form of disjoining pressure. This is distinct from the low humidity 'hindered' adsorption effect (adsorption region of the isotherm) described by the P-B model as synonymous to 'disjoining pressure'.

Additional evidence against the 'disjoining pressure' concept includes the following arguments:

- the relative constancy of modulus of elasticity up to about 50% RH followed by a continuous and significant increase to saturation. This is unlike cellulosic and other materials that show a decrease in modulus value due to attenuation of hydrogen bonds by the water molecules.
- there is no correlation with strength change and the amount adsorbed as there is for cellulosic materials.
- the length change due to physically adsorbed water is less than 20% of the total. Only 15% of the total water (D-dried as reference) at 30% RH (dried from saturation) is physically adsorbed

4.4 Model of Daimon and Co-workers

This model is based on sorption experiments conducted on fully hydrated C_3S pastes [14]. Two types of specimens were studied. One type was untreated and the other had the calcium hydroxide extracted. The isotherms for both types were completely irreversible exhibiting large primary and secondary hysteresis. The adsorption branch of the isotherm (following first drying) was considered to represent the true pore structure. It is suggested that adsorption is hindered by the presence of calcium hydroxide as its extraction from the paste results in a significant increase in the volume of small pores. A graphic of the model is presented in Figure 4.16. It is very similar to the F-S model with some minor distinctions. It is suggested that there are two kinds of pores-a wider intergel pore and a smaller intragel pore. The wider

pores are said to be observable in the inner C-S-H product by scanning electron microscopy and the smaller pores not. The model further classifies intragel pores as intercrystallite and intracrystallite. The intercrystallite pore type is similar to that reported by Brunauer et. al. [34]. The intracrystallite pore corresponds to the poorly ordered interlayer space in the F-S model [9].

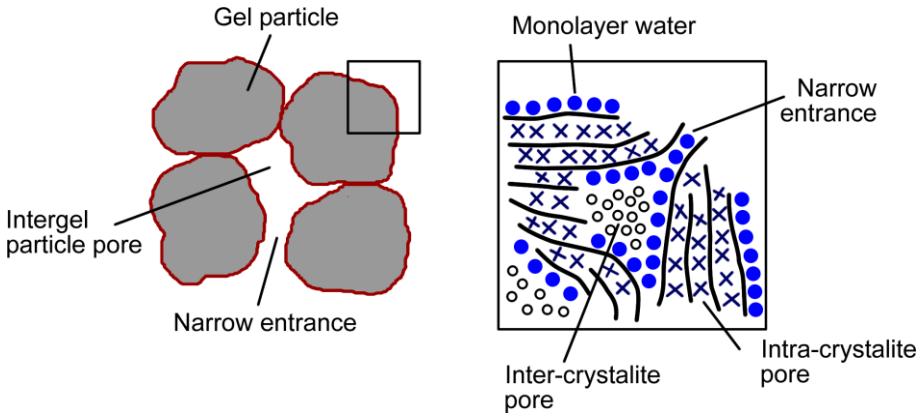

Figure 4.16 A simplified pore model for C-S-H gel after Daimon et. al. [14]

There are some difficulties with the conclusion that it is valid to use the adsorption branch of the isotherm for surface area calculations. The isotherm is not reversible at any value of partial pressure indicating that processes other than adsorption are simultaneously taking place. This invalidates the use of water as an adsorbate in the B.E.T. surface area calculation as has been extensively discussed in the previous section on the F-S-model. There is some evidence based on helium-inflow methods for the existence of 'trapped' space between aggregates of C-S-H layers in cement paste when the water/cement ratio < 0.38 [26]. There is a significant increase in the time-dependent inflow at the 11%RH condition in these pastes. The inflow, then, is apparently not due to the removal of interlayer water as the layers are essentially full at 11%RH. Rather helium enters into the 'trapped' space or space similar to the intercrystallite pores described by Daimon et. al. The inflow would be controlled by narrow entrances. The 'trapped' spaces are not 'gel' pores as described in the P-B model.

They are likely spaces created by the poorly aligned C-S-H layers that agglomerate and are deposited in confined space during the hydration process.

4.5 Jennings (J) Model

A colloidal model for the nanostructure of hydrated cement paste was proposed by Jennings [35] in 2000 and has been referred to as CM-I. This was later refined in 2008 [36] and referred to as CM-II. The model is essentially a hybrid incorporating features of the F-S layered model and the colloidal P-B model. The input data for the computations at the core of the J-model is largely based on the publications of Feldman [13, 16, 37, 38] that relate to a detailed assessment of the completely irreversible water sorption isotherm and the nanostructural implications of the helium inflow experiments. The J-model is used to provide explanations for certain aspects of the physical and chemical behavior of cement paste and relies heavily on 'granular' behavior analogies. The focus in this chapter will be on the refined model as this is the most recent colloidal-based model at the time of writing. The primary features of the model (CM-II) will be described. This will be followed by a discussion of the main tenets of the model. Alternate points of view and critical commentary is integrated into the discussion.

The C-S-H is modeled as a network of prismatic-shaped aggregates or particles referred to as 'globules' for consistency with the original model (CM-I). A schematic of the model is illustrated in Figure 4.17. The particles have a least dimension of about 5 nm and the other dimensions vary from 30-60nm.The particles are depicted as having outer surface and internal porosity as well as interlayer space. The model utilizes three types of pores: pores within the 'globule' referred to as intraglobular pores (IGP);small gel pores (SGP) (1-3 nm in diameter) trapped between the globules that are percolated to the outer regions; large gel pores (LGP) (3-12 nm in diameter) or space created as a result of the overlap of globular flocs. Clusters of 'globules' pack together in two packing densities termed high density (HD) C-S-H and low density C-S-H (LD) C-S-H. The C-S-H, itself, is considered intrinsically similar, the difference due solely to the porosity as a result of the packing arrangement.

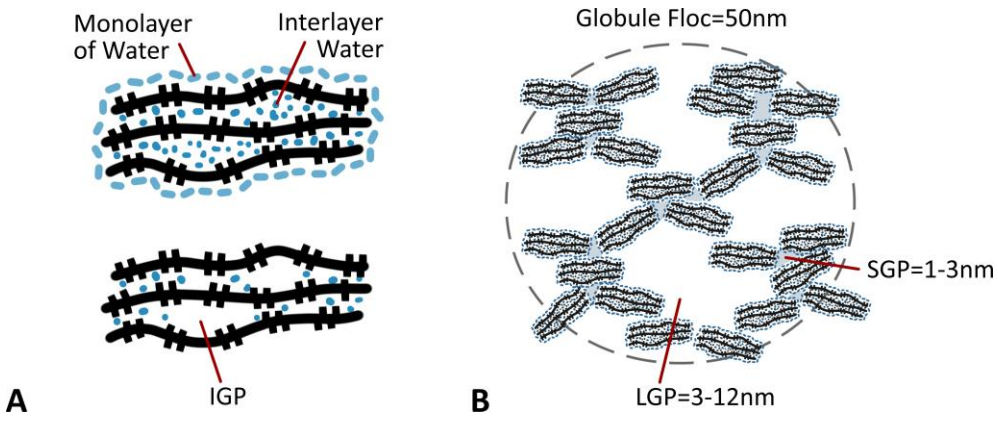

Figure 4.17 A schematic of the Jennings model for C-S-H. A: A D-dried globule and a rewet globule depicting a layered structure and empty/full intraglobular pores (IGP). B: A globule floc depicting small gel pores outside of the globule and large gel pores (LGP). [36]

There are a number of difficulties with the J-model. Some of these are discussed as follows. The issue of correct density values for C-S-H is important. Jennings cites a value of 2.604 gcm^{-3} for saturated 'globules' based on small angle neutron scattering (SANS) measurements [39]. Earlier work by Powers and Brownyard cited density values of 2.60 g/cm^3 for D-dried cement paste when lime-saturated water was used as a displacement fluid [40]. This is similar to the density of quartz (2.60- 2.65 g/cm^3). This value would likely represent the density of the silicate sheets (including the Ca-O backbone) themselves as the water enters the space between the layers and thus the volume occupied by interlayer water would not be considered as part of the solid. This is also the case for the density value of 2.85 g/cm^3 reported by Brunauer and Greenberg [41]. Density values of D-dried hydrated cement pastes determined using helium and methanol as displacement fluids (Feldman, [42]) were about 2.20-2.30g/cm^3. Heller and Taylor [43] reported values of 2.00-2.20g/cm^3 for semi-crystalline C-S-H (I) obtained by calculation using crystallographic data. Cement paste density values determined at the 11%RH condition using helium, water, or methanol as displacement fluids had values of about 2.30-2.40g/cm^3 for all fluids. A value of 2.18 g/cm^3 was obtained for hydrated C_3S from which calcium hydroxide had been depleted i.e. essentially for C-S-H [44]. A density value of phase pure C-S-H (I) (2.40 g/cm^3, C/S= 0.80) was determined experimentally by the writers using helium pycnometry. Density values reported to be 2.35

and 2.45 g/cm^3 for C-S-H were also obtained by atomistic modeling using Monte Carlo algorithms and geometrical calculi for the saturated and dry state, respectively. Further, Richardson [45] has corrected the unit cell for C-S-H (the 'a' parameter was twice the correct value) reported by Pellenq [46] and obtained a value of 2.33 g/cm^3. This density is significantly lower than the estimate based on neutron scattering experiments. The SANS value of 2.60 g/cm^3 was incorrectly considered as a validation of their atomistic numerical model by Pellenq and co-workers.

Changes in density of the C-S-H on first-drying from 11%RH and adsorption back to 11%RH are explained by the J-model as follows. Water, on drying, is removed from the interlayer space and the surface both of which act to increase the density. Removal of water from the IGP spaces with 'fixed' boundaries has the effect of decreasing density values, the net effect of removal of water from all three locations being a density increase. The assertion that both the volume and mass change from the first two locations are the same amount on drying is erroneous. For example, the separation of the length-change isotherm into 'reversible' and 'irreversible' components indicates that the 'reversible' length-change on drying is < 0.01% whereas the 'irreversible' length-change > 0.35%. The separation itself is 'model-less'. The 'reversible' isotherm, however, is by definition attributed to surface adsorption as the latter is a thermodynamically reversible process. It is clear then that there are significant differences in the magnitude of volume change due to the removal of adsorbed water and interlayer water. The assumption that the IGP boundaries are fixed is unlikely as the structural collapse of the layers on drying would bring the surfaces closer together. Water in the IGP, if present, would appear to be under a similar force field as the interlayer water. It is also concluded on the basis of similar density values estimated after resorption to 11% RH that water does not re-enter the layers of the C-S-H at this humidity but rather resides on the surface and in the IGP. This explanation is untenable as given the location of the IGP, water in the J-model would have to enter the interlayer in order to reach the IGP sites. Further, the scanning loops emanating from the adsorption branch, in the water mass-change isotherm indicate that there is significant irreversibility at very low humidity levels. This irreversibility can be readily explained by the entry and exit of interlayer water on adsorption even at humidities <11%RH. The increase in density on first drying is due to the removal of interlayer water. The sharp decrease is due to the collapse of layers not allowing helium to

enter fully in 40 hours. The increase in density on rewetting then can only be explained by water returning to the interlayer structure without an equivalent re-expansion. The density increase at higher humidities is due to the large volume increase because of the swelling of the layers as more water is associated with the structure.

The arguments advanced for the J-model based on thermodynamics for reasons discussed in the previous discussion of the F-S model are invalid. The rationale for surface area contributions including surfaces of the IGP spaces is based on water adsorption calculations. These are untenable due to the irreversible nature of the isotherms. B.E.T surface area calculations require data representing reversible adsorption processes. In addition, helium inflow into the cement paste nanostructure with the exception of low water/cement ratio pastes reaches equilibrium in 40 hours. Helium penetrates all the available space. Density values accounting for interlayer space detected by helium are consistent with values for C-S-H based on X-ray crystallographic determinations [42] i.e. 2.20-2.40. Helium gas can flow into nanospaces <1nm in size instantaneously [16]. Density values of, for example, porous vycor glass (mean pore size <3nm) determined using helium pycnometry agree with standard values .This calls into question the existence of IGP spaces. A value for the density of water of about 2.0g/cm^3 is estimated using the J-model as only the outside surface water is considered to change the measured volume. Feldman's estimate of 1.20± 0.08 g/cm-3 for the density of interlayer water (based on the F-S model) is more realistic and consistent with water densities for interlayer water in clay systems [17]. The J-model provides estimates of water density of about 1.20 g/cm-3 in the region of the isotherm between 11-40% RH. This region is the flattest part of the isotherm and it would be expected that the bulk of the interlayer water would have previously entered the system at humidities < 11%RH. The density value for the water in this region is accurate and reflects the incremental amount of interlayer water that has intercalated between the C-S-H layers.

The packing of 'globules' into different arrangements appears to be a useful concept. It allows properties to vary without changing the globular structure. In this respect it is compatible with the F-S model where aggregates of layers can 'pack' into connected arrays. The constancy of water surface area is however an issue. The calculation itself is 'model-less' and meaningless as indicated in the previous discussions. Since the water isotherm is totally irreversible a B.E.T. surface area calculation is invalid.

The J-model postulates the existence of small gel porosity (SGP) trapped between 'globules' and percolated to the outside surfaces. This is compatible with the F-S model for paste at low porosity (low water/cement ratio) and the Daimon model. These type of pores have been detected by helium inflow experiments as described previously.

The J-model assigns irreversible shrinkage to drying from 100-50% RH. It appears then that these are ascribed mainly to capillary effects. The F-S model attributes these effects primarily to the region of humidity < 11%RH. The latter is based on the observation that the 'irreversible' length change accounts for about 80% of the length change ,most of which occurs below 11%RH. Further the length-change isotherm is completely irreversible exhibiting large primary and secondary hysteresis. This is contrary to the assertion based on the J-model that drying is mostly reversible below 50% RH. The J-model argues that irreversible shrinkage involves a 'pushing' of the globule flocs closer together through the action of meniscus effects i.e. compressive stress on the solid. This is consistent with some aspects of a layered model (F-S) and correlates with an increased degree of polymerization of the silicates and the observed reductions in surface area.

In an attempt to assess length-change below 40% RH Jennings applied the Bangham equations using Eglobule = 60GPa [36] and a surface area value of $70m^2/g$. Length change was far lower than that observed. The values for Eglobule and surface area are reasonable. The difficulty is that the equations must be applied to the 'reversible' portion of the isotherm and not the 'total' water isotherm for reasons discussed previously. Jennings argues that the large shrinkages of 1% or more that have been measured directly for small regions of C-S-H using microscopic techniques [36] was the motivation for the development of a colloidal model and suggests that the shrinkage at low RH's is due to the removal of interlayer water. It would appear that on this basis the F-S model is more appropriate. Large local deformations, then, can easily be rationalized by a layered model as opposed to a 'globular' model.

Jennings rationalizes the creep process as beginning when the SGP are full and increases as the LGPs fill at higher humidities. In the J-model creep involves reorientation of the globules producing denser local packing and perhaps reducing the surface area. This argument would appear to be wanting as creep of cement paste has been shown to occur in the 'dry' state. Further, relaxation experiments performed on pure C-S-H, have shown that at any given

equilibrium condition with respect to moisture content the basal spacing does not change when the specimens are subjected to a sustained load. The predominating mechanism, then, would appear to be one that involves 'sliding of C-S-H sheets. A reorientation of aggregates of 'sheets' is possible but it is likely a minor contributor to the process.

Aging is associated with volume change/collapse of the LGP in the J-model. The globules deform as water is removed and reenters the interlayer spaces. It is argued that there are several ways of rearranging the globules to collapse the LGP. The process of pulling water out of the LGP causes them to collapse with the greatest effect occurring while the meniscus is outside the gel. It is suggested here that aging as described by the F-S model is more consistent with experimental observations [47]. In the F-S model aging is ascribed to the creation of new interlayer space as the silicate sheets translate and layer surfaces approach each other under sustained stress. Examination of the 'irreversible' water isotherm indicates that length-change on drying from the saturated state is insignificant until humidities below 11%RH are reached where shrinkage can exceed 0.20%.This clearly indicates that the role of menisci in this regard is not likely a factor. The meniscus effect on 'reversible' desorption is greater. However the effect is small as the total 'reversible shrinkage' at humidities above 40%RH (where the meniscus ruptures) is about 0.05%.

Slow diffusion of water on drying is attributed to the desorption of hindered or load-bearing water (J-model) that is accompanied by rearrangement of the globules. The arguments contravening the necessity of introducing this concept have been presented previously in the discussion related to disjoining pressure.

Jennings argues that the reduction in surface energy as surfaces come into close proximity is probably the driving force for natural aging. This is attributed to a measurable decrease in the LGP and a possible rearrangement of the SGP. The F-S model attributes the reduction in surface energy to layered surfaces coming closer together resulting in an increase in the amount of interlayer space. An increase in solid volume on drying as measured by helium pycnometry supports this view [47].

4.6 Taylor's Model- A Composition-Based Nanostructural Model

Taylor suggested that the C-S-H consisted of layers containing elements of both 1.4 nm tobermorite (T-type) and jennite (J-type) structure [48]. It was further suggested that these elements could reside in individual layers in conformance with poorly defined regions containing highly disordered material including small amounts of monomeric silicate ions. A schematic of a silicate chain representing 1.4 nm tobermorite and jennite is illustrated in Figure 4.18.

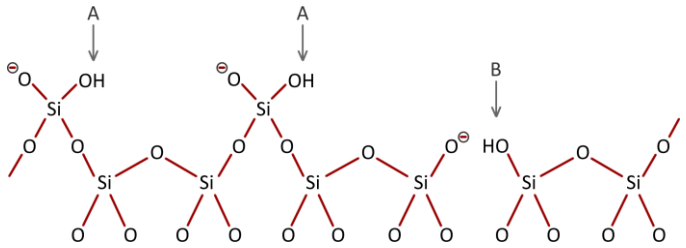

Figure 4.18 A schematic of a silicate chain of the type present in jennite and 1.4 nm tobermorite showing the probable positions of the H atoms marked A and suggested modification at B by the omission of a bridging tetrahedron.

It is instructive to examine the plot of the calculated Ca/Si ratio versus chain length for 1.4 nm tobermorite and jennite (Figure 4.19). Taylor assumed that each bridging tetrahedron and one of the two end group tetrahedra are associated with one H atom. The average C/S ratio in cement paste is about 1.75. This can be obtained by the presence of a mixture of T-type and J-type structures, both with dimeric anions or a single element J-type structure with a mean chain length of 5 tetrahedra. In the T-type structure the main layer consists of a central Ca-O part sandwiched between parallel silicate chains. In the J-type structure –OH groups contain half the oxygen atoms of the central component.

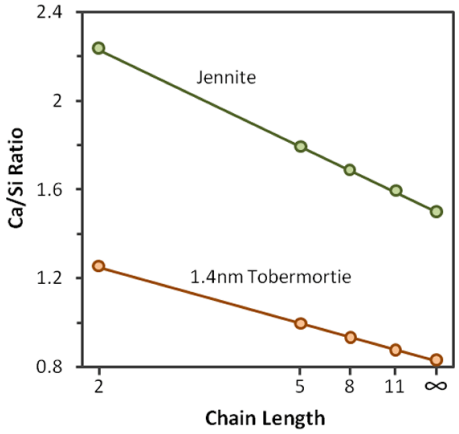

Figure 4.19 The calculated Ca/Si ratio plotted against a function of chain length for jennite and 1.4nm tobermorite structures modified by the omission of bridging tetrahedra. [48]

Observed temporal changes in ion distribution are compatible with an initial formation of the former followed by a gradual transition to the latter-a change towards a more highly ordered structure. The changes in distribution of local Ca/Si ratio reported by Richardson and Groves can be explained [49]. The early age distribution ranges from 1.2-2.3, the lower value approximating the C/S ratio of the tobermorite structure and the upper value that of jennite. At later ages there is a narrowing of the distribution and a tendency toward a higher value with a mean value of 1.75 consistent with a jennite structure. In Taylor's model the Ca/Si ratio can be raised above 0.83 by removal of some of the bridging tetrahedra with replacement by interlayer Ca^{2+} ions. The Ca-O cores of the layers then conform to the J-type structure. The silicate ions and OH- groups are then located in an ordered arrangement.

4.7 Richardson and Groves (R-G) Model

The R-G model is arguably the most comprehensive compositional model for C-S-H currently available [50-52]. A summary of the principal features of this model will be presented here. The reader is referred to the original sources for a detailed analysis of its basic tenets. Tobermorite-'solid-solution' calcium hydroxide (T/CH) and tobermorite-jennite (T/J) nanostructures are rationalized for a diverse range of cement systems. The most suitable combination of nanostructures is dependent on the nature of the cement system.

A brief description of the composition of the T/CH nanostructure follows. Richardson and Groves argue that the calcium silicate hydrate is composed of isolated variable length silicate

chains with a variable number of –OH groups attached to Si atoms in 'solid- solution' with varying amounts of calcium hydroxide. They proposed a general formula [39]:

$$Ca_XH_{2(N+1-X)}Si_NO_{(3N+1)}.zCa(OH)_2.mH_2O$$

where: N is the mean silicate chain length;

X is the number of Ca^{2+} ions required for charge balance of the silicate chains;

2(N+1-X) is the number of hydroxyl units attached to the chains;

z is the number of $Ca(OH)_2$ units in 'solid-solution';

m is the number of bound water molecules excluding those present as hydroxyl groups.

An alternate formulation accounting for the experimentally observed sequence of chain lengths i.e., 3n-1 where n is an integer (1,2,3,…n) was also reported:

$$[Ca2nHwSi(3n-1)O(9n-2)] . (OH)w+n(y-2).Ca(n.y)/2.mH2O$$

where: w is the number of silanol groups;

w/n is the degree of protonation of the silicate chains.

Layer structure and neutrality require the following limiting values:

$0 \leq y \leq 2$, $n(2-y) \leq w \leq 2n$

$2 \leq y \leq 4$, $0 \leq w \leq 2n$

$4 \leq y \leq 6$, $0 \leq w \leq n(6-y)$

and $X=1/2\ (6n-w)$

$z=1/2\ (w+n(y-2))$

The formula in square brackets represents the tobermorite-like core. It is comprised of a highly disordered layer structure consisting of silicate chains of mean length, 3n-1. Dimers (n=1) are linked during polymerization by bridging tetrahedral to form pentamers (n=2) and polymers of higher degree. The main layer calcium ions are indicated as $2nCa^{2+}$ within the square brackets. The interlayer Ca^{2+} ions required for charge-balance are denoted as

n-(w/2) of the (n.y)/2Ca^{2+} ions outside the square brackets. The remainder of the (n.y)/2Ca^{2+} ions in the T/CH nanostructure occupy positions in layers of C-H sandwiched between silicate layers of tobermorite-like structure. These ions, in the T/J nanostructure form part of the main layer of jennite-based structural units (Si-O-Ca-OH). Local compositional variations are due to regional variation of the structural units of C-S-H.

Schematics showing varying degrees of protonation of the silicate chains in tobermorite-based and jennite-based dimers are shown in Figure 4.20 (A, B and C).

The T structures in the R-G model are a derivative of the dreierkette structure of 1.4 nm tobermorite. Structural modifications that can account for changes in the Ca/Si ratio greater or less than 0.83 include: (i) an omission of bridging tetrahedra resulting in an increase in the chain length and an increase in the Ca/Si ratio, (ii) an increase in the content of Ca^{2+} ions balanced by a reduction in Si-OH groups i.e a decrease in the level of protonation of the silicate chains resulting in an increase in the Ca/Si ratio, (iii) a decrease in the content of Ca^{2+} ions balanced by an increase in Si-OH groups i.e. an increase in the extent of protonation resulting in a decrease in Ca/Si ratio, (iv) additional calcium ions balanced by OH ions resulting in an increase in Ca/Si ratio-the difference between the T and J-based structural units. Modifications (i), (ii) and (iii) also apply to J-based structures.

Alternatively changes to Ca/Si ratio of T/CH structures involve the incorporation of layers of CH.

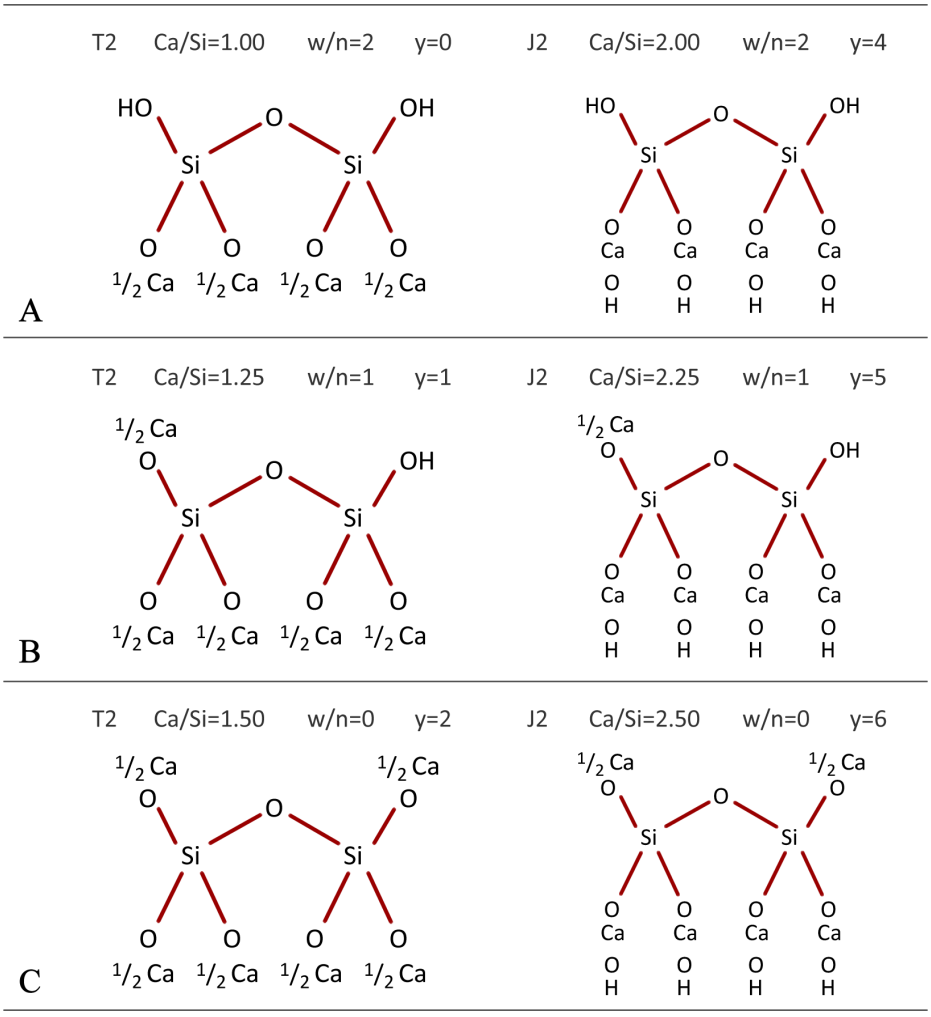

Figure 4.20 Schematics of Tobermorite-based (T2) and Jennite-based (J2) dimers showing maximum (A), intermediate (B) and minimum (C) degrees of protonation; values of the variables in the R-G model are indicated. [53]

The R-G model was modified to account for substituents in the C-S-H structure [39]. It is described by the formula:

$[Ca_2nHwSi1\text{-}aRa)(3n\text{-}1)O(9n\text{-}2)]\ \ Ic+a/c(3n\text{-}1)\ .\ (OH)w+n(y\text{-}2).Ca(n.y)/2.Can.y\ .mH_2O$

where: R is a trivalent cation, e.g. Al^{3+};

Ic+is a monovalent cation or Ca^{2+} acting to correct the charge imbalance resulting

from the substitution of S^{4+} by R^{3+}.

Al substitutes for Si at sites within the bridging tetrahedra (see schematic in Figure 4.21 the value of 'a' corresponding to the n-1 bridging sites is, $0 \leq a \leq (n-1)/(3n-1)$.

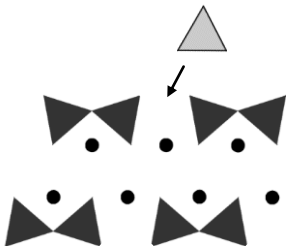

Figure 4.21 Schematic of a pentameric silicate chain with Al substituted for Si in the bridging site: circles:Ca; dark grey triangles: silica tetrahedra; light grey triangles: alumina tetrahedra.

The R-G model enabled a number of conclusions to be drawn regarding the nanostructure of several hydrated silicates originating from C_3S, Portland cement (PC) or PC blends containing activated synthetic slag glass. These are as follows:

(1) The C-S-H in PC pastes can be modeled as essentially a T/J-type nanostructure. Polymerization processes occurring at later ages in J-type units (and not T-type) can explain the tendency toward a unimodal distribution of Ca/Si ratio. The bimodal distribution of Ca/Si ratio observed at early ages can be accounted for with a nanostructure composed of T/J structural units. The large amount of dimer remaining at advanced ages can be rationalized on this basis. It is emphasized that the presence of some T-type units is required to accommodate tetrahedral Al^{3+}.

(2) The nanostructure of hydrated PC-slag pastes is comprised entirely of T-type units involving a relatively low degree of protonation of the silicate chains.

(3) The nanostructure of KOH-activated PC-slag pastes is likely comprised of T/CH structural units. This is similar to the nanostructure of KOH activated PC-metakaolin paste. The latter cannot be described in terms of a T/J-based nanostructure.

(4) The nanostructure of hydrated KOH-activated synthetic slag glass is entirely based on T-type units with varying degrees of protonation of the silicate chains.

(5) The nanostructure of hydrated blends of PC and colloidal silica is entirely T-type.

(6) The nanostructure of C-S-H in small alite grains is essentially composed of dimeric T-type material. It is suggested that the properties of this C-S-H can be substantially than that formed elsewhere in a paste. It is postulated that significant edge effects can occur due to the small size of the particles of C-S-H.

It is emphasized that there are several models for C-S-H nanostructure in the literature not described here to which the reader can refer [54-56].The models described in this chapter were selected to elucidate the approaches used to modify C-S-H nanostructure that will be introduced in the following chapters.

References

1. Powers T. C. and Brownyard T. L. (1946). Studies of the physical properties of hardened Portland cement paste. Part 3. Theoretical interpretation of adsorption data, J. Am. Concr. Inst. Proc. Vol. 43, pp. 469-504.
2. Powers T. C. (1960). Physical properties of cement paste, Proc. 4th Int. Symp. Chem. Cem., Washington D.C., Monograph 43, Vol. II, Session V, Paper V-1, pp.577-609.
3. Diamond S. (1976). Cement paste microstructure-An overview at several levels, Proc. of Conf. on Hydraulic Cement Pastes: Their Structure and Properties, University of Sheffield, Session I, pp. 2-30.
4. Diamond S. (2004).The microstructure of cement paste and concrete-A visual primer, Cem. Concr. Comp., 26(8), pp.919-933.
5. Diamond S. and Bonen D. (1993). Microstructure of hardened cement paste- A new interpretation, J. Am. Ceram. Soc., 76(12), pp. 2993-2999.
6. Goto S., Daimon M., Hosaka G. and Kondo R. (1976). Composition and morphology of hydrated tricalcium silicate, J. Am. Ceram. Soc., 59(7-8), pp.281-284.
7. Taylor H. F. W. (1997). Hydration of calcium silicate phases, Chapter 5 in Cement Chemistry, Thomas Telford, London, pp.113-156.
8. Feldman R. F. and Sereda P.J. (1970). A new model for hydrated Portland cement and its practical implications, Eng. Journal, 53(8-9), pp. 53-59.
9. Feldman R. F. and Sereda P.J. (1969). A model for hydrated Portland cement paste as deduced from sorption-length change and mechanical properties, Matls and Struct., 1(6), pp.509-520.
10. Feldman R. F. (1972). Assessment of experimental evidence for models of hydrated Portland cement, Highway Res. Rec., No. 370, pp. 8-24.
11. Feldman R. F. (1970). Sorption and length-change scanning isotherms of methanol and water on hydrated Portland cement, Proc. 5th Int. Symp. Chem. Cem., Tokyo, Vol.III, pp.53-66.
12. Ramachandran V. S., Feldman R. F., Beaudoin J. J., Concrete Science, Heyden, 1981.

13. Feldman R. F. (1972). Assessment of experimental evidence for models of hydrated Portland cement, Highway Res. Rec., No. 370, pp. 8-24.
14. Daimon M., Abo-El-Enein S. A., Hosaka G., Goto S. and Kondo R. (1976). Pore structure of calcium silicate hydrate in hydrated tricalcium silicate, J. Am. Ceram. Soc., 60(3-4), pp. 110-114.
15. Helmuth R. A. (1965). Dimensional changes and water adsorption of hydrated Portland cement and tricalcium silicate, MSc. Thesis, Illinois Institute of Technology, 64p.
16. Feldman R. F. (1971). The flow of helium into the interlayer spaces of hydrated cement paste, Cem. Concr. Res., 1(3), pp. 285-300.
17. Martin R. T. (1962). Adsorbed water on clay: A review. Proc. 9th Nat. Conf. Clay and Clay Min. Ed. A. Swineford, Pergamon Press, New York, p28.
18. Brunauer S. (1943). The adsorption of gases and vapors, Princeton University Press, pp. 420.
19. Alizadeh R., Beaudoin J. and Raki L. (2007). C-S-H (I)-A nanostructural model for the removal of water from hydrated cement paste, J. Am. Ceram. Soc., 90(2), pp.670-672.
20. Young J. F. (1988). Investigations of calcium silicate hydrate structure using silicon-29 nuclear magnetic resonance spectroscopy, J. Am. Ceram. Soc., 71(3), pp. 118-120.
21. Yu P. and Kirkpatrick R. J. (1999). Thermal dehydration of tobermorite and jennite, Concr. Sci. and Eng., 1(3), pp. 185-191.
22. Sato H. and Grutzeck M. (1992). Effect of starting materials on the synthesis of tobermorite, Proc., Mat. Res. Soc. Symp., Vol 45, pp. 235-240.
23. Van Damme H. and Gmira A. (2006). Cement hydrates, Chapter 13.3 in Handbook of Clay Science, Ed. Bergaya F., Thang B.K.G. and Lagaly G., Elsevier (Oxford) pp. 1113-1128.
24. Pellenq R. J.-M., Lequeux N., vanDamme H. (2008), Engineering the bonding scheme in C-S-H: The iono-covalent framework, Cem. Concr. Res., 38(2),pp. 159-174.
25. Alizadeh R., Beaudoin J. J. and Raki L., Mechanical properties of calcium silicate hydrates, *Matls and Struct.*, 44, 13-28, 2011.
26. Vichit-Vadakan W. and Scherer G. W. (2003). Measuring permeability and stress relaxation of young cement paste by beam bending, Cem. Concr. Res., 33(12), pp.1925-1932.
27. Beaudoin J. and Alizadeh R. (2007). Detection of nanostructural anomalies in hydrated cement systems, Cem. Concr. Comp., 29(2), pp.63-69.
28. Vichit-Vadakan W. and Scherer G.W. (2002). Measuring permeability of rigid materials by a beam bending method: III Cement paste. J. Am. Ceram. Soc., 85(6), pp. 1537-1544.
29. Valenza II J. and Scherer G. W. (2004). Measuring permeability of rigid beams by the beam-bending method: V. Isotropic rectangular plates of cement paste, J. Am. Ceram. Soc.,87(10), pp.1927-1931.
30. Tamtsia B. T. and Beaudoin J. (2000). Basic creep of hardened cement paste-A re-examination of the role of water, Cem. Concr. Res., 30(9), pp. 1465-1475.
31. Alizadeh R., Beaudoin J. and Raki L. (2010). Viscoelastic nature of calcium silicate hydrate, Cem. Concr. Comp., 32 (5), pp. 369-375.

32. Glucklich J. and Ishai O. (1962). Creep mechanism in cement mortar, J. Am. Concr. Inst., 59(7), pp. 923-948.
33. Seligman P. (1968). Nuclear magnetic resonance studies of the water in hardened cement paste, J. Res. Dev. Labs Portland Cement Association, 10(1), pp. 52-65.
34. Brunauer S., Skalny J. and Odler I. (1973). Complete pore structure analysis, Proc. Int. Symp.-Pore Structure and Properties of Materials, RILEM/UPAC, Part I-C Academia, Prague, pp3-26.
35. Jennings H. M. (2000). A model for the microstructure of calcium silicate hydrate in cement paste, Cem. Concr. Res., 30(1), pp.101-116.
36. Jennings H. M. (2008). Refinements to colloidal model of C-S-H in cement: CM-II, Cem. Concr. Res., 38(3), pp.275-289.
37. Feldman R. F. (1972). Helium flow and density measurement of the hydrated calcium silicate-water system, Cem. Concr. Res., 2(1), pp. 123-136.
38. Feldman R. F. (1973). Helium flow characteristics of rewetted specimens of dried Portland cement paste, Cem. Concr, Res., 3(6), pp. 777-790.
39. Allen A. J., Thomas J. J. and Jennings H. M. (2007). Composition and density of nanoscale calcium-silicate-hydrate in cement, Nature Materials, 6(4), pp. 311-316.
40. Powers T. C. and Brownyard T. L. (1947). Physical properties of hardened cement paste. Part 5. Studies of hardened cement paste by means of specific volume measurements. J. Am. Conc. Inst. Proc., Vol 43., pp.669-712.
41. Brunauer S. and Greenberg S. (1962). The hydration of tricalcium silicate and β-dicalcium silicate at room temperature, Proc. 4th Int. Symp. Chem. Cem., London, Vol. I, pp. 135-163.
42. Feldman R. F. (1972). Density and porosity studies of hydrated Portland cement, Cement Technology, 3(1), pp. 5-14.
43. Heller L. and Taylor H.F.W. (1956). Crystallographic data for the calcium silicates, HMSO London, 79p.
44. Young J. F. and Hansen W. (1987). Volume relationship for C-S-H formation based on hydration stoichiometry, Proc. Mater. Res. Soc. Symp. Vol. 85, pp. 313-322.
45. Richardson I. (2010). Private communication.
46. Pellenq R.J.-M. et al. (2009). A realistic molecular model of cement hydrates, Proc. Nat. Acad. Sci. USA., 106(38), pp. 16102-16107.
47. Feldman R. F. (1972). Mechanism of creep of hydrated Portland cement paste, Cem. Concr. Res., 2(5), pp.521-540.
48. Taylor H. F. W. (1986). Proposed structure for calcium silicate hydrate gel, J. Am. Ceram. Soc., 69(6), pp. 464-467.
49. Richardson I. G. and Groves G.W. (1993). Microstructure and microanalysis of hardened ordinary Portland cement pastes, J. Mater. Sci., 28(1), pp.265-277.
50. Richardson I. G. and Groves G.W. (1992). Models for the composition and structure of calcium silicate hydrate (C-S-H) gel in hardened tricalcium silicate pastes, *Cem. Concr. Res.*, 22(6), pp.1001-1010.
51. Richardson I. G. (2004). Tobermorite/jennite and tobermorite/calcium hydroxide-based models for the structure of C-S-H: Applicability to hardened pastes of tricalcium silicate, β-dicalcium silicate, Portland cement and blends of Portland cement with blast-furnace slag, metakaolin, or silica fume, *Cem. Concr. Res.*, 34(9), pp. 1733-1777.

52. Richardson I. G. (2008). The calcium silicate hydrates, *Cem. Concr. Res.*, 38(2), pp. 137-158.
53. Richardson I. G., Tobermorite/jennite- and tobermorite/calcium hydroxide-based models for the structure of C-S-H: applicability to hardened pastes of tricalcium silicate, β-dicalcium silicate, Portland cement, and blends of Portland cement with blast-furnace slag, metakaolin, or silica fume, *Cem. Concr. Res.*, 34, 1733-1777, 2004.
54. Kantro D. L., Brunauer S. and Weise C. H. (1962). Development of surface in the hydration of calcium silicates. II. Extension of investigations to earlier and later stages of hydration, *J. Phys. Chem.*, 66(10), pp.1804-1809.
55. Birchall J. D. and Thomas N. L. (1984). The mechanism of retardation of setting of OPC by sugars, *Proc. Brit. Ceram. Soc.*, Vol.35, pp.305-315.
56. Glasser F. P., Lachowski E. E. and Macphee D. E. (1987). Compositional model for calcium silicate hydrate (C-S-H) gels, their solubilities and free energies of formation, *J. Am. Ceram. Soc.*, 70(7), pp.481-485.

Chapter 5

Experimental Techniques Utilized in the Study of Layered Calcium silicates

The experimental techniques utilized in investigation of the chemical, physical and mechanical properties of cement-based materials are now well established [1, 2]. In this chapter, some of the test methods that are used to study the nanostructure of C-S-H and that are of interest to the current research documented in this thesis are described. It is important to mention that, in general, a combination of these techniques is employed in order to strengthen certain conclusions about the structure and behavior of materials since each individual technique is limited in some aspects.

5.1 *X-ray Diffraction*

X-ray diffraction (XRD) is one of the most frequently used methods in cement chemistry. It is generally used for the characterization of crystalline materials and the determination of their chemical composition. The X-ray pattern of each material is a unique "fingerprint". This technique is based on the analysis of the intensity and the angle of diffracted X-ray beam after encountering a plane of atoms in a material.

In a crystalline material, various atoms are located in the structure in a repeating order. This can produce similar atomic planes as shown in Figure 5.1. The distance between these planes is called the d-spacing. X-ray beams are diffracted partially when they hit various parallel layers. The diffracted beams can be detected decently if they are in phase. This is occurs according to Bragg's law:

$n \lambda = 2 d \sin\theta$

where λ is the wavelength of the X-ray (~0.15 nm for the Cu source), d is the distance between the atomic planes, θ is the angle of incidence and n is an integer.

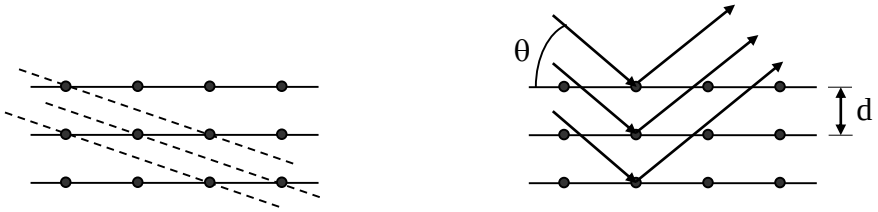

(a) **(b)**

Figure 5.1. (a) Two possible atomic planes in a crystalline structure. (b) Diffraction of X-rays expressed by Bragg's law.

In an XRD instrument that has the Bragg-Brentano geometry, the X-ray tube rotates around the sample so that the beams are emitted typically at angles from 2 to 30 degrees. Since the detector rotates at the same angle to receive the diffracted beams, only the atomic planes parallel to the surface of the sample are detected. The intensity of the X-rays is plotted versus the 2θ (the angle between the emitted and diffracted beam).

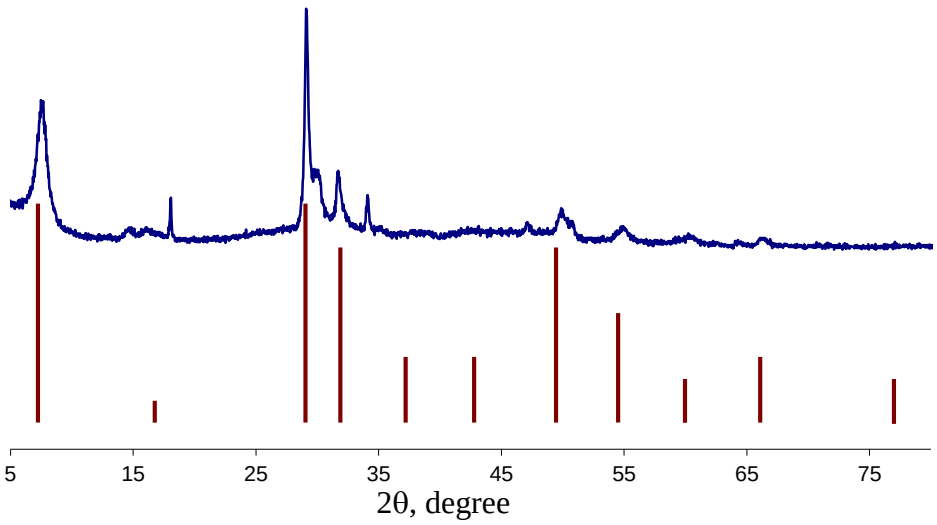

Figure 5.2. The X-ray diffraction pattern for C-S-H (C/S=1.5 on top) compared to the reference data for Calcium Silicate Hydrate (ICDD data No. 34-0002 on the bottom).

This spectrum is then compared to known reflections in the database in order to identify the compounds in the sample. The XRD pattern of C-S-H (C/S = 1.5) is shown in Figure 5.2 and compared to that from the ICDD database (data No. 34-0002). The peaks that are not matched at all are from the calcium hydroxide (data No. 04-0733).

5.2 Thermal Methods

Chemical materials are usually decomposed or may experience a phase transition upon heating to high temperatures. Water, for example, is evaporated at about 100 ºC. Calcium hydroxide is decomposed to CaO and H_2O at about 400 ºC. It is possible to measure the decrease in the weight during these transformations as well the heat adsorbed (if the change is endothermic) or generated (when the change is exothermic). These measurements are called thermogravimetric analysis (TGA) and differential thermal analysis (DTA), respectively. Differential weight change measurements can be used to estimate the amount

of each chemical compound. Various types of materials can also be identified based on the heat flow during the transitions.

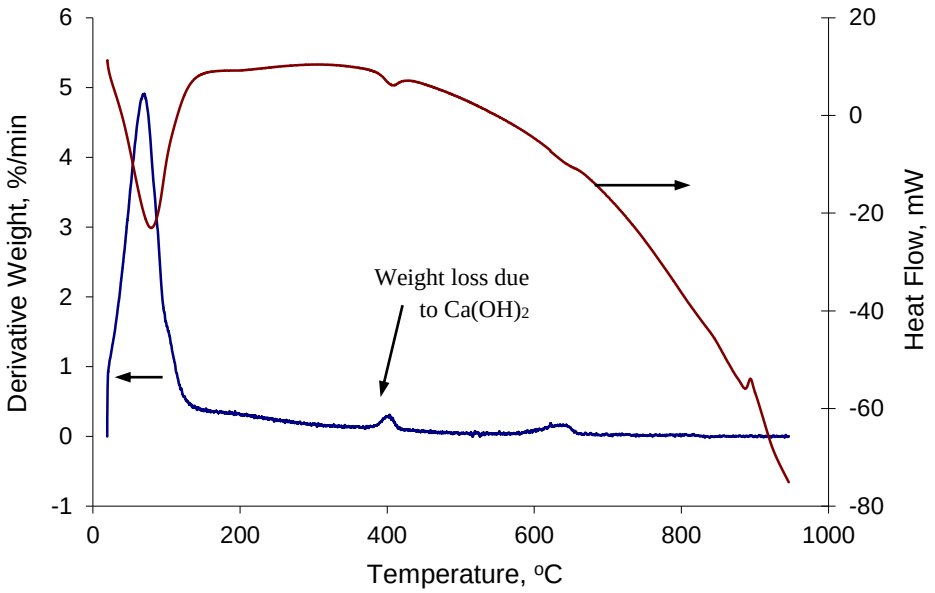

Figure 5.3 The TGA-DTA curves for C-S-H (C/S=1.5 heated from room temperature at 10 °C/min to 950 °C under nitrogen gas flow at 100 mL/min).

The TGA-DTA curves for the C-S-H (C/S: 1.5) are shown in Figure 5.3 Analysis of the derivative weight change, for example, at the temperature range around 400 °C shows that there is about 0.4% weight loss due to the decomposition of $Ca(OH)_2$ and evaporation of H_2O. Since the H_2O mass proportion in calcium hydroxide is 24%, it is calculated that 1.7% $Ca(OH)_2$ is present in the material. Similar calculations are possible for other components such as calcium carbonate that decomposes at about 600 °C. Similar analyses using the DTA curve can also be conducted once it is calibrated.

5.3 *Nuclear Magnetic Resonance Spectroscopy (NMR)*

The concept of this technique was first discovered at 1902. But, it was not until 1952 when the practical experimental technique was developed. NMR found its place in cement chemistry in the early eighties [3, 4, 5]. NMR, which is a nondestructive technique, is based on the analysis of the interaction between an oscillating radio frequency electromagnetic field with a collection of atomic nuclei in the presence of an external strong magnetic field.

In NMR, nuclei with odd mass number and half-integer spins such as ^{17}O and ^{29}Si are of most interest because of their magnetic moment. In the presence of a magnetic field the degeneracy of spin energy levels is lifted. This change of energy state in an individual nucleus results in absorbing or emitting a photon with a specific frequency. This frequency is detected and analyzed in NMR [6]. The most useful aspect of NMR in molecular structure studies is that the electrons in the vicinity of the observed nucleus shield it from the magnetic field, which results in a slightly different frequency. Therefore, depending on the neighborhood nucleus and their bonds, this interaction can be different for the same atom. Since it is difficult to measure the absolute values of these frequencies accurately, they are always been reported as chemical shifts relative to an experimentally useful standard [7].

Study of the location of the chemical shifts reveals fundamental information on the molecular structure of materials. For solid state NMR, the magic angle spinning (MAS) method is often used in order to avoid large peak broadenings caused by several nuclear interactions. This is conducted by spinning the sample at frequencies of 1-35 kHz around an axis oriented 54.7˚ to the magnetic field [6].

The most investigated nucleus in cement chemistry is silicon. A relatively high natural abundance of ^{29}Si (4.67%) as well as its principal structural role in the calcium silicate hydrates makes it favorable for such studies. Silicate tetrahedra are present in hydrated cement systems in various degrees of polymerization. In NMR, polymerization that results in more electron shielding makes the chemical shifts more negative and ranges from –60 to 120 ppm [8]. The polymerization of a silicate tetrahedron (Q) is expressed by Q^n, where n is the number bridging oxygens per tetrahedron. If the oxygen is shared with other silicate

tetrahedra, the possible Q^n sites (n=0 to 4) are usually observed at the following ranges shown in the Figure 5.4 [9]:

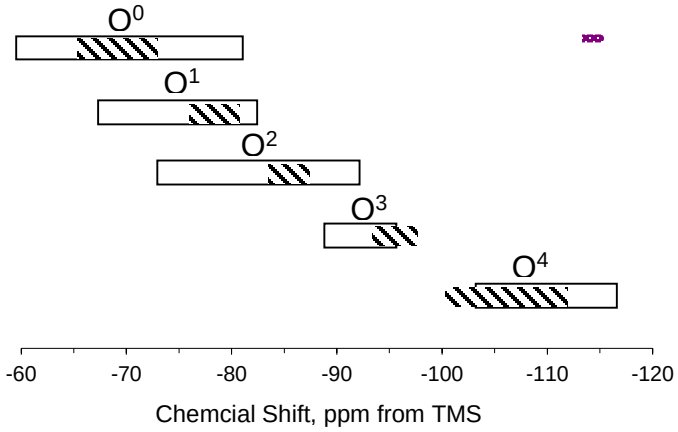

Figure 5.4. Ranges of ^{29}Si chemical shifts of Q^n units in solid silicates. The well-separated ranges are hatched.

In hydrated Portland cement, some Q^0 might be observed due to the unhydrated C_3S and C_2S. The usual acquired peaks (as schematically shown in Figure 5.5) are for Q^1 (chain end group) and Q^2 (chain middle group) silicate sites. Q^3 has rarely been reported in cement paste and is attributed to the chain branching silicate sites (between the layers) [10, 11, 12]. Q^4 is the polymerization of the quartz and can be seen in silica fume, for example.

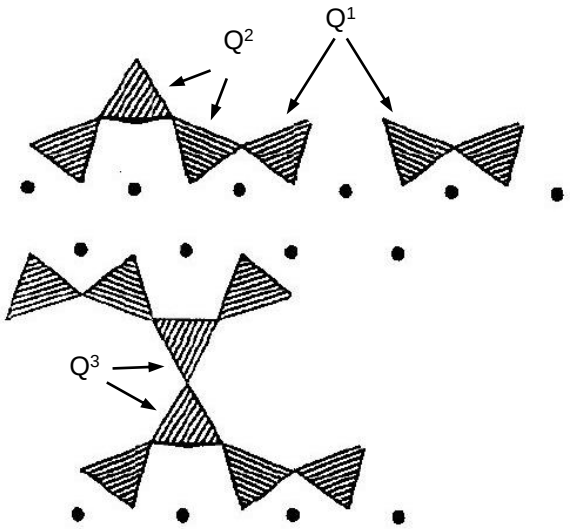

Figure 5.5. Schematic presentation of the possible silicate sites (triangles) in C-S-H. Circles are calcium atoms from the Ca-O layer.

The structure of calcium-silicate-hydrates (including various tobermorite systems) has been widely studied by ^{29}Si NMR. The reported chemical shifts for Q^1, Q^2 and Q^3 in C-S-H are ~ -79 to -80, ~ -85 to -86 and near –96 ppm, respectively [4, 13, 14, 15, 16]. Various peaks have also been observed on the shoulder of Q^2 peak that are attributed to the difference in the local environment of Q^2 sites as in the bridging positions and paired groups [14, 17, 18]. The chemical shift of bridging sites may also vary depending on the chemical attachments such as OH^- or Ca^{2+}.

5.4 Dynamic mechanical analysis (DMA)

Dynamic Mechanical Analysis (DMA) involves the analysis of the response of an oscillating force in sinusoidal form applied on a specimen. DMA is a widely used technique in polymer science and is often used to study the temperature transitions of molecular forms [19]. The theory of viscoelasticity in such materials implies that the steady state vibrational response involves frequency dependent moduli and stress and strain will not be in the same phase. (See Figure 5.6) The strain generally lags with the stress by an angle δ. The tan δ, which is

referred to as internal friction, is a function of frequency [20]. Consider a sinusoidal load that is applied on a sample in the form of

$$\sigma = \sigma_A \sin(\omega t)$$

where σ is the stress at time t, σ_A is the maximum stress and ω is the frequency of the oscillation.

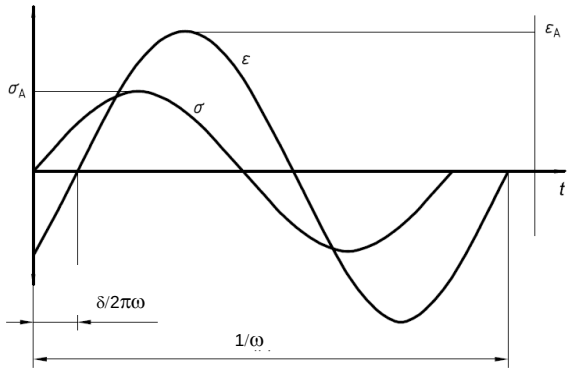

Figure 5.6. The phase shift between the stress and strain in a viscoelastic material subjected to sinusoidal oscillation.

If the stress remains within the elastic region of the material, the strain response (Figure 5.6) will be in a sinusoidal form as well and can be expressed as

$$\varepsilon = \varepsilon_A \sin(\omega t + \delta)$$

where ε is the strain at time t, ε_A is the maximum strain (if the stress-strain remains in the linear region) and δ is the phase difference angle. All of the properties of a DMA analysis are calculated based on the maximum strain under sinusoidal stress and the angle defining the lag between the force and the response.

Equations can be derived for two types of modulus; *E': storage modulus* and *E": loss modulus* [19]:

$$E' = (\sigma_A / \varepsilon_A)\cos\delta$$
$$E'' = (\sigma_A / \varepsilon_A)\sin\delta$$

The storage modulus (also called the elastic modulus) is a measure of how elastic the material is and ideally is equivalent to Young's modulus although the nature of the loading is different. This may not be completely true since Young's modulus is determined from the slope of a line obtained from a range of stress-strain values, while E' represents a point at a specific stress. Loss modulus (also known as the viscous modulus) is a measure of the loss of energy due to internal friction and motions. The complex modulus (E^*) is defined as *E'+iE"*.

The tangent of the phase angle (tan δ, also called the damping angle) is an indicator of how efficiently the material loses energy to molecular rearrangements and internal friction and is independent of geometry effects.

$$\tan\delta = \varepsilon'' / \varepsilon' = E'' / E'$$

DMA was introduced in the seventies as a nondestructive analysis technique for cement-based materials. Radjy and colleagues first investigated states of water in cement hydration products using a temperature controlled DMA (or DTMA) [20, 21, 22]. Recent applications in cement science use DMA primarily for studying the polymer modified cementitious materials. It is also possible to study other phenomena such as creep and stress relaxation with a DMA instrument.

5.5 Microindentation measurements (MI)

Facility description

All the microindentation tests were performed using a CSM Instruments Instrumented Indentation Tester. The CSM microindentation instrument (see schematic shown in Figure 5.7) has a load range of 0.03 – 30 N with a resolution of 0.3 mN. The apparatus is housed in

an environmental chamber (Figure 5.7). All tests were conducted at 11% RH on specimens equilibrated at 11%RH. Tests were conducted using a Berkovich indenter.

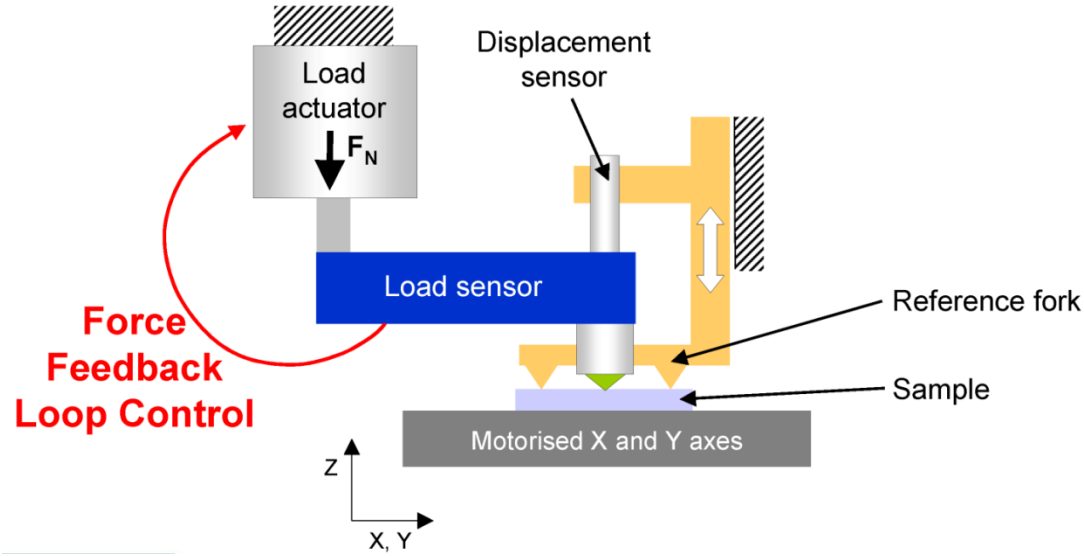

Figure 5.7 Microindentation testing machine

Test specifications

The rate of loading in the current experiments was 2000 mN/min. The specimens were tested over a wide range of porosity values varying from about 10% to as high as 60%. There were approximately 25 indents on each sample at each porosity level for a total of approximately 125 indents for each material system. The indentation depth was recorded as a function of time at the maximum load of 1000 mN for a 600s dwell period.

Microindentation parameters

Creep Modulus

A typical load-displacement curve with a period of constant load is shown in Figure 5.8

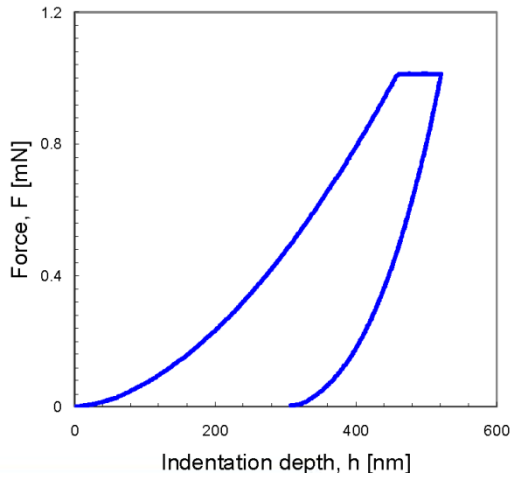

Figure 5.8. Typical load-displacement curve

The logarithmic creep can be determined through curve fitting of the indentation-depth (h) versus time curves during the 600s dwell time by the following equation:

$\Delta h(t) = x_1 \ln (x_2 t + 1) + x_3 t + x_4$

The creep modulus, C, is then calculated from: $C = F_{max} / (2a_U x_1)$ where $a_U = [A_c/\pi]^{1/2}$. A_c is the projected area of contact between the indenter probe and the indenter surface. The projected area is required due to the 'sink-in' effect of the surface profile under load (see Figures 5.9, 5.10). It is determined using the Oliver and Pharr method as a function of the maximum indentation depth [23]. These authors determined that the projected area (A_c) for a perfect cone or pyramid could be estimated from the relation, $A_c = C_0 h^2$ where C_0 is a constant (24.5 for a Vickers or Berkovich indenter) and h is as defined above.

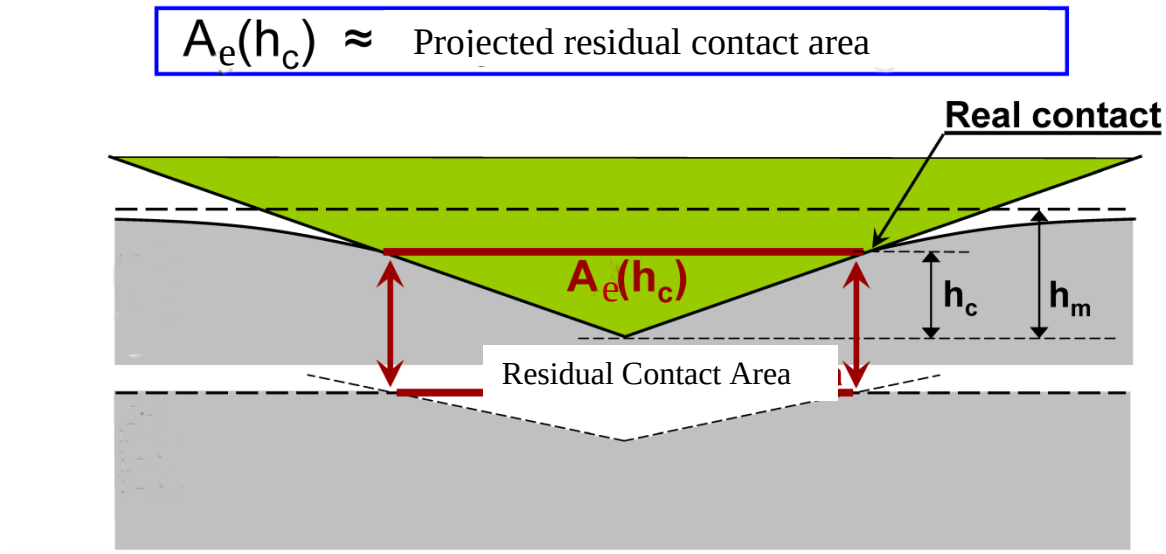

Figure 5.9 Projected Area of Microindentation

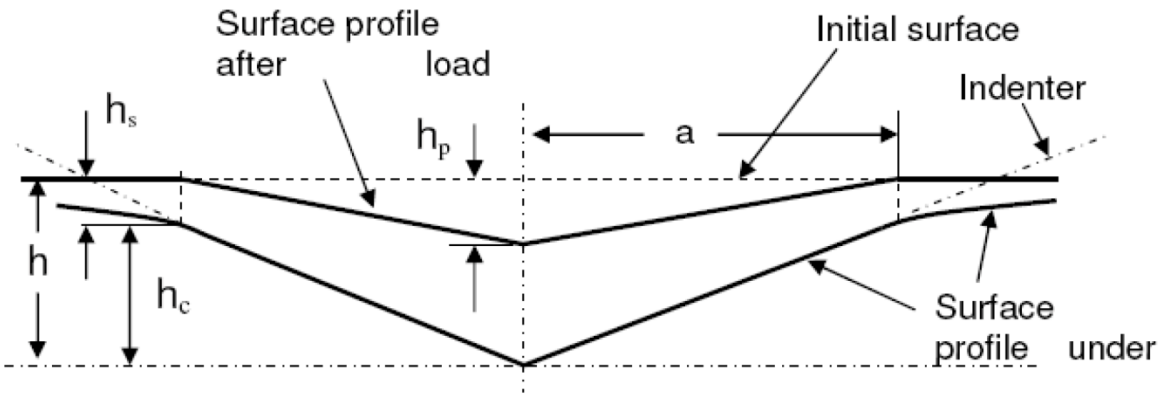

Figure 5.10 Schematic of depth descriptors

Indentation Modulus and Indentation Hardness

The indentation modulus (M) and indentation hardness (H) were obtained from the software that uses the Oliver and Pharr method. $M = \pi^{1/2}S/ [2\beta(A_c)^{1/2}]$ where :

$S = dP/dh |_{h = hmax}$ is the initial slope of the unloading branch of the F-h curve and $\beta \approx 1.0$. F is the maximum indentation load. Determination of S is illustrated in Figure 5.11.

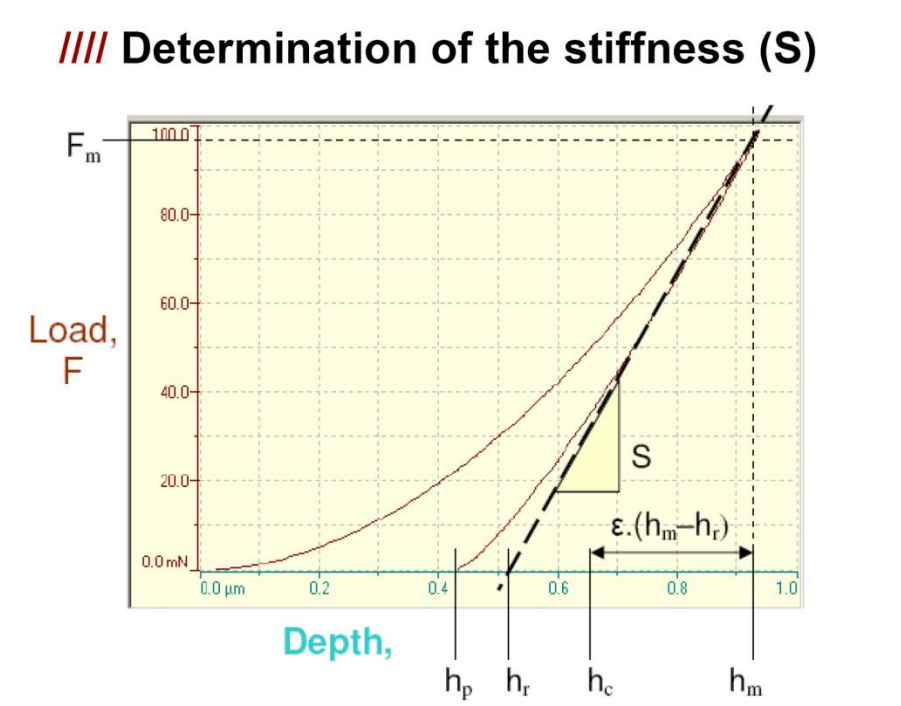

Figure 5.11 Determination of the stiffness

The various depths, h_p, h_r, h_c and h_m utilized for the calculations are defined in the figure. The geometric constant ϵ is a function of the exponent 'm' in the power-law fit of the unloading curve and can be calculated from Sneddon's equations [24]. Indentation hardness $H = F/A_c$. A schematic outlining the calculations is provided in Figure 5.12

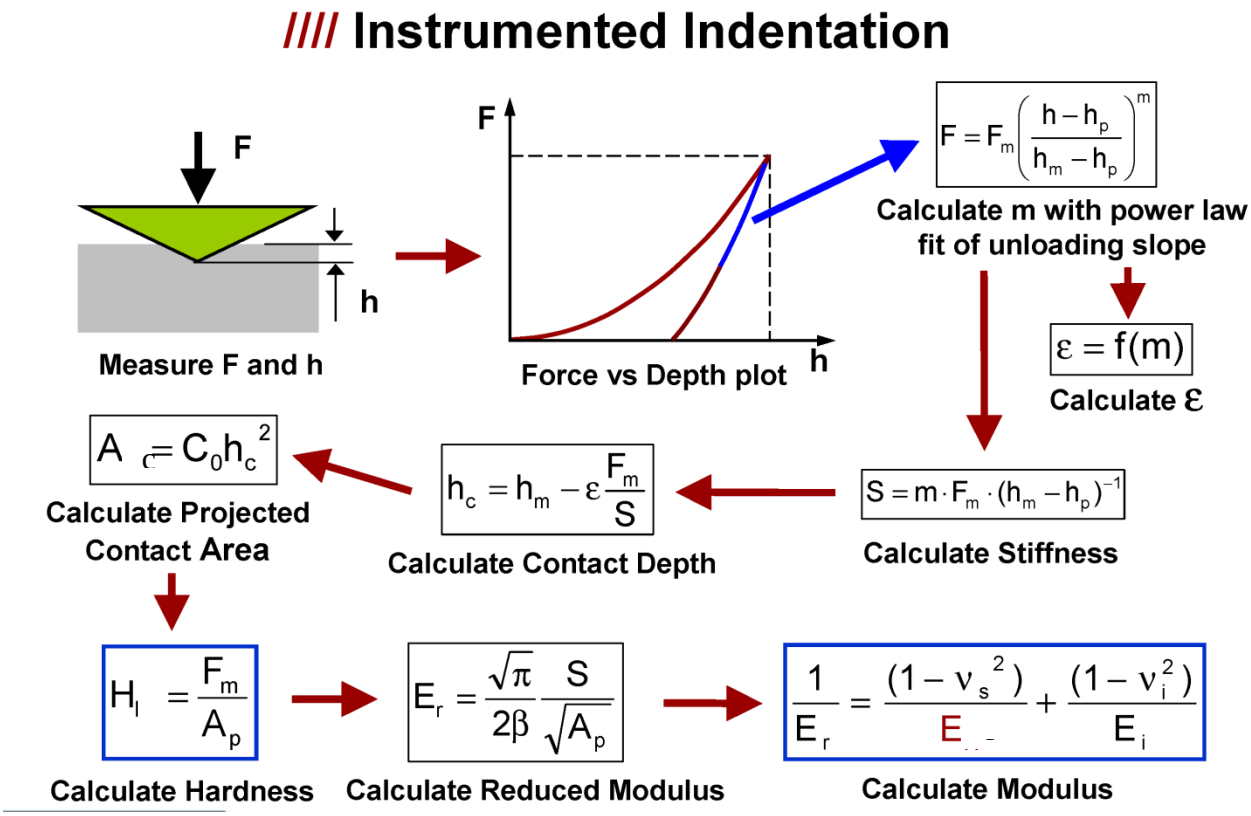

Figure 5.12 Schematic of Modulus of Elasticity Calculation

5.6 *Other analytical methods*

Several other techniques can be employed in cement science investigations depending on the information required about a specific chemical compound.

In order to investigate the morphology and surface characterization of materials, images at the micro and nano scales can be captured using a Scanning Electron Microscope (SEM). High-resolution images of up to about 110,000K magnification are easily obtained from various cementitious minerals. Different crystalline shapes of materials such as long prisms in ettringite and the hexagonal form of calcium hydroxide are readily observed. In this technique, a focused beam of electrons strikes the surface of the material. The surface interactions result in the emission of secondary and backscattered electrons as well as X-ray. The electrons are collected and converted to the image of the surface. It is also possible to

produce back-scattered images, the contrast of which is based on the atomic number. This helps differentiate regions rich in a specific atom. Elemental analysis is also possible through energy dispersive X-ray spectroscopy (EDX) that enables estimates of the proportion of each atom in the mixture. EDX imaging allows mapping the distribution of various elements in the material.

Unknown components of a mixture of either organic or inorganic material can be detected using Fourier Transform Infrared Spectroscopy (FTIR). This technique can be applied quantitatively for gases, liquids and solids. FTIR is a powerful tool in identifying the nature of the chemical bonds of molecules. Chemical bonds vibrate at certain frequencies depending on the type of atoms and bonds. The adsorption of the energy of infrared portion of light by a molecular bond can change the vibrational state of a chemical bond from ground level to an exited level. The energy required for this transition is unique for each bond and thus can be measured and used for the detection of various bonds in molecules. Various IR techniques have been employed to study the structure of cement-based materials [25, 26].

Other methods such as BET surface area measurement, static measurement of dynamic modulus of elasticity, nanoindentation and AFM analysis can be employed in order to obtain additional information about the materials and enhance the discussion of arguments that are advanced.

References

1. ASTM book of standards, volume 04.01 “Cement; Lime; Gypsum,” also volume 04.02 “Concrete and Aggregates,” *American Society for Testing and Materials*, 2007/2008.
2. Ramachandran V. S. and Beaudoin J. J. (edt.), “Handbook of Analytical Techniques in Concrete Science and Technology,” William Andrew, 2001.
3. Lippmaa E., Mägi M., Samoson A., Engelhardt G., Grimmer A.-R., “Structural studies of silicates by solid-state high-resolution 29Si NMR,” *J Am Chem Soc*, 102, 4889–4893, 1980.

4. Wieker W., Grimmer A.-R., Winkler A., Mägi M., Tarmak M. and Lippmaa E., "Solid-state high-resolution 29Si NMR spectroscopy of synthetic 14Å, 11and 9Å tobermorites," Cem. Concr. Res. 12, 333-339, 1982.
5. Lippmaa E., Mägi M., Tarmak M., Wieker W., Grimmer A.-R., "A high-resolution ^{29}Si NMR study of the hydration of tricalciumsilicate," *Cem. Concr. Res*. 12, 597-602, 1982.
6. Macomber R. S., A complete introduction to modern NMR spectroscopy, John Wiley & Sons, 1998.
7. Duer M. J. (edt.), Solid-State NMR spectroscopy – Principles and applications, Blackwell Science, 2002.
8. Engelhardt G. and Michel D., High-resolution solid-state NMR of silicates and zeolites, John Wiley & Sons, 1987.
9. Mägi M., Lippmaa E., Samoson A., Engelhardt G. and Grimmer A.-R., "Solid state high-resolution silicon-29 chemical shifts in silicates," *J Phys Chem*, 88, 1518-1522, 1984.
10. Young J. F., "Investigations of Calcium Silicate Hydrate Structure Using Silicon-29 Nuclear Magnetic Resonance Spectroscopy," J. Am. Ceram. Soc., 71(3) C118-C120, 1988.
11. Yu P., Kirkpatrick R. J. "Thermal dehydration of tobermorite and jennite," Concrete Science and Engineering, 1, 185-191, 1999.
12. Sato H., Grutzeck M. "Effect of starting materials on the synthesis of tobermorite," Mat. Res. Soc. Symp. Proc., vol. 245, 235-240, 1992.
13. M. Grutzeck, A. Benesi, and B. Fanning, ''Silicon-29 magic-angle spinning nuclear magnetic resonance study of calcium silicate hydrates,'' J. Am. Ceram. Soc., 72, 665-668, 1989.
14. Bell G. M. M., Bensted J., Glasser F. P., Lachowski E. E., Roberts D. R. and Taylor M. J., "Study of Calcium Silicate Hydrates by Solid State High Resolution ^{29}Si Nuclear Magnetic Resonance," *Advances in Cement Research*, 3, 23-37, 1990.

15. Cong X. and Kirkpatrick R. J., "29Si MAS NMR Study of the Structure of Calcium Silicate Hydrate," Adv. Cem. Based Mat., 3, 144-156, 1996.
16. Young J. F., "Investigations of Calcium Silicate Hydrate Structure Using Silicon-29 Nuclear Magnetic Resonance Spectroscopy," J. Am. Ceram. Soc., 71(3) C118-C120, 1988.
17. Klur I., Pollet B., Virlet J., Nonat A., "C-S-H structure evolution with calcium content by multinuclear NMR," 2nd International conference on NMR spectroscopy of cement based materials, 119-141, 1998.
18. Brough A. R., Dobson C. M., Richardson I. G., Groves G. W., "Application of Selective 29Si Isotopic Enrichment to Studies of the Structure of Calcium Silicate Hydrate (C-S-H) Gels," *J Am Ceram Soc*, 77(2) 593-596, 1994.
19. Ferry J., Viscoelastic Properties of Polymers, Wiley, New York, Ch. 5–7, 1980.
20. Menard K. P., Dynamic Mechanical Analysis – A practical introduction, CRC Press LLC, 1999.
21. Radjy F., Sellevold E. J. "Internal friction peaks due to adsorbed and capillary water in microporous substances," Nature Physical Science, 241, 133-135, 1973.
22. Radjy F. and Richards C.W. "Effect of curing and heat treatment history on the dynamic mechanical response and the pore structure of hardened cement paste," *Cement and Concrete Research*, 3, 7-21, 1973.
23. Oliver W. C. and Pharr G. M., "An improved technique for determining hardness and elastic modulus using load and displacement sensing indentation experiments", *J. Mater. Res.*, 7, 1564-1583, 1992.
24. Sneddon I. N., "The relation between load and penetration in the axisymmetric Boussinesq problem for a punch of arbitrary profile", *Int. J. Eng. Sci.*, 3, 47-57, 1965.
25. Delgado A. H., Paroli R. M., Beaudoin J. J. "Comparison of IR techniques for the characterization of construction cement minerals and hydrated products," *Applied Spectroscopy*, 50(8), 970-976, 1996.
26. Ghosh S.N. and Chatterjee A.K. "Absorption and reflection infrared spectra of major cement minerals, clinkers and cements," *J. Mater. Sci.*, 9, 1577-1584, 1974.

Chapter 6

Synthesis of Layered Calcium Silicate Hydrates

6.1 General

C-S-H from Portland Cement

The C-S-H formed in the Portland cement hydration incorporates various elements and has a variable and nearly amorphous structure. Therefore, the main research related to the C-S-H systems has focused on the hydration products of pure C_3S or α-C_2S. The reaction product is chemically treated to remove the $Ca(OH)_2$ and achieve almost pure C-S-H [1]. This type of C-S-H usually has an average C/S ratio of about 1.7. In some cases it is required to study the properties of low C/S ratio C-S-H systems, for which the initial preparation of C-S-H from hydrated C_3S is decalcified. This is possible by leaching the calcium in either distilled water or ammonium nitrate [2, 3]. The latter is more favorable as it results in a minor loss of Si from the structure and thus a nearly pure decalcification.

Synthetic C-S-H

C-S-H can be readily made from mixing lime and silica in an excess of water (pozzolanic reaction). The properties of such systems made at various temperatures and different C/S ratios have been intensively studied. The first of these contributions were made by Taylor [4, 5-7]. Hydrothermal conditions are often used in order to promote crystallization of the C-S-H. Curing temperatures of about 60 ºC are experienced in the formation of C-S-H systems.

Another commonly employed method for C-S-H synthesis is the double decomposition of calcium salts (most commonly calcium nitrate) with a soluble silicate (eg. Na_2SiO_3-$5H_2O$). The C-S-H precipitate is washed with the CH solution. Mixing calcium hydroxide and hydrous silica in aqueous suspension can also be used to produce C-S-H [8]. In these

methods, after the formation of the C-S-H the final material is filtered and washed and stored under nitrogen gas. The crystallinity of synthetic C-S-H depends on the reaction time and temperature.

Pozzolanic reaction results in the formation of more crystalline C-S-H, but it is slower that the double precipitation method. [9]

6.2 Materials preparation for this study

Different cementing systems were prepared: synthetic calcium-silicate-hydrate (C-S-H with C/S = 0.8 to 1.5); 1.4nm tobermorite; jennite; high temperature phases i.e. gyrolite, xonotlite and hillebrandite; hydrated Portland cement paste (water/cement ratio = 0.40) at different ages.

C-S-H: synthetic C-S-H was produced from the pozzolanic reaction between CaO and amorphous silica in excess water (water/solids = 11). Calcium oxide was obtained by calcining reagent grade calcium carbonate at 900◦C. Reactive silica (CAB-O-SIL, grade M-5 from Cabot Corporation, USA) was heated at 110◦C to remove any surface adsorbed water. Distilled water was de-aired and used for the reactions. All materials were kept sealed in N_2 purged bottles until they were used. Variation in C/S ratio was achieved by adjusting the stoichiometric amounts of the reactants. The reaction period was 6 months. The material was then filtered and dried under vacuum for 4 days at room temperature. The dried C-S-H was stored in nitrogen purged glass vials before the experiments. Characterization of these materials by X-ray diffraction (XRD) and thermal methods gave results directly comparable to C-S-H (I) as reported by Taylor [10].

1.4nm tobermorite: the reactants (CaO and SiO_2) were prepared as described above. The C/S ratio was 0.9. The reactants were placed in a high density polyethylene bottle mixed in excess deionized water (water/solids = 11) and maintained at 80 °C using a heating wrap. The mixture was continuously agitated with a magnetic stirrer for a period of 4 months. The XRD spectrum and TGA curve were similar to those obtained by Yu and Kirkpatrick [11].

Jennite: the reactants (CaO and SiO_2) were prepared as described above. The C/S ratio was 1.4. The reactants were placed in a high density polyethylene bottle mixed in excess deionized water (water/solids = 11) and maintained at 80 °C using a heating wrap. The mixture was continuously agitated with a magnetic stirrer for a period of 4 months. The XRD pattern was similar to that obtained by Yu and Kirkpatrick [11], Gard and Taylor [12] and Hara and Inoue [13]. The TGA curve matched that published by Yu and Kirkpatrick [11].

Cement pastes:

The 45 year old paste specimens were cast in glass cylinders with circular cross-section (25mm in diameter). The paste was prepared with water/cement ratios of 0.50, 0.80, 0.90 and 1.00. The cylinders were continuously rotated for 24h and the specimens were subsequently demolded and sheathed in a rubber membrane containing a few drops of lime saturated water. They were then stored in stoppered glass tubes for 45 years. Slices 1mm thick were then cut and ground into a fine powder for fabrication into compacted specimens. The use of compacted specimens provided an effective means for controlling the porosity. The cement used was a normal type I Portland cement. The oxide analysis for the cement (percentages are given in brackets) used was as follows: SiO_2 (20.72); Al_2O_3 (5.87); Fe_2O_3 (3.07); CaO (62.66); MgO (3.46);SO_3 (2.18). Ignition loss was 1.10 %; Insoluble residue was 0.24%. Free CaO was 0.24%. The Bogue compound composition was: C_3S (46.5%); C_2S (24.6%); C_3A (10.4%); C_4AF (9.3%). Blaine fineness was 3279 cm^2/g. The 'old' pastes were characterized using X-ray diffraction, TGA and 29Si NMR methods.

The 3 year old paste (made with Type I Portland cement) was prepared using a water/cement ratio of 0.40. Rectangular prisms (250 x 100 x 12mm) were cast. The samples were vibrated and stored in a moist curing room for 24 h. They were then demoulded and curing was continued for 3 years in a saturated lime solution. Thin slices (1 x 12 x 60 mm) were cut from the paste prism using an Isomet diamond saw. Selected slices were also ground into a fine powder for fabrication into compacted specimens.

Young pastes (water/cement = 0.40) hydrated for short periods (e.g. 3 and 7 days) were prepared in a similar manner to the 3 year old paste.

Gyrolite:

The reactants (CaO and SiO_2) were prepared as described above. The C/S ratio was 0.5. Several experiments were made using an autoclave in the temperature range between 200 °C to 220 °C for 3 days.

After reaction the products were removed from the autoclave and conditioned at 11%RH for one week. The XRD pattern of products is on the paper.

Xonotlite:

The reactants (CaO and SiO_2) were prepared as described above. The C/S ratio was 1.0. Several experiments were made using an autoclave in the temperature range between 200 °C to 220 °C for 2 days. The XRD pattern of products is on the paper.

Hillebrandite:

The reactants (CaO and SiO2) were prepared as described above. The C/S ratio was 1.8. Several experiments were made using an autoclave in the temperature range between 200 °C to 220 °C for 6 hours.

6.3 Humidity Conditioning:

Specimens for all cementing systems investigated were conditioned at 11% RH in vacuum desiccators containing saturated lithium chloride solution. The powders were conditioned at 11%RH for several weeks before compaction and for one week after compaction. Theoretically there is a monolayer of water on the surfaces of the particles in addition to interlayer water at this humidity.

References

1. Chen J.J., Thomas J.J., Taylor H.F.W., Jennings H.M., “Solubility and Structure of Calcium Silicate Hydrate,” Cement and Concrete Research, 34(9) 1499-1599, 2004.
2. Carde C., Escadeillas G., Francois R., “Use of ammonium nitrate solution to simulate and accelerate the leaching of cement pastes due to deionized water,” Mag. Concr. Res., 49(181) 295–301, 1997.

3. Lea F. M. "The action of ammonium salts on concrete," *Magazine of Concrete Research*, 17(52), 115-116, 1965.
4. Taylor H.F.W., "Hydrated calcium silicates: part I. Compound formation at ordinary temperatures," J. Chem. Soc. 3682-3690, 1950.
5. Heller L., Taylor H.F.W., "Hydrated calcium silicates: part 2. Hydrothermal reactions: lime:silica ratio 1:1," J. Chem. Soc. 2397– 3401, 1951.
6. Heller L., Taylor H.F.W., "Hydrated calcium silicates: part 3. Hydrothermal reactions of mixture of lime:silica molar 3:2," J. Chem. Soc. 1018– 1019, 1952.
7. Heller L., Taylor H.F.W., "Hydrated calcium silicates: part 4. Hydrothermal reactions lime:silica ratios 2:1 and 3:1," J. Chem. Soc. 2535– 2541, 1952.
8. Beaudoin, J. J., "Why Engineers Need Materials Science," Concrete International, 21(8), 86-89, 1999.
9. Taylor H.F.W., The chemistry of cements, Ch5: The Calcium Silicate Hydrates, V.1, Academic Press, 1964.
10. Taylor H. F. W., "Cement Chemistry", 2nd Edition, Thomas Telford Pub., pp. 459, 1997.
11. Yu P., Kirkpatrick R. J. "Thermal dehydration of tobermorite and jennite," Concrete Science and Engineering, 1, 185-191, 1999.
12. M. Grutzeck, A. Benesi, and B. Fanning, ''Silicon-29 magic-angle spinning nuclear magnetic resonance study of calcium silicate hydrates,'' J. Am. Ceram. Soc., 72, 665-668, 1989.
13. Hara N. and Inoue N., Formation of jennite from fumed silica, Cem. Concr. Res., 10, 677-682, 1980.

Chapter 7

Experimental Outline

The experimental work described in the thesis is comprised of four parts.

The following parts of thesis were designed to establish the compatibility of compositional models of C-S-H nanostructure in hydrated Portland cement (HPC) paste with the engineering behavior of pure mineral systems (T, J, C-S-H) that comprise the principal elements of these models. Insights into the structural role of water in layered silicates are an intrinsic outcome of this work.

The thesis contains four parts briefly described below.

Part 1 – Dynamic Mechanical thermal analysis of layered calcium silicate hydrates

This work involves extensive use of dynamic mechanical analysis (DMA) techniques and the application of dynamic mechanical thermo analysis (DMTA) to the studied systems. There were papers will be introduced and discussed in Chapter 8.

Paper 1. Dynamic mechanical thermoanalysis of layered calcium silicate hydrates

Paper 2. Correlation between dynamic mechanical thermo-analysis and composition-based models for C-S-H in hydrated portland cement paste

Paper 3. Effect of Thermal Treatment of 1.4nm Tobermorite and Jennite on Mechanical Performance

Part 2 – Mechanical properties and dimensional stability of layered calcium silicate hydrates

The results contained in this part are reported in three journal papers. Three papers will be introduced and discussed in chapter 8.

Paper 4. Mechanical property–porosity relationships of layered calcium silicate hydrate phases

Paper 5. Dimensional Stability of 1.4nm Tobermorite, Jennite and Other Layered Calcium-Silicate-Hydrates

Paper 6. Drying of Calcium Silicate Hydrates: Regeneration of Elastic Modulus

Part 3 – The effects of prolonged hydration on the engineering behavior of hydrated Portland cement paste

The results contained in this part are reported in three journal papers. These papers will be introduced and discussed in chapter 10.

Paper 7. Drying of Calcium Silicate Hydrates: Regeneration of Elastic Modulus

Paper 8. Dynamic Mechanical Thermo- Analysis of Portland cement Paste Hydrated for 45 Years

Paper 9. Creep of 45 Year Old Cement Paste- The Role of Structural Water

Part 4 – Layered calcium-silicate-hydrates engineering performance and the structural role of interlayer water

The results contained in this part are reported in three journal papers. Three papers will be introduced and discussed in Chapter 11.

Paper 10. Engineering Performance of Pure Calcium-Silicate-Hydrates Phases: The Structural Role of Interlayer Water

Paper 11. Structural Factors Affecting the performance of Layered Calcium Silicate Hydrates

Paper 12. The Effect of Drying History and the Role of Water on the Engineering Behavior of Layered Calcium-Silicate Hydrates

Chapter 8

Application of Dynamic Mechanical Thermo-Analysis Methods for Assessing Engineering Performance of Layered Calcium Silicate Hydrates

Solutions to sustainable concrete infrastructure problems and design are rooted in a comprehensive understanding of the calcium-silicate-hydrate phase in cement-based binders. The most recent composition-based models for C-S-H in hydrated Portland cement are based on 1.4 nm tobermorite-jennite structures (T-J models).

Three papers (from Part 1 of the experimental program) addressing nanostructural issues related to composition-based models for C-S-H in hydrated Portland cement paste are presented in this chapter. Research results demonstrating the application of Dynamic Mechanical Thermo-Analysis (DMTA) for assessing mechanical performance of the layered silicate minerals investigated are reported. Sensitivity of these techniques to phase changes at higher temperatures are useful for establishing links between engineering properties and composition i.e. cement chemistry. It is demonstrated that variations of T-J composition-based models can be invoked that are dependent on degree of hydration and ageing effects. The latter are shown to be influenced by temperature and porosity.

The titles of the papers in this chapter are as follows:

Paper 1: Dynamic Mechanical Thermoanalysis of Layered Calcium- Silicate-Hydrates, Journal of Thermoanalysis and Calorimetry, 118(1), 1-14, 2014.

Paper 2: Correlation Between Dynamic Mechanical Thermo-analysis and Composition-Based Models for C-S-H in Hydrated Portland Cement Paste, Materials and Structures, DOI 10.1617/s11527-014-0330-7, 2014.

Paper 3: Effect of Thermal Treatment of 1.4 nm Tobermorite and Jennite on Mechanical Performance, Materials and Structures, under review.

8.1 Introduction

The utility of the DMTA technique for determining the mechanical performance of 1.4 nm tobermorite and jennite (the key structural units for composition-based models of C-S-H in hydrated Portland cement systems) is explored in the three papers presented in this chapter. It is demonstrated in Paper 1 that DMTA results (E' and tan∂) mimic those of DMA (E' and tan∂ versus equilibrium mass-loss curves) in the temperature range (25-110°C) greatly reducing data acquisition times. The method provides a means of assessing the influence of other factors such as high temperature phase changes and microstructural features (e.g. porosity) that can affect behavior. The results are germane to an assessment of the concept of a tobermorite - jennite model for the C-S-H present in hydrated cement paste.

Original data to assess the practical validity of the Richardson-Groves composition-based models for the C-S-H in cement paste is provided in Paper 2. The DMTA method was used

to obtain this data. Differences in mechanical performance between 'young' paste and 'old' paste are accounted for using these models.

The effects of thermal treatment of 1.4nm tobermorite and jennite on mechanical performance are described in Paper 3. Irreversible changes to the tobermorite system due to pre-heating for prolonged periods at temperatures associated with phase transformations are followed using the DMTA method. These were not observed for jennite. DMTA appears to be a valuable research tool for studies of dehydration phenomena and their correspondence to the engineering behavior of layered calcium-silicate-hydrates.

8.2 Paper 1: Dynamic Mechanical Thermoanalysis of Layered Calcium Silicate Hydrates

The first paper is a comprehensive study of the application of the DMTA method to examine the mechanical behavior of compacted systems of C-S-H, 1.4 nm tobermorite (T) and jennite (J) powders. The study focuses on the nanostructural effects due to the removal of water from the 11% RH condition. Sensitivity of DMTA to phase changes and their relevance to mechanical performance is a useful outcome of this work and a contribution to improving our understanding of the current composition-based models. Changes to the DMTA parameters (E' and tan∂) of C-S-H, tobermorite and jennite are explained in terms of the removal of interlayer water, interactions of interlayer Ca^{2+} with the silicate sheets and potentially cross-linking effects. Mechanical mixtures of T and J were also utilized to assess the behavior of these bi-mineral systems with respect to similarities and differences to that

of hydrated cement paste. Porosity and the amorphous nature of cement paste are also taken into consideration in the discussion.

Dynamic Mechanical Thermo-Analysis of Layered Calcium-Silicate Hydrates

(Journal of Thermal Analysis and Calorimetry 118 (1), pp. 1-14)

P. Pourbeik[a], J. J. Beaudoin[b], R. Alizadeh[c] and L. Raki[b]

[a] Department of Civil Engineering, University of Ottawa, Ottawa, ON, Canada

[b] National Research Council Canada, Construction Portfolio, Ottawa, ON, Canada

[c] Giatec Scientific Inc., Ottawa, ON, Canada

Abstract

Dynamic mechanical thermoanalysis (DMTA) was conducted on compacted specimens of C-S-H, 1.4nm tobermorite, jennite and compacted hydrated Portland cement paste powders as well as hardened cement paste. The synthetic silicates are key elements for compositional models of the hydrated calcium silicates present in cement paste. The study focuses on the the nanostructural effects due to the removal of water from the 11% RH condition. The DMTA results (E' and tan∂ versus temperature curves) in the 25°C - 110 °C range mimicked those of DMA (E' and tan∂ versus mass loss curves) conducted at room temperature for C-S-H and cement paste. In addition the DMTA curves for 1.4nm tobermorite and jennite in the temperature range 110-300°C were sensitive to phase changes including the transition of

1.4 nm tobermorite to 1.1 nm tobermorite and other forms as well as the transition of jennite to metajennite.

The DMTA curves of a 50/50 mixture of 1.4nm tobermorite and jennite exhibit similarities and differences to that of hydrated cement paste that are influenced by porosity and the amorphous nature of C-S-H in the cement paste. The study provides useful data for evaluating Taylor's concept of a possible tobermorite-jennite model for the C-S-H present in hydrated cement paste.

1 Introduction

The calcium-silicate-hydrate (C-S-H) binding phases in hydrated Portland cement paste are known to be ill-crystalline [1]. This has led to the development of various generically different structural models for C-S-H [2-5]. These models describe the silicate hydrates as layered calcium-silicate hydrates [2, 5], microporous colloidal gels [3], or assemblies of globular particles [4]. The state of water in cement paste, depending on the model, has been described as adsorbed, interlayer or bulk or combinations of these. Numerous attempts and investigations to elucidate the nanostructure of C-S-H produced by cement hydration have led to the development of various compositional models [6-9]. The focus of this paper is on the latter. Current layered silicate models developed by Richardson and Groves [6] and Taylor and Richardson are comprised primarily of tobermorite-type and jennite-type structures [7, 8]. The state of water in these models is primarily adsorbed and interlayer. Richardson also discusses systems better described by tobermorite-calcium hydroxide structures e.g. slag-Portland cement pastes. The primary objective of any structural model for C-S-H is to better understand and eventually predict the underlying physico-mechanical

and physico-chemical factors responsible for engineering performance. There is a paucity of experimental data related to the engineering properties of synthetic C-S-H, 1.4nm tobermorite and jennite. The application of dynamic mechanical thermo analysis (DMTA) to obtain this data for these synthetic minerals will be described in this paper. Alizadeh et. al. further demonstrated that C-S-H(I) –a layered silicate- is a useful model for the C-S-H present in hydrated Portland cement paste [10].

Dynamic mechanical thermo-analysis (DMTA) in the temperature range -160°C to +100°C was first used by Radjy and coworkers to study the effects of low temperature phase changes in porous hydrated cement pastes on engineering parameters [11-14]. They identified two low temperature transitions which were described as an 'adsorbate' transition (-160°C to - 60 °C) and a 'capillary' transition (-50°C to 0°C) [10]. They also observed a modulus decrease for saturated paste in the temperature range 25°C-100°C and a slow recovery with time. They further suggested that the slow rate of recovery was consistent with an intercalation process as proposed by Feldman [15] and raised the question as to whether the removal of water from 1.4nm tobermorite would be analogous. More recent work by Foray-Thevenin et. al. demonstrated that DMTA can be used as a complimentary tool to characterize cement paste samples [16]. Their investigation of silicate-rich cement pastes cured at 80°C and tested in the temperature range -150°C to + 230°C provided useful characterization data related to porosity, silicate hydration and dehydration.

Recent work by three of the authors has demonstrated the utility of dynamic mechanical analysis (DMA) in following changes to the physical parameters (storage modulus (E') and internal friction, tan ∂) accompanying mass loss due to drying of synthetic C-S-H from the

11%RH condition [17]. It was apparent that the removal of surface adsorbed water and interlayer water played a significant role in the behavior of C-S-H systems. Alizadeh et. al. have [17] demonstrated that thermal dynamic mechanical analysis (DMTA) can mimic the room temperature DMA results for the C-S-H systems and in addition detect thermally activated phase transitions. The investigation strategy for this current work included the synthesis of 1.4 nm tobermorite, jennite, C-S-H (variable C/S ratios) and production of samples by powder compaction. Portland cement paste samples were also utilized. Experimental data on mechanical performance were obtained using DMTA techniques on all samples conditioned to 11% RH. The 11%RH condition is significant as the silicates are covered with a monolayer of water at this condition and therefore contain only interlayer water and surface adsorbed water [15]. No capillary water is present. This study follows the effects of removal of this water on engineering behavior through application of DMTA methods. It was expected that the information generated would provide a basis for comparison of all the layered silicates studied permitting inferences to be made on the significance of structural models for hydrated cement. There is a paucity of experimental data on the engineering properties of the systems studied in this investigation. The information is expected to be useful to cement science modelers especially those engaged in dynamic molecular modeling.

2 Experimental

2.1 Materials

Four cementing systems were prepared: synthetic calcium-silicate-hydrate (C-S-H with C/S = 0.8 to 1.5)); 1.4nm tobermorite; jennite and hydrated Portland cement paste (water/cement ratio = 0.40).

C-S-H: synthetic C-S-H was produced from the pozzolanic reaction between CaO and amorphous silica in excess water. Calcium oxide was obtained by calcining reagent grade calcium carbonate at 900°C. Reactive silica (CAB-O-SIL, grade M-5 from Cabot Corporation, USA) was heated at 110°C to remove any surface adsorbed water. Distilled water was de-aired and used for the reactions. All materials were kept sealed in N_2 purged bottles until they were used. Variation in C/S ratio was achieved by adjusting the stoichiometric amounts of the reactants. The reaction period was 6 months. The material was then filtered and dried under vacuum for 4 days at room temperature. The dried C-S-H was stored in nitrogen purged glass vials before the experiments. Characterization of these materials by X-ray diffraction (XRD) and thermal methods gave results directly comparable to C-S-H (I) as reported by Taylor [1].

1.4nm tobermorite: the reactants (CaO and SiO_2) were prepared as described above. The C/S ratio was 0.9. The reactants were placed in a high density polyethylene bottle mixed in excess deionized water (water/solids = 11) and maintained at 80 °C using a heating wrap. The mixture was continuously agitated with a magnetic stirrer for a period of 4 months. The XRD spectrum and TGA curve were similar to those obtained by Yu and Kirkpatrick [18].

Jennite: the reactants (CaO and SiO_2) were prepared as described above. The C/S ratio was 1.4. The reactants were placed in a high density polyethylene bottle mixed in excess deionized water (water/solids = 11) and maintained at 80 °C using a heating wrap. The mixture was continuously agitated with a magnetic stirrer for a period of 4 months. The XRD pattern was similar to that obtained by Yu and Kirkpatrick [18], Gard and Taylor [19] and Hara and Inoue [20]. The TGA curve matched that published by Yu and Kirkpatrick [18].

Portland Cement Paste: The Portland cement paste (made with Type I Portland cement) was prepared using a water/cement ratio of 0.40. Rectangular prisms (250 x 100 x 12mm) were cast. The samples were vibrated and stored in a moist curing room for 24 h. They were then demoulded and curing was continued for two months in a saturated lime solution. Thin slices (1 x 12 x 60 mm) were cut from the paste prism using an Isomet diamond saw. Lime-saturated water was used for cutting the cement paste samples. Selected slices were also ground into a fine powder for fabrication into compacted specimens. It was not necessary to rotate the cement paste during casting as the water/cement ratio of 0.40 was sufficiently low to minimize segregation.

The cement used was a normal type I Portland cement. The oxide analysis for the cement used was as follows: SiO_2, 20.72%; Al_2O_3, 5.87%; Fe_2O_3, 3.07%; CaO, 62.66%; MgO, 3.46%; SO_3, 2.18%. Loss on ignition was 1.10%, the insoluble residue was 0.24% and free CaO was 0.24%. The Bogue compound composition was C_3S, 46.5%; C_2S, 24.6%; C_3A, 10.4%; C_4AF, 9.3%. Blaine fineness was 3279 cm^2/g.

2.2 Humidity Conditioning

Specimens for all four cementing systems were conditioned for 3 weeks at 11%RH in vacuum desiccators containing saturated lithium chloride solution. The powders were conditioned at 11%RH before compaction and for a few days after compaction. Theoretically there is a monolayer of water on the surfaces of the particles in addition to interlayer water at this humidity.

2.3 Preparation of Compacted Specimens

Solid rectangular prism samples for all the powdered materials (from the four cementing systems) were prepared by pressure compaction in steel moulds with a cross-section of 12.8 x 83 mm. The thickness of most of the prism samples was approximately 1mm. The thickness of each sample was measured to 0.1mm.Numerous studies on the use and validity of compacts as models for hydrated cement systems have been published [21-25]. It has been shown that compacted specimens of powdered hydrated Portland cement have similar mechanical property-porosity relationships to that of the original hardened paste of the same material [21]. The porosity of compacted samples was determined using helium pycnometry or in the case of the phase pure minerals by calculation using published density values. The calculation is made knowing the apparent volume and the solid volume of the sample. Porosity is varied by controlling the compaction pressure. The density measurements obtained using helium pycnometry or by calculation were accurate to $\pm$ 0.01 g/cm^3 as verified by calibration with standard microporous materials e.g. vycor glass of similar geometry.

2.4 Dynamic Mechanical Analysis (DMA) and Dynamic Mechanical Thermal Analysis (DMTA)

Principles

The dynamic mechanical analysis (DMA) method involves the application of an oscillating force to the sample and measurement of displacement [26]. The elastic property obtained by DMA is referred to as the storage modulus (E'); it is analogous to the static modulus of elasticity. There is usually a time lag between the applied force and the resulting displacement. The time lag can be quantified in terms of a phase angle between the load and the displacement due to their ideally sinusoidal nature. The tangent of this angle ($\tan\partial$) represents the damping property of the material often referred to as internal friction.

2.5 Apparatus

The DMA analysis was conducted using a Rheometrics RSA II instrument on all samples in this investigation. Tests were conducted in the three point bending mode. Specimens were rectangular beams (12.8mm x 83mm x 1mm thick). A very low amplitude oscillation was applied on the brittle, thin samples in order to prevent any damage or micro-cracking. This was confirmed by microscopic analysis after the experiment. Moreover, no decrease was observed in the E' value when a trial specimen was repeatedly subjected to the same loading procedure. Samples were tested at a frequency of 0.10Hz at a maximum strain level of 0.01% and an initial static load of 20g in order to ensure a good contact between the upper fixture and the surface of the specimen throughout the dynamic loading process. The induced stress was kept below 2MPa in order not to introduce any significant damage or micro-cracking to

the sample. The original experiments were conducted in the frequency range from 0.10Hz to 10Hz. It was observed that the E' and tan∂-mass loss curves had similar features at all frequencies. They were more distinguishable, however, at 0.10Hz. Prior to conducting the experiments the calibration of the equipment was checked using standard weights and a steel bar.

2.6 The room temperature test

The DMA tests in this study involved step by step drying on test samples at room temperature. The removal of water was achieved by the application of vacuum or a combination of vacuum and heat in a special drying cell. Maximum care was taken in the sample treatment. The combination of vacuum and heat was applied over a lengthy drying period in order to avoid any physical damage to the samples. The initial mass-loss levels were obtained only through vacuum at room temperature. The temperature was gradually increased and only exceeded 50°C at mass-loss values above about 8%. Additional drying temperatures at higher mass-losses did not exceed 110 °C .The experiments involved the incremental removal of water from each sample prior to each test run. E' and tan∂ versus mass-loss curves were constructed for each test specimen. The construction of each curve involved up to 15 DMA tests on the same sample and took up to two weeks to complete. Specimens were covered with a very thin polyethylene film during testing to minimize mass-loss during a test. It was pre-determined that the film had a negligible effect on modulus values. It also minimized any effect of carbonation. Further thermogravimetric analysis (TGA) was performed on samples before and after testing. The extent of carbonation was very small. Three separate tests were conducted for each series of samples.

2.7 The DMTA test

The DMTA experiments were performed on the same instrument as the DMA experiments. The samples were heated from 25°C to 300°C. Temperature was increased in increments of 2°C every 5 minutes. E' and tan∂ versus temperature curves were plotted. Each test took about 11h and 45min.to complete. It is apparent that the DMTA tests are much less tedious and time consuming to perform compared to DMA tests at room temperature. Mass-loss occurred during the test due to temperature increases. Temperatures associated with mass-loss or phase transition events for the pastes or the clay minerals studied are well known and are referred to in the following sections.

3 Results and Discussion

Published data on the experimentally determined mechanical properties of 1.4nm tobermorite and jennite are essentially non-existant. The primary objective of this work was to obtain this basic information through the application of DMTA methods to these systems as it is germane to any assessment of compositional models for C-S-H in hydrated cement systems. The discussion will also draw on published data concerning the structure and character of the clay minerals and synthetic C-S-H utilized in this study. In addition it was felt that the simultaneous monitoring of mechanical behavior accompanying the removal of water from the 11% RH condition would enhance discussion of the nanostructural role of surface and interlayer water on mechanical performance of the layered silicates investigated in this work.

Drying of cement paste is of considerable interest in cement science as the physical and chemical mechanisms are not fully resolved [15]. It was of interest in the current work to establish whether a DMA test at room temperature on specimens that have undergone step by step equilibrium drying from 11%RH would yield similar results (at least qualitatively) to a test where the removal of water is achieved by thermal means (as in the DMTA test). Once this premise was established inferences as to the role of interlayer water and its removal on engineering performance could be made from the results of either test.

Samples were examined using a Scanning Electron Microscope after the DMTA test. No visible microcracks were observed. In addition E' versus mass-loss curves for layered silicates are often cyclic in nature i.e. decreases in E' can be followed by increases in E'. It is unlikely that these increases would be observed if microcracking had occurred.

3.1 A brief discussion and interpretation of the results of the dynamic mechanical analysis (DMA) of C-S-H at room temperature and the similarities of the curves with those obtained by thermal DMA (referred to as DMTA) are presented in order to facilitate the broader discussion and inferences made from comparisons of the DMTA experiments on C-S-H, 1.4nm Tobermorite, Jennite and hydrated Portland cement paste systems.

Changes in the dynamic mechanical response (DMA) of synthetic C-S-H due to removal of water from the 11%RH condition at room temperature have been previously reported [17]. Plots of storage modulus (E') and the tangent of the phase angle between the load and displacement (tan∂-a measure of internal friction), as a function of mass-loss (Figure 1(a) and 1(b)) serve to illustrate the nanostructural features that influence these parameters. This includes the role of interlayer water on mechanical performance. Results for two C-S-H

systems (C/S = 1.2, Figure 1(a) and C/S = 1.5, Figure 1(b)) are plotted. The oscillatory trend in the E' and tan∂ curves was observed at all frequencies (0.1 to 10Hz) to be independent of the moisture content. The intensity of the peaks in the curves decreased with increasing frequency.

3.1 E' versus Mass-Loss-C-S-H

The E' versus mass-loss curves exhibit an inflection point at a mass-loss of 0.5% followed by a rapid decrease up to a mass-loss of about 2%. It is suggested that the removal of surface water increases the surface energy and contributes to the decrease in stiffness of C-S-H. The combined removal of surface water and interlayer water (which contributes significantly to the stiffness of the C-S-H) results in the rapid decrease. This is followed by an increase in E' up to a maximum value at about 5% mass loss (Figure 1(a)) with a further decrease in E' as mass loss increases from about 5% to about 12%.The stiffening effect is less pronounced for C/S = 1.5 and the maximum occurs at about 6% mass loss (Figure 1 (b)). This is possibly the result of structural features such as shorter average silicate chain-lengths and structural defects due to missing bridging silica tetrahedra [17]. It is known that the degree of polymerization of C-S-H is lower at higher C/S ratios [8]. Further, drying of C-S-H from the 11%RH condition to mass-loss values >5% results in an increase in the degree of polymerization [27]. The calcium ions in the interlayer region can also play a role in stiffening the silicate layers i.e. in this mass-loss region the influence of the interlayer calcium may be less dominant at C/S = 1.5 due to the effects of a larger number of structural defects. It is possible that partially dehydrated calcium ions can interact with the ≡ Si-O- groups of the short silicate chains [28]. There is a possibility of strong 'surface-cation-surface' ionic-

covalent interactions. Calcium ions can contribute to the electrostatic interactions between C-S-H sheets that are as strong as Si-O-Si chemical bonds [29]. Changes in the 002 basal spacing on drying of C-S-H (for C/S ratios > 1.0) as followed by X-ray diffraction methods also indicate that a significant decrease in basal-spacing occurs at a mass loss between 4 and 5% bringing the silicate sheets into closer proximity [17]. The decrease in E' with mass loss >5% is a result of the removal of the final quantities of interlayer water which provide structural stability to the layered nanostructure.

3.2 Tan∂ versus Mass-Loss-C-S-H

The removal of water from a layered silicate such as C-S-H is influenced by the process itself that include incremental changes that are taking place in the nanostructure. A description of these processes follows. There are two peaks observed in the tan∂ versus mass-loss figures for C/S = 1.2. The two peaks occur due to the progressive structural collapse and its influence on the energy requirements for water removal. Tan∂ initially increases with mass-loss when E' decreases (Figure 1(a)). The initial removal of surface adsorbed water and interlayer water results in an increase in tan∂ values. This may be due to the increased ability of the layers to translate since water molecules are considered to restrain the C-S-H sheets [17, 22]. This increase in internal friction reaches a maximum at about 2% mass loss which matches well the minimum reached in the E' versus mass loss curve. The decrease in internal friction following the peak at 2% mass loss is likely a result of cross-linking between the silicate layers and an increase in the degree of polymerization. An increase in the interaction of calcium ions with the silicate sheets may contribute to this effect. The damping behavior of

C-S-H may be reduced by bridging of the C-S-H and an increase in the number of strong bonds (either Si-O-Si or ≡Si-O^-- Ca^{2+}). Subsequent increase in damping as more interlayer water is removed may be due to sliding of the silicate sheets as they come closer together. The decline after the second maximum is attributed to the remaining amount of interlayer water and possibly some constitutional water at higher mass-loss. The second peak is significantly reduced. The magnitude of the second peak is affected by the processes and parameters that influence structural collapse and water removal. It is emphasized that the C-S-H solid is constantly changing during the test and that the restraint on particle translation decreases the magnitude of internal friction. The shift of the peaks to a higher temperature reflects the minimal energy required to overcome these constraints. The extent of the latter is dependent on the C/S ratio (number of structural defects) and the initial pore structure and the constraints on mass transfer of water.

Tan∂ for C/S = 1.5 has a similar cyclic behavior exhibiting two maxima but at different mass-loss values. Higher C/S ratio C-S-H contains a greater amount of interlayer water that may have an influence on the position of these peaks (Figure 1(b)).

3.3 Comparison of DMTA and DMA Results- C-S-H

The range of values of E' and tan∂ differ significantly for the C/S = 1.2 material in Figure 1(a) (DMA results) and in Figure 2 (DMTA results). The curves in Figure 1(a) represent the results for compacted specimens prepared at about 44% porosity. The curves in Figure 2 were plotted for specimens prepared at 20% porosity. Emphasis in the choice of porosity levels

was placed on clarity of presentation given similarities in oscillatory behavior at different porosity levels.

The DMTA curves for C-S-H essentially mimic those obtained from room temperature DMA experiments (Figure 2). The initial value of E' is referred to as the first peak. The E' versus temperature curves then exhibit a decrease in stiffness with a minimum occurring at about 50°C followed by an increase reaching a maximum or second peak at about 75°C (C/S = 1.2). These peaks are associated with the removal of adsorbed and interlayer water. The second peak is significantly reduced at lower C/S ratios e.g. C/S = 0.8, (not shown). Similarly the tan∂ versus temperature curves exhibit two low temperature peaks at about 35 and 70°C (C/S = 1.2). The second peak shifts to higher temperatures at lower C/S ratios i.e. C/S = 0.8.These two peaks are due to the removal of interlayer water occurring with the continual collapse of structure. The translation of the layers into closer proximity results in a partial increase in tan∂. A small increase in the values of E' and tan∂ occurs at about 150 to 175 °C possibly due to the loss of some chemically bound water. Chemically bound water is continuously removed as 1.4nm tobermorite, jennite and C-S-H is heated from 100-1000 °C [8]. These and the TG results of Kirkpatrick show that a significant part of the chemically bound water is removed by 175°C [18]. Mass-loss curves obtained in this study for C-S-H (C/S = 0.8 and 1.2), jennite and 1.4 nm tobermorite on heating from 25°C to 1000 °C correspond to those of Taylor and Kirkpatrick. These are plotted in Figure 3. Moreover Alizadeh et. al. argued that a small increase in tan∂ is due to removal of interlayer water occurring with the continuous collapse of structure [27]. An increase in the frequency generally results in less intensified peaks for both E' and tan∂ curves, similar to observations for the DMA experiments. The

general features of the DMTA curves can be explained as described in the previous section for the DMA curves. It appears that the virtually continuous DMTA curves (containing a large number of data points) provide similar information on the nanostructural behavior of C-S-H due to removal of water as can be obtained in DMA experiments with fewer data points (about 15). The DMA room temperature experiments generally take up to two weeks to complete given the quasi- equilibrium nature of the water removal process. The DMTA experiments provide qualitatively similar information in considerably less time.

3.4 Comparison of DMTA and DMA Results- Hydrated Portland Cement

The DMTA curves for hydrated Portland cement (Figure 4(a)) are also similar to those obtained from room temperature DMA experiments (Figure 4(b)). The E' versus temperature curve for cement paste (w/c ratio = 0.40) continuously decreases with temperature. There is an initial decrease in E' to about 65°C followed by a more gradual decrease (change in slope) as the temperature is increased to about 200°C. The tan∂ versus temperature curve increases to a maximum at about 60°C and then decreases at about 85°C. This is followed by an increase in internal friction to an inflection point at 110°C and subsequent decrease to 125°C. Further heating to 200°C results in a gradual increase. The DMA results plotted in Figure 4(b) show variations in stiffness and damping. These can be explained in a similar manner to those for C-S-H described previously. There is an initial significant decrease up to a 2% mass-loss due to the removal of adsorbed and some interlayer water. This is followed by a plateau in the curve. The C-S-H in cement paste is nearly amorphous and incorporates in its structure elements such as aluminum. This may reduce the cross-linking potential and

interaction of silicate sites in cement paste that contribute to the increase in stiffness of C-S-H. It is noteworthy that C-S-H has only a small increase in stiffness in this mass-loss region when the C/S = 1.5. It is apparent that nanostructural effects of C-S-H i.e. larger number of defects and smaller silicate chain-lengths influence the magnitude of stiffness at these moisture contents [17]. The C/S ratio in cement paste is typically around 1.70 [1]. An additional decrease in E' (although it is only about 2GPa) results from a further decrease in mass-loss (6% to 9.5%). This is likely due to further collapse of the silicate layers and the removal of the remaining interlayer water. The tan∂ curve shows two maxima and their appearance corresponds well with similar behavior of synthetic C-S-H. The explanation of these similarities is also provided in the previous section on DMA of C-S-H. These results will be revisited and discussed in a section to follow that compares all the systems investigated and their relevance to behavioral models of the nanostructure of hydrated Portland cement. It can be stated however that DMTA and room temperature DMA parameters, as a function of mass-loss, provide fundamentally similar information for the systems studied.

3.5 DMTA of 1.4 nm Tobermorite

DMTA curves of E' and tan∂ versus temperature for 1.4 nm tobermorite conditioned at 11% RH are presented in Figure 5. The thermal dehydration studies of Yu and Kirkpatrick [18], ^{43}Ca NMR investigations of Bowers and Kirkpatrick [30], Raman spectroscopy studies of Kirkpatrick et. al. [31] and the ^{27}Al and ^{29}Si MAS NMR studies of Komarneniet et. al. [32], provide useful insights on the features of these curves. The data included observations related

to the determination of the temperature ranges for the various phase transitions that occur on thermal treatment of tobermorite obtained by using a variety of analytical and spectroscopic methods. Specifically these entailed the following: surface and interlayer water removal at temperatures up to 60°C ;conversion from the 1.4nm form to the 1.2nm form and removal of additional interlayer water between 60 and 100 °C; conversion from the 1.2nm form to the 1.1nm form between 130 to 200 °C; conversion to the 0.96nm form at temperatures up to 260°C.

3.6.1 E' versus Temperature

There is a decrease in E' over four distinct temperature ranges (Figure 5) involving changes in the slope as the temperature increases to about 130°C (i.e. 25-35°C; 35-60°C; 60-100°C; 100-130°C). The results for a specimen porosity of 59% were chosen for clarity as the peak and inflections of the curves in the figure are clear and distinct. The frequency level was 3.98 Hz. Peaks and inflections at other porosity levels occur in similar locations but vary in intensity level. Additional discussion of porosity effects is provided in a discussion to follow. The removal of adsorbed water occurs in the first temperature range possibly overlapping with the removal of interlayer water. The second range likely corresponds to further removal of interlayer water. Interlayer water (as discussed previously) can have a structural role in layered calcium silicate hydrate systems contributing a stiffening effect [25]. The decrease in E' results from the removal of both surface water and interlayer water as the temperature increases to about 60°C. Removal of a further amount of interlayer water and the conversion of 1.4nm tobermorite to the 1.2nm form occurs in the third temperature range (60-100°C).

The conversion is accompanied by a significant density change (2.23 g/cm^3 to about 2.40 g/cm^3, [33]) resulting in an increase in porosity along with a loss of 4 moles of structural water [18]. The additional loss of interlayer water and increase in porosity are responsible for the continuing decrease in E' throughout this temperature range. There is a small increase in E' reaching a maximum as the temperature increases from 130 to 160°C followed by a continuous decrease to 300°C. There is a conversion from the 1.2nm tobermorite to the 1.1nm form in the temperature range, 130-200°C and a transformation to the 0.96 form at about 260°C. This is accompanied by loss of an additional 2 moles of water at 200°C and a further 2 moles of water at about 260°C. There is also an increase in density and porosity associated with these conversions. A density of 2.48 g/cm^3 has been reported for the 1.1nm form [33]. The maximum value of E' at 160°C may be explained as follows. The gradual decrease in the basal spacing coupled with possible interaction of the interlayer Ca^{2+} ions with the silicate sheets (as described previously for C-S-H systems) and the stiffening effect of the remaining water molecules in the interlayer space may override any weakening effect due to conversion to the 1.1nm form and the resulting porosity increase [17,18,33]. The decrease in E' upon further heating beyond 160°C may be a result of the combined effects of the final removal of interlayer water and the conversion to the 0.96nm form of tobermorite.

3.6.2 Tan∂ versus Temperature

There are four distinct peaks at about 35°C, 75°C, 100°C and 130°C in the tan∂ versus temperature curves for 1.4nm tobermorite where tan∂ increases to a maximum and then

decreases (Figure 5). There is a significant decrease in the value of tan∂ in the temperature range 130-175°C. Following this the slope of the curve significantly decreases as the temperature increases to 300°C. The first two peaks occur in the temperature region associated with the removal of surface and interlayer water. This process results in an increase in internal friction. The decrease in tan∂ following the peak maxima is possibly due to cross-linking effects and the interaction of Ca^{2+} ions with the silicate sheets. The second maximum arises due to the continued removal of interlayer water. The peak at 100°C is likely associated with the conversion of 1.4nm tobermorite to the 1.2 form. The associated increases in density and porosity and any additional removal of interlayer water are likely contributors to the increase in internal friction. The decrease is again possibly due to ionic-covalent interactions between the sheets as the basal spacing is reduced with further increments of interlayer water removal. The increase in tan∂ beginning at about 110°C, reaching a maximum at 130°C, and subsequently decreasing as the temperature increases to about 200°C is associated with the transformation of 1.2nm tobermorite to the 1.1nm form. The increase in internal friction is apparently influenced by the increased porosity and removal of interlayer water in this temperature range. The decrease after the maximum may be due to additional cross- linking and ionic-covalent interactions with the silicate sheets that may occur as the basal spacing decreases. The gradual decrease in tan∂ after 275°C results from the loss of the final 2 moles of interlayer water and the increased porosity resulting from the conversion to the 0.96 nm form of tobermorite. The loss of interlayer water and additional decrease in basal-spacing would appear to dominate the effect as an increase in porosity would generally tend to increase the internal friction.

3.7 DMTA of Jennite

DMTA curves of E' and tan∂ versus temperature for jennite conditioned at 11%RH are presented in Figure 6.Yu and Kirkpatrick studied the thermal dehydration of jennite and identified, using a variety of techniques, the corresponding phase transition to metajennite and mass changes that occur at temperatures up to 300°C [18]. The curves for jennite in the figure are for compacts prepared at a porosity of 48%. They were chosen for clarity as the peaks and inflections in the curves are clear and distinct. Further details about porosity effects are provided in a section to follow.

3.7.1 E' versus Temperature

There are 4 distinct temperature ranges in the E' versus temperature curve in Figure 6 (25-35°C, 35-85°C, 85-175°C, 175-300°C) [18,19]. There is a gradual decrease in the value of E' between 25 and 35°C largely due to the loss of adsorbed surface water. This is followed by a more rapid decrease in E' as the temperature increases to about 85°C that is attributed primarily to the loss of interlayer water. It is clear that interlayer water has a structural role in the mechanical behavior of jennite. Metajennite forms in the third temperature range as the basal spacing changes from 1.06nm to 0.86nm. There is a loss of 4 water molecules from the structural unit and a large change in density from 2.33g/cm^2 to 2.62 g/cm^2 accompanied by an increase in porosity [33]. The values of E' in this temperature range remain relatively constant suggesting that the new phase is intrinsically stiffer than jennite itself as it would otherwise be expected that increases in porosity would result in a reduction in stiffness.

Further removal of interlayer water (about 2 moles) on heating to 300°C results in a further decrease in E' suggesting that the final 2 moles of water have a significant effect in maintaining the structural integrity of metajennite. Metajennite is also transformed into a disordered phase above 250°C [18]. This phase appears to contribute to the low stiffness values that are observed.

3.7.2 Tan∂ versus Temperature

The phase transitions and thermal events that correspond to the dehydration of jennite have been well documented as was previously mentioned for 1.4nm tobermorite [18-21]. The removal of interlayer water from layered silicates involves continual changes to the solid as the water is considered part of the solid crystallite. The mass transport is affected by these changes and the structural collapse processes that occur. Decreases in tan∂ or internal friction of layered silicates result from restraints on translation of silicate sheets that are affected by these processes. The oscillatory nature of the curves is a result of the transient collapse process that interferes with the removal of interlayer water. The tan∂ versus temperature curves illustrate this.

There are three distinct peaks at about 50, 80 and 145°C in the tan∂ versus temperature curves, Figure 6. There are also 3 clear points of inflection at about 35, 110 and 175°C. The increase in tan∂ (internal friction) from 25 to 35°C is largely due to loss of surface adsorbed water and possibly some interlayer water. The increase from 35°C to 50°C is likely due to the removal of interlayer water. The decrease in tan∂ from 50 to 75°C may also be linked to

the interactions of interlayer Ca^{2+} ions with the silicate sheets as there are Ca^{2+} and water molecules in the interlayer space. There are no Q^3 signals observed in the ^{29}Si MAS NMR experiments [18] with jennite unlike the case for tobermorite suggesting that any cross-linking of the silicate sheets may be minimal in the jennite system. The small increase in tan∂ leading to a maximum in the 75 to 85°C temperature range is consistently present over a wide range of frequencies and is possibly due to further removal of interlayer water and additional interaction of Ca^{2+} ions with the silicate sheets. The large increase in tan∂ between 85 and 145°C is associated with the formation of metajennite, the accompanying loss of 4 water molecules from the interlayer and the significant increase in density and porosity as indicated in the previous section. Further removal of 2 moles of water from metajennite in the temperature range 145 to 220°C likely results in additional interactions involving interlayer Ca^{2+}. The removal of water may be a two step process as there is a change in slope at 175°C that also corresponds with the beginning of a significant decrease in E' as noted in the previous section. There is a gradual increase in tan∂ as the temperature increases from 220 to 300°C. This is likely related to the formation of a disordered phase [18].

3.8 DMTA-Porosity/Compaction Effects

Porosity of compacted cement systems is controlled by the pressure used to compact the hydrated cement powders. It has been shown that the porosity dependence of the elastic modulus of compacted pastes is similar to that for paste hydrated specimens [25]. Hence compaction effects translate into porosity effects.

E' for the compacted C-S-H preparations (at room temperature) has been generally shown to be porosity dependent [17]. The E' versus porosity curves for the C-S-H systems used in this study are plotted in (Figure 7(a)). Plotted on the same curve are the results for 1.4 nm tobermorite and jennite. The data for jennite is shifted to lower porosity values relative to tobermorite. The data for tobermorite is closer to the curve for C-S-H with C/S = 1.5. The data for hydrated cement paste (2-3 months old; degree of hydration determined by TGA methods is 77%) is close to the trend line for jennite. The C-S-H present in cement paste has been reported to have C/S ratios varying from 1.5 to 2.3 with typical values being about 1.7 [8].The range of E' values (5-25 GPa) for all these systems including hydrated cement paste is similar.

The tan∂-porosity curves for the systems studied are plotted in Figure 7(b).The curve for 1.4nm tobermorite lies above the curve for jennite. The curves for the C-S-H preparations and cement paste lie between these two curves indicating that the latter could be represented by an average of the curves for tobermorite and jennite.

A brief description of the porosity dependence of the E' and tan∂ versus temperature curves (not shown) for jennite follows (frequency = 3.98 Hz). The porosity range investigated was 23% to 48%.

The E' versus temperature curves at each porosity level were all very similar. This can be seen in Figure 8 where plots are shown for jennite specimens with porosity values varying from 23 to 48%. The initial region from 25-35°C due primarily to the removal of adsorbed

water was unaffected except for the lowest porosity material at 24% porosity where the initial region extended to 50°C. This was likely due to the more restricted diffusion path for the removal of water. The second region exhibiting a rapid decrease in E' extended to temperatures varying between 85 and 120°C with the higher temperatures associated with lower porosity. This region was associated primarily with the removal of interlayer water. The third or 'plateau' region extended from about 170 to 250◦C with higher temperatures associated with lower porosities. This region is associated with the formation and slow decomposition of metajennite. The final region exhibits a more rapid decline in E' associated with the formation of a disordered phase. In general higher porosity materials tend to shift the regions to higher temperatures. The general nature of the E' relationships, however, remains unchanged.

The low temperature tan∂ maxima associated with removal of surface and interlayer water shift slightly to higher temperatures at lower porosities. The intensities of the peaks are not significantly different. The peaks associated with the formation and subsequent slow decomposition of metajennite do not significantly change in intensity except at the lowest porosity levels where the peak is reduced to an inflection point at 130°C following a decrease in slope beginning at about 110°C. Initial tan∂ values are higher at the lowest porosity values, i.e. 24.8%.The porosity related effects do not alter the general nature of the E' and tan∂ versus temperature curves.

Variations in porosity have only a minor effect over most of the porosity range (30 to 59%) on the E' and tan∂ versus temperature curves for 1.4 nm tobermorite (Figure 9). The shape of the E' curves at each porosity level is similar with a gradual decrease in E' as temperature

increases to 300°C (Figure 9(a). There are also similarities in the tan∂ curves with notable differences for the tan∂ curve of the lowest porosity system (porosity = 30%), (See plots of the curves for porosity values of 30 and 59%, Figure 9(b)). The low temperature inflections and slope changes in the tan∂ curve for the low porosity curve (30%) were not as readily apparent. The peak at 150°C associated with the transformation to 1.1nm tobermorite is present but with reduced intensity. It is apparent that low porosity systems can restrict the translation of silicate sheets resulting in lower increases in internal friction.

3.9 Commentary on the DMTA of the Layered Calcium Silicate Hydrates

A comparison of the DMTA results of the layered calcium silicate hydrate systems studied (all initially at 11%RH) and hydrated Portland cement follows. It will be limited to the temperature range 25°C to 100°C as thermally activated structural transitions occur at higher temperatures for the 1.4nm tobermorite and jennite materials.

The E' versus temperature curves for jennite are remarkably similar to those for hydrated Portland cement paste. There is a rapid continuous and monotonic decrease in E' (between 25 and 110°C) of about 3.8GPa at a similar porosity level e.g.33-35%, as surface and interlayer water is removed. The decrease in E' for 1.4nm tobermorite over the same temperature range is continuous but not monotonic as the conversion of 1.4nm tobermorite to the 1.2 nm form occurs in this temperature range. The decrease in E' at 32% porosity is about 1.8 GPa, significantly less than that for jennite and hydrated Portland cement paste.

The Portland cement paste investigated here (water/cement ratio =0.40) was hydrated for 2 months. One of Taylor's hypotheses was that the C-S-H that forms when cement hydrates is a mixture of tobermorite-type and jennite-type structures [8]. It was suggested that the initial formation of tobermorite–type followed by jennite-type structures could provide an explanation for the observed changes of anion size distribution with time while maintaining a Ca/Si ratio of about 0.8. The E' versus temperature curve for a 50/50 mixture of 1.4nm tobermorite and jennite (24% porosity) (Figure 10 (a)) has a higher value of E' at 25°C than that for Portland cement paste (water/cement ratio = 0.40, 30% porosity). E' remains higher up to 60°C when both systems have values of E' = 11GPa. This is also the case for phase pure tobermorite (porosity = 40%) where E' at 25°C is 11GPa. E' for HCP then decreases from about 13GPa at 25°C to about 10 GPa at 110°C which is similar for 50J/50T and tobermorite.for both systems. The shape of the E' versus temperature curve is well matched for both systems. E' for phase pure jennite (porosity = 33%) is 16.3 GPa at 25°C. The E' data in this study indicate that there is a similar mechanical response (qualitative) for cement paste to that of the pure jennite (with reference to the shape of the curve). This suggests the possibility that more mature cement pastes may have more jennite type C-S-H structures or that jennite-type structures have a dominate contribution to E'.

The decrease in E' for synthetic C-S-H (C/S ratio = 1.2, Figure 2) from its initial value of 7.3 GPa to its minimum value is about 4.2GPa obtained at the same frequency (3.98Hz) as the 1.4 tobermorite and jennite systems. This occurs at about 50°C for synthetic C-S-H and is followed by an increase in E' as previously noted. There are much larger decreases in E' with temperature for synthetic C-S-H having low C/S ratio values e.g. the system with C/S = 0.80

has a drop in E' value of about 7 GPa at a similar frequency. The results for the higher C/S ratio C-S-H systems are more analogous to those for hydrated cement paste than those for the lower C/S ratio systems as might be expected.

The tan∂ curves for the 50/50 mixtures exhibit three low temperature peaks at about 35, 60, and 85 °C. The characteristics of the corresponding curves for pure jennite and tobermorite phases have been described in previous sections.

The tan∂ curve for hydrated Portland cement is significantly different than those for the other layered silicate systems (Figure 10(b)) largely due to the amorphous nature of the C-S-H present.

There is an increase in tan∂ up to about 75°C as surface adsorbed and interlayer water is removed followed by a small decrease as temperature increases to about 120°C. The C-S-H in hydrated Portland cement does not exhibit an X-ray basal-spacing.

The tan∂ versus temperature curves for all the layered calcium silicate hydrate systems studied, other than hydrated Portland cement, exhibit some general similarities. They contain two regions featuring peaks where increases in internal friction occur reaching a maximum followed by decreases in internal friction. In the preceding discussions these peaks have been attributed to the removal of surface and interlayer water and the role of interlayer Ca^{2+}.These peaks occur at the following temperatures for the corresponding silicate type: 40 and 80°C (1.4nm tobermorite); 55 and 80°C (jennite) ; 35 and 65°C (C-S-H;C/S = 1.2); 60 and 110°C (hydrated cement paste); 45 and 95°C (50/50 1.4nm tobermorite/jennite mixture).The tan∂ curves for the 50J/50T, HPC phase pure jennite are shown in Figure 10(b).The porosity

levels were 24 and 30%. and frequencies, 3.98-5Hz. The curves provide useful data for evaluating Taylor's views of a possible tobermorite- jennite structural model for the C-S-H present in hydrated cement paste as mentioned above [8].

4 Conclusions

1. Dynamic mechanical thermal analysis (DMTA) information is similar to that obtained using dynamic mechanical analysis (DMA) at room temperature when mass-loss occurs due to equilibrium drying of thin specimens. Nanostructural changes due to drying of thin C-S-H specimens from 11%RH can be detected using DMTA

2. Thermally activated phase transitions in 1.4 nm tobermorite (e.g. the 1.4 form to the 1.2 and 1.1 forms) and in jennite (e.g. jennite to metajennite) can be detected using DMTA.

3. Changes to the storage modulus (E') and internal friction (tan∂) due to drying of synthetic C-S-H, 1.4nm tobermorite and jennite can be explained by the removal of interlayer water, interactions of interlayer Ca^{2+} with the silicate sheets and potentially cross-linking effects.

4. The changes in E' and tan∂ for all the layered silicate systems studied can be rationalized using a layered calcium silicate hydrate model.

5. Changes in E' and tan∂ for hardened cement paste on drying from 11%RH have both differences and similarities to those for 1.4nm tobermorite, jennite and C-S-H (C/S = 1.5).

6. The DMTA response (E' and tan∂ versus temperature) for a 50/50 mixture of 1.4nm tobermorite and jennite (porosity = 32%) and for hydrated cement paste (water/cement =

0.40) have significant differences. This is due to the amorphous nature of C-S-H in cement paste and porosity differences.

5 References

1. Taylor H. F. W., Chapter 5, Hydration of the calcium silicate phases, Cement Chemistry, Thomas Telford Publishing, London, pp 459, 1997.

2. Feldman R. F., Sorption and length-change scanning isotherms of methanol and water on hydrated Portland cement, Vol. III, 53-56, 1968.

3. Powers T. C. and Brownyard T. L., Studies of the physical properties of hardened Portland cement paste-part 3: theoretical interpretation of adsorption data. J. Amer. Concr. Inst., 18(4), 469-504, 1946.

4. Jennings H. M., Refinements to colloid model of C-S-H in cement: CM-II. Cem. Concr. Res. 38, 275-289, 2008.

5. Daimon M., Abo-El-Enein S. A., Hosaka G., Goto S. and Kondo R., Pore structure of calcium silicate hydrate in hydrated tricalcium silicate, J. Amer. Ceram. Soc. , 60(3-4), 110-114,1977.

6. Richardson I.G. and Groves G.W., Models for the composition and structure of calcium silicate hydrate (C-S-H) gel in hardened tricalcium silicate pastes, Cem. Concr. Res., 22, 1001-1010, 1992.

7. Richardson I. G., Tobermorite/jennite- and tobermorite/calcium hydroxide-based models for the structure of C-S-H: applicability to hardened pastes of tricalcium silicate, Portland cement, and blends of Portland cement with blast-furnace slag, metakaolin, or silica fume, Cem. Concr. Res., 34, 1733-1777, 2004.

8. Taylor H.F.W., Proposed structure for Calcium Silicate Hydrate Gel, J. Amer. Ceram. Soc. 69, (6), 464-467, 1986.

9. Richardson I. G., The calcium silicate hydrates, Cem. Concr. Res., 38(2), 137-158, 2008.

10. Alizadeh R., Beaudoin J. J. and Raki L., C-S-H(I)-A nanostructural model for the removal of water from hydrated cement paste, J. Amer. Ceram. Soc., 90(2), 670-672, 2007.

11. Radjy F. and Sellevold E. J., Internal friction peaks due to adsorbed and capillary water in microporous substances, Nature Physical Science, 241, 133-135, 1973.

12. Radjy F. and Richards C. W., Effect of curing and heat treatment history on the dynamic mechanical response and the pore structure of hardened cement paste, Cem. Concr. Res., 3, 7-21, 1973.

13. Sellevold E. J. and Radjy F., Drying and resaturation effects on internal friction in hardened cement paste, J. Amer. Ceram. Soc., 59(5-6), 256-258, 1976.

14. Radjy F. , Sellevold E. J. and Richards C. W., Effect of freezing on the dynamic mechanical response of hardened cement paste down to -60°C, Cem. Concr. Res.,2 , 697-715, 1972.

15. Feldman R. F., Assessment of experimental evidence for models of hydrated Portland cement, Highway Res. Rec. No. 370, 8-24, 1971.

16. Foray-Thevenin G., Vigier G., Vassoille R. and Orange G., Characterization of cement paste by dynamic mechanical thermo-analysis, Materials Characterization, 56, 129-137, 2006.

17. Alizadeh R., Beaudoin J. J. and Raki L., Mechanical properties of calcium silicate hydrates, Matls. and Struct., 44, 13-28, 2011.

18. Yu P. and Kirkpatrick R.J., Thermal dehydration of tobermorite and jennite, Concr. Sci. and Eng., 1, 185-191, 1999.

19. Gard J. A. and Taylor H. F. W., Calcium silicate hydrate (II) ("C-S-H(II)"), Cem. Concr. Res., 6, 667-678, 1976.

20. Hara N. and Inoue N., Formation of jennite from fumed silica, Cem. Concr. Res., 10, 677-682, 1980.

21. Soroka I. and Sereda P.J., The structure of cement- stone and use of compacts as structural models, Proc. 5th Int. Symp. on the Chem. of Cem., Vol. 3., Tokyo, 67-73,1968.

22. Feldman R. F., Factors affecting the Young's modulus-porosity relation of hydrated Portland cement compacts, Cem. Concr. Res., 2(4), 375-386, 1972.

23. Sereda P.J. and Feldman R. F., Compacts of powdered material as porous bodies for use in sorption studies, J. Appl. Chem., 13, 150-158, 1963.

24. Beaudoin J.J., Comparison of mechanical properties of compacted calcium hydroxide and Portland cement paste systems, Cem. Concr. Res., 13, 319-324, 1983.

25. Sereda P.J., Feldman R.F. and Swenson E.G., Effect of sorbed water on some mechanical

Properties of hydrated Portland cement pastes and compacts, Highway Research Board, Special Report 90, 58-73, 1966.

26. Menard K. P., Dynamic Mechanical Analysis-A Practical Introduction, CRC Press LLC, Boca Raton, pp. 208, 1999.

27. Alizadeh R., Nanostructure and engineering properties of basic and modified calcium-silicate-hydrate systems, PhD thesis, University of Ottawa, pp. 231, 2009.

28. Van Damme H. and Gmira A., Cement hydrates, Chapter 13.3 in Handbook of Clay Science, Eds.Bergaya F., Theng B.K.G. and Lagaly G., Elsevier Ltd., pp.1246, 2006.

29. Pellenq R. J.-M., Lequeux N. and Van Damme H., Engineering the bonding scheme in C-S-H: The iono-covalent framework, Cem. Concr. Res., 38, 159-174, 2008.

30. Bowers G.M. and Kirkpatrick J. R., Natural abundance ^{43}Ca NMR spectroscopy of tobermorite and jennite: Model compounds for C-S-H, J. Amer. Ceram. Soc., 92(2), 545-548, 2009.

31. Kirkpatrick J.R., Yarger J. L., McMillan P.F., Yu P. and Cong X., Raman spectroscopy of C-S-H, tobermorite and jennite., Advn. Cem. Bas. Matls, 5, 93-99, 1997.

32. Komarneniet S., Roy D.M., Fyfe C. A. and Kennedy G. J., Naturally occurring 1.4nm tobermorite and synthetic jennite characterization by ^{27}Al and ^{29}Si MAS NMR spectroscopy and cation exchange properties, Cem. Concr. Res., 17, 891-895, 1987.

33. Thomas, Jefferey J., Jennings H. M. and Allen A.J., Relationships between composition and density of tobermorite, jennite and nanoscale CaO-SiO2-H2O, J. Phys. Chem. C, 114, 7594-7601, 2010.

Figure Captions

Figure 1. DMA (room temperature) of synthetic C-S-H dried from the 11% RH condition. E' and tan∂ versus mass loss: (a) C/S = 1.2 (b) C/S = 1.5. Frequency = 0.1 Hz.

Figure 2. DMTA curves (25-300°C) of synthetic C-S-H (C/S = 1.2) heated from the 11%RH condition: E' and tan∂ versus temperature. Frequency = 3.98 Hz.

Figure 3. Mass-loss curves for C-S-H (C/S = 0.8 and 1.2), jennite and 1.4nm tobermorite on heating from 25°C to 1000°C.

Figure 4. DMTA and DMA curves for hydrated Portland cement (HPC) (w/c = 0.40): (a) DMTA- E' and tan∂ versus temperature curves for HPC heated from the 11% RH condition; (b) DMA- E'and tan∂ verses mass loss curves for HPC dried from the 11% RH condition. Frequency = 5Hz.

Figure 5. DMTA curves for 1.4nm tobermorite heated from the 11%RH condition: E' and tan∂ versus temperature curves. Frequency = 3.98Hz. Porosity = 59%.

Figure 6. DMTA curves for jennite heated from the 11%RH condition: E' and tan∂ versus temperature curves. Frequency = 3.98Hz. Porosity = 48%.

Figure 7. E' versus porosity curves (room temperature) for C-S-H, 1.4nm tobermorite, jennite and HPC.

Figure 8. E' versus temperature curves for jennite specimens prepared at porosities ranging from 23 to 43%.

Figure 9. (a) E' and (b) tan∂ versus temperature curves for 1.4nm tobermorite specimens prepared at porosities ranging from 30 to 59%.

Figure 10. E' and tan∂ versus temperature curves for a 50/50 (% by mass) mixture of 1.4nm tobermorite and jennite (30% porosity), phase pure jennite (30% porosity) and HPC (w/c = 0.40; 24% porosity).

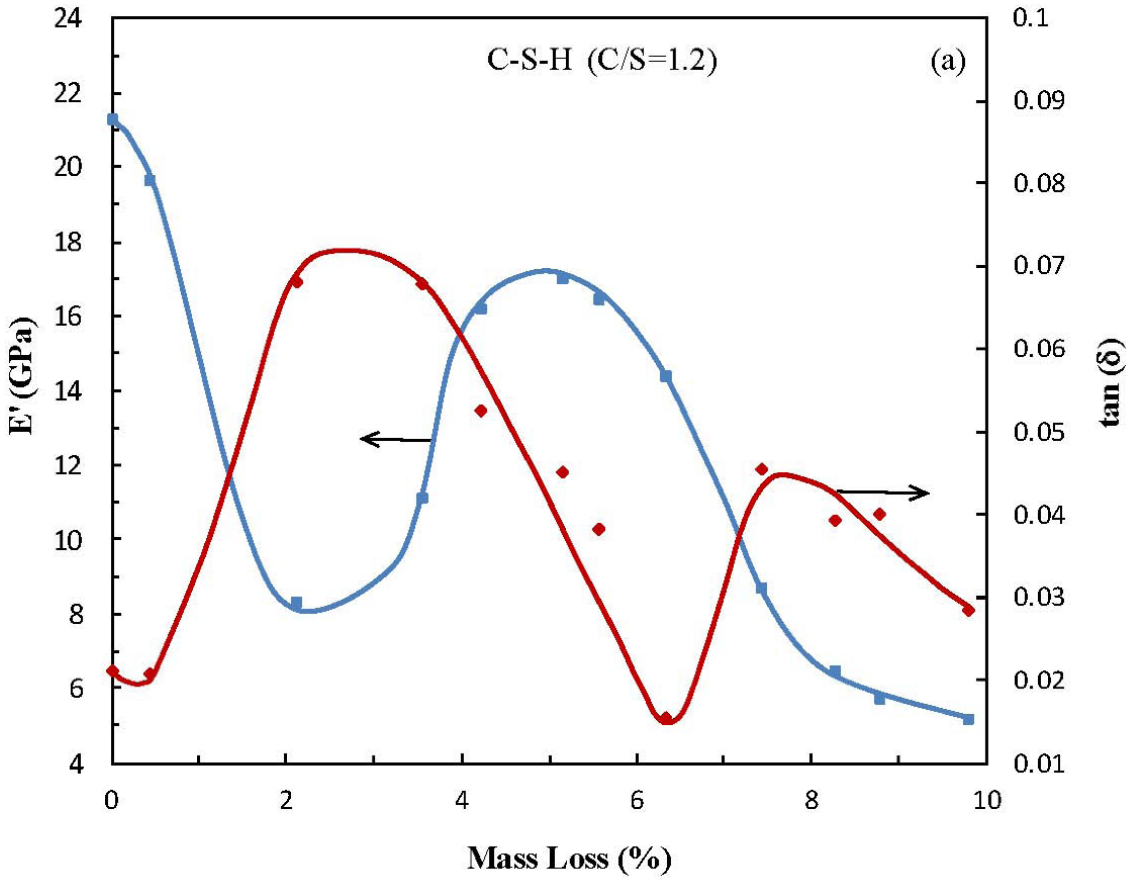

Figure 1. DMA (room temperature) of synthetic C-S-H dried from the 11% RH condition. E' and tan∂ versus mass loss: (a) C/S = 1.2. Frequency = 0.1 Hz.

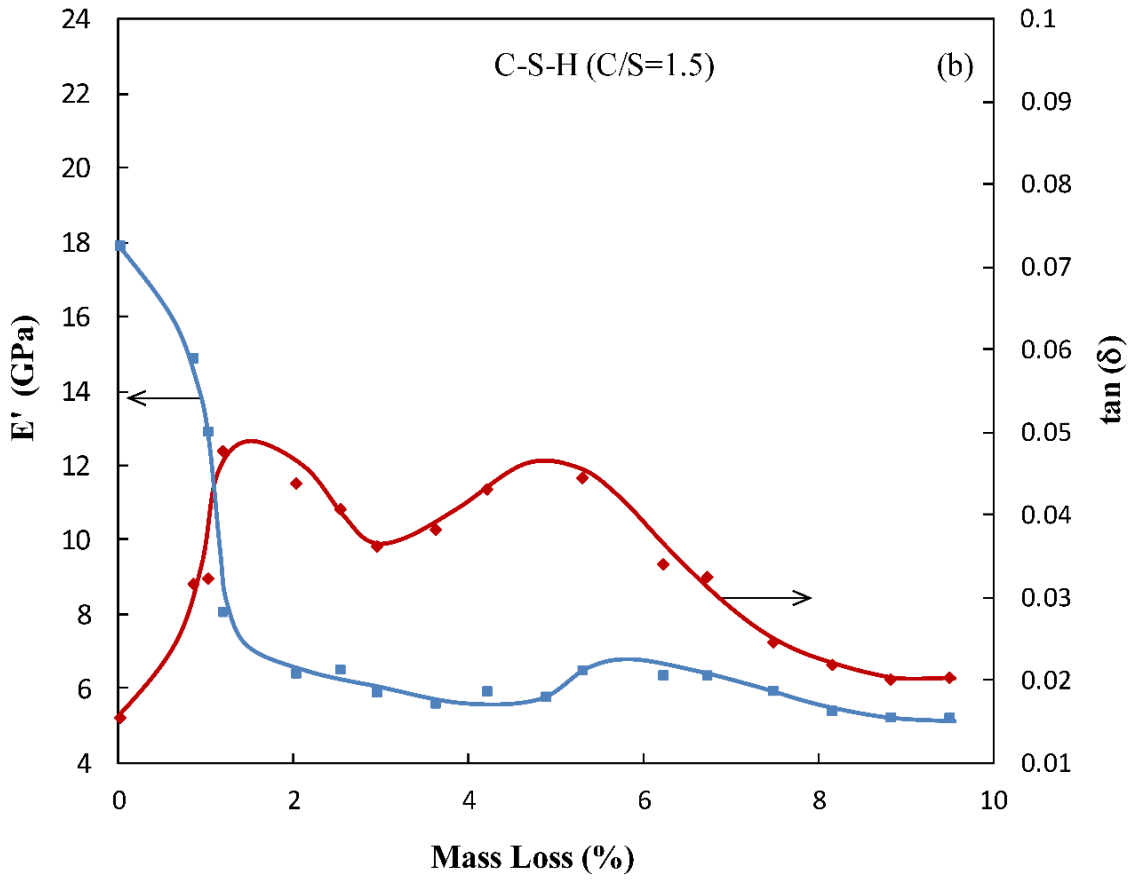

Figure 1. DMA (room temperature) of synthetic C-S-H dried from the 11% RH condition. E' and tan∂ versus mass loss: (b) C/S = 1.5. Frequency = 0.1 Hz.

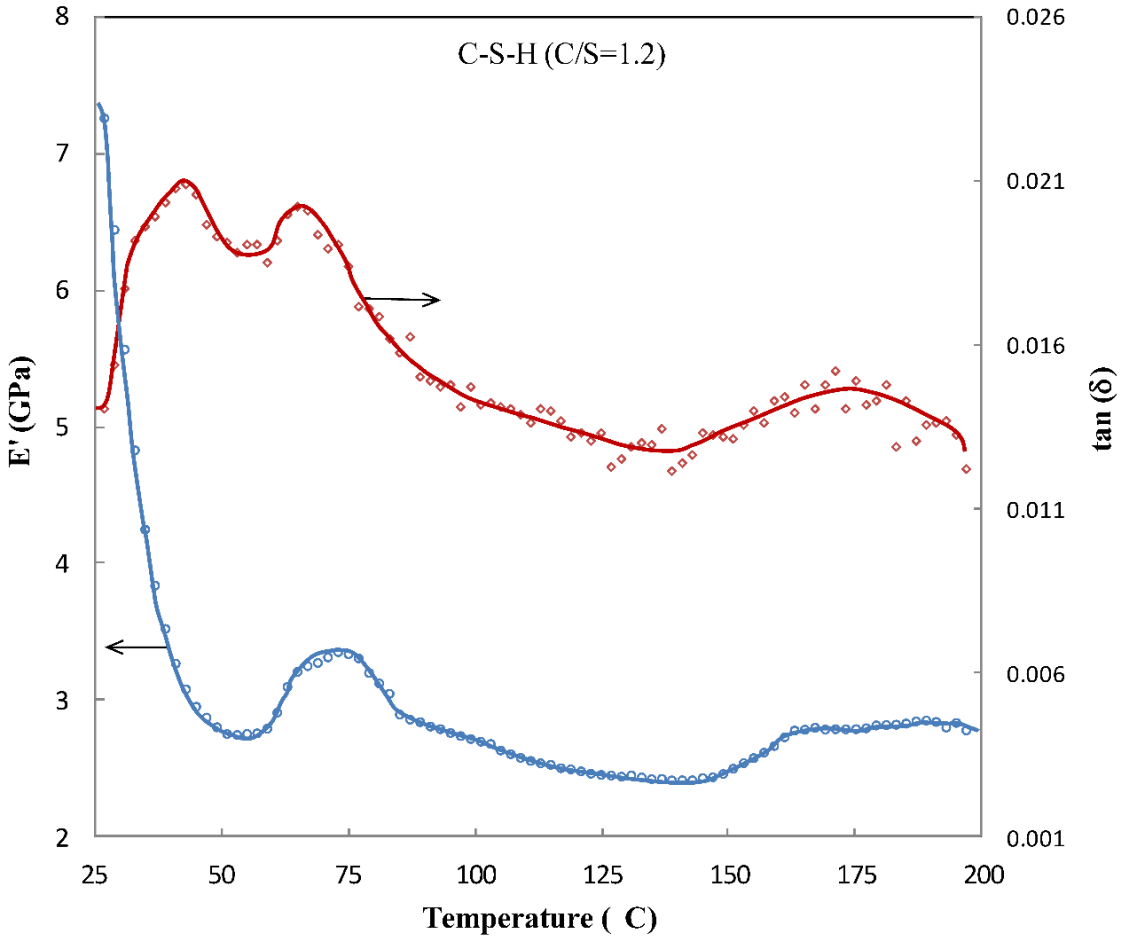

Figure 2. DMTA curves (25-300˚C) of synthetic C-S-H (C/S = 1.2) heated from the 11% RH

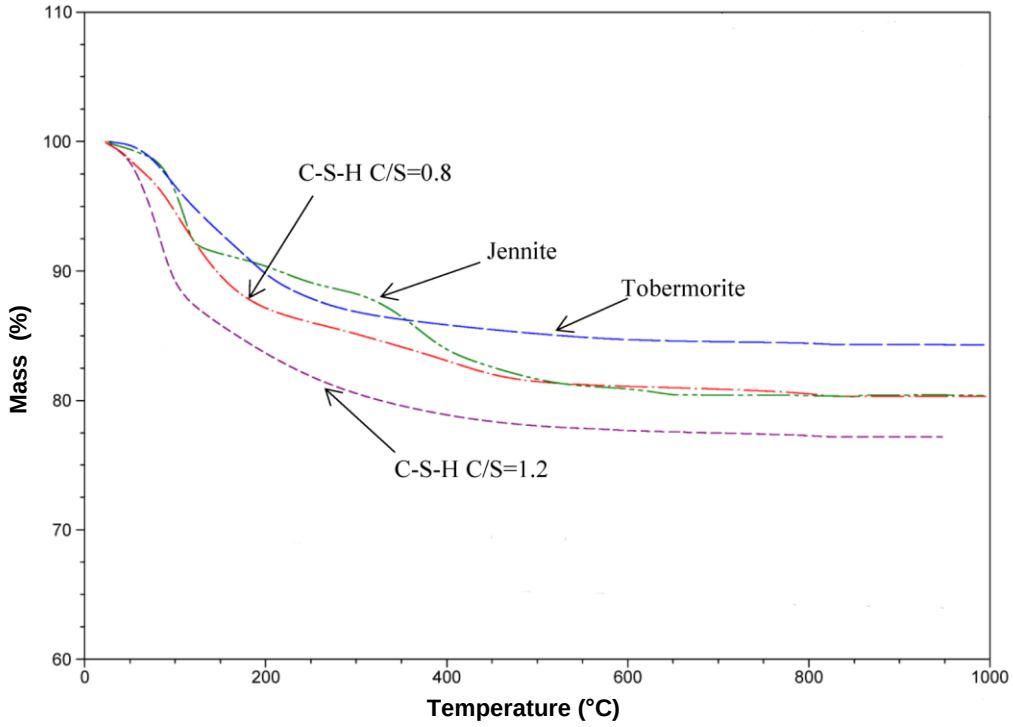

Figure 3. Mass-loss curves for C-S-H (C/S = 0.8 and 1.2), jennite and 1.4nm tobermorite on heating from 25°C to 1000°C.

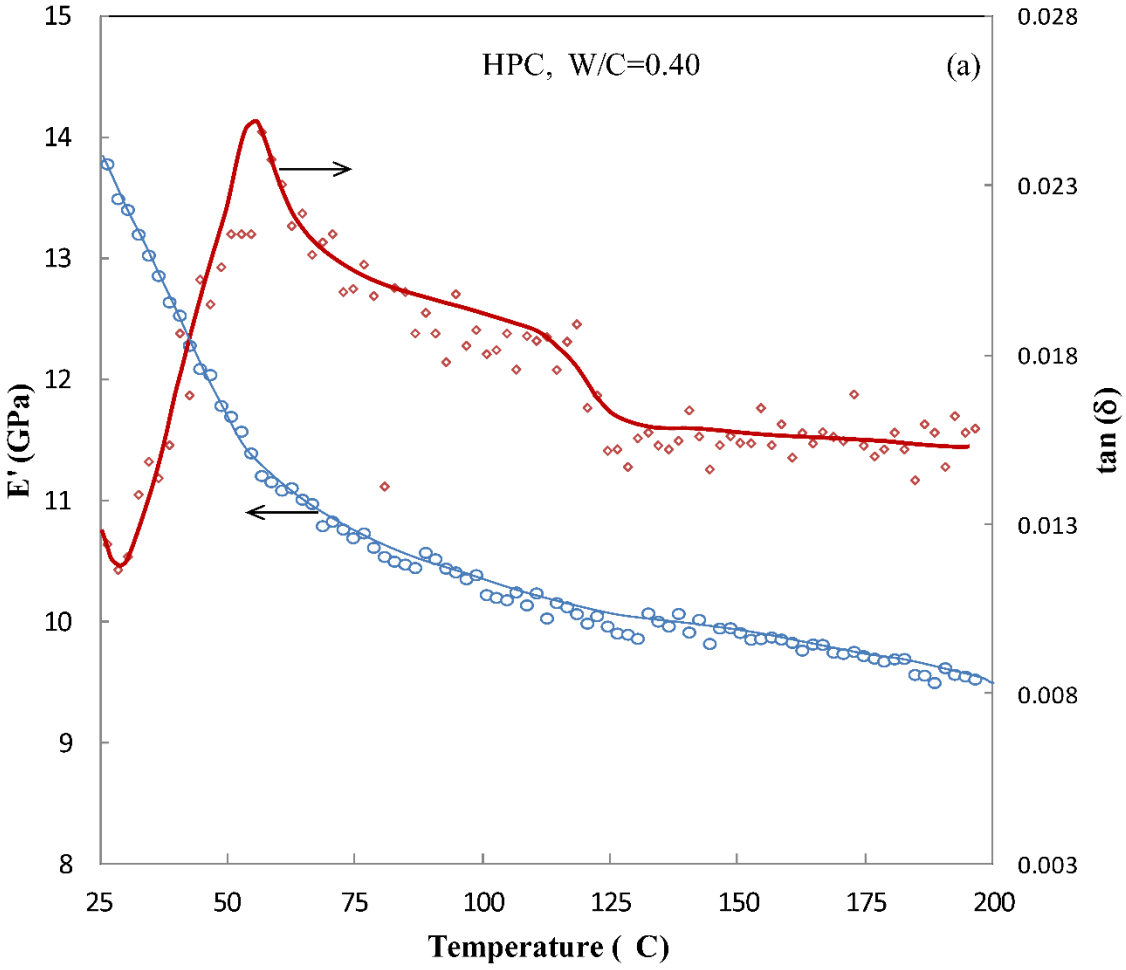

Figure 4. DMTA and DMA curves for hydrated Portland cement (HPC) (w/c = 0.40): (a) DMTA- E' and tan∂ versus temperature curves for HPC heated from the 11% RH condition.

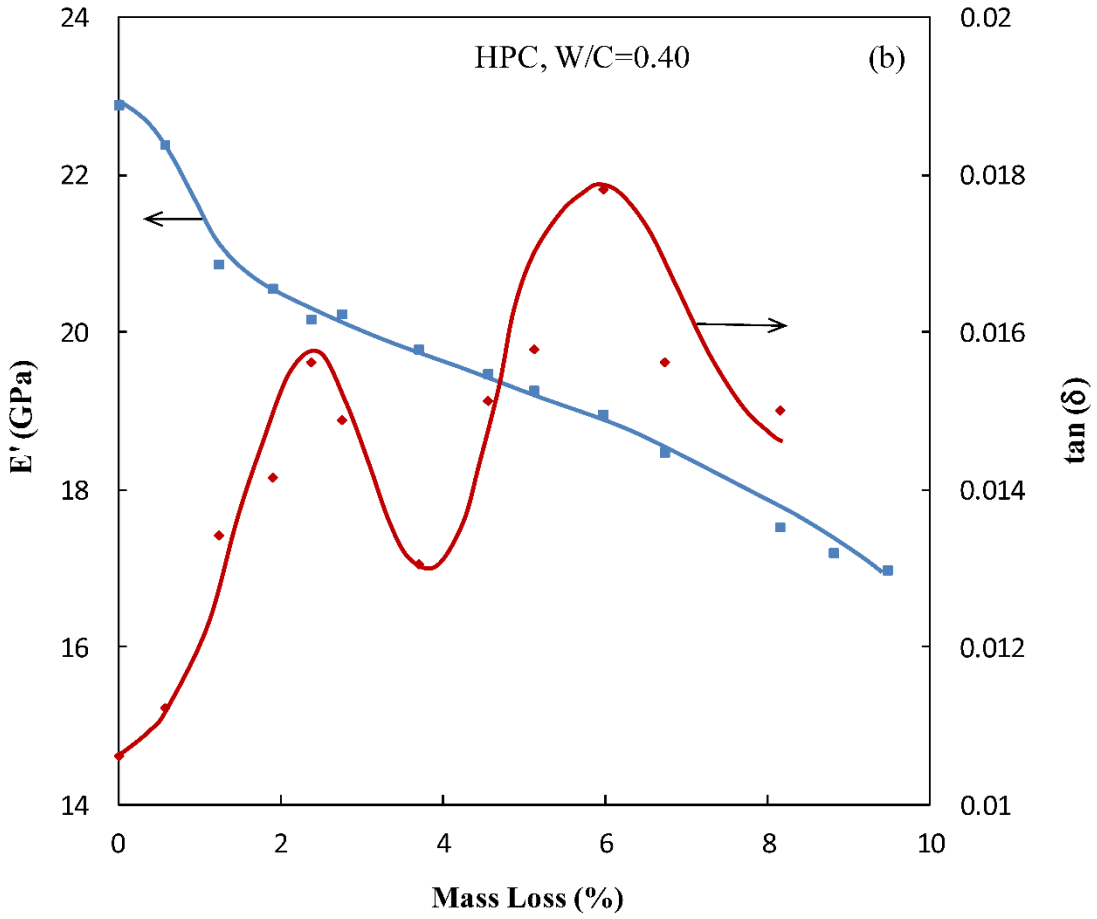

Figure 4. DMTA and DMA curves for hydrated Portland cement (HPC) (w/c = 0.40): (b) DMA- E'and tan∂ verses mass loss curves for HPC dried from the 11% RH condition. Frequency = 5Hz.

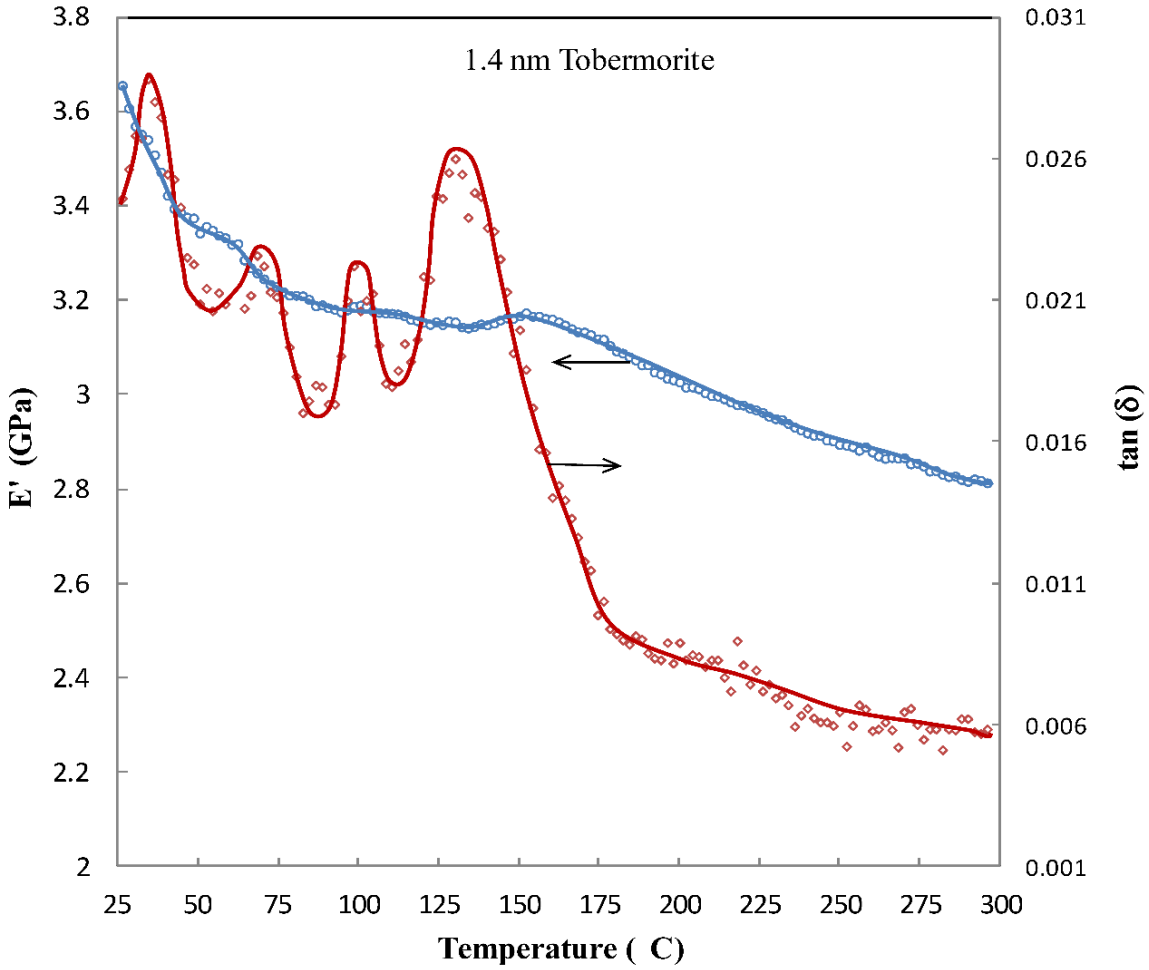

Figure 5. DMTA curves for 1.4nm tobermorite heated from the 11%RH condition: E' and tan∂ versus temperature curves. Frequency = 3.98Hz. Porosity = 59%.

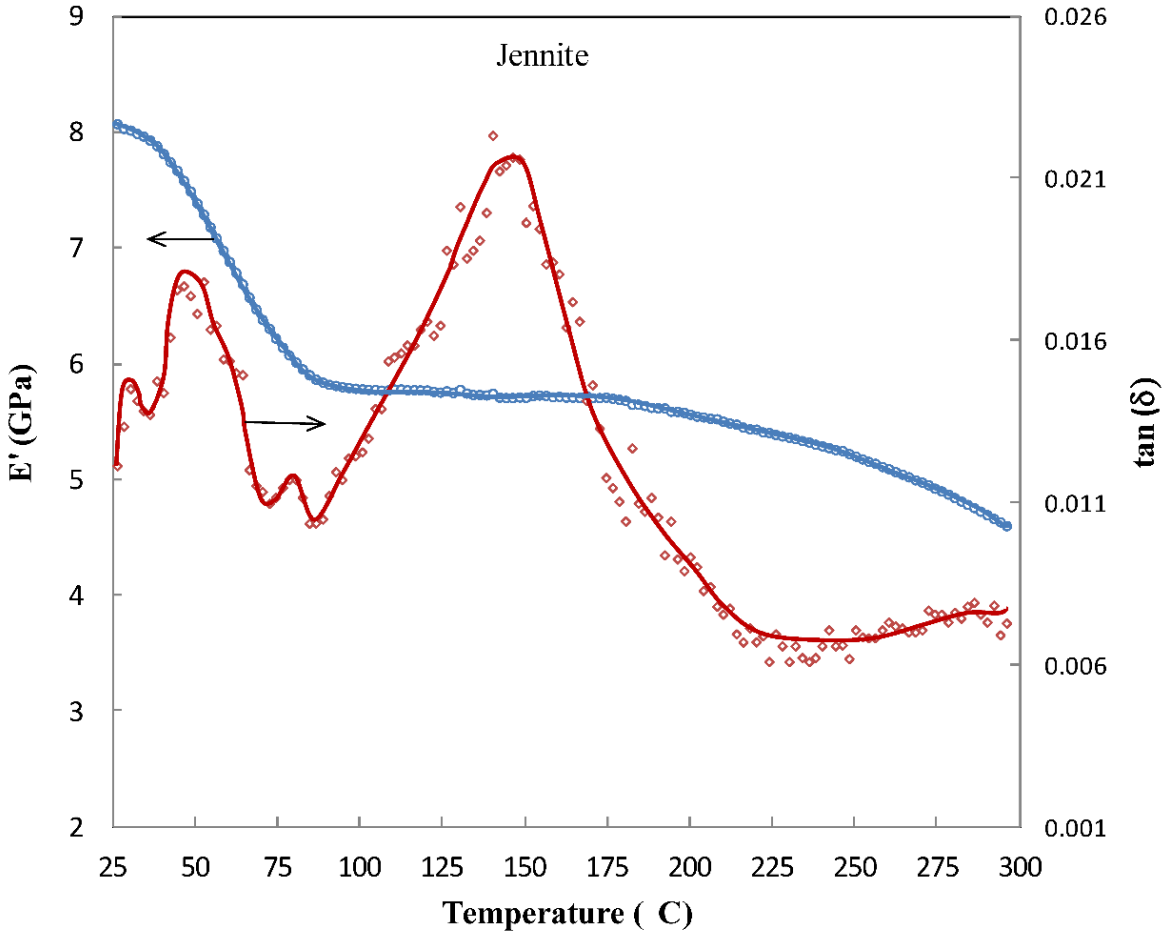

Figure 6. DMTA curves for jennite heated from the 11%RH condition: E' and tan∂ versus temperature curves. Frequency = 3.98Hz. Porosity = 48%.

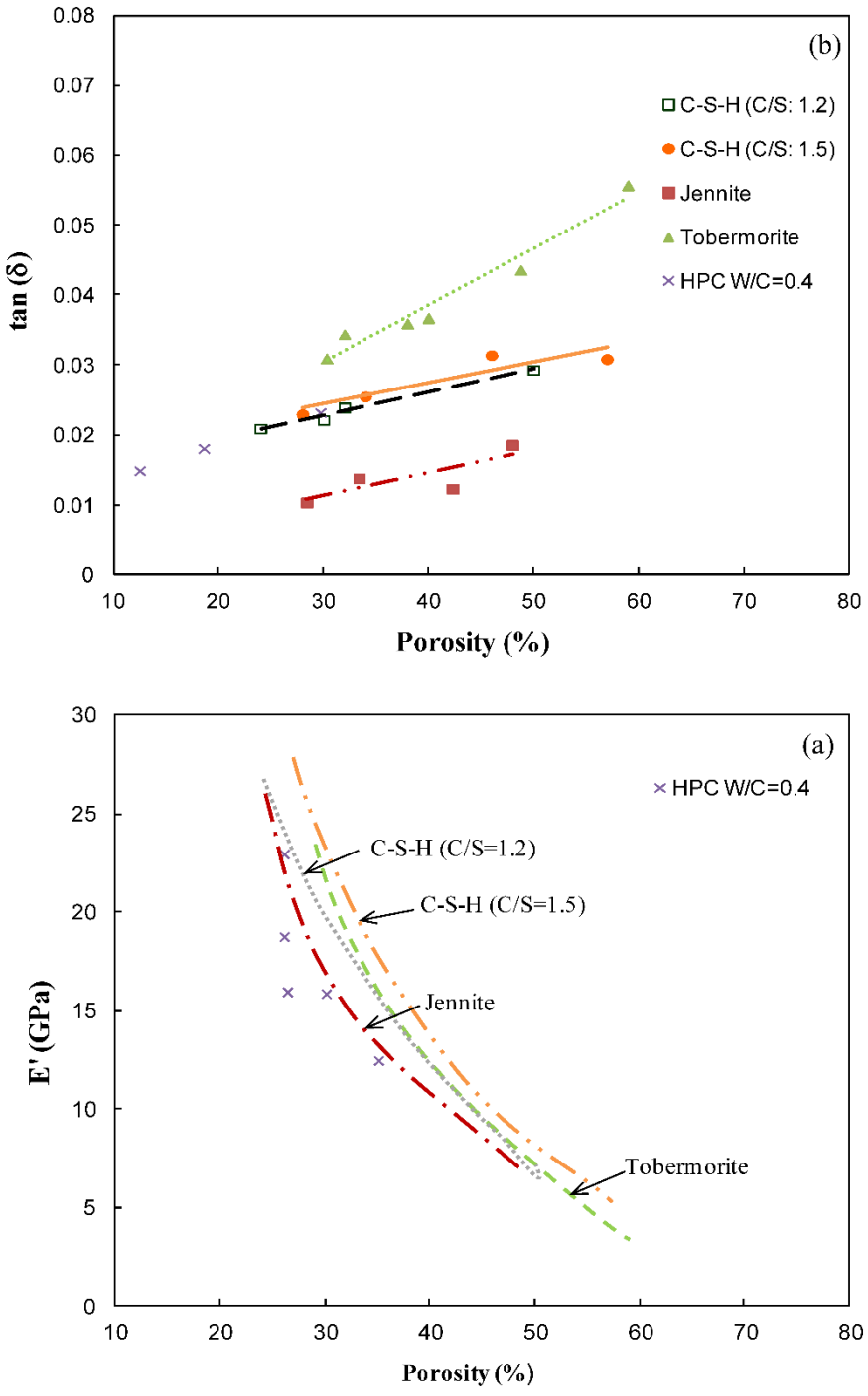

Figure 7. E' versus porosity curves (room temperature) for C-S-H, 1.4nm tobermorite, jennite and HPC.

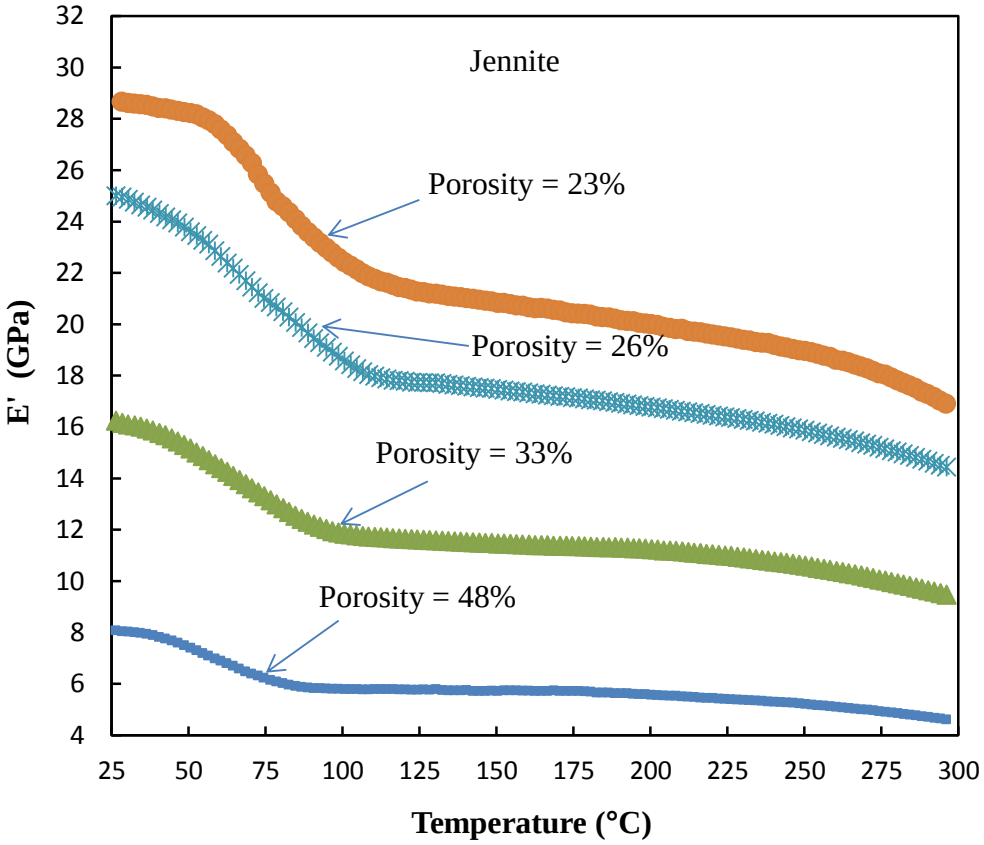

Figure 8. E' versus temperature curves for jennite specimens prepared at porosities ranging from 23 to 43%.

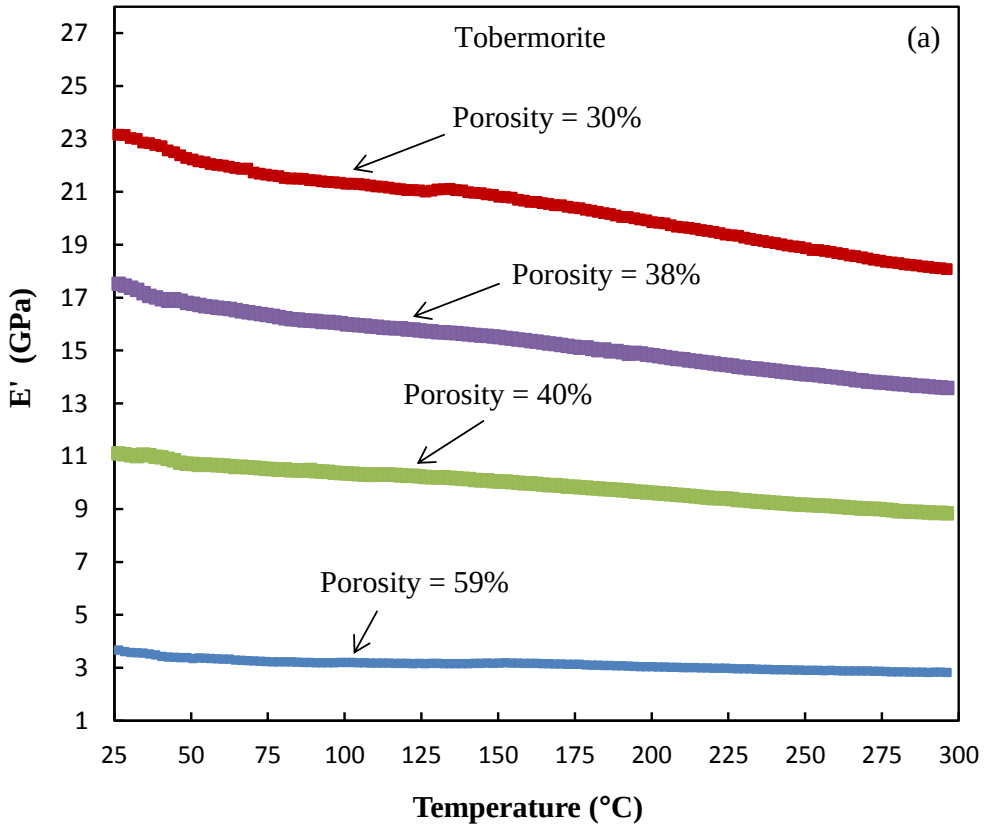

Figure 9. (a) E' versus temperature curves for 1.4nm tobermorite specimens prepared at porosities ranging from 30 to 59%.

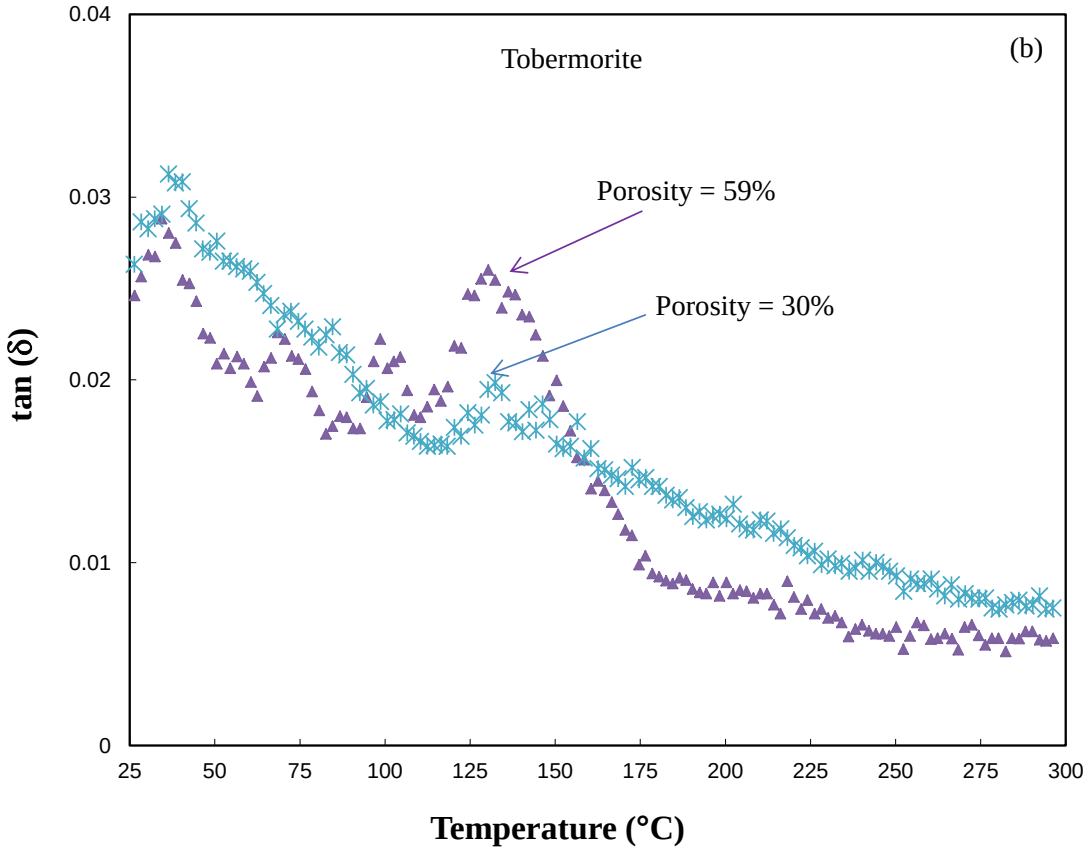

Figure 9. (b) tan∂ versus temperature curves for 1.4nm tobermorite specimens prepared at porosities ranging from 30 to 59%.

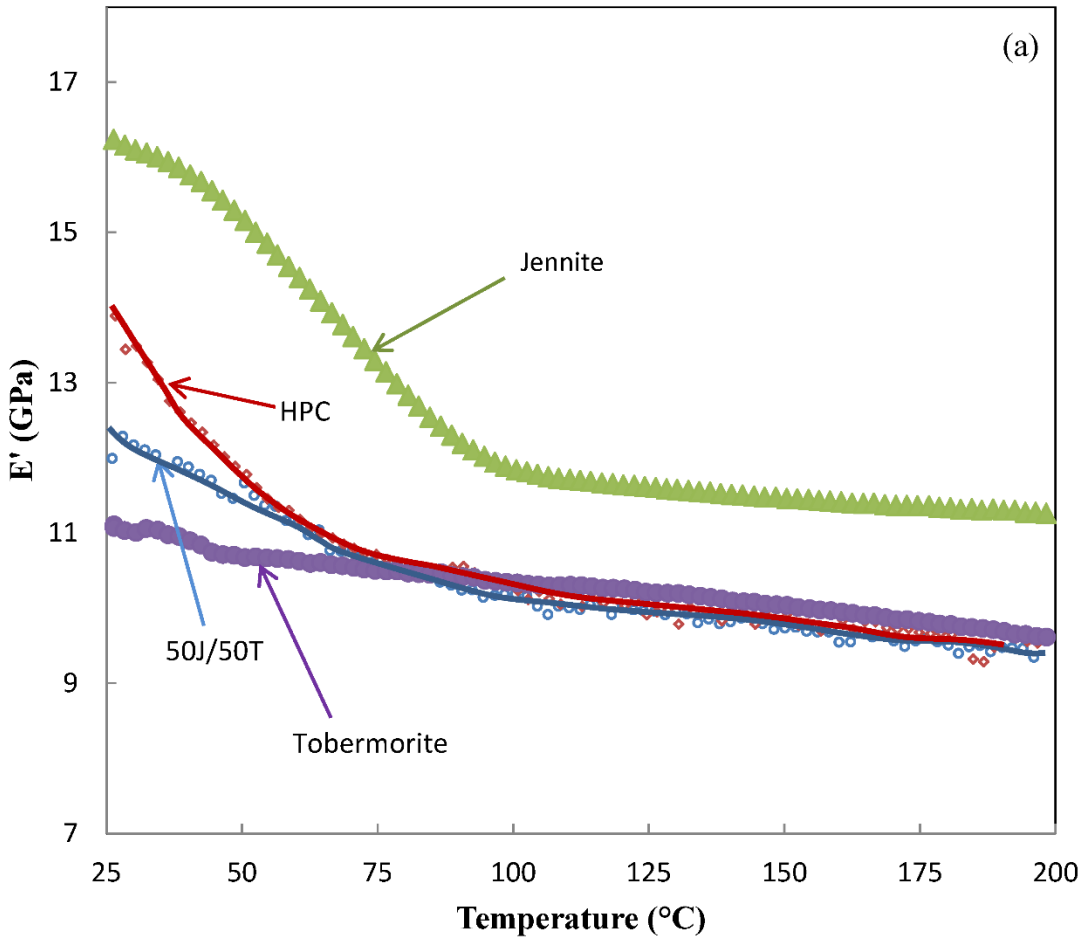

Figure 10. (a) E' versus temperature curves for a 50/50 (% by mass) mixture of 1.4nm tobermorite and jennite (30% porosity), phase pure jennite (30% porosity) and HPC (w/c = 0.40; 24% porosity).

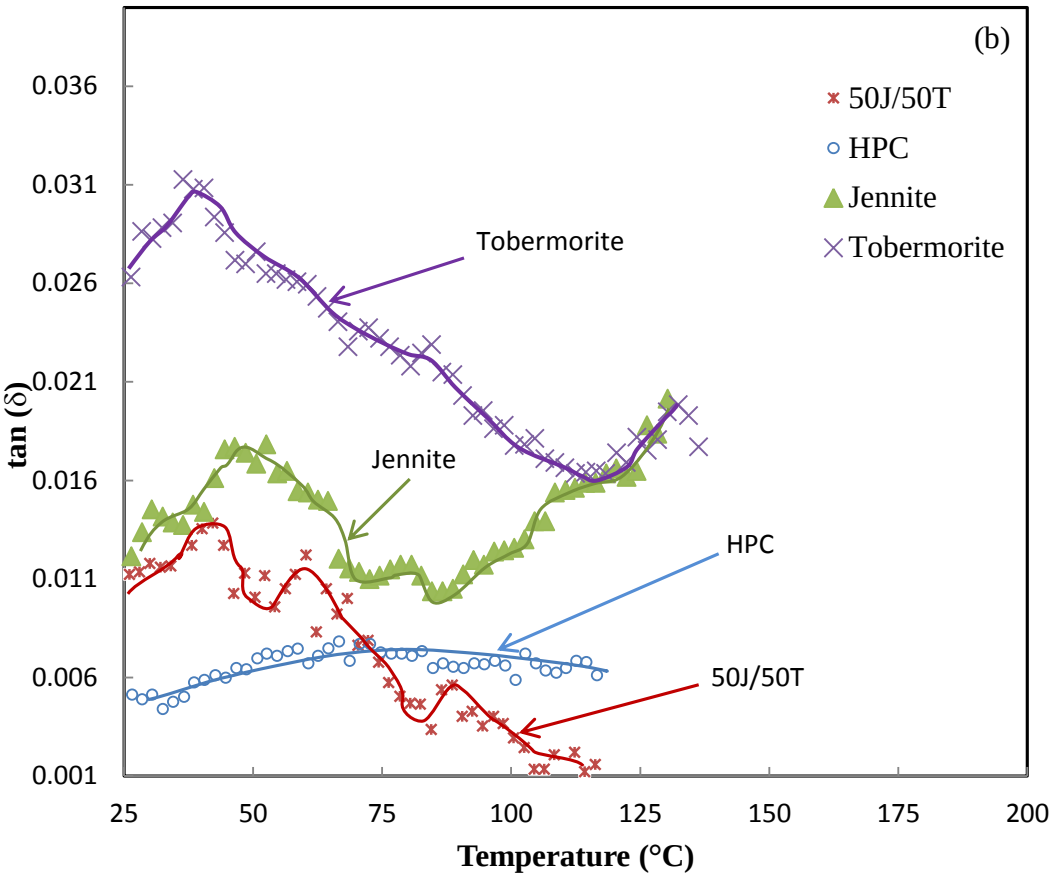

Figure 10. (b) tan∂ versus temperature curves for a 50/50 (% by mass) mixture of 1.4nm tobermorite and jennite (30% porosity), phase pure jennite (30% porosity) and HPC (w/c = 0.40; 24% porosity).

8.3 Paper 2: Correlation between Dynamic Mechanical Thermo-analysis and Composition - Based Models for C-S-H in Hydrated Portland Cement Paste

The DMTA method was used to compare the mechanical performance of compacted bodies of T, J and CH with cement paste hydrated for periods of 2 months, 3 years and 45 years. Differences in engineering behavior between 'young' and 'old' paste were explained by application of a T/J dominant model ('young' paste) and a J-T/CH structural model with a minor amount of T ('old paste').

Correlation between Dynamic Mechanical Thermo-Analysis and Composition-Based Models for C-S-H in Hydrated Portland Cement Paste

(Materials and Structures, DOI 10.1617/s11527-014-0330-7, 2014)

P. Pourbeik[a], J. J. Beaudoin[b], R. Alizadeh[c] and L. Raki[b]

[a] Department of Civil Engineering, University of Ottawa, Ottawa, ON, Canada

[b] National Research Council Canada, Construction Portfolio, Ottawa, ON, Canada

[c] Giatec Scientific Inc., Ottawa, ON, Canada

Abstract

A Dynamic Mechanical Analysis (DMTA) technique was used to assess the mechanical performance of 1.4nm tobermorite (T), jennite (J) and mixtures of tobermorite and jennite and tobermorite and calcium hydroxide (CH). A comparison of E' (storage modulus) and tan∂ (internal friction) versus temperature curves for compacted solid bodies of these mineral systems with corresponding curves for cement paste hydrated for 2 month and 3 years (both referred to as 'young') and 45 year old paste (referred to as 'old') was made. Original data was provided to assess the practical validity of the Richardson–Groves composition-based models for the C-S-H in cement paste. Differences in mechanical performance between the 'young' paste and the 'old' paste could be accounted for by application of a T/J dominant model ('young' paste) and a J- T/CH structural model with a minor amount of T ('old paste').

Keywrods: Dynamic Mechanical Thermo-Analysis, Cement Paste, C-S-H, tobermorite, jennite

Introduction

Details of the nanostructure of the C-S-H binding phase in concrete have been the subject of considerable controversy for decades [1]. Different models have been proposed that are comprised of structures that range from colloidal particles to layered silicates [2-9]. Evidence in support of the various models has been largely indirect as the C-S-H in cement paste is X-ray amorphous. Recently nanostructural models based on tobermorite/jennite (T/J) and tobermorite/'solid-solution' CH (T/CH) advanced by Taylor and Richardson and Groves have been useful in clarifying a number of nanostructural ambiguities [4-6]. These models were constructed on the basis of careful examination of the compatibility of the compositional, spectroscopic and transmission electron microscopy (TEM) evidence of hydrated Portland cement and cement systems containing slags, metakaolin and other supplementary cementing materials. The Dynamic Mechanical Thermo-Analysis (DMTA) method was first applied in cement science to detect low temperature phase changes by Radjy and coworkers [10-13]. The authors have utilized this technique for investigating the mechanical properties of both hardened pastes and solid bodies formed by powder compaction. The DMTA has been shown to be sensitive to dehydration effects including the loss of interlayer water and phase transitions that occur on heating [14]. An attempt was made to correlate the compositional models described above with mechanical performance of 'young' cement paste hydrated for two months and three years and 'old' cement paste hydrated for 45 years. Several systems including compacted powders of 1.4nm tobermorite, jennite and mixtures of these two phases as well as tobermorite/CH mixtures were subjected to DMTA for this purpose. The conformance of the mechanical response of the mineral

systems with the paste materials was assessed and forms the basis for the discussion that follows.

Experimental

Materials

Four cementing systems were prepared: 1.4nm tobermorite; jennite; hydrated Portland cement paste (water/cement ratio = 0.40, hydrated for both 2 months and 3 years); hydrated Portland cement paste (water/cement ratio = 0.70 and 1.00, hydrated 45 years).

In addition several mechanical mixtures of 1.4 nm tobermorite, jennite and calcium hydroxide powders were prepared.

1.4nm tobermorite: the reactants (CaO and SiO_2) were prepared as follows. Calcium oxide was obtained by calcining reagent grade calcium carbonate at 900◦C. Reactive silica (CAB-O-SIL, grade M-5 from Cabot Corporation, USA) was heated at 110◦C to remove any surface adsorbed water. Distilled water was de-aired and used for the reactions. All materials were kept sealed in N_2 purged bottles until they were used. The C/S ratio was 0.9. The reactants were placed in a high density polyethylene bottle, mixed in excess deionized water (water/solids = 11) and maintained at 80 °C using a heating wrap. The mixture was continuously agitated with a magnetic stirrer for a period of 4 months. The XRD spectrum and TGA curve were similar to those obtained by Yu and Kirkpatrick [15].

Jennite: the reactants (CaO and SiO_2) were prepared as described above. The C/S ratio was 1.4. The reactants were placed in a high density polyethylene bottle mixed in excess deionized water (water/solids = 11) and maintained at 80 °C using a heating wrap. The

mixture was continuously agitated with a magnetic stirrer for a period of 4 months. The XRD pattern was similar to that obtained by Yu and Kirkpatrick [15], Gard and Taylor [16] and Hara and Inoue [17]. The TGA curve matched that published by Yu and Kirkpatrick [15].

Portland Cement Paste: Three sets of Portland cement paste were used for these experiments. The first set (made with Type I Portland cement) was prepared using a water/cement ratio of 0.40. Rectangular prisms (250 x 100 x 12.8 mm) were cast. The samples were vibrated and stored in a moist curing room for 24 h. They were then demoulded and curing was continued for 3 years in a saturated lime solution. Thin slices (1.0 x 12.8 x 60.0 mm) were cut from the paste prism using an Isomet diamond saw. Selected slices were also ground into a fine powder for fabrication into compacted specimens with similar geometry. The second set was prepared 45 years ago using water/cement ratios of 0.70 and 1.0. The freshly mixed paste was placed in a tightly stoppered plastic tube 3.17 cm in diameter and allowed to rotate horizontally on rollers at the rate of 0.70 rpm. The paste cylinders were removed after 24 h and covered in a rubber membrane containing drops of lime saturated water and kept saturated by storage in glass cylinders for 45 years. Prior to testing thin discs (1 mm thick) were cut and ground into a fine powder for fabrication into the prism shaped compacted specimens described above. The geometry of the 45 year old samples (circular cross-section) was unsuitable for both DMTA and DMA tests. Compacted samples in the form of thin beams (1.0 x 12.8 x 60.0 mm) were therefore fabricated from the powdered paste preparations. The use of compacted specimens was also strategic for comparison purposes as the 1.4nm tobermorite and jennite preparations were powders and test samples were in the form of compacted beams having the same geometry. Hydrated cement paste specimens having the same geometry were also tested to further demonstrate the validity of the

procedures used. Use of compacts as porous bodies for investigation in cement science is well documented. Their use is very convenient as it is possible to vary the porosity while keeping the composition of the solid phase constant. It should also be noted that the porosity of a compact consists of the porosity of the 'solid' phase (internal) and the porosity outside the 'solid' phase (external) referred to generally as 'capillary' porosity. It is therefore possible (at the same total porosity) for a lower water/cement ratio paste to have a greater volume of 'capillary' pores. The 45 year 'old' pastes were characterized by ^{29}Si MAS NMR and found to have a mean silicate chain length of approximately 4.1 units. The nitrogen BET surface areas were 46 and 41 m^2/g for pastes with water /cement ratios of 0.70 and 1.00 respectively. The third set was identical to the first set except that curing in saturated lime solution was limited to two months.

Humidity Conditioning

Specimens for all four cementing systems were conditioned for several days at 11%RH in vacuum desiccators containing saturated lithium chloride solutions. The powders were conditioned at 11%RH before compaction and for a few days after compaction. Theoretically there is a monolayer of water on the surfaces of the particles in addition to interlayer water at this humidity.

Preparation of Compacted Specimens

Solid rectangular prism samples for all the powdered materials (from the four cementing systems) were prepared by pressure compaction in steel moulds with a cross-section of 12.8 x 83 mm. The thickness of most of the prism samples was nominally 1mm but varied between

the limits of 1-2 mm. Numerous studies on the use and validity of compacts as models for hydrated cement systems have been published [18-22]. It has been shown that compacted specimens of powdered hydrated Portland cement have similar mechanical property-porosity relationships to that of the original hardened paste of the same material [18]. The porosity of compacted samples was determined using helium pycnometry or in the case of the phase pure minerals by calculation using published density values. The calculation is made knowing the apparent volume and the solid volume of the sample. Porosity is varied by controlling the compaction pressure.

Dynamic Mechanical Thermo-Analysis (DMTA)

The dynamic mechanical analysis (DMA) method in general involves the application of an oscillating force to the sample and measurement of displacement [23] The DMTA curves were obtained in the frequency range of 0.10 Hz to 10 Hz. The data reported in the paper was obtained at frequencies of 3.98 Hz. The curves were similar at all frequencies but changes were more pronounced at 3.98 Hz. The elastic property obtained by DMA is referred to as the storage modulus (E'); it is analogous to the static modulus of elasticity. There is usually a time lag between the applied force and the resulting displacement. The time lag can be quantified in terms of a phase angle between the load and the displacement due to their ideally sinusoidal nature. The tangent of this angle ($\tan\partial$) represents the damping property of the material often referred to as internal friction. Additional details are given in a previous publication [24]. Internal friction of the 'solid' phase is mainly related to the content of interlayer/structural water. It is dependent on the resistance to shear stress effects and the

ability of the layers to translate relative to one another. Nevertheless it is suggested that large pores can contribute to increasing internal friction as they may facilitate the translation of silicate sheets. Higher values of internal friction in normally hydrated cement paste are generally associated with higher water/cement ratio. Several mechanisms are thought to influence the magnitude of internal friction in systems comprised essentially of layered calcium silicate hydrates. Samples conditioned at 11%RH contain essentially a monolayer of surface water and interlayer water. The latter has a structural role and its removal affects the potential translation of the silicate sheets relative to each other. Decreases in stiffness are associated with the removal process and partial collapse of structure facilitating translation of the silicate sheets. Further removal of water can result in a more complete collapse of structure increasing the resistance to translation of sheets. This is likely associated with an increase in the degree of polymerization, crosslinking between sheets and interactions between interlayer calcium ions and the silicate sheets. A secondary effect is possibly related to water/cement ratio. The magnitude of internal friction is likely dependent on 'capillary' porosity referred to above as it generally increases with water/cement ratio. The DMTA analysis involves heating the sample at a constant rate during the experiment. It was conducted using a Rheometrics RSA II instrument on all samples in this investigation. The samples were heated from 25◦C to 300◦C. Temperature was increased in increments of 2◦C every 5 minutes. E' and tan∂ versus temperature curves were plotted. Each test took about 11h and 45min.to complete. It is apparent that the DMTA tests are much less tedious and time consuming to perform compared to DMA tests at room temperature that involve multiple measurements as dehydration occurs in equilibrium steps of water removal. The general characteristics of the E and tan∂ versus temperature DMTA curves mimic those of

the E and tan∂ versus mass-loss DMA curves even though the latter are obtained under quasi-equilibrium conditions. The mass-loss due to removal of free water in the dynamic DMTA test is substantially but not totally complete at 100○C. A slower heating rate in the DTMA would not likely change the response very much especially as the DMTA curves already mimic those obtained with the room temperature DMA test. Previous work by Alizadeh indicated that the information provided by the equilibrium DMA and DMTA tests is similar in nature [14]. Measures were taken to minimize carbonation. Specimens were stored in vacuum desiccators at 11% RH until the time of test. The test chamber volume of the DMA instrument was relatively small (225cm^3) and sealed during the entire test period. Transfer of the specimens to the chamber took less than 1 minute. Thermogravimetric analysis of selected specimens following the test indicated that carbonation was not significant. The surfaces of the samples were examined using both optical and scanning electron microscopy. There was no apparent evidence of microcracking. Previous DMA work on phase pure C-S-H using specimens with identical geometry indicated initial decreases in storage modulus followed by decreases [14, 24]. This reversal in stiffness values would be unlikely to occur in the presence of any significant microcracking.

Results and Discussion

The cement and mineral systems investigated were selected in order to assess the compliance of their mechanical properties with the tobermorite and jennite-based nanostructural models for cement pastes advanced by Richardson and Groves, Taylor and others. The DMTA analysis of cement paste (hydrated for 3 days to 45 years), 1.4nm tobermorite (T), jennite (J)

and mixtures of T, J and CH phases was used to evaluate the mechanical response of these materials in the temperature range 25-300°C. A comparison of the temperature dependence of the primary DMTA parameters E' (storage modulus) and tan∂ (internal friction) provided a basis for assessing the compatibility of the T/J and T/CH models with mechanical performance. Evidence for these model constructs has been based primarily on compositional, spectroscopic and electronmicroscopy investigations. The thermally activated events that occur during DMTA experiments involving heating to 300 °C also provide insight as to the role of interlayer water and phase changes (with T and J) on the processes that influence the mechanical performance of these systems. A useful precursor to discussion of the DMTA results is an examination of the E' versus porosity curves for the systems studied [25].

DMTA curves- E' and tan∂ versus temperature (cement paste hydrated for periods of 3 years and 2 months).

E' versus temperature curves for cement paste samples (w/c = 0.40; hydrated for both 2 months and 3 years) and a 50/50 mixture (by mass) of jennite and 1.4nm tobermorite (50J-50T) are plotted in Figure 1(a). The paste hydrated for 2 months and the 50J-50T system have similar porosity values i.e. 30%. The initial E' values (13.0 and 12.3 GPa) are similar. The E'-temperature curve for the paste is coincident with that of the curve for the 50J-50T system over most of the temperature range. The curve for the paste hydrated for 3 years lies above the curve for the 50J/50T system. Despite the difference in porosity of the latter two systems (30% for the 50J-50T specimen and 15% for the 3 year old paste specimen) accounting for variance in the initial values of E' (12.5 and 18 GPa) and the phase changes

that occur for both jennite (metajennite formation and disordered phases above 250 °C) and tobermorite (changes to 1.2, 1.1 and 0.96 nm forms) on heating the shapes and general character of the curves are remarkably similar. A curve for a 45/45/10 blend of J, T and CH (not shown) is also similar. The E' values for each system decrease over the entire temperature range. In addition each curve has four distinct temperature regions (25-40 °C; 40-75°C; 75-200°C and 200-300°C). The first two regions involve the loss of surface and interlayer water. Interlayer water continues to be lost in the higher temperature regions. Additional details on the effects of phase changes and concomitant density and porosity changes have been reported elsewhere [26]. Although the C-S-H in hydrated cement paste is generally amorphous in nature it appears to behave as a layered silicate in response to dynamic mechanical stimuli.

Richardson has stated that the bimodal distribution in Ca/Si ratio observed at early ages in water-activated neat pastes is compatible with a T/J composition-based model [2]. Here we consider both the two month and three year period of hydration to be 'early' with respect to the 45 year period to be discussed later. It would appear that based on the correspondence of shape and relative magnitude of the E' curves for the T/J mixtures and both the 2 month and 3 year old paste that a T-J nanostructural model appears to be reasonable.

The above arguments for E' data and the compatibility of mechanical behavior of early age paste with that for the 50T-50J system can be extended to the tan∂ versus temperature curves for these materials, Figure 1(b). The general character of all the curves appears to be similar. Low temperature maxima were observed between 50 and 75 °C for all three systems. These are attributable to the removal of surface and interlayer water that accompany phase changes and ancillary processes due to the dehydration process as referred to above. The magnitude

in this temperature region is less for the two month old paste possibly due to the restraining effect of a larger number of unhydrated cement particles. There is a gradual increase in tan∂ following the initial peak. This begins at temperatures of 100, 150 and 150°C for the 2 month, 3year and 50J-50T system respectively. There is also a small peak at about 200°C for the latter two systems. A peak at about 140°C for the 50J-50T system is likely due to metajennite formation. The peak at 200°C may be due to additional interactions involving interlayer Ca^{2+}. The increase in tan∂ above 220 °C may involve formation of a disordered phase [15].

DMTA curves-E' and tan∂ versus temperature (cement paste hydrated for 45 years)

The cement paste in this section was hydrated for 45 years and is considered 'old'. It is well polymerized with average chain lengths generally greater than 4.0 as determined by 29Si MAS NMR. The E' versus temperature curves for compacts of the old paste (w/c = 0.70 and 1.0), a mixture of 75% 1.4nm tobermorite and 25 % CH (75T/25CH) , jennite (J), tobermorite (T) and various mixtures of J and T (e.g. 45J-45T-10 CH; 50J-50T; 75J-25T) are shown in Figure 2(a). The porosity values for these materials are: 36.1, 30.6, 33.6, 33.4%, 30% and 30% for all J-T mixtures respectively. This accounts for the lower initial value of E' for the paste with w/c = 0.70 relative to that for the paste with w/c = 1.0. The initial E' values are 6.6, 9.2, 15.8, 16.2, 18.4 GPa for the old pastes and J, 75T-25CH and T respectively. The corresponding E' values for the J-T mixtures are 13.8, 12.7 and 11.2 GPa for the J-T mixtures in order of increasing jennite content. The E' curves for the old paste, 50J-50T system and jennite are very similar in character with four distinct temperature regions; 35-50°C; 50-

100°C; 100-250°C; 250-300°C. The influence of surface and interlayer water removal as well as metajennite formation is as described previously. The general conformance of the curves is noteworthy considering the generally amorphous nature of C-S-H in hydrated cement paste. Nevertheless the differences in the magnitude of E' for the studied systems warrants further discussion.

It has been suggested by Richardson that the compositional and structural data for C-S-H in old C_3S pastes, for example, cannot be accounted for by an entirely J-type structure unless there is very significant protonation of the silicate chains. It would appear that the results for jennite mixtures in Figure 2(a) support this view. It is clear that a decrease in the tobermorite content of the jennite-tobermorite mixtures shifts the E' curves closer to those for the old cement paste.

It would appear that the 75T-25CH would not be a suitable model for the mechanical performance of the old cement paste. The magnitude of the E' values relative to those for the old paste is much too high. The similar characteristics of the curve to those for the old pastes however merits some additional comment. The shape of the curve is similar up to 100°C, the difference being the much smaller decrease in E' due to the removal of interlayer water i.e. <1GPa. This is likely due to the restraining effect of the CH phase. The decrease in E' from 100 to 200 °C is about 0.70GPa and from 200 to 300 °C about 0.20GPa. This is similar to the decreases in E' observed in these temperature regions for jennite. It would appear that the influence of CH on stiffening the system is reduced after 100 °C. In accordance with Richardson's suggestion that it is possible that structural elements based on tobermorite, jennite and CH can all occur within the same system it would appear that old cement pastes can be modeled as system comprised of primarily J units with some T-CH units. This is

supported by the trend of the E'-temperature curves for the J-T mixtures in Figure 2(a). It is noted that this premise is also supported by the results of a previous study of mechanical property-porosity relationships of layered calcium silicate hydrate phases where the data (obtained at 25°C) for the 75T/25CH system was nested along the curve for jennite [25]. Arguments for correspondence of the DMTA E' data for these systems can be extended to the tan∂ versus temperature data for all these systems, Figures 2(b) and 2(c). The tan∂ curves for these materials are complex and are plotted in two separate figures for clarity.

Figure 2(b) is a plot for J, J-T mixtures and old cement paste (w/c = 1.0). They all exhibit low temperature tan∂ peaks (40-60°C) that are primarily due to the removal of surface and interlayer water. There is a subsequent decrease in internal friction in all systems up to about 125°C. The magnitude of the internal friction values (in the temperature region, 40-125°C) for the curves representing J, 75J-25T and old cement paste (w/c = 1.0) is similar The decrease may be a result of interactions between interlayer Ca^{2+} ions and the silicate sheets.

Figure 2(c) is a plot of the tan∂ curves for the old cement paste systems, J, T and the 75T-25CH materials. The magnitude of the tan∂ values for the 75T-25CH and old cement paste is similar at temperatures above 60 °C. The data for J and 75T-25CH are coincident at temperatures up to 125 °C. Jennite subsequently converts to metajennite resulting in higher values of tan∂ due to changes in porosity of the system. In the case of old cement paste and the 75T-25CH system cross-linking between the silicate layers and an increase in the degree of polymerization may occur. Subsequent increases in tan∂ values are in the case of jennite and 1.4 nm tobermorite due to phase changes (e.g. to metajennite and 1.1nm tobermorite) as referred to above and associated changes in density and porosity [26]. The peaks in the curves for cement paste occurring between 150 and 300°C are likely due to further removal

of interlayer water. The decreases in internal friction values following these peaks are likely the result of further interactions involving interlayer Ca2+ ions and the silicate sheets as well as cross-linking.

It is apparent that an increase in the amount of jennite in a J-T mixture reduces the magnitude of internal friction (in the temperature range (25-125 °C) .This brings the curves into closer proximity with the old cement paste (w/c = 1.0) which has a similar porosity of about 30%. The old paste (w/c = 0.70) as a consequence of the compaction pressures utilized has a higher total porosity than the old paste (w/c = 1.0). The 'solid' phase of the sample, however, had fewer capillary pores which may account for the lower values of internal friction.

It is suggested that despite the phase changes that occur in both the jennite and 1.4nm systems the DMTA response of old cement paste (i.e. E' and tan∂ versus temperature) mimics a combination of both these silicate minerals (especially at temperatures less than 100 °C) when the amount of tobermorite is low. This is also the case for the 75T-25CH system.

Conclusions

1. Dynamic mechanical analysis (DMTA) is a useful tool to assess the role of water and any concomitant phase changes that occur due to dehydration of calcium silicate hydrates.

2. A comparison based on the DMTA response (E' and tan∂ versus temperature curves) of jennite , 1.4nm tobermorite and mixtures of these silicates with cement paste hydrated for 3 years and 45 years can provide a basis for the assessment of the compatibility of T/J and T/CH models of C-S-H nanostructure in cement paste with mechanical performance parameters.

3. The DMTA response of three year old cement paste (‘young’) mimics the response of 1.4 nm tobermorite/jennite (T/J) mixtures. It is suggested that the Richardson-Groves and Taylor composition-based models for C-S-H nanostructure based on T/J structural units is compatible with the mechanical behavior of ‘young’cement paste.

4. The DMTA response of 45 year old cement paste (‘old’) mimics the response of jennite (J) and 1.4 nm tobermorite/calcium hydroxide (T/CH) mixtures when the amount of tobermorite is relatively small. It is suggested that the Richarson-Groves composition-based model for C-S-H based on the presence of both J and T/CH structural units is compatible with the mechanical behavior of ‘old’ cement paste.

5. A small amount of CH in the J-T system does not appear to have an effect on mechanical performance due to thermal changes in the temperature region 100-300 °C.

References

1. Taylor H. F.W., Hydration of the calcium silicate phases, Cement Chemistry, Chapter 5, Thomas Telford Publishing, London, pp.459, 1997.

2. Richardson I. G., Tobermorite/jennite- and tobermorite/calcium hydroxide-based models for the structure of C-S-H: applicability to hardened pastes of tricalcium silicate, β-dicalcium silicate, Portland cement, and blends of Portland cement with blast-furnace slag, metakaolin, or silica fume, Cem. Concr. Res., 34, 1733-1777, 2004.

3. Taylor H.F.W., Proposed structure of calcium silicate hydrate gel, J. Amer. Ceram. Soc.69 (6), 464-467, 1986.

4. Richardson I. G., The calcium silicate hydrates, Cem. Concr. Res., 38(2), 137-158, 2008.

5. Richardson I. G. and Groves G. W., Models for the composition and structure of calcium silicate hydrate (C-S-H) gel in hardened tricalcium silicate pastes, Cem. Concr. Res., 22, 1001-1010, 1992.

6. Taylor H. F.W., Nanostructure of C-S-H: current status, Adv. Cem. Based Mater. 1, 38-46, 1993.

7. Chen J. J., Thomas J. J., Taylor H.F.W., Jennings H. M., Solubility and structure of calcium silicate hydrate, Cem. Concr. Res., 34, 1499-1519, 2004.

8. Grutzek M. W., A new model for the formation of calcium silicate hydrate (C-S-H), Mater. Res. Innov., 3, 160-170, 1999.

9. Powers T. C. and Brownyard T. L., Studies of the physical properties of hardened Portland cement paste: Part 3. Theoretical interpretation of adsorption data, J. Amer. Concr. Inst., 43,469-504, 1946.

10. Radjy F. and Sellevold E. J., Internal friction peaks due to adsorbed and capillary water in microporous substances, Nature Physical Science, 241, 133-135, 1973.

11. Radjy F. and Richards C. W., Effect of curing and heat treatment history on the dynamic mechanical response and the pore structure of hardened cement paste, Cem. Concr. Res., 3, 7-21, 1973.

12. Sellevold E. J. and Radjy F., Drying and resaturation effects on internal friction in hardened cement paste, J. Amer. Ceram. Soc., 59(5-6), 256-258, 1976.

13. Radjy F. Sellevold E. J. and Richards C. W., Effect of freezing on the dynamic Mechanical response of hardened cement paste down to -60°C, Cem. Concr. Res., 2, 697-715, 1972.

14. Alizadeh R., Nanostructure and engineering properties of basic and modified calcium-silicate-hydrate systems, PhD thesis, University of Ottawa, pp.230,2009.

15. Yu P. and Kirkpatrick R. J., Thermal dehydration of tobermorite and jennite, Concr. Sci. and Eng., 1, 185-191, 1999.

16. Gard J. A. and Taylor H. F. W., Calcium silicate hydrate (II) ("C-S-H(II)"), Cem. Concr. Res., 6, 667-678, 1976.

17. Hara N. and Inoue N., Formation of jennite from fumed silica, Cem. Concr. Res., 10, 677-682, 1980.

18. Soroka I. and Sereda P.J., The structure of cement- stone and use of compacts as structural models, Proc. 5th Int. Symp. on the Chem. of Cem., Vol. 3., Tokyo, 67-73,1968.

19. Feldman R. F., Factors affecting the Young's modulus-porosity relation of hydrated Portland cement compacts, Cem. Concr. Res., 2(4), 375-386, 1972.

20. Sereda P.J. and Feldman R. F., Compacts of powdered material as porous bodies for use in sorption studies, J. Appl. Chem., 13, 150-158, 1963.

21. Beaudoin J.J., Comparison of mechanical properties of compacted calcium hydroxide and Portland cement paste systems, Cem. Concr. Res., 13, 319-324, 1983.

22. Sereda P.J., Feldman R.F. and Swenson E.G., Effect of sorbed water on some mechanical properties of hydrated Portland cement pastes and compacts, Highway Research Board, Special Report 90, 58-73, 1966.

23. Menard K. P., Dynamic Mechanical Analysis-A Practical Introduction, CRC Press LLC, Boca Raton, pp. 208, 1999.

24. Alizadeh R., Beaudoin J. J. and Raki L., Mechanical properties of calcium silicate hydrates, Matls. and Struct., 44, 13-28, 2011.

25. Pourbeik P., Beaudoin J. J., Alizadeh R. and Raki L., Mechanical property-porosity relationships of layered calcium silicate hydrate phases, Matls. and Struct. 46(9), 1489- 1495, 2013.

26. Pourbeik P., Beaudoin J. J., Alizadeh R. and Raki L., Dynamic Mechanical Thermo-Analysis of Layered Calcium-Silicate Hydrates, Submitted to Journal of Thermal Analysis and Calorimetry, 2013.

Figure captions

Figure 1(a): DMTA – E' versus temperature curves for 'young' cement paste hydrated for 3 years (w/c = 0.40) and a 50/50 mixture (by mass) of 1.4 nm tobermorite and jennite. All samples were conditioned at 11% RH at the start of the test. Symbols: CP = cement paste; T = 1.4nm tobermorite; J = jennite.

Figure 1(b): DMTA-tan∂ versus temperature curves for 'young' cement paste hydrated for 3 years (w/c = 0.40) and a 50/50 mixture (by mass) of 1.4 nm tobermorite and jennite. All samples were conditioned at 11% RH at the start of the test. Porosity values are the same as shown in Figure 1(a). Symbols: CP = cement paste; T = 1.4nm tobermorite; J = jennite.

Figure 2(a): DMTA- E' versus temperature curves for 'old' cement paste hydrated for 45 years (w/c = 0.70 and 1.00), a 75/25 mixture (by mass) of 1.4 nm tobermorite and CH, jennite, tobermorite and mixtures of J and T (45J-45T-10CH; 50J-50T; 75J-25T). All samples were conditioned at 11% RH at the start of the test. Symbols: CP = cement paste; T = 1.4nm tobermorite; J = jennite; CH = calcium hydroxide. Porosity for all systems except old paste (w/c = 0.70) is approximately 30%.

Figure 2(b): DMTA- tan∂ versus temperature curves for 'old' cement paste hydrated for 45 years (w/c = 1.00), J and mixtures of J and T (50J-50T; 75J-25T). All samples were conditioned at 11% RH at the start of the test. Symbols: CP = cement paste; T = 1.4nm tobermorite; J = jennite. Porosity for all systems is approximately 30%.

Figure 2 (c): DMTA- tan∂ versus temperature curves for 'old' cement paste hydrated for 45 years (w/c = 1.00 and 0.70), J, T and a mixture of T and CH (75T-25CH). All samples were conditioned at 11% RH at the start of the test. Symbols: CP = cement paste; CH = calcium hydroxide; T = 1.4nm tobermorite; J = jennite. Porosity for all systems except old paste (w/c = 0.70) is approximately 30%.

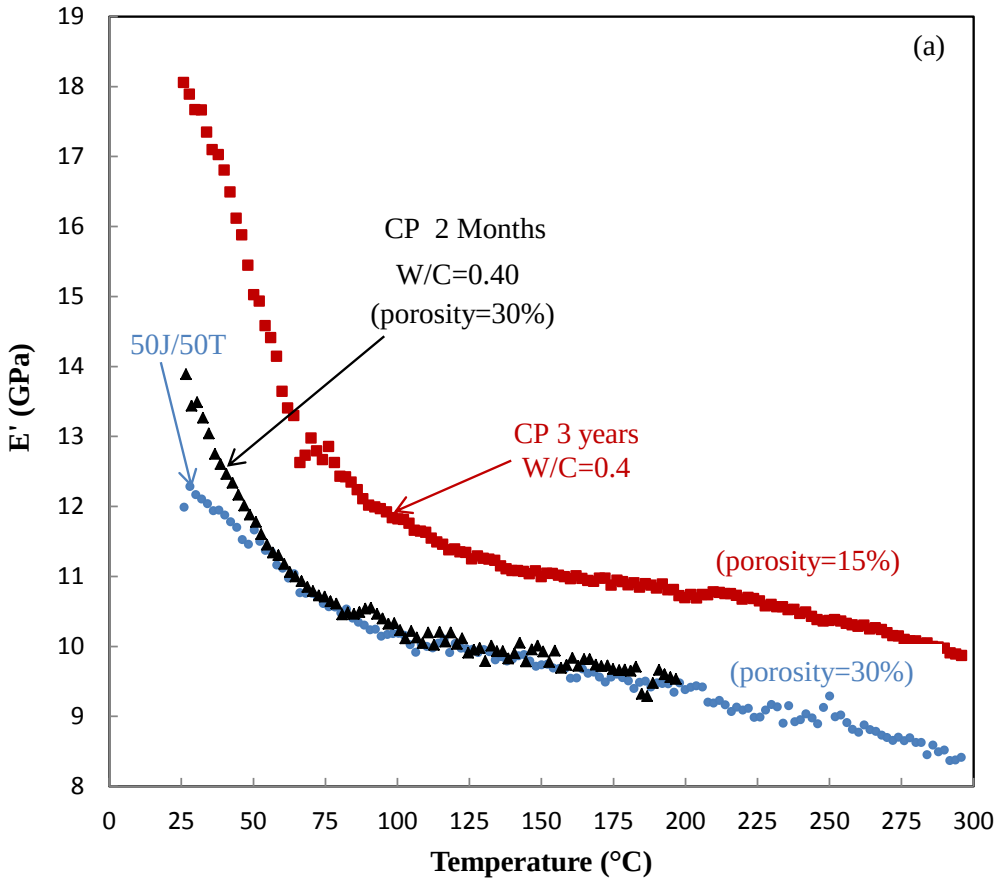

Figure 1(a): DMTA – E' versus temperature curves for 'young' cement paste hydrated for 3 years (w/c = 0.40) and a 50/50 mixture (by mass) of 1.4 nm tobermorite and jennite. All samples were conditioned at 11% RH at the start of the test. Symbols: CP = cement paste; T = 1.4nm tobermorite; J = jennite.

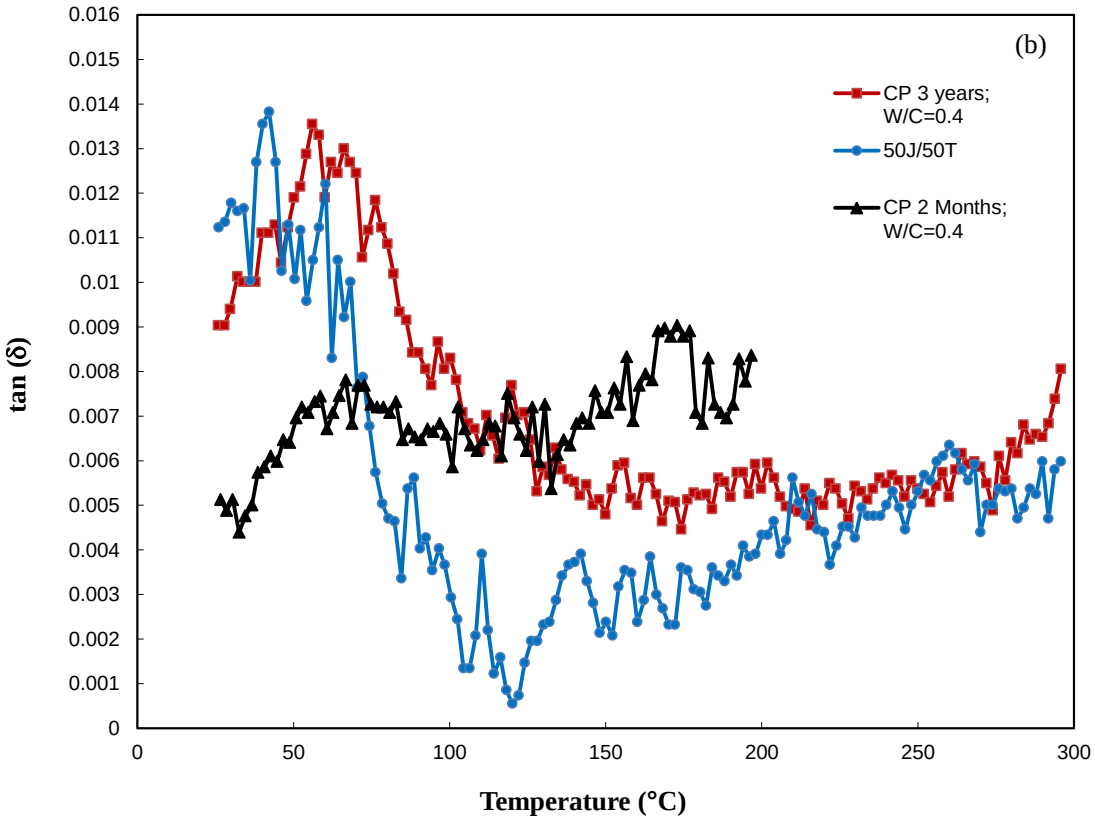

Figure 1(b): DMTA-tan∂ versus temperature curves for 'young' cement paste hydrated for 3 years (w/c = 0.40) and a 50/50 mixture (by mass) of 1.4 nm tobermorite and jennite. All samples were conditioned at 11% RH at the start of the test. Porosity values are the same as shown in Figure 1(a). Symbols: CP = cement paste; T = 1.4nm tobermorite; J = jennite.

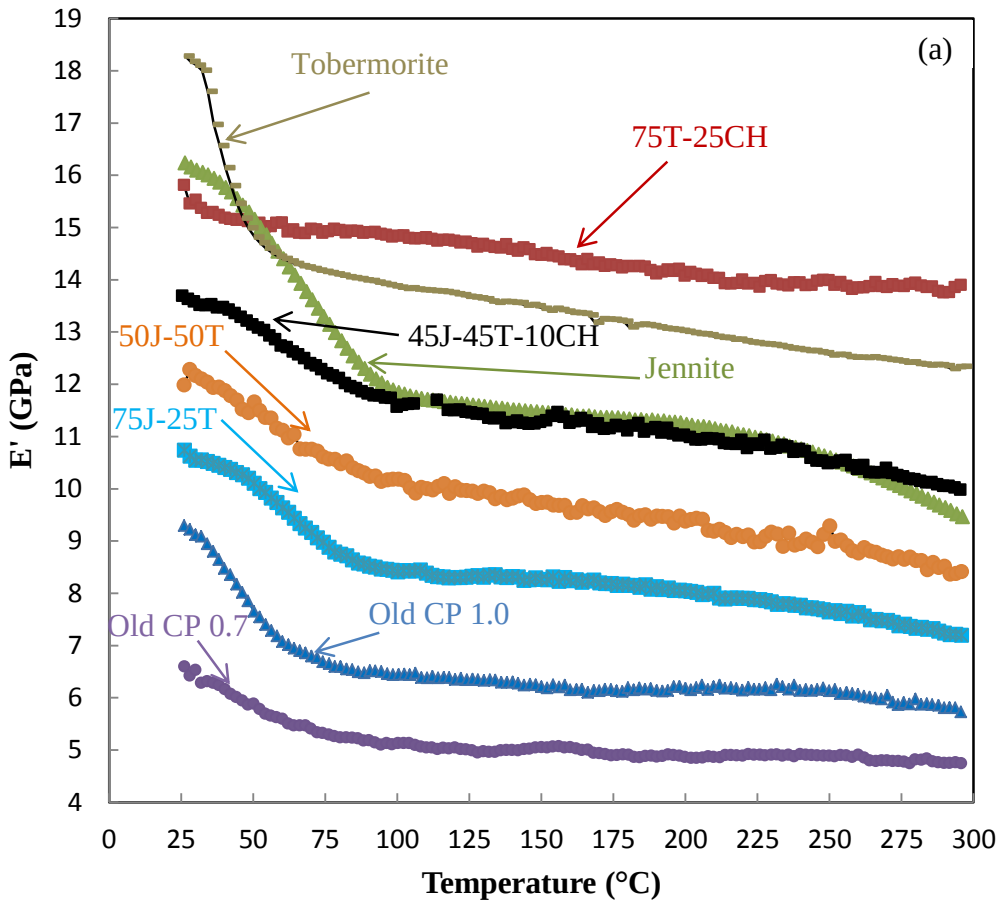

Figure 2(a): DMTA- E' versus temperature curves for 'old' cement paste hydrated for 45 years (w/c = 0.70 and 1.00), a 75/25 mixture (by mass) of 1.4 nm tobermorite and CH, jennite, tobermorite and mixtures of J and T (45J-45T-10CH; 50J-50T; 75J-25T). All samples were conditioned at 11% RH at the start of the test. Symbols: CP = cement paste; T = 1.4nm tobermorite; J = jennite; CH = calcium hydroxide. Porosity for all systems except old paste (w/c = 0.70) is approximately 30%.

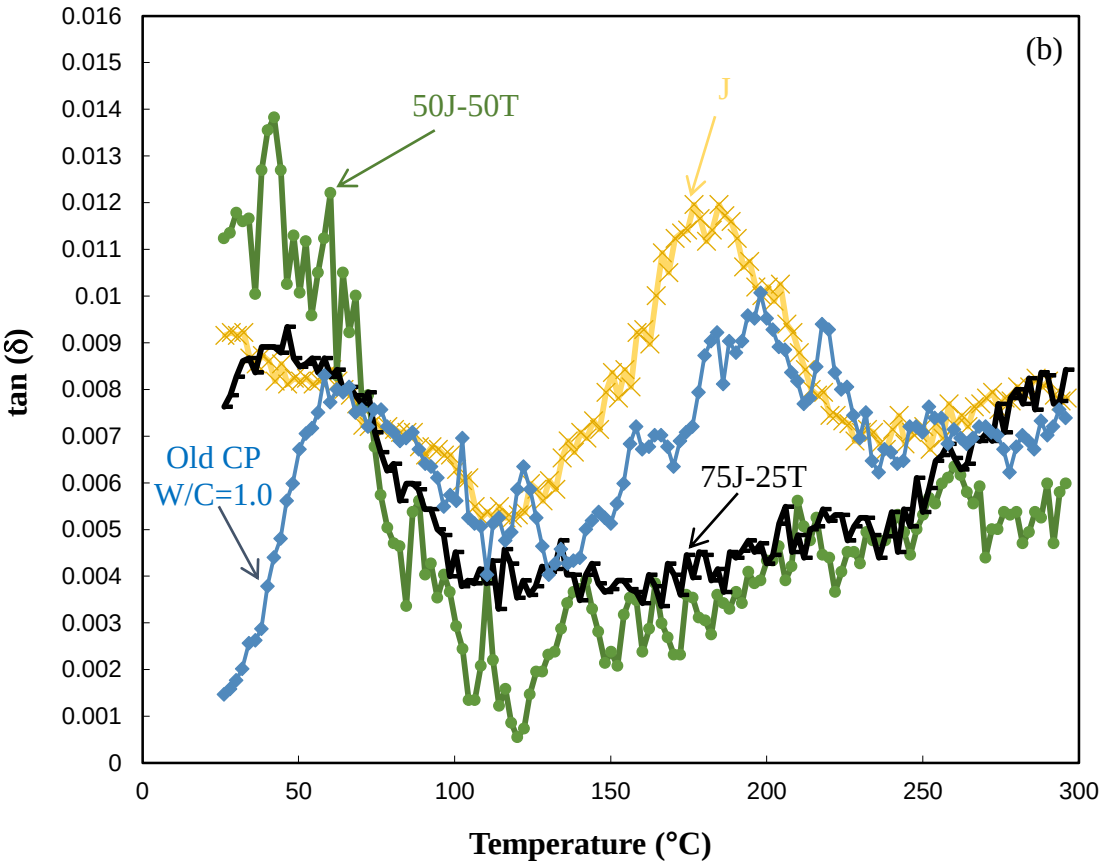

Figure 2(b): DMTA- tan∂ versus temperature curves for 'old' cement paste hydrated for 45 years (w/c = 1.00), J and mixtures of J and T (50J-50T;75J-25T). All samples were conditioned at 11% RH at the start of the test. Symbols: CP = cement paste; T = 1.4nm tobermorite; J = jennite. Porosity for all systems is approximately 30%.

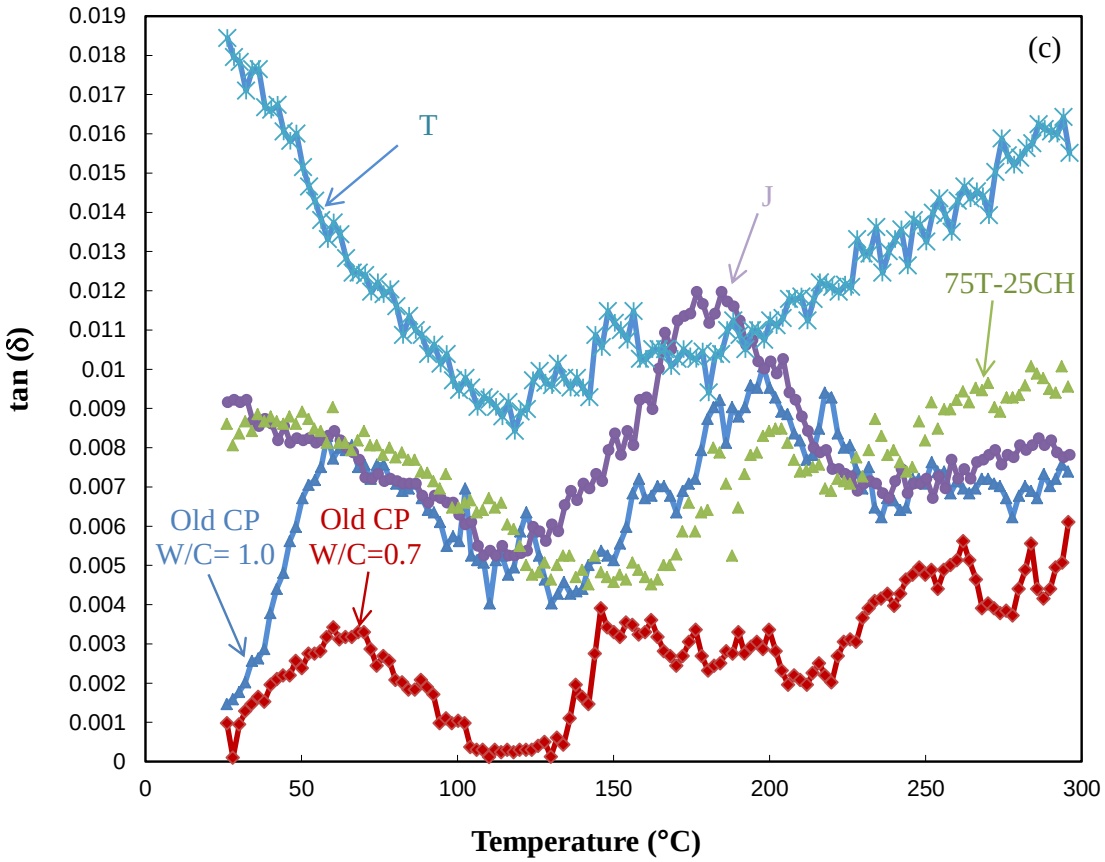

Figure 2 (c): DMTA- tan∂ versus temperature curves for 'old' cement paste hydrated for 45 years (w/c = 1.00 and 0.70), J, T and a mixture of T and CH (75T-25CH). All samples were conditioned at 11% RH at the start of the test. Symbols: CP = cement paste; CH = calcium hydroxide; T = 1.4nm tobermorite; J = jennite. Porosity for all systems except old paste (w/c = 0.70) is approximately 30%.

8.4 Paper 3: Effect of Thermal Treatment of 1.4 nm Tobermorite and Jennite on Mechanical Performance

DMTA appears to be a promising method for studying the effect of dehydration on the engineering behavior of layered calcium silicate hydrate systems.The DMTA method was able to detect irreversible effects (including increases in E' at 25°C) associated with pre-heating T for prolonged periods at temperatures associated with phase transformations. This was not the case for jennite. Thermal events associated with disordered phases that form at higher temperatures in the jennite system pre-heated to 175°C could be detected by the DMTA method.

Effect of Thermal Treatment of 1.4nm Tobermorite and Jennite on Mechanical Performance

(Materials and Structures, to be submitted)

P. Pourbeik, J. J. Beaudoin, R. Alizadeh and L. Raki

Abstract

Dynamic mechanical thermoanalysis (DMTA) was conducted on compacted specimens of 1.4nm tobermorite and jennite powders conditioned to 11%RH at 25°C or pre-heated for prolonged periods at temperatures associated with phase transformations i.e. 65, 79 and 175°C. The DMTA curves for the reference systems conditioned at 11%RH were sensitive to phase changes including the transition of 1.4nm tobermorite to other forms e.g. 1.1 nm tobermorite and jennite to metajennite. This sensitivity was also observed for phase transformations resulting from the effects of pre-heating. Pre-heating results in irreversible effects for the 1.4nm tobermorite as reflected in the E' and tan∂ results. This was not the case for jennite. The DMTA method was able to detect thermal events associated with disordered phases that form at higher temperatures in the jennite system pre-heated to 175°C. DMTA appears to be a promising method for studying the effect of dehydration on the engineering behavior of layered calcium silicate hydrate systems.

Introduction

The calcium-silicate-hydrate phases (C-S-H) are the principal binding components of Portland cement-based materials. These phases are major contributors to the engineering behavior of concrete including mechanical properties, volume stability and durability [1]. Investment in the sustainability of concrete infrastructure is a global issue. Long-term solutions are likely to involve advances in the fundamental understanding of the performance of C-S-H systems in various aggressive environments and elevated temperatures. Models for the nanostructure of the hydrated calcium silicates (in hydrated Portland cement or hydrated cement systems containing slag, fly ash or silica fume) that contain structural elements of 1.4nm tobermorite and jennite or 1.4nm tobermorite and calcium hydroxide have been proposed by Taylor and Richardson [2, 3]. Studies on the crystal structure and dehydration of these minerals have been reported [4-7]. There is little or no experimental information available, however, on the mechanical properties of these layered silicates. This study is an attempt to address this issue applying the dynamic mechanical thermoanalysis (DMTA) method on specimens made by compacting powders of synthetic 1.4nm tobermorite and jennite. The investigation also includes thermal pre-treatment of these minerals prior to DMTA testing to promote the formation of 1.1nm tobermorite and metajennite in order to assess their influence on mechanical performance.

Experimental

Materials

CaO: Calcium oxide was obtained by calcining reagent grade calcium carbonate at 900◦C.

SiO_2: Reactive silica (CAB-O-SIL, grade M-5 from Cabot Corporation, USA) was heated at 110°C to remove any surface adsorbed water.

The synthetic 1.4nm tobermorite and jennite were produced from the pozzolanic reaction between CaO and amorphous silica in excess water. Distilled water was de-aired and used for the reactions. All materials were kept sealed in N_2 purged bottles until they were used. Details of the synthesis are given below.

1.4nm Tobermorite: the reactants (CaO and SiO2) were prepared as described above. The C/S ratio was 0.9. The reactants were placed in a high density polyethylene bottle mixed in excess deionized water (water/solids = 11) and maintained at 80 °C using a heating wrap. The mixture was continuously agitated with a magnetic stirrer for a period of 4 months. The XRD spectrum and TGA curve were similar to those obtained by Yu and Kirkpatrick [4].

Jennite: the reactants (CaO and SiO2) were prepared as described above. The C/S ratio was 1.4. The reactants were placed in a high density polyethylene bottle mixed in excess deionized water (water/solids = 11) and maintained at 80 °C using a heating wrap. The mixture was continuously agitated with a magnetic stirrer for a period of 4 months. The XRD pattern was similar to that obtained by Yu and Kirkpatrick [4], Gard and Taylor [8] and Hara and Inoue [9]. The TGA curve matched that published by Yu and Kirkpatrick [4].

Humidity Conditioning

Specimens of 1.4 nm tobermorite and jennite were conditioned for several days at 11%RH in vacuum desiccators containing saturated lithium chloride solutions. The powders were conditioned at 11%RH before compaction and for several days after compaction.

Theoretically there is a monolayer of water on the surfaces of the particles in addition to interlayer water at this humidity.

Preparation of Compacted Specimens

Solid rectangular prism samples for the powdered materials were prepared by pressure compaction in steel moulds with a cross-section of 12.8 x 83 mm. The thickness of most of the prism samples was nominally 1mm but varied between the limits of 1-2mm.Numerous studies on the use and validity of compacts as models for hydrated cement systems have been published [10-14].It has been shown that compacted specimens of powdered hydrated Portland cement have similar mechanical property-porosity relationships to that of the original hardened paste of the same material[14]. The porosity of compacted samples was determined using helium pycnometry or by calculation using published density values. The calculation is made knowing the apparent volume and the solid volume of the sample.

Dynamic Mechanical Thermoanalysis (DMTA)

The dynamic mechanical analysis method (DMA) involves the application of an oscillating force to the sample and measurement of displacement [15].The elastic property obtained by DMA is referred to as the storage modulus (E'); it is analogous to the static modulus of elasticity. There is usually a time lag between the applied force and the resulting displacement. The time lag can be quantified in terms of a phase angle between the load and the displacement due to their ideally sinusoidal nature. The tangent of this angle ($\tan\partial$) represents the damping property of the material often referred to as internal friction. Additional details are given in a previous publication [16]. The DMTA experiments were

performed using a Rheometrics RSA II instrument on all samples in this investigation. The samples were heated from 25◦C to 300◦C. Temperature was increased in increments of 2◦C every 5 minutes. E' and tan∂ versus temperature curves were plotted. Each test took about 11h and 45min.to complete. The frequency ranged from 0.1 to 10 Hz.

Results and Discussion

The layered calcium silicate hydrates, 1.4nm tobermorite (T) and jennite (J), are the principal cementing minerals in composition-based models for the structure of hydrated Portland cement. The thermal stability and mechanical performance of these materials can potentially provide valuable insight into the engineering behavior of cement-based materials. Results from a dynamic mechanical thermoanalysis (DMTA) study of heat treated 1.4nm tobermorite and jennite are presented here. The influence of thermally induced phase changes, the removal of interlayer water and their effects on the reversible - irreversible nature of DMTA parameters (E' and tan∂) are also discussed.

DMTA-1.4nm tobermorite

Heat treatment of 1.4 nm tobermorite

The thermal treatment of 1.4nm tobermorite conditioned to 11% RH (reference sample) was followed by X-ray diffraction (Figure 1). A series of consecutive vacuum heat treatments (i.e. specimens for each thermal treatment were previously heated according to the preceding steps in the series) was employed as follows: 24 h at room temperature; 48h at 46°C; 72h at 65°C;48h at 70°C; 48h at 79°C;72h at 96°C;24h at 108°C and 72h at 175○C. The 002 basal reflections were approximately 1.34, 1.17, 1.14, 1.14, 1.12, 1.10, 1.10 and 1.10nm

respectively. A separate treatment of a sample conditioned at 11%RH and heated for 72h at 175°C was made. The product of the latter was 1.1nm tobermorite as confirmed by x-ray diffraction. It is apparent that the applied heat treatments resulted in a progressive decrease in basal-spacing reaching the 1.1nm form of tobermorite in the last three steps.

The thermal treatment of 1.4 nm tobermorite selected for discussion in this section included pre-heating for 3days under vacuum at 65°C and 3 days at 175°C. The DMTA results (E' and tan∂ versus temperature curves) for the reference (no previous heat treatment, equilibrated at 11%RH) and the 65°C treated sample (frequency = 3.98 Hz) are presented in Figure 2(a) and 2(b) respectively. The samples were comprised of compacted 1.4nm tobermorite (420 MPa compaction pressure, 30% porosity). This is a relatively low porosity value and was chosen to investigate the effects of any nanostructural changes that would occur in a confined space. The results for the powdered samples compacted at 70 MPa (59% porosity) are presented in Figure 3(a) and 3(b) respectively. Details of the DTMA experiments are as follows.

E' versus temperature curves at low porosity- reference and system pre-heated at 65°C

Differences in the E' versus temperature curves for the reference and the 65°C heat-treated sample (Figure 2(a)) are discussed as follows.

There is a small decrease in E' for the reference sample (25 to 35°C) from about 18.25 to 18 GPa, primarily due to the removal of surface adsorbed water and possibly some interlayer water [17]. This is followed by a rapid decrease to a value of about 14.2 GPa at 70°C. This

decrease corresponds to the removal of both surface and interlayer water. Removal of additional interlayer water and the conversion of 1.4nm tobermorite to the 1.2 form occurs as the temperature increases further to about 100°C [4]. E' decreases slightly to 13.8 GPa during this period. In addition there is a density increase (2.23 g/cm^3 to 2.40 g/cm^3, [18]) resulting in an increase in porosity along with a loss of 4 moles of structural water. E' continues to decrease to a value of 12.2 GPa as the temperature decreases to 300°C. This is accompanied by a conversion to the 1.1nm form in the temperature region, 130-160°C and a transformation to the 0.96 form at about 260°C. Two moles of water are lost at about 200°C with an additional 2 moles at about 260°C. The continued decrease in E' may be due to density increases accompanying phase changes along with the removal of additional interlayer water. These effects would appear to counteract any stiffening due to interactions of interlayer Ca^{2+} ions with the silicate sheets [18]. The E' curve decreases in a smooth monotonic fashion unlike that of the curve for samples at higher porosity levels (to be discussed later).

The initial value of E' for the sample vacuum treated at 65°C increased to 20.5 GPa relative to the reference sample at the 11%RH condition (18.3 GPa) inspite of the loss of surface and interlayer water due to the treatment. The 002 basal-spacing has decreased to about 1.14nm during the heat treatment prior to the DMTA experiment. It would appear that this transformation resulting from 3 days treatment at 65°C is sufficient to stiffen the system relative to the reference sample. This may possibly be due to interactions of interlayer Ca2+ ions with the silicate sheets. E' then decreases to 15 GPa at 50°C similar to the reference sample. E' reduces to 10 GPa at 70°C, a much larger decrease than the reference sample. E'

then slowly decreases to 9 GPa as heating continues and the temperature increases to 300°C. The phase changes and loss of the remaining interlayer water apparently have little effect on the resultant values of E' in this temperature region. These are possibly counterbalanced by interactions of Ca^{2+} with the silicate sheets and cross-linking effects.

Tan∂ versus temperature curves at low porosity-reference and system pre-heated at 65°C

The tan∂ versus temperature curves of the reference and the pre-heated sample (Figure 2(b)) are similar in character with one major exception. The tan∂ value for the pre-heated sample is initially much lower at the starting temperature of 25°C. It has a steep rise to a maximum value at about 55°C. The remainder of the curve at higher temperatures is similar in both systems. The tobermorite layers in the pre-heated system have come closer together as evidenced by the basal-spacing changes restricting translation and resulting in a low value of internal friction. The rapid increase in internal friction is due to the additional removal of interlayer water and possibly porosity increase due to density changes accompanying a gradual phase change. There is a subsequent decrease in tan∂ which is similar in magnitude for both systems. This decrease terminates between 120 and 140°C. It is suggested that continual removal of interlayer water and lack of uniformity in consolidation of the layers in confined space (i.e. low porosity) is restrictive and results in a decrease in internal friction. The 1.4nm tobermorite converts to the 1.1nm form in the temperature range of 130-160°C. This is likely rate dependent to some extent. There is however a peak in the tan∂ curve at 150°C and 170°C of similar magnitude for the reference and pre-heated sample respectively.

The increase to the maximum, in both cases, is likely due to the conversion to the 1.1nm form along with an increase in solid density and porosity. The continued removal of interlayer water after the maximum is reached results in a decrease in internal friction up to a temperature of about 180 and 200°C for the reference and pre-heated systems respectively. In both systems this is followed by an increase in internal friction up to 300°C. Yu and Kirkpatrick have reported the loss of two moles of water at 200°C and again at 260°C, the latter accompanying a phase change to the 0.96 form of tobermorite [4]. These events, coincident with density and porosity increases, would appear to be conducive to translation of the layers as evidenced by the increase in internal friction.

E' versus temperature curves at high porosity- reference and system pre-heated at 175°C

Differences in the E' curves for the reference and the heat treated systems compacted to a porosity of 59% (Figure 3(a)) are as follows. The initial value of E' after heat treatment is 4.58GPa representing a 25% increase from the value for the reference sample. Heat treatment results in the formation of the 1.1nm form of tobermorite. The increase in the initial value of E' is likely due to Ca^{2+} interactions with the silicate sheets and possible cross-linking effects (Q3 sites have been observed using ^{29}Si MAS NMR spectroscopy) during the phase transformation to the 1.1 nm form [4, 5]. The E' values for the pre-heated sample continuously decrease with temperature with a change in slope at about 100°C. The nearly linear decrease in E' from 100 °C to 300°C is attributed to the loss of two moles of water at both 200 °C and 260°C as well as increased porosity due to the transition to the 0.96 form.

The E' versus temperature curve for the reference 1.4nm tobermorite sample (initially at 11%RH) is more complex than the reference curve for lower porosity samples containing several points of inflection at the following temperatures: 40 °C; 60°C; 100°C. The first two inflections correspond to the removal of surface and interlayer water. The third corresponds to the formation of the 1.2nm form. There is also a clearly visible peak at about 150°C associated with formation of the 1.1nm form of tobermorite. The linear decrease in E' values from about 175°C to 300°C is similar in character to that of the reference sample described previously.

Tan∂ versus temperature curves at high porosity- reference and system pre-heated at 175°C

The tan∂ versus temperature curve for the reference system (Figure 3(b)) exhibits peaks having maximum values at about 40, 75, 100 and 130°C. These peaks correspond to similar events described above for the E' data i.e. the removal of surface and interlayer water and the transformation from the 1.4nm form to the 1.2 and 1.1nm form. Following the peak at 130°C there is a relatively steep decrease in internal friction until about 175°C where there is an abrupt decrease in slope. A point of inflection at about 220°C occurs followed by a further gradual decrease in tan∂ values as temperature is increased to 300°C. The latter decreases correspond to further removal of interlayer water and the phase transition to the 0.96 form of tobermorite.

The tan∂ versus temperature curve for the pre-heated sample is similar in character to the latter part of the reference curve following the peak at 130°C. There is a decrease in tan∂ up to 100°C followed by an increase to a maximum at about 220°C. This is not unexpected as

the starting material in this case has already been converted to the 1.1nm form. The observations are also associated with the removal of interlayer water and the phase transition to the 0.96 form of tobermorite.

DMTA-jennite

Heat treatment of jennite

The thermal treatment of jennite conditioned to 11% RH (reference sample) was followed by x-ray diffraction (Figure 4).Jennite was vacuum treated for 24h at room temperature and subsequently heated at 46°C for 48h and at 70°C for 48h . Jennite conditioned at 11%RH was also directly heated at 79°C for 72h and 175°C for 72h. The 70°C heat treatment resulted in the formation of metajennite as evidenced by a shift in the x-ray basal-spacing from 1.04 to 0.87nm.Jennite remained present with heat treatments at lower temperatures. Specimens for the DMTA tests included room temperature reference jennite samples conditioned to 11%RH, and those treated at 79°C and 175°C as the latter were comprised of metajennite or its dehydration products. DMTA results for high porosity (48%) and low porosity (33%) systems were selected for the discussion that follows.

E' versus temperature curves at low porosity-reference system and system pre-heated at 79°C

The E' versus temperature curve for the reference has four distinct regions: 25-35°C; 35-90°C; 90-175°C; 175-300°C (Figure 5(a)). There is a continuous decrease in E' over the entire temperature range. The loss of surface and interlayer water occur over the first two regions. The formation of metajennite occurs in the third temperature region. This is accompanied by the loss of 4 water molecules and a large change in density (2.33g/cm^3 to

2.62g/cm^3 [18]) with a concomitant increase in porosity. A significant decrease in E' occurs on heating to 300°C. This is accompanied by removal of the final 2 moles of water and the transformation of metajennite into a disordered phase [4].

The E' versus temperature curve for the heat-treated jennite (at 79°C) is similar in character to that of the reference system in the 175-300°C region. The corresponding dehydration events and transformation to a disordered phase are also similar. It is noteworthy that the value of E' is about 11.9 GPa for the reference beginning in the third temperature region and the initial value of the heat- treated sample is about 13.7 GPa.It would appear that the metajennite formed through heat treatment at 79 °C is only marginally different than the metajennite formed by gradually heating jennite (conditioned to 11% RH) from room temperature.

Tan∂ versus temperature curves at low porosity-reference system and system pre-heated at 79 °C.

The tan∂ values for the reference (Figure 5(b)) decrease on heating from 25 to 110°C with a small peak occurring at about 60°C and an inflection point at 80°C. The general decrease in tan∂ is possibly due to the interactions of interlayer Ca^{2+} ions with the silicate sheets as there are Ca^{2+} and water molecules in the interlayer space. There are no Q^3 signals observed in the ^{29}Si MAS NMR experiments [4] with jennite unlike tobermorite suggesting that any cross-linking of the silicate sheets may be minimal in the jennite system. Events at 60 and 80°C are likely associated with the removal of interlayer water allowing for small increases in internal friction. The large increase in tan∂ in the temperature range 110 to 145°C is associated with the formation of metajennite, the accompanying loss of 4 water molecules

from the interlayer and a significant increase in density and porosity. Further removal of 2 moles of water from metajennite in the temperature range 145 to 220°C likely results in additional interactions involving interlayer Ca^{2+}. The gradual increase in tan∂ as temperature is increased from 220 to 300°C is likely related to the formation of a disordered phase [4].

The pre-heated sample is primarily composed of metajennite. The tan∂ versus temperature curve mimics the reference curve beginning at 110 °C. The interpretation of the thermal events is similar.

E' versus temperature curves at high porosity-reference system and system pre-heated at 175°C

The E' versus temperature curve for the reference system (high porosity) has four distinct regions at similar locations to those of the low porosity system (Figure 6(a)). The initial E' value (8.1GPa) is lower than the low porosity value as expected. The interpretation of the thermal events is similar.

The E' versus temperature curve for the pre-heated system mimics the reference curve from 175 °C to 300°C. E' for the reference sample at 175°C is 5.5GPa. The initial E' for the pre-heated sample is 5.5GPa. E' for the pre-heated system decreases continuously as the temperature is increased from 25 to 300°C. Dehydration and the transition from metajennite to disordered phases at temperatures above 200°C occur.

Tan∂ versus temperature curves at high porosity-reference system and system pre-heated at 175°C

The tan∂ versus temperature curve for the high porosity reference system has similarities to the reference curve for the low porosity reference system, at temperature above 100°C the

primary difference is the increase in intensity of the low temperature peaks (Figure 6(b)). The interpretation of the thermal events is the same.The tan∂ curve for the pre-heated system reflects the further dehydration and transition to disordered phases. Peaks at 100°C and 225°C may possibly be associated with the disordering process. The presence of disordered phases at higher temperatures was confirmed by Yu and Kirkpatrick [4].

Conclusions

1. Dynamic mechanical thermoanalysis (DMTA) is sensitive to nanostructural changes that occur on drying of 1.4nm tobermorite and jennite including removal of surface and interlayer water.

2. DMTA can detect phase changes of 1.4nm tobermorite and jennite that occur on heating these systems from the 11%RH condition.

3. DMTA exhibits thermal events that are sensitive to the effects of pre-heating 1.4nm tobermorite and jennite to temperatures associated with phase transformations.

4. Differences in the character of the E' and tan∂ versus temperature curves due to pre-heating 1.4nm tobermorite to 65 and 175°C can be explained by changes in basal spacing, phase changes e.g. to the 1.1nm form and accompanying changes in density and porosity. Pre-heating results in irreversible effects including increases in E' (stiffness) at 25°C.

5. Differences in the character of the E' and tan∂ versus temperature curves due to pre-heating jennite to 79°C and 175°C are not pronounced as is the case for pre-heating 1.4nm tobermorite.

6. The DMTA response resulting from the formation of metajennite (79°C) and the dehydration of metajennite (175 °C) during the pre-heating treatment mimics that part of the DMTA curve for the reference sample obtained at those temperatures.

7. The pre-heating treatment does not significantly affect the E' and tan∂ values for metajennite or its dehydration products as determined from DMTA tests on the reference system conditioned to 11% RH.

8. The DMTA method is able to detect thermal events associated with disordered phases that form at higher temperatures in the jennite system pre-heated to 175°C.

9. DMTA is a promising method for studying the effect of dehydration on the engineering behavior of layered calcium silicate hydrate systems.

References

1. Taylor H. F.W., Hydration of the calcium silicate phases, Cement Chemistry, Chapter 5, Thomas Telford Publishing, London, pp.459, 1997.

2. Taylor H.F.W., Proposed structure of calcium silicate hydrate gel, J. Amer. Ceram. Soc.69 (6), 464-467, 1986.

3. Richardson I. G., The calcium silicate hydrates, Cem. Concr. Res., 38(2), 137-158, 2008.

4. Yu P. and Kirkpatrick R. J., Thermal dehydration of tobermorite and jennite, Concr. Sci. and Eng., 1, 185-191, 1999.

5. Taylor H.F.W., The dehydration of tobermorite, Clay and Clay Minerals, 6(1), 101-109, 1956.

6. Viehland D., Yuan L. J., Xu Z., Kong X.-D., Kirkpatrick R. J., Structural studies of jennite and 1.4nm tobermorite. Disordered layering along the [100] of jennite. J. Amer. Ceram. Soc., 80(12), 3021-3028, 2005.

7. Bonacorrsi E., Merlino S., Taylor H.F.W., The crystal structure of jennite, $Ca_9Si_6O_{18}(OH)_6.8H_2O$, Cem. Concr. Res., 34, 1481-1488, 2004.

8. Gard J. A. and Taylor H. F. W., Calcium silicate hydrate (II) ("C-S-H(II)"), Cem. Concr. Res., 6, 667-678, 1976.

9. Hara N. and Inoue N., Formation of jennite from fumed silica, Cem. Concr. Res., 10, 677-682, 1980.

10. Soroka I. and Sereda P.J., The structure of cement- stone and use of compacts as structural models, Proc. 5th Int. Symp. on the Chem. of Cem., Vol. 3., Tokyo, 67-73,1968.

11. Feldman R. F., Factors affecting the Young's modulus-porosity relation of hydrated Portland cement compacts, Cem. Concr. Res., 2(4), 375-386, 1972.

12. Sereda P.J. and Feldman R. F., Compacts of powdered material as porous bodies for use in sorption studies, J. Appl. Chem., 13, 150-158, 1963.

13. Beaudoin J.J., Comparison of mechanical properties of compacted calcium hydroxide and Portland cement paste systems, Cem. Concr. Res., 13, 319-324, 1983.

14. Sereda P.J., Feldman R.F. and Swenson E.G., Effect of sorbed water on some mechanical properties of hydrated Portland cement pastes and compacts, Highway Research Board, Special Report 90, 58-73, 1966.

15. Menard K. P., Dynamic Mechanical Analysis-A Practical Introduction, CRC Press LLC, Boca Raton, pp. 208, 1999.

16. Alizadeh R., Beaudoin J. J. and Raki L., Mechanical properties of calcium silicate hydrates, Matls. and Struct., 44, 13-28, 2011.

17. Feldman R. F. and Ramachandran V. S., Differentiation of interlayer and adsorbed water in hydrated Portland cement by thermal analysis, Cem. Concr. Res., 1(6), 607-620, 1971.

18. Thomas, Jefferey J., Jennings H. M. and Allen A.J., Relationships between composition and density of tobermorite, jennite and nanoscale CaO-SiO2-H2O, J. Phys. Chem. C, 114, 7594-7601, 2010.

Figure Captions

Figure 1. X-ray diffraction spectra for 1.4nm tobermorite subjected to various dehydration treatments- changes in 002 basal-spacing.

Figure 2. (a) E' versus temperature curves: (1) 1.4nm tobermorite conditioned at 11% RH (2) 1.4nm tobermorite pre-heated under vacuum at 65°C for 3 days. Porosity = 30%.

Figure 2. (b) tan∂ versus temperature curves: (1) 1.4nm tobermorite conditioned at 11% RH (2) 1.4nm tobermorite pre-heated under vacuum at 65°C for 3 days. Porosity = 30%.

Figure 3. (a) E' versus temperature curves: (1) 1.4nm tobermorite conditioned at 11% RH (2) 1.4nm tobermorite pre-heated at 175°C for 3 days. Porosity = 59%.

Figure 3. (b) tan∂ versus temperature curves: (1) 1.4nm tobermorite conditioned at 11%RH (2) 1.4nm tobermorite pre-heated at 175°C for 3 days. Porosity = 59%.

Figure 4. X-ray diffraction spectra for jennite subjected to various dehydration treatments- changes in 002 basal spacing.

Figure 5. (a) E' versus temperature curves: (1) jennite conditioned at 11% RH (2) jennite pre-heated under vacuum for 3 days at 79°C. Porosity = 33%.

Figure 5. (b) tan∂ versus temperature curves: (1) jennite conditioned at 11% RH (2) jennite pre-heated under vacuum for 3 days at 79°C. Porosity = 33%.

Figure 6. (a) E' versus temperature curves: (1) jennite conditioned at 11% RH (2) jennite pre-heated under vacuum for 3 days at 175°C. Porosity = 48%.

Figure 6. (b) tan∂ versus temperature curves: (1) jennite conditioned at 11% RH (2) jennite pre-heated under vacuum for 3 days at 175°C. Porosity = 48%.

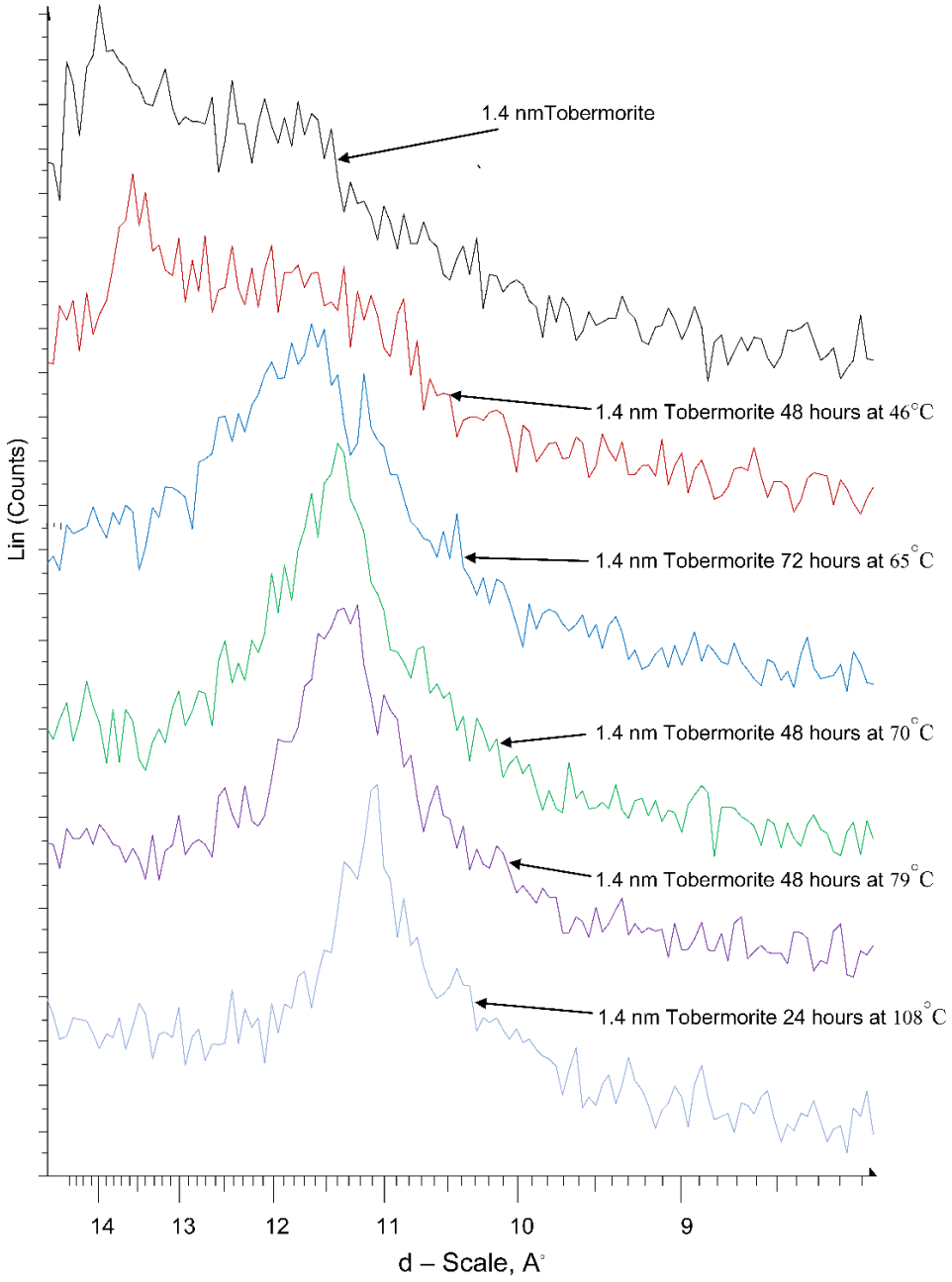

Figure 1. X-ray diffraction spectra for 1.4nm tobermorite subjected to various dehydration treatments- changes in 002 basal-spacing.

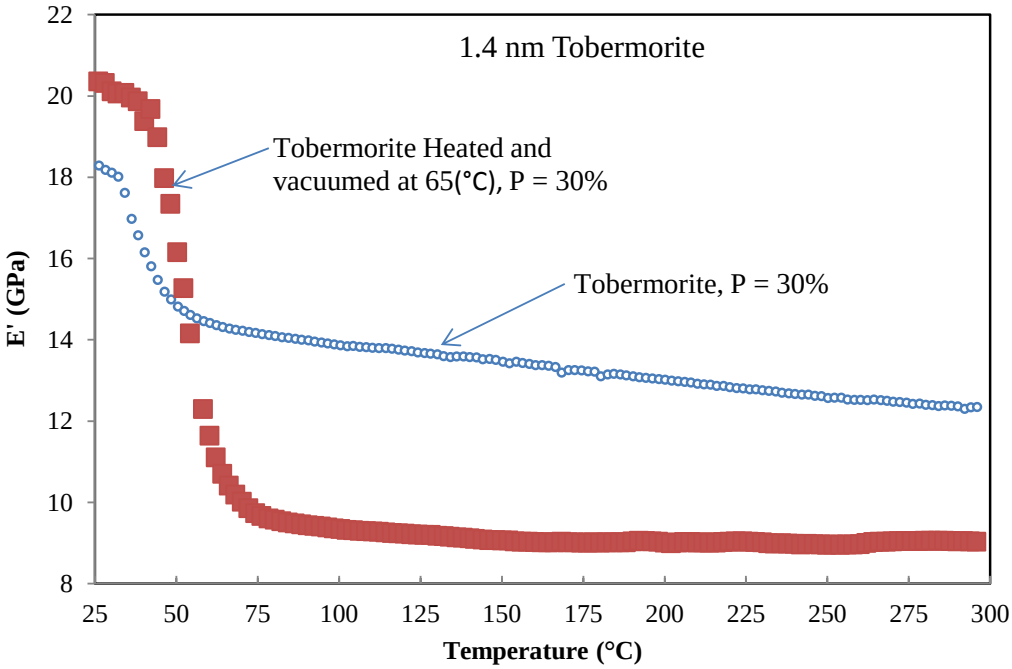

Figure 2. (a) E' versus temperature curves: (1) 1.4nm tobermorite conditioned at 11% RH (2) 1.4nm tobermorite pre-heated under vacuum at 65°C for 3 days. Porosity = 30%.

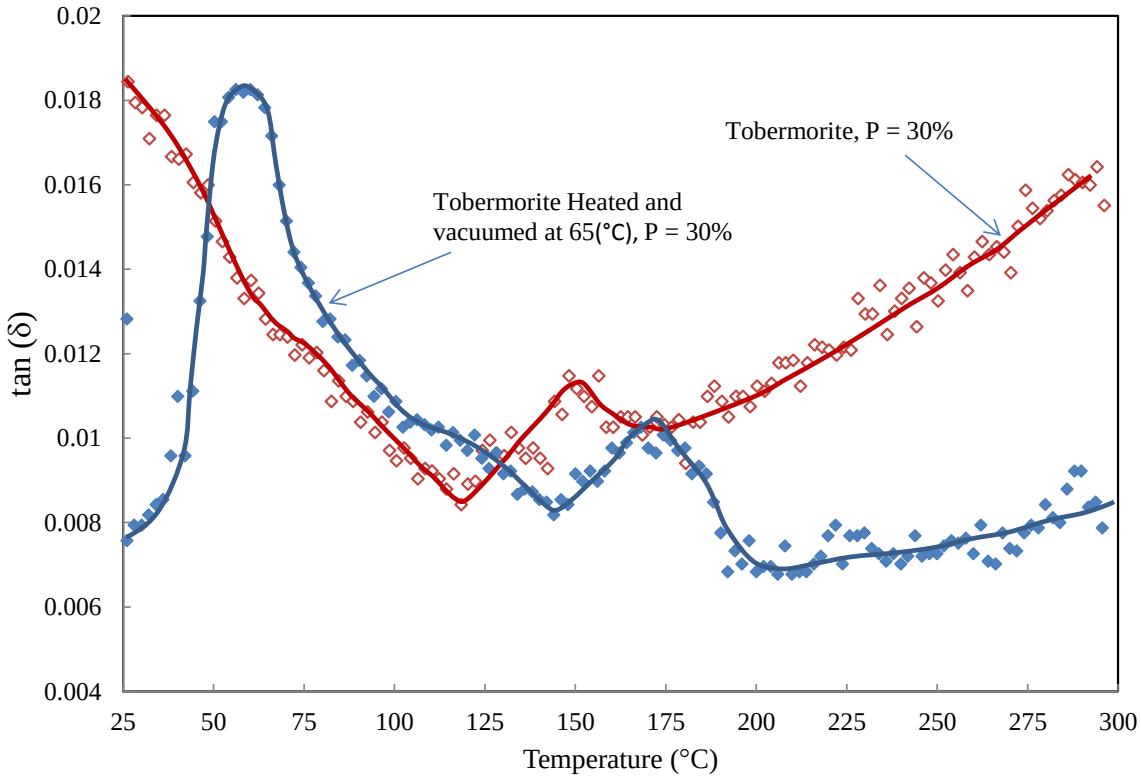

Figure 2(b). tan∂ versus temperature curves: (1) 1.4nm tobermorite conditioned at 11% RH (2) 1.4nm tobermorite pre-heated under vacuum at 65°C for 3 days. Porosity = 30%.

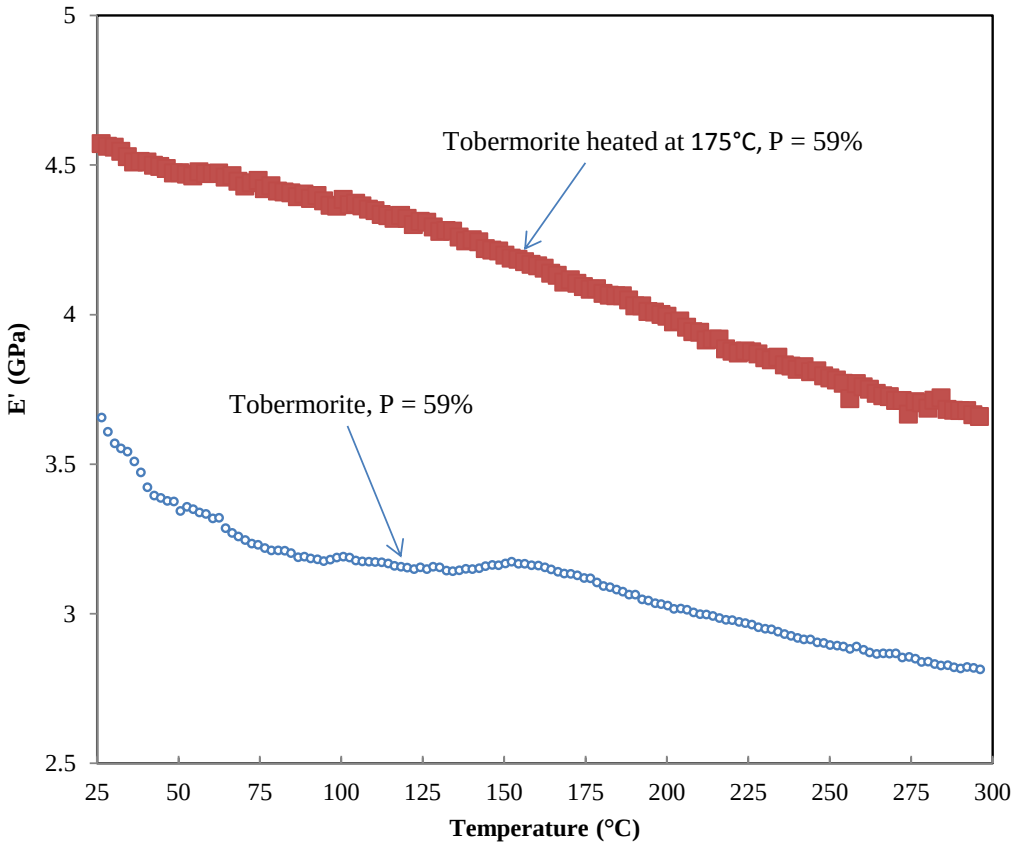

Figure 3. (a) E' versus temperature curves: (1) 1.4nm tobermorite conditioned at 11% RH (2) 1.4nm tobermorite pre-heated at 175°C for 3 days. Porosity = 59%.

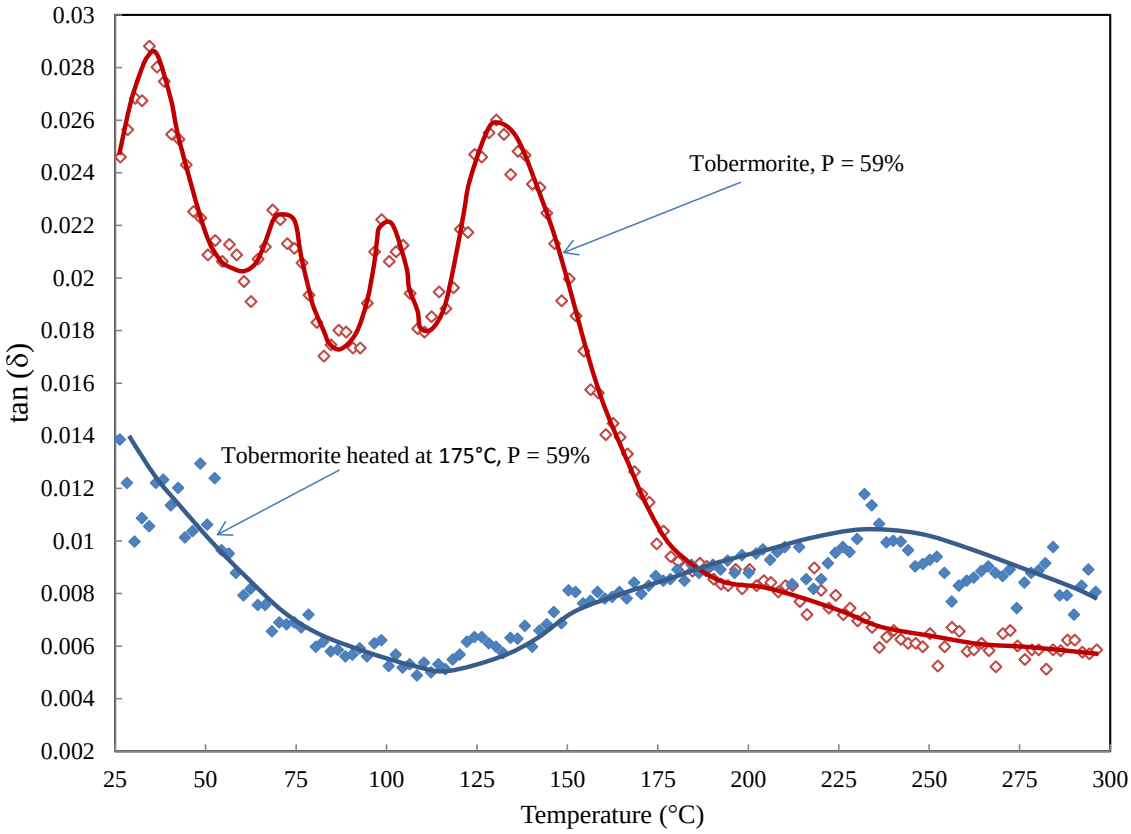

Figure 3(b). tan∂ versus temperature curves: (1) 1.4nm tobermorite conditioned at 11% RH (2) 1.4nm tobermorite pre-heated at 175°C for 3 days. Porosity = 59%.

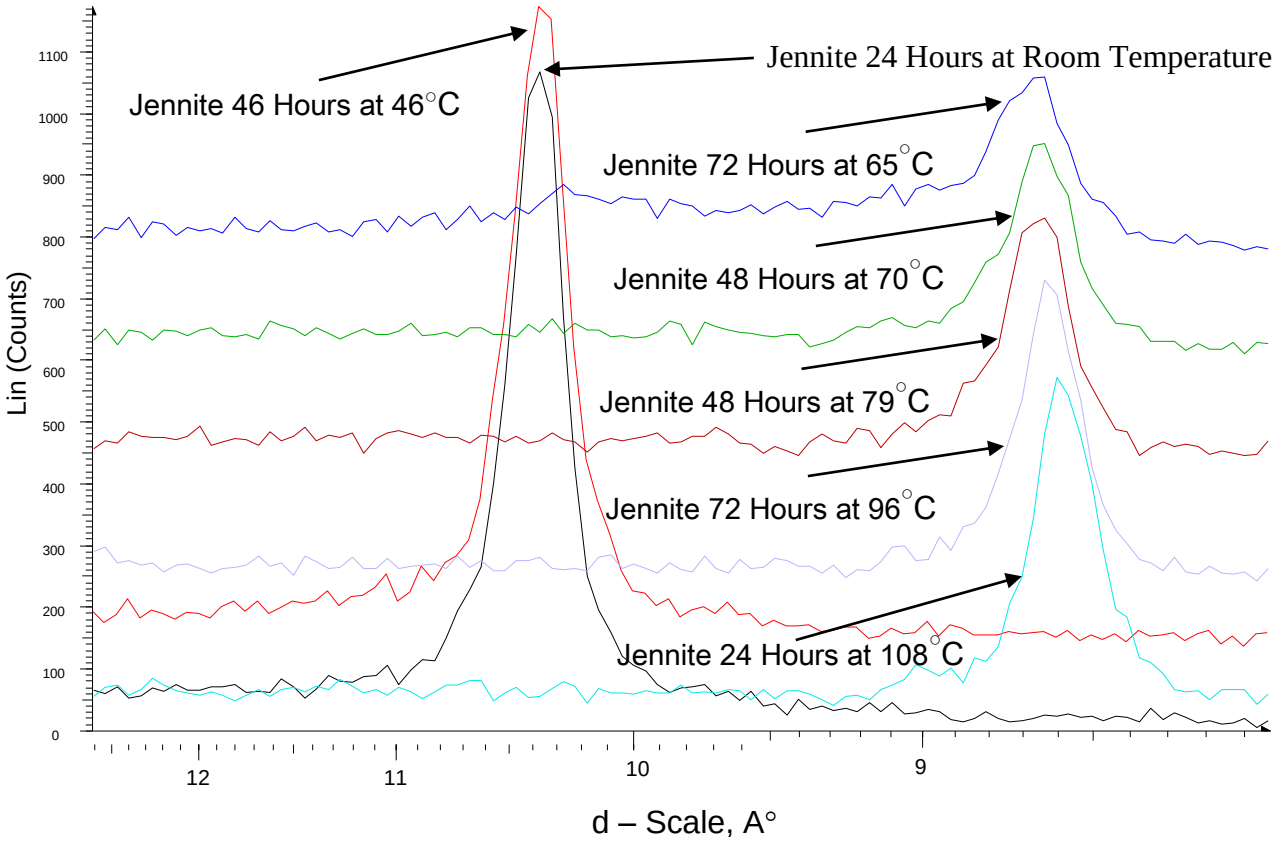

Figure 4. X-ray diffraction spectra for jennite subjected to various dehydration treatments-changes in 002 basal spacing.

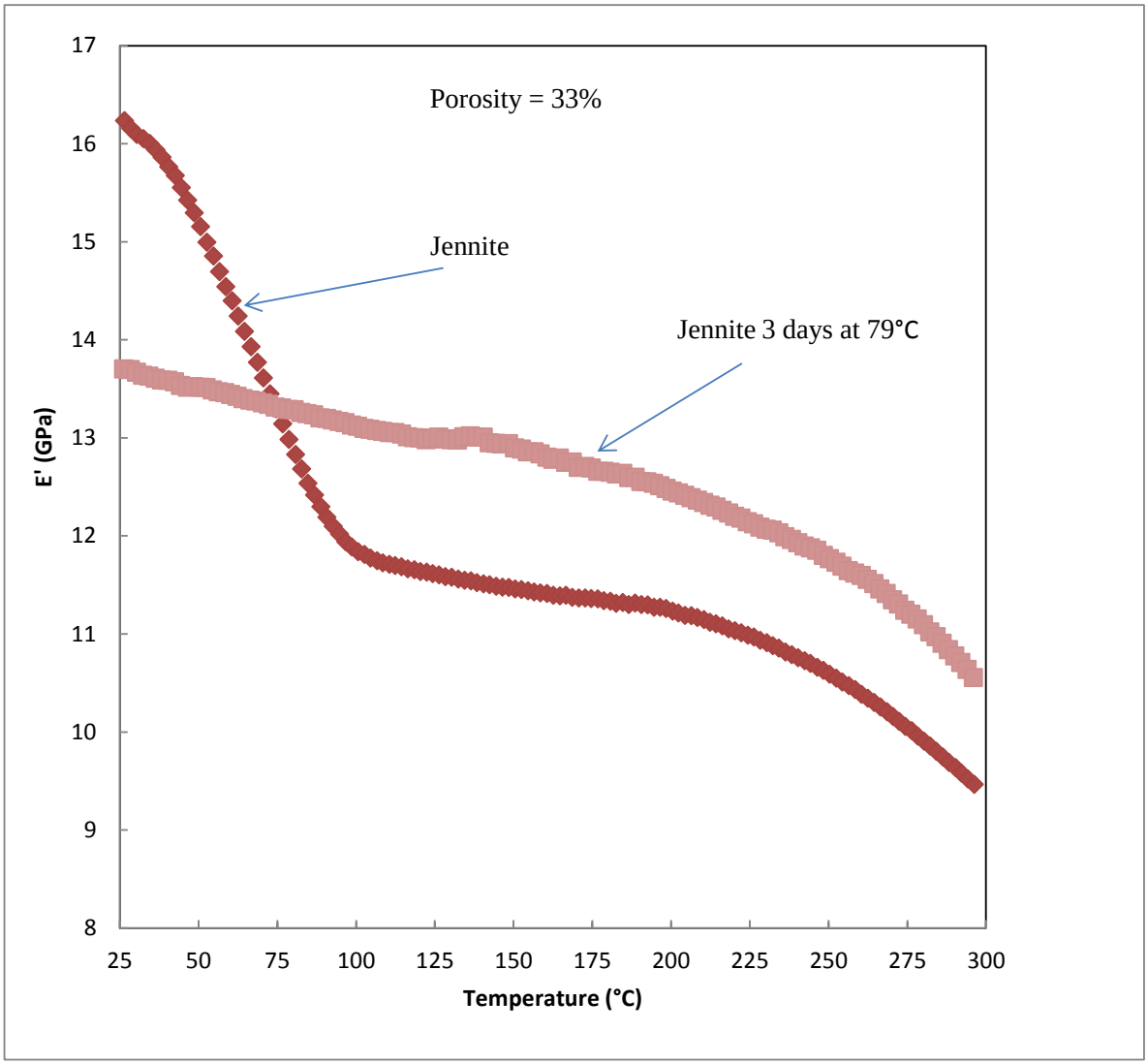

Figure 5(a). E' versus temperature curves: (1) jennite conditioned at 11% RH (2) jennite pre-heated under vacuum for 3 days at 79°C. Porosity = 33%.

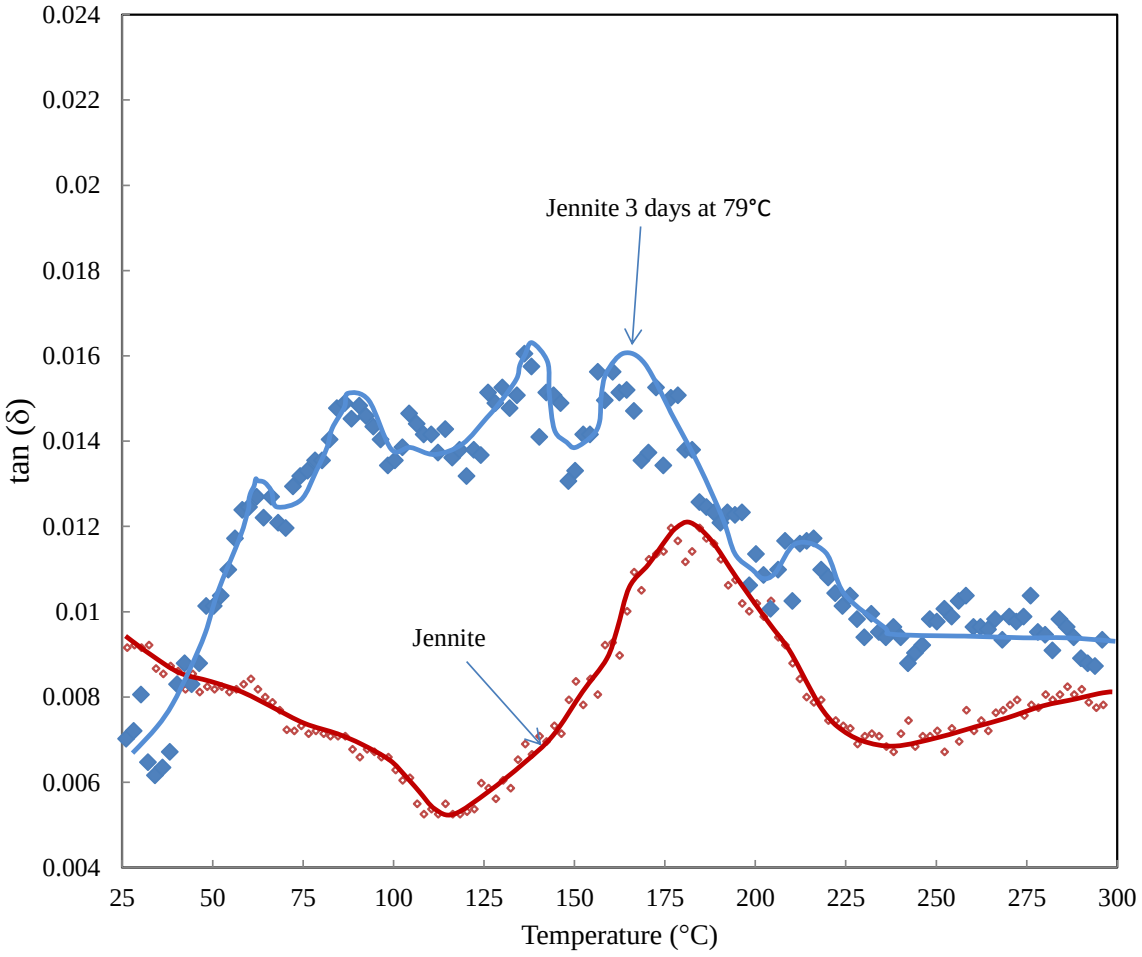

Figure 5(b) tan∂ versus temperature curves: (1) jennite conditioned at 11% RH (2) jennite pre-heated under vacuum for 3 days at 79°C. Porosity = 33%.

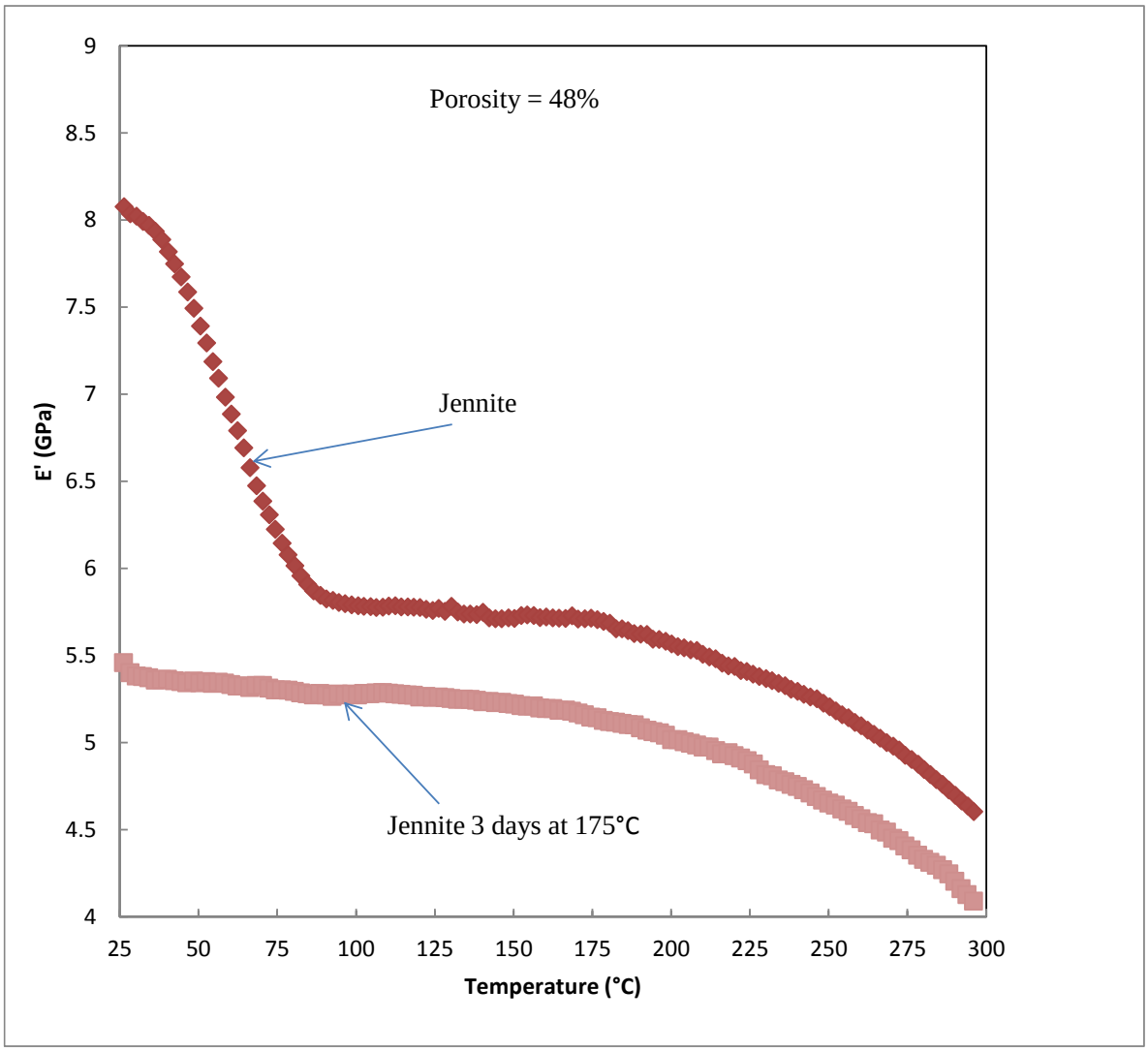

Figure 6(a). E' versus temperature curves: (1) jennite conditioned at 11% RH (2) jennite pre-heated under vacuum for 3 days at 175°C. Porosity = 48%.

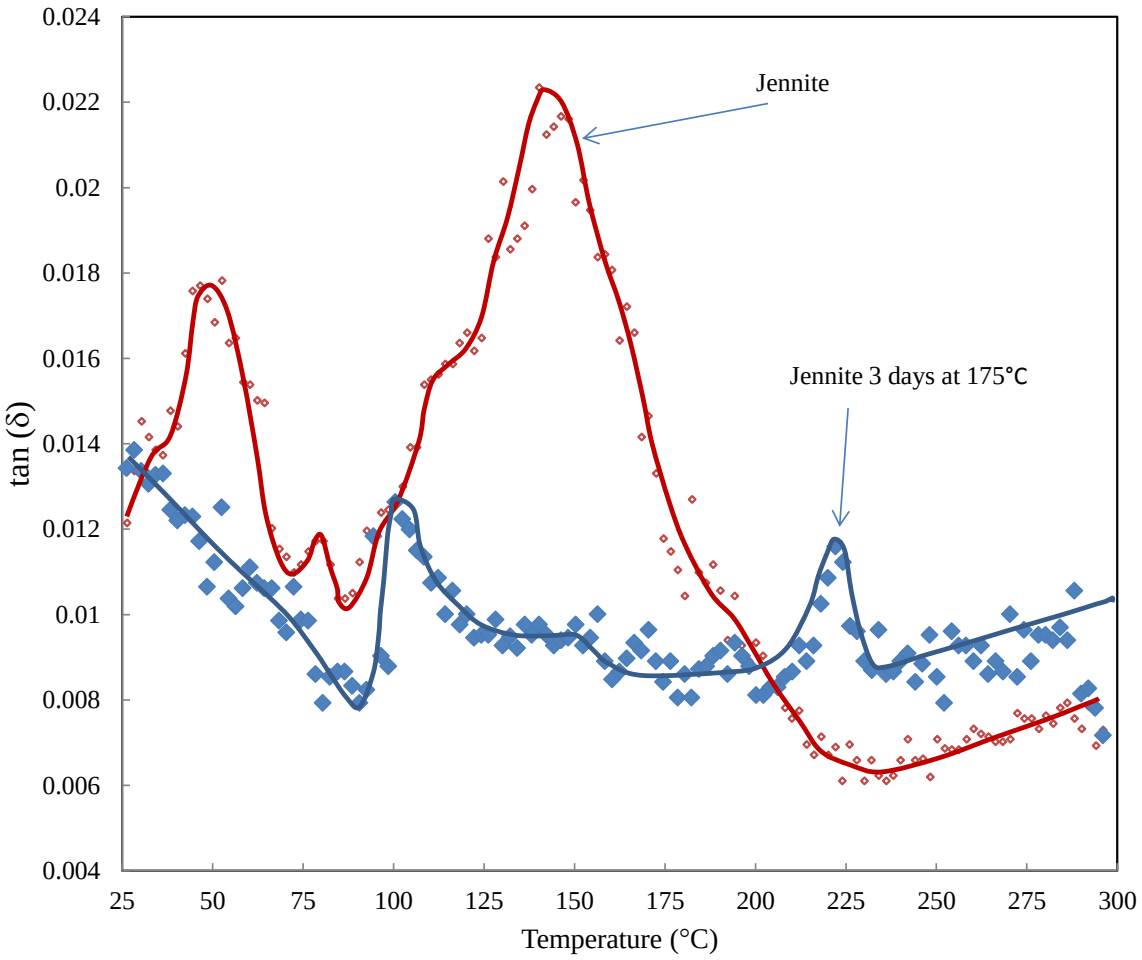

Figure 6(b). tan∂ versus temperature curves: (1) jennite conditioned at 11% RH (2) jennite pre-heated under vacuum for 3 days at 175°C. Porosity = 48%.

Chapter 9

Volume Stability and Mechanical Property-Porosity Relationships of Layered Calcium-Silicate-Hydrates

Research results that focus on the volume stability and mechanical property-porosity relationships of layered calcium-silicate-hydrates are described in this chapter (Part 2 of the experimental section of the thesis). The research findings are presented in three journal papers i.e. Papers 4, 5 and 6. The work addresses these characteristics of the 1.4 nm tobermorite and jennite mineral systems that are key elements of composition-based models for C-S-H in hydrated cementitious materials. Comparisons are made with hydrated Portland cement paste. The non-uniqueness of storage modulus-porosity curves obtained using DMA methods is discussed in Paper 4 of the series with reference to Taylor's analysis of strength-porosity curves and the influence of particle type, density and crystallinity. Additional insights regarding the practical application of T-J and T-CH nanostructural models for the C-S-H phase in hydrated cements is provided**.**

Length-change –mass-loss curves on drying from the 11% RH condition for C-S-H, T and J were critically examined in Paper 5. Mechanisms of shrinkage in terms of the contribution of adsorbed and interlayer water are discussed. The x-ray basal-spacing changes of the layered silicates on drying were assessed and inferences drawn regarding nano-structural models for C-S-H in hydrated cement paste. The dimensional stability and the role of the

removal of 'structural' water from the layered silicates are discussed in terms of their relevance to cement-based materials. The research findings strengthen the case for compliance of experiment with the composition-based structural models for hydrated cement.

The thermodynamic instability and the ability to 'regenerate' elastic properties following prolonged thermal drying of layered silicates was demonstrated in Paper 6.Decreases in elastic modulus relative to the 11% RH condition typically observed in a DMTA test were recovered subsequent to the prolonged thermal treatment. The recovery or 'regeneration' was observed for all the calcium-silicate systems studied. The results are compatible with the notions expressed for nanostructural models of C-S-H in cement paste that are comprised of structural units of T and J.

The titles of the papers in this chapter are as follows:

Paper 4: Mechanical Property-Porosity Relationships of Layered Calcium Silicate Hydrate Phases, Materials and Structures 46(9), 1489-1495, 2013.

Paper 5: Dimensional Stability of 1.4 nm Tobermorite, Jennite and Other Layered Calcium Silicate Hydrates, Advances in Cement Research, 26(1), 1-9, 2014.

Paper 6: Drying of Calcium Silicate Hydrates: Regeneration of Elastic Modulus, Advances in Cement Research, DOI: 10.1680/adcr.14.00048.

9.1 Introduction

The three papers in this chapter form contributions related to the physico-mechanical behaviour of layered calcium-silicate hydrates. The experimental results presented support arguments for the compatibility of existing composition-based models for C-S-H present in cement paste and are consistent with models comprised of 1.4 nm tobermorite and jennite. It is believed that the mechanical properties presented in the thesis for the latter two layered silicate minerals are the first to be published and represent novel and unique data. The behavioural characteristics reported in this chapter i.e. storage modulus and shrinkage are fundamental to the satisfactory performance of cement-based materials. The performance of the pure silicate phases should be first determined and then satisfactorily understood in the context of their compatibility with practical materials such as cement paste. A brief summary of the content and theme of each paper presented in this chapter will precede the inclusion of the full paper.

9.2 Paper 4: Mechanical Property-Porosity Relationships of Layered Calcium Silicate Hydrate Phases

Storage modulus (obtained from DMA experiments) versus porosity curves were generated for several pure layered calcium silicate hydrate systems in addition to Portland cement paste. Taylor's porosity-proportion of dense crystalline material-strength diagram was a useful tool for explaining the porosity dependence of the pure phases in this study. Other important factors that influence the relative position of these curves include the average silicate chain length/number of defects, C/S ratio of the C-S-H, BET nitrogen surface area, degree of hydration (in the case of Portland cement). The storage modulus versus porosity curves are

consistent with other published evidence for a tobermorite-jennite-based model for C-S-H nanostructure in hydrated cement paste.

Mechanical Property-Porosity Relationships of Layered Calcium Silicate Hydrate Phases

(Materials and Structures 46(9), 1489-1495, 2013)

P. Pourbeik[a], J. J. Beaudoin[a], R. Alizadeh[b] and L. Raki[a]

[a] *National Research Council Canada, Construction Portfolio, Ottawa, ON, Canada*

[b] *Giatec Scientific Inc., Ottawa, ON, Canada*

Abstract

Dynamic Mechanical Analysis (DMA) measurements were made on the following calcium-silicate- hydrate systems: 1.4 nm tobermorite (T), jennite (J), synthetic C-S-H (C/S = 0.80, 1.20 and 1.50) and cement paste. The age of the cement paste varied from 3days to 45 years. Plots of storage modulus versus porosity were constructed for all these materials. The non-uniqueness of the curves is discussed with reference to Taylor's analysis of strength-porosity curves and the influence of particle type, density and crystallinity. Additional insights regarding the practical application of T-J and T-CH nanostructural models for the C-S-H nanostructure in hydrated cements is provided.

Keywords: Layered Calcium Silicate Hydrate; Mechanical Properties; Dynamic Mechanical Analysis (DMA); Porosity

1 Introduction

Mechanical property-porosity relationships for cement-based materials have been studied extensively [1-4]. It was suggested by Taylor [5] and, Feldman and Beaudoin [6] that there is no unique strength-porosity relationship but rather a family of system specific curves that depend on other factors that include the proportion of coarse, dense and crystalline material. It is apparent that nanostructural aspects of C-S-H-the principal binding phase in hydrated Portland cements-influence mechanical performance. Current compositional models for the nanostructure of the silicate phases in hydrated cement are based on 1.4nm tobermorite-jennite (T-J) or 1.4nm tobermorite-calcium hydroxide (T-CH) structures [7-9]. It is suggested here that some insight as to the practical applicability of these models in terms of mechanical performance can be obtained directly from dynamic mechanical analysis (DMA) of pure phases including: 1.4nm tobermorite, jennite and synthetic C-S-H. A study was designed to determine the relationships between the storage modulus (E') and porosity for these phases and their mixtures in addition to cement pastes hydrated for periods up to 45 years. Taylor's approach was used to assess the mechanical performance of all the systems studied and its porosity dependence.

2 Experimental

2.1 Materials

Synthetic 1.4nm tobermorite, jennite, synthetic C-S-H and Portland cement paste were prepared as follows:

CaO: Calcium oxide was obtained by calcining reagent grade calcium carbonate at 900°C.

SiO_2: Reactive silica (CAB-O-SIL, grade M-5 from Cabot Corporation, USA) was heated at 110°C to remove any surface adsorbed water.

The synthetic 1.4nm tobermorite and jennite were produced from the pozzolanic reaction between CaO and amorphous silica in excess water.Distilled water was de-aired and used for the reactions. All materials were kept sealed in N_2 purged bottles until they were used. Details of the synthesis are given below.

1.4nm tobermorite: the reactants (CaO and SiO_2) were prepared as described above. The C/S ratio was 0.9. The reactants were placed in a high density polyethylene bottle mixed in excess deionized water (water/solids = 11) and maintained at 80 °C using a heating wrap. The mixture was continuously agitated with a magnetic stirrer for a period of 4 months. It was then filtered to remove excess water and placed in a desiccator over a saturated lithium chloride solution (11% RH) for several weeks. The XRD spectrum and TGA curve were similar to those obtained by Yu and Kirkpatrick [10].

Jennite: the reactants (CaO and SiO_2) were prepared as described above. The C/S ratio was 1.4. The synthesis procedure was similar to that described above for 1.4nm tobermorite. It was then filtered to remove excess water and placed in a desiccator over a saturated lithium chloride solution (11% RH) for several weeks. The XRD pattern was similar to that obtained by Yu and Kirkpatrick [10], Gard and Taylor [11] and Hara and Inoue [12]. The TGA curve matched that published by Yu and Kirkpatrick [10].

C-S-H: synthetic C-S-H was produced from the pozzolanic reaction between CaO and amorphous silica in excess water (water/solids = 11). Distilled water was de-aired and used for the reactions. All materials were kept sealed in N_2 purged bottles until they were used. Variation in C/S ratio was achieved by adjusting the stoichiometric amounts of the reactants.

The reaction period was 6 months. The material was then filtered and dried under vacuum for 4 days at room temperature. The dried C-S-H was stored in nitrogen purged glass vials before the experiments. Characterization of these materials by XRD and thermal methods gave results directly comparable to C-S-H (I) as reported by Taylor [13].

Portland Cement Paste: Three sets of Portland cement paste were used for these experiments. The first set (made with Type I Portland cement) was prepared using a water/cement ratio of 0.40. Rectangular prisms (250 x 100 x 12mm) were cast. The samples were vibrated and stored in a moist curing room for 24 h. They were then demoulded and curing was continued for 3 years in a saturated lime solution. Thin slices (1 x 12 x 60 mm) were cut from the paste prism using an Isomet diamond saw. Selected slices were also ground into a fine powder for fabrication into compacted specimens.

The second set of paste samples was prepared using water/cement ratios of 0.50, 0.70, 0.80, 0.90 and 1.00. The freshly mixed paste was placed in a tightly stoppered plastic tube 3.17 cm in diameter and allowed to rotate horizontally on rollers at the rate of 0.70 rpm. The paste cylinders were removed after 24 h and covered in a rubber membrane containing drops of lime saturated water and kept saturated by storage in glass cylinders for 45 years. Prior to testing, thin discs (1 mm thick) were cut and ground into a fine powder for fabrication into compacted specimens. The 45 year 'old' pastes were characterized by ^{29}Si MAS NMR and found to have a mean silicate chain length of approximately 4.1 units. The nitrogen BET surface areas were 65, 46, 40, 62 and 41m^2/g for the pastes respectively.

The third set of specimens was similar to the first set but differed only in that the hydration times were very short i.e. 3, 7 and 28 days.

2.2 Humidity Conditioning

All specimens were conditioned for at least one week after compaction at 11%RH in vacuum desiccators containing saturated lithium chloride solutions. The powders were conditioned at 11%RH before compaction for three weeks.

2.3 Preparation of Compacted Specimens

Solid rectangular prism samples for the powdered materials were prepared by pressure compaction in steel moulds with a cross-section of 12.8 x 83 mm. The thickness of most of the prism samples was nominally 1mm but varied between the limits of 1-2mm.Numerous studies on the use and validity of compacts as models for hydrated cement systems have been published [14-18]. It has been shown that compacted specimens of powdered hydrated Portland cement have similar mechanical property-porosity relationships to that of the original hardened paste of the same material [18]. The porosity of compacted samples was determined using helium pycnometry or by calculation using published density values. The calculation is made knowing the apparent volume and the solid volume of the sample.

2.4 Dynamic Mechanical Analysis (DMA)

The dynamic mechanical analysis method (DMA) involves the application of an oscillating force to the sample and measurement of displacement [19]. The elastic property obtained by DMA is referred to as the storage modulus (E'); it is analogous to the static modulus of elasticity. There is usually a time lag between the applied force and the resulting displacement. The time lag can be quantified in terms of a phase angle between the load and the displacement due to their ideally sinusoidal nature. The tangent of this angle (∂) is referred to as internal friction. Additional details are given in a previous publication [20].

The storage modulus measurements were found to be nearly frequency independent within the range tested i.e. 0.1 to 5Hz.

3 Results and Discussion

Taylor and Crennan and El-Hemaly and Taylor provided, for the first time, a rational approach for explaining the wide variation in strength properties of various normally cured and hydrothermally treated cement systems [5, 21]. The primary postulate was that there was no single or unique strength-porosity function for these materials. Other factors played important roles in strength determination. The authors of the current study found Taylor's approach useful for explaining the porosity dependence of the elastic or storage modulus (E') obtained from dynamic mechanical analysis (DMA). Storage modulus data for several pure phases (1.4nm tobermorite, jennite, synthetic C-S-H having variable C/S ratio) and cement pastes varying in age from a few days to 45 years was obtained. Many investigators have demonstrated a correlation between modulus of elasticity and compressive strength of concrete [22].

3.1 Strength versus porosity relationships for cement systems- Taylor's approach

It was suggested by Taylor [5] that Feldman and Beaudoin (F-B) [6] that at a given porosity the highest strength is obtained with an optimum blend of relatively dense well-crystallized material (type 1) and less dense poorly crystallized material (type 2).The proportion of type 1 material required increases at low porosity values. The F-B concept is that strength is

dependent on ***both*** the bonding properties of the particles and their intrinsic strength. The relative influence of these factors varies with porosity. Interparticle bonding is more important at high porosities requiring a high proportion of poorly crystallized material. It is also less important at low porosities as the intrinsically higher strengths of the denser particles influences the behavior of the composite. It was also noted that properties of some materials can only be described in terms of a distribution. Fly ash and granulated slag particles, for example, are large and dense but largely non-crystalline.

Taylor constructed a porosity-particle type-strength diagram to rationalize the variation in strength property for a wide range of cement systems including hydrothermally produced calcium- silicate- hydrates (see Figure 1, [5,21]). Lines AB, EF and CD in the figure (data from Feldman and Beaudoin ref. [6]) represent normally cured pastes, autoclaved cement-silica products and high density materials respectively.

Taylor emphasized that for a given blend of particle types different arrangements of particles are possible including different distributions of pore size and shape. His diagram will be used in the next section to explain the results of the systems investigated in the current study. In this context a few additional points are germane: (1) the strengths of normally cured pastes at a given porosity would likely increase if they contained a higher proportion of well-bonded larger and stronger particles; (2) highest strengths are generally obtained if the reaction product consists of a blend of poorly crystalline and semi-crystalline types of C-S-H; (3) curves in the diagram representing any given set of specimens are not necessarily linear and are referred to as data lines. Several data lines for autoclaved materials (in addition to EF in the figure that represents a 1:1 autoclaved cement-fly ash mixture) can be obtained by suitable choice of starting materials.

3.2 Storage modulus (E')- porosity relationships-current study

E' data obtained by the DMA method for the systems in this study are plotted against porosity in Figure 2. There is no curve that uniquely represents all the systems as might be expected. The curves are displaced along the porosity axis at a given value of E' in the following order: cement paste hydrated 3 yrs. < cement paste hydrated 45yrs. < jennite, cement paste hydrated up to 30days and blended systems of jennite, 1.4nm tobermorite and calcium hydroxide < C-S-H preparations (C/S = 1.2 and 1.5) < 1.4nm tobermorite < C-S-H (C/S = 0.80). The relative displacement of all these curves can be explained using the concepts embodied in the Taylor diagram of Figure 1. The thesis is that the position on a strength contour is a function of both porosity and the proportion of coarse, dense, crystalline material in the composite. Indicators of crystallinity include such nanostructural descriptors as the average silicate chain-length.

Examination of the curves in Figure 2 reveals the importance of the relative crystallinity of the silicate phases. There appears to be a correlation between the average chain-length of the silica tetrahedra as determined by ^{29}Si MAS NMR data (Q^2/Q^1 ratio) [10] and the position along the porosity axis. The average chain-length is approximately in the following order: cement paste (3yr.) < cement paste (45yr.) < C-S-H (C/S = 1.2 and 1.5) < C-S-H (C/S = 0.80) < synthetic jennite and blended systems of jennite, 1.4nm tobermorite and calcium hydroxide, < 1.4nm tobermorite. The 3yr. paste has a mean chain-length of about 3 units and the 45 yr. paste about 4 units. The C-S-H (C/S = 1.2 and 1.5) has a mean chain length of about 4.0 and 2.8 respectively. The C-S-H (C/S = 0.80) has a mean chain length > 10.0 units. The synthetic jennite (C/S = 1.4) and 1.4nm tobermorite (C/S = 0.90) have predominately Q^2 sites with long continuous chains [10].

It is also noted that the relative position of the curves for 1.4nm tobermorite, jennite and composite blends would be expected to shift to lower values of porosity were these mineral systems to become more disordered (concomitant with missing silica tetrahedral and lower average chain lengths) as has been postulated in various models of the nanostructure of C-S-H in hydrated cement paste [7-9]. Further it can also be stated (with other factors -including porosity- held constant) that as mean chain length (crystallinity) of the systems under investigation increases the value of E' increases. These observations would seem to conform with Taylor's approach as previously described.

Other factors affect the relative position of the E' versus porosity curves. For example the data points for the young paste (up to 30 days hydration) lie along the jennite curve. They are also shifted to higher values along the porosity axis relative to the 3 year and 45 year pastes. Young pastes contain both C-S-H and significant amounts of unhydrated cement. The density of the latter is significantly higher than that of C-S-H itself. It would then appear that in this case the proposed idea that highest strength can be achieved with an optimum blend of relatively dense well- crystallized material and less dense poorly crystallized material applies.

The nitrogen surface area (determined by the BET method) of these systems would also appear to be a contributing factor. For example, the surface area of the C-S-H (C/S = 0.80) used in this study as determined by the authors has a very high value of 186 m^2/g. The combination of high average chain-length (about 10 units) and high surface area may account for the higher values of E' at high porosity values. This would also appear to be in concert with Taylor's postulates and the F-B ideas expressed earlier. The low C/S ratio C-S-H material has greater intrinsic strength due to provision of greater surface for bonding of the

fundamental particles and a more favorable pore size distribution. The BET surface area for the 1.4nm tobermorite preparation is about double that of jennite i.e. 58 m^2/g versus 32 m^2/g as determined by the authors. Accordingly the curve for 1.4nm tobermorite is shifted to higher values of porosity indicating that this system has greater structural stiffness than the jennite material. Similarly the BET surface area values for the other two C-S-H preparations (C/S = 1.2 and C/S = 1.5) are 30 and 52 m^2/g respectively which may contribute to the shift of the curve for the C/S = 1.5 preparation to higher values for reasons similar to those described previously.

3.3 Hydrated paste and compacted specimens

The data for the E' versus porosity curves for the cement pastes hydrated for 3 years and those hydrated for periods up to 30 days was obtained using both hydrated paste and compacted specimens. The data for both types of preparations fall on the same curve in each case. The synthetic C-S-H, 1.4nm tobermorite and jennite powders were all compacted at different pressures to produce solid bodies for the DMA experiments.

4 Conclusions

1. There are no unique mechanical property-porosity relationships for hydrated cement paste and structurally related layered calcium-silicate hydrates.

2. Particle crystallinity, density and surface area are contributing factors that influence specific mechanical property-porosity relationships for layered calcium-silicate-hydrates.

3. Taylor's porosity-proportion of dense crystalline material- strength diagram is a useful tool for explaining the porosity dependence of the mechanical properties of 1.4nm

tobermorite, jennite, synthetic C-S-H and other layered calcium- silicate-hydrates of interest in cement chemistry investigations.

4. The storage modulus (E') versus porosity curves generated from DMA measurements on the title systems are consistent with other published evidence for a jennite-tobermorite-based model for C-S-H nanostructure in hydrated cement paste.

5. Compacted solid bodies made from ground cement paste, 1.4nm tobermorite, jennite and synthetic C-S-H powders are useful for determining the mechanical performance of these materials. The coincidence of E' versus porosity data for normally hydrated cement paste and ground and compacted paste confirm the view that similar bonds are formed with either process.

5 References

1. Odler I. and Roβler M., Investigation on the relationship between porosity, structure and strength of hydrated Portland cement pastes. II Effect of pore structure and of degree of hydration, Cem. Concr. Res., 15, 401-410, 1985.

2. Odler I. and Roβler M., Investigation on the relationship between porosity, structure and strength of hydrated Portland cement pastes. I. Effect of porosity, Cem. Concr. Res., 15, 320-330, 1985.

3. Mindess S., Relation between the compressive strength and porosity of autoclaved calcium silicate hydrates, J. Amer. Ceram. Soc., 53(11), 621-624, 1970.

4. Beaudoin J. J., Feldman R. F. and Tumidajski, P. J., Pore structure of hardened Portland cement pastes and its influence on properties, Adv. Cem. Bas. Mat., 1, 224-236, 1994.

5. Taylor H. F. W., Discussion of the paper, 'Microstructure and strength of hydrated

Cements' by R.F. Feldman and J. J. Beaudoin, Cem. Concr. Res., 7,465-468, 1977.

6. Feldman R. F. and Beaudoin J. J., Microstructure and strength of hydrated Cements, Cem. Concr. Res., 6, 389-400, 1976.

7. Taylor H. F.W., Hydration of the calcium silicate phases, Cement Chemistry, Chapter 5, Thomas Telford Publishing, London, pp.459, 1997.

8. Richardson I. G., Tobermorite/jennite- and tobermorite/calcium hydroxide-based models for the structure of C-S-H: applicability to hardened pastes of tricalcium silicate, β-dicalcium silicate, Portland cement, and blends of Portland cement with blast-furnace slag, metakaolin, or silica fume, Cem. Concr. Res., 34, 1733-1777, 2004.

9. Taylor H.F.W., Proposed structure of calcium silicate hydrate gel, J. Amer. Ceram. Soc.69 (6), 464-467, 1986.

10. Yu P. and Kirkpatrick R. J., Thermal dehydration of tobermorite and jennite, Concr. Sci. and Eng., 1, 185-191, 1999.

11. Gard J. A. and Taylor H. F. W., Calcium silicate hydrate (II) ("C-S-H(II)"), Cem. Concr. Res., 6, 667-678, 1976.

12. Hara N. and Inoue N., Formation of jennite from fumed silica, Cem. Concr. Res., 10, 677-682, 1980.

13. Taylor H. F. W., Chapter 5, Hydration of the calcium silicate phases, Cement Chemistry, Thomas Telford Publishing, London, pp 459, 1997.

14. Soroka I. and Sereda P.J., The structure of cement- stone and use of compacts as structural models, Proc. 5th Int. Symp. on the Chem. of Cem., Vol. 3., Tokyo, 67-73,1968.

15. Feldman R. F., Factors affecting the Young's modulus-porosity relation of hydrated Portland cement compacts, Cem. Concr. Res., 2(4), 375-386, 1972.

16. Sereda P.J. and Feldman R. F., Compacts of powdered material as porous bodies for use in sorption studies, J. Appl. Chem., 13, 150-158, 1963.

17. Beaudoin J.J., Comparison of mechanical properties of compacted calcium hydroxide and Portland cement paste systems, Cem. Concr. Res., 13, 319-324, 1983.

18. Sereda P.J., Feldman R.F. and Swenson E.G., Effect of sorbed water on some mechanical Properties of hydrated Portland cement pastes and compacts, Highway Research Board, Special Report 90, 58-73, 1966.

19. Menard K. P., Dynamic Mechanical Analysis-A Practical Introduction, CRC Press LLC, Boca Raton, pp. 208, 1999.

20. Alizadeh R., Beaudoin J. J. and Raki L., Mechanical properties of calcium silicate hydrates, Matls. and Struct., 44, 13-28, 2011.

21. Crennan J. M., El-Hemaly S. A. S. and Taylor H. F. W., Autoclaved lime-quartz materials I. Some factors influencing strength, Cem. Concr. Res., 7, 493-502, 1977.

22. Neville A. M., Properties of Concrete, John Wiley &Sons Inc., New York, pp.532, 1963.

Figure Captions

Figure 1. Porosity-particle type-strength diagram for cement pastes and other calcium-silicate hydrate systems (after Taylor, ref. [5]). Compressive strength contours are labeled in MPa. Lines AB, EF and CD (data from Feldman and Beaudoin ref. [6]) represent normally cured pastes, autoclaved cement-silica products and high density materials respectively.

Figure 2. Dynamic Mechanical Analysis (DMA) – Storage modulus (E') versus porosity curves for: cement paste hydrated 3 to 28days, 3 years, 45 years; 1.4nm tobermorite (T); jennite (J); mixtures of T and J and CH; C-S-H with C/S = 0.80, 1.20 and 1.50. Frequency = 3.98 Hz.

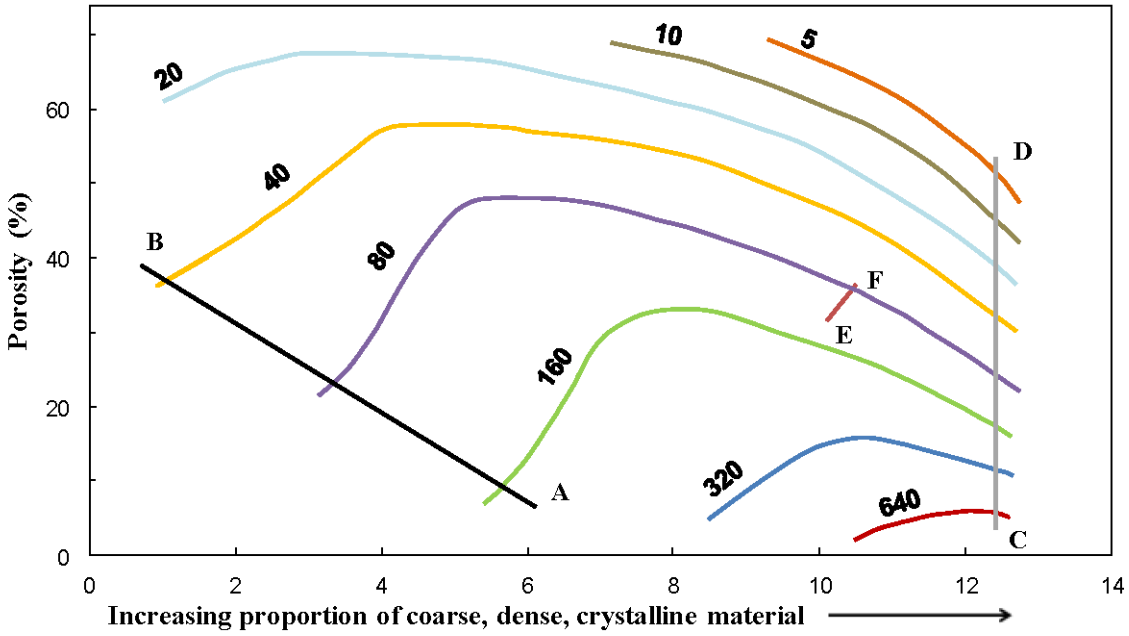

Figure 1. Porosity-particle type-strength diagram for cement pastes and other calcium-silicate hydrate systems (after Taylor, ref. [5]). Compressive strength contours are labeled in MPa. Lines AB, EF and CD (data from Feldman and Beaudoin ref. [6]) represent normally cured pastes, autoclaved cement-silica products and high density materials respectively.

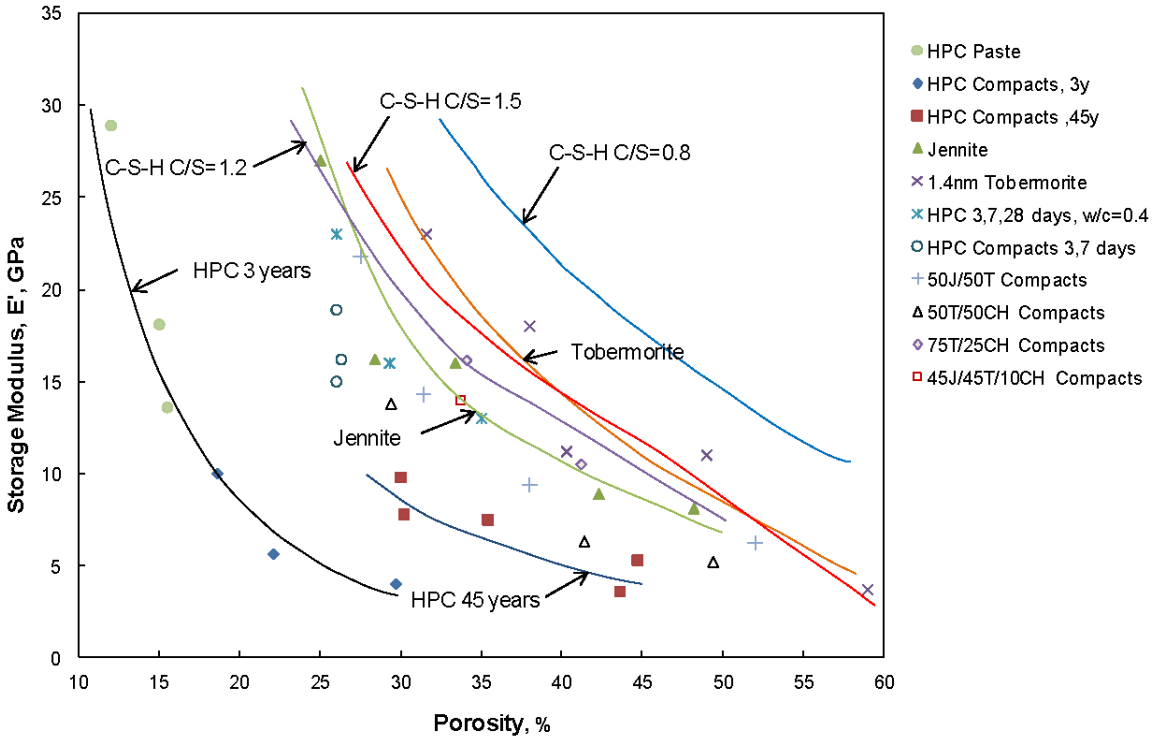

Figure 2. Dynamic Mechanical Analysis (DMA) – Storage modulus (E') versus porosity curves for: cement paste hydrated 3 to 28days, 3 years, 45 years; 1.4nm tobermorite (T); jennite (J); mixtures of T and J and CH; C-S-H with C/S = 0.80, 1.20 and 1.50. Frequency = 3.98 Hz.

9.3 Paper 5: Dimensional Stability of 1.4 nm Tobermorite, Jennite and Other Layered Calcium Silicate Hydrates

Length change versus mass-loss curves on drying the title layered silicate systems from 11% RH were obtained. Similar curves were obtained for hydrated Portland cement paste.In addition to mass-loss phase changes could be detected from changes in slope of the mass-loss curves. The dimensional stability of the solid phase of the layered silicates could be assessed using the change in basal-spacing versus mass-loss curves in conjunction with the corresponding curves of length-change. Nanostructural constructs for calcium silicate hydrate in hydrated cement paste based on T and J are consistent with a shrinkage potential assessment based on length and basal-spacing changes due to drying.

Dimensional Stability of 1.4nm Tobermorite, Jennite and Other Layered Calcium-Silicate-Hydrates

(Advances in Cement Research, 26(1), 1-9, 2014)

P. Pourbeik[a], J. J. Beaudoin[a], R. Alizadeh[b] and L. Raki[a]

[a] *National Research Council Canada, Construction Portfolio, Ottawa, ON, Canada*
[b] *Giatec Scientific Inc., Ottawa, ON, Canada*

Abstract

Length-change measurements of 1.4nm tobermorite, jennite and C-S-H preparations (with varying C/S ratio) subjected to drying from the 11% relative humidity condition are reported. The dimensional stability investigation is focused on the role of adsorbed and interlayer water as shrinkage mechanisms involving menisci effects in capillary pores are eliminated in this humidity range. Length-change versus mass-loss curves and the corresponding d_{002} basal-spacing change (obtained by x-ray diffraction) with mass-loss are assessed and inferences drawn regarding nanostructural models for C-S-H in hydrated Portland cement paste. Length-changes of the pure phases were significantly greater than those for hydrated cement paste due to the restraining effect of unhydrated cement particles and CH crystals in the paste. The dimensional stability and the role of the removal of 'structural water' from the systems studied is discussed in terms of its relevance to cement-based materials.

Keywords: Dimensional Stability, 1.4nm Tobermorite, Jennite, layered calcium-silicate-hydrates, nanostructure

Introduction

New generation models for the nanostructure of C-S-H in hydrated Portland cement paste are based on constructs comprised of 1.4nm tobermorite (T) and jennite (J) units (Taylor, 1986 and Richardson, 2008). Evidence in support of these models is largely physico-chemical in nature. There is a paucity of information linking the nanostructural behavior of T and J with engineering performance. An understanding of the dimensional stability of cement binders is central to the resolution of concrete sustainability issues. A review of the superposition of several shrinkage mechanisms by (Young et al., 1978) identified two of the primary shrinkage mechanisms for cement pastes as related to 'capillary drying' and 'gel drying'. The dimensional stability of synthetic T, J and C-S-H during drying from 11% RH is the focus of this study. The influence of adsorbed and interlayer water on the shrinkage of the 'solid-phase' can be studied in this humidity region as menisci effects due to the presence of capillary pore water are effectively eliminated. The objective of this study is to provide basic shrinkage data for specific layered silicates of relevance in cement science. An assessment of the compatibility of length-change of cement systems with the shrinkage potential of the 'solid-phase' of relevant hydrated cement minerals determined from basal-spacing versus mass-loss curves on drying from 11% RH is provided. Inferences regarding the consistency of the results with nanostructural models are made.

Experimental

Materials

Four cementing systems were prepared: synthetic calcium-silicate-hydrate (C-S-H with C/S = 0.8, 1.2 to 1.5); 1.4nm tobermorite; jennite and hydrated Portland cement paste (water/cement ratio = 0.40).

C-S-H: synthetic C-S-H was produced from the pozzolanic reaction between CaO and amorphous silica in excess water (water/solids = 11). Calcium oxide was obtained by calcining reagent grade calcium carbonate at 900°C. Reactive silica (CAB-O-SIL, grade M-5 from Cabot Corporation, USA) was heated at 110°C to remove any surface adsorbed water. Distilled water was de-aired and used for the reactions. All materials were kept sealed in N_2 purged bottles until they were used. Variation in C/S ratio was achieved by adjusting the stoichiometric amounts of the reactants. The C-S-H prepared for this study had C/S ratios of 0.80, 1.20 and 1.50. The reaction period was 6 months. The material was then filtered and dried under vacuum for 4 days at room temperature. The dried C-S-H was stored in nitrogen purged glass vials before the experiments. Characterization of these materials by X-ray diffraction (XRD) and thermal methods gave results directly comparable to C-S-H (I) as reported (Taylor, 1997). The C/S ratio in this classification varies from about 0.80 to 1.50. The XRD patterns for C-S-H samples (C/S=0.80 and 1.20) are shown in Figure 1(a). The degree of crystallinity generally increases with time. The sharpness of the XRD peaks also increases with crystallinity. The XRD peaks at six months reaction time are relatively sharp and typical of many reported in the literature. The reaction took place at a relatively high water-solid ratio of 11. A reasonably high degree of homogeneity would be expected as the

degree of dispersion of the reactants is quite high. Characterization data e.g. XRD and NMR spectra are highly reproducible.

1.4nm tobermorite ($Ca_5Si_6O_{16}(OH)_2.7H_2O$(Bonaccorsi and Merlino, 2005)): the reactants (CaO and SiO_2) were prepared as described above. The C/S ratio was 0.9. The reactants were mixed in excess deionized water (water/solids = 11) and placed in a high density polyethylene bottle maintained at 80 °C using a heating wrap. The mixture was continuously agitated with a magnetic stirrer for a period of 4 months. The XRD spectrum and TGA curve were similar to those obtained by Yu and Kirkpatrick (Yu and Kirkpatrick, 1999) The XRD spectrum is shown in Figure 1(b).

Jennite ($Ca_9Si_6O_{18}(OH)_6.8H_2O$) (Bonacorrsi et al., 2004)): the reactants (CaO and SiO_2) were prepared as described above. The C/S ratio was 1.4. The reactants were placed in a high density polyethylene bottle, mixed in excess deionized water (water/solids = 11) and maintained at 80 °C using a heating wrap. The mixture was continuously agitated with a magnetic stirrer for a period of 4 months. It was then filtered to remove excess water and placed in a desiccator over a saturated lithium chloride solution (11% RH) for several weeks. The XRD pattern was similar to that obtained by several authors (Yu and Kirkpatrick, 1999; Gard and Taylor, 1976; Hara and Inoue, 1980). The TGA curve matched that previously published (Yu and Kirkpatrick, 1999). The XRD spectrum is shown in Figure 1(c).

The use of off-stoichiometric ratios of CaO and SiO_2 was intentional. It was based on the experience of several other researchers (Viehland et. al., 1997; Komameni et. al., 1987; Cong and Kirkpatrick, 1996; Hara and Inoue, 1980.) and their attempts to synthesize pure phases

of 1.4nm tobermorite and jennite. The authors experiments also reflected similar results. For example, it was found that the use of bulk calcium/silica ratios in the range (1.2 to 1.5) only resulted in the formation of phase pure jennite for the C/S = 1.4 preparation (Cong and Kirkpatrick, 1996).Other preparations contained mixtures of C-S-H and jennite.

Portland Cement Paste: The Portland cement paste (made with Type I Portland cement) was prepared using a water/cement ratio of 0.40. Rectangular prisms (250 x 100 x 12mm) were cast. The samples were vibrated and stored in a moist curing room for 24 h. They were then demoulded and curing was continued for 3 years in a saturated lime solution. Additional paste samples (w/c = 0.40) made from the same cement were hydrated for 3 months. Thin slices (1 x 12 x 60 mm) were cut from the paste prisms using an Isomet diamond saw. Selected slices were also ground into a fine powder for fabrication into compacted specimens.

Preparation of Compacted Specimens

Solid circular disc samples for all the powdered materials (from the four cementing systems) were prepared by pressure compaction in steel moulds with a diameter of 31.75 mm. The thickness of most of the disc samples was nominally 1mm but varied between the limits of 1-2mm. Specimens of rectangular shape, approximately 25.4 x 6.4mm were cut from the circular compacts for the length change measurements. Numerous studies on the use and validity of compacts as models for hydrated cement systems have been published (Soroka and Sereda, 1968; Feldman, 1972; Sereda and Feldman, 1963; Beaudoin, 1983; Sereda et al., 1966) .It has been shown that compacted specimens of powdered hydrated Portland cement have similar mechanical property-porosity relationships to that of the original hardened paste of the same material (Soroka and Sereda, 1968). The porosity of compacted samples was determined using helium pycnometry or in the case of the phase pure minerals by calculation

using published density values. The calculation is made knowing the apparent volume and the solid volume of the sample. Porosity is varied by controlling the compaction pressure.

The pressed discs or compacts were all prepared at a porosity of approximately 30%. This includes the 3 month old cement paste that was ground into a powder and then compacted. It is important for comparisons of length-change as the 'active' component or 'solid-phase' of the systems studied is then similar.

Humidity Conditioning

Specimens for all four cementing systems were conditioned for several days at 11%RH in vacuum desiccators containing saturated lithium chloride solution. The powders were conditioned at 11%RH for three weeks before compaction and for one week after compaction. Theoretically there is a monolayer of water on the surfaces of the particles in addition to interlayer water at this humidity.

Length-Change Measurements

Modified Tuckerman gage extensometers were used for the length change measurements. A description of the device and operational details are provided elsewhere (Feldman et al., 1964). A schematic of the extensometer with the sample in place is provided in Figure 2. The sample is inserted into a holder (number 5) and is held against the knife edges (numbers 2 and 3) by a light spring (number 4). The optical system consists of two mirrors: a fixed one (number 6) and a tilting one (number 7). The latter is on the face of a rocking lozenge. The whole set-up is supported by a stand (number 8). The tilting of the mirror is correlated to the

length change of the sample and is monitored using an auto collimator. This optical instrument measured the length-change with an accuracy of 1 microstrain. The samples were placed in a vacuum cell with an optical window through which the extensometer was read. The cell is made so that the sample can be subjected to high vacuum. Ground glass joints and valves were used in its construction to exclude CO_2. Heating tapes connected to a rheostat were wrapped around the cell to apply heat as required.

X-ray Diffraction

The changes in the d_{002} basal spacing with drying were followed for all the layered silicates investigated. The XRD patterns were obtained using a Scintag XDS 2000 diffractometer using CuK_α radiation and a graphite monochromator. A diffraction angle range of $2\theta = 5\text{-}15^\circ$ was used with a step size of 0.03° . This range was selected because of the primary interest in the 002 basal spacing reflection. A 7-s count interval with an accelerating voltage of 45kV and a current of 35mA was employed.

Mass-Change Measurements

The initial measurements of mass for all the studied systems were made at the 11% RH condition. Drying took place in a vacuum cell similar to the one used for the length-change measurements. A drying protocol consisting of 14 steps was utilized with mass change measurements taking place after each step. The steps involved: vacuum at room temperature for periods varying from 18 hours to 3.75 days; heating under vacuum at 46°C for periods varying from 1 day to 14 days; at 65°C for periods varying from 1 day to 6 days; at 70°C for

2 days; at 79°C for 2 to 6days; at 96°C for 1 to 5 days; at 100°C for 2 days; at 113°C for 2days. All specimens dried to a given step were dried through all the preceding steps before testing. Mass loss is expressed as a per cent of the mass at 11%RH.

Surface Area Measurements

Nitrogen surface area determinations (BET method) were performed on all the systems studied using a Nova 2200e surface area analyzer. Samples were outgassed (vacuum dried) for 24 h prior to obtaining the sorption isotherms. Nitrogen surface area values were 186, 30 and 52 m^2/g for C-S-H, C/S = 0.8, 1.2 and 1.5 respectively. Nitrogen surface area values were 58 and 32 m^2/g for 1.4nm tobermorite and jennite respectively.

Results and Discussion

Length-Change

An indication of the multiplicity of possible shrinkage mechanisms in porous cement systems has been previously discussed (Young et.al., 1978).The current paper focuses on the contribution to length-change by the 'solid-phase' only which consists primarily of layered calcium-silicate-hydrates. The starting point for all the length-change measurements is 11% RH. All the studied systems therefore contain no pore water (with the possible exception of water that might be present in a small amount of microporosity) and only surface adsorbed and interlayer water. The absence of pore water (in predominately capillary pores) precludes a deconvolution of the mechanisms involving this type of water. Changes in the internal pore volume have largely taken place as a result of the prior removal of the 'capillary water'. The

discussion is necessarily centered on the two species of water present at 11%RH and their role in volume change. The volume of 'solid-phase' is the same in all the compacted systems as the porosity is similar i.e. about 30%. It is the chemical composition of the solids that varies. The effect of 'capillary' pore water on dimensional change is therefore beyond the scope of this study and would require an investigation in the upper humidity regions of the water adsorption isotherm. Separating the effects of surface and interlayer water on dimensional change (as referred to in the text) would require a separation of the water sorption isotherm into reversible and irreversible components which is also beyond the scope of this investigation.

The Bangham effect (derived from the Gibbs adsorption equation) relating length change to changes in solid surface tension would appear to be operative. The loss of interlayer water, however, has been shown to be the dominant mechanism in hydrated cement systems and is estimated to account for about 80% of the length change (Feldman, 1968). Further the length change due to the Bangham effect would be difficult to determine for the layered silicate minerals as it requires thermodynamic reversibility. This condition is not met by application of the theory to sorption isotherms of layered silicates (as stated above) due to the presence of both primary and secondary hysteresis. Therefore the two length change mechanisms are combined for purposes of this discussion.

Length-change versus mass-loss curves for 1.4nm tobermorite, jennite, C-S-H and hydrated Portland cement paste (HPC) are presented in Figure 3. A brief description of the length-change curves is as follows. The starting condition for all experiments was 11% RH. This is the position on the sorption isotherm where the surface is covered with a monolayer of water and all the interlayer positions are filled with water. No capillary pore water is present.

Jennite (J) shrinks less than tobermorite (T) up to a mass-loss of about 2.25%. Jennite has a much lower basal-spacing than tobermorite (1.06 compared to 1.40 nm) and likely contains a lower amount of interlayer water. In addition Taylor reports that the central CaO part of the layer is distorted from that in CH in a way that differs from 1.4 nm tobermorite (Taylor, 1997). These factors may contribute to the lower initial shrinkage. The larger shrinkage of T may also be dependent on the degree of stacking of the silicate sheets. This may also account for the larger surface area observed for T. Shrinkage of cement pastes has been shown to be dependent on surface area (Feldman and Swenson, 1975). The transformation to a new phase i.e. metajennite (M-J; $C_9S_6H_7$ (Taylor, 1997)) occurs at approximately this mass-loss (2.25%) and is accompanied by both a 0.2nm change in basal-spacing and a change in density from 2.33 to 2.62 g/cm^3 (Thomas et al., 2010). An increase in density of the new phase is manifested by a volumetric decrease of the solid. This results in a significant increase in total shrinkage to about 0.65% surpassing the amount of shrinkage exhibited by tobermorite which itself undergoes transformation to the 1.2nm form at this mass-loss (Yu and Kirkpatrick, 1999). The crystallographic reorientation of the solid phase in the specimen abruptly affects the dimensional stability at this point. The subsequent shrinkage of M-J continues to exceed that of T over the entire mass loss range. It is noteworthy that the shrinkage curve for C-S-H (C/S = 1.2) lies between the curves for 1.4 nm tobermorite and jennite (up to 2.25% mass-loss) and between 1.2 nm tobermorite and metajennite at higher mass-losses. The shrinkage of C-S-H (C/S = 1.5) with respect to T, J and M-J is similar to that for C-S-H (C/S = 1.2) up to a 6% mass-loss. The shrinkage for the former exceeds the latter and M-J at higher mass-losses.

The shrinkage curves for HPC paste (w/c = 0.40) hydrated for both 3 months and 3 years show that the shrinkage is significantly less than that of all the synthetic systems studied. This is, in part, due to the restraining effect of unhydrated cement clinker grains and the presence of calcium hydroxide crystals. The paste is about 62% hydrated at 3 months and 85% hydrated at 3 years. The extent of hydration of these pastes was determined by thermo gravimetric analysis (TGA). The non-evaporable water content (mass-loss between 110˚C and 1000˚C per unit mass of cement) corrected for loss on ignition of the cement was determined. This quantity was expressed as a ratio of the non-evaporable water at complete hydration taken to be 0.253 in order to estimate the extent of hydration, (Powers and Brownyard, 1948). This is not unique to a cement paste with a w/c = 0.40. It was shown that the amount of shrinkage of cement pastes below 40% RH (equilibrium conditions prevailing) is similar for a variety of conditions and admixture use (Feldman and Swenson, 1975; Roper, 1966). Drying from the 11% RH condition, as stated previously, removes the effect of pore water on dimensional change. Generally, the total amount of shrinkage for HPC paste varies up to about 1% when water removal due to drying takes place from the 11% RH condition. Length-change in this humidity region does not significantly affect the relative position of the HPC shrinkage curves relative to those of the synthetic materials even with variances in the porosity or water/cement ratio. The length-change for the HPC pastes in Figure 3 is similar to jennite up to a 1% mass loss. This will be discussed further in the next section when the effects of basal-spacing changes are discussed. The length-change of the paste is significantly less than exhibited by all the synthetic silicates studied at mass losses exceeding 1%.

The issue of the possible existence of microcracks and/or it effects was considered. The thin specimens brought to equilibrium at 11%RH were examined in the SEM. Despite the high vacuum no microcracks were observed. This was validated by dynamic mechanical analysis (DMA) investigations by three of the authors on various C-S-H systems (Alizadeh et. al., 2011). Decreases in storage modulus values were observed to be followed by subsequent increases as mass-loss took place from the 11% RH condition. Increases on drying would be unlikely in a system containing microcracks.

Changes in basal-spacing (d_{002})

The change in basal-spacing (d_{002}) versus mass-loss curves are presented in Figure 4.These curves enable an assessment of the shrinkage potential of the various calcium-silicate-hydrates and their relevance to the volume stability of HPC paste. The calcium-silicate-hydrates, 1.4 nm tobermorite and jennite are the principal minerals that are integral components of current models for the nanostructure of hydrated Portland cement (Taylor, 1986; Richardson, 2008). Their dimensional change characteristics on drying from 11% RH, along with those of synthetic C-S-H preparations, should provide insight about the shrinkage potential and stability of the solid phases in cement-based binding materials. A brief analysis follows.

The basal-spacing for all systems shifts to lower values as water is removed. The curve for jennite is relatively flat with a phase transition to metajennite occurring at about a 3.5% mass-loss. The curve for 1.4nm tobermorite approaches the curve for C-S-H (C/S = 1.5) at a mass-loss of about 3.5% at d_{002} = 1.15 nm and continues along the same path to a d_{002} value of 1.12 at a mass-loss of 6%. In this mass-loss region the shrinkage potential of tobermorite and C-

S-H (C/S = 1.5) are similar. The d_{002} value for C-S-H (C/S = 1.5) subsequently decreases and reaches a plateau at a mass-loss value of 7.6%. The transition of the d_{002} values of C-S-H (C/S = 1.2) from proximetry to the tobermorite curve to significantly lower values begins at 4% mass-loss and reaches a plateau at a mass loss of about 7.6% when it meets the curve for C-S-H (C/S=1.5).

The shrinkage potential for C-S-H with C/S ratios that can be encountered in cement-based materials would appear to lie between that of tobermorite and metajennite depending on the drying conditions. C-S-H with low values of C/S ratio e.g. C/S = 0.80 would on the basis of changes in d_{002} values (0.20 nm compared to 0.22 nm for a mass change of 10%) alone appear to have moderately less shrinkage potential than C-S-H with higher values of C/S ratio. This is not actually the case as the shrinkage of C-S-H is similar for both C/S = 0.8 and 1.2. This can be partially explained by considering other factors that influence shrinkage. Shrinkage of hydrated cement has been shown to be dependent on several factors including surface area, water/cement ratio, degree of hydration, temperature and pore size distribution (Ramachandran et al., 1981). The surface area of the C-S-H(C/S =0.80) system is significantly higher than that of the C-S-H (1.20). The significance of surface area on hydrated cements was investigated (Feldman and Swenson, 1975). Generally shrinkage increases with surface area. It was concluded by these authors that shrinkage is associated with the degree of dispersion of the pastes rather than its chemical composition or morphology. Surface area values of HPC typically lie between 30-60m^2/g. Shrinkage of cement-based materials generally increases with surface area (Feldman and Swenson, 1975).The very high surface area value of C-S-H (C/S = 0.80) could account for a larger than

expected shrinkage. The initially greater shrinkage for tobermorite with respect to jennite (up to 2.25% mass-loss) may be partially due to its larger surface area (Figure 3). The reversal of relative shrinkages following subsequent transitions to the 1.2 and 1.1nm form of tobermorite and the formation of metajennite may be influenced by interactions of interlayer calcium with the silicate sheets in the tobermorite structure following drying.

The primary components of current compositional models of the nanostructure of C-S-H in hydrated Portland cement are 1.4nm tobermorite and jennite (Taylor, 1986). A structural framework based on these two minerals (in view of the basal-spacing changes on drying) is not incompatible with changes to the C-S-H (C/S = 1.2 or 1.5). It is apparent that the shrinkage potential of HCP would be dependent on the relative amounts of these minerals constituting the structural framework of the C-S-H network in the paste. It is suggested that the shrinkage potential under normal ambient conditions i.e. 25-35°C would be reduced with increasing amounts of jennite (prior to any phase changes i.e. formation of M-J) as structural elements. Another contributing factor to the potential shrinkage of 1.4nm tobermorite and jennite is the change in density accompanying a phase change. The density of tobermorite and jennite increase from 2.23 to 2.40 g/cm^2 and 2.33 to 2.62 g/cm^2 respectively following phase changes (e.g.the 1.4 to the 1.2nm form of tobermorite and jennite to metajennite).It follows, since there is no pore water present at this humidity, that any increased shrinkage is due to a solid-phase change. The corresponding change in density results in a decrease in volume of the solid phase and a concomitant increase in pore volume of the sample.

Conclusions

1. Length-change of 1.4 nm tobermorite, jennite and C-S-H (C/S = 0.8, 1.2, 1.5) specimens of similar porosity due to drying from the 11%RH condition is significantly greater than the corresponding values for hydrated cement paste up to a mass loss of 10%. This is attributed to the restraining effect of unhydrated cement particles and calcium hydroxide crystals in the paste.

2. Length-change due to drying of 1.4nm tobermorite and jennite from the 11%RH condition is sensitive to phase changes that occur in these minerals e.g. conversion of 1.4nm to 1.2 and 1.1nm tobermorite and jennite to metajennite. These phase changes can be detected by changes in slope of the length-change-mass-loss curves.

3. Length-change of C-S-H (C/S = 0.8) is larger than expected (based on the relatively low basal spacing change on drying) due to its very high surface area relative to higher C/S ratio preparations.

4. The dimensional stability of the solid phase of the porous layered silicate samples investigated can be assessed using the change in basal-spacing versus mass-loss curves in conjunction with the corresponding length-change curves.

5. The dimensional stability of C-S-H (C/S = 1.5) solids on drying from 11% RH is similar to 1.4nm tobermorite and its derivatives up to a mass loss of 6.5%. The shrinkage potential shifts to that of metajennite at higher values of mass loss. The dimensional response of C-S-H (C/S = 1.2) gradually shifts toward that of metajennite beginning at a mass-loss of 4%.

6. Nanostructural constructs for C-S-H in hydrated cement paste based on 1.4nm tobermorite and jennite are consistent with a shrinkage potential assessment based on length-change and basal-spacing changes due to drying.

References

Alizadeh R., Beaudoin J.J. and Raki L. (2011), Mechanical properties of calcium silicate hydrates, Materials and Structures, 44, 13-28.

Beaudoin J.J (1983) Comparison of mechanical properties of compacted calcium hydroxide and Portland cement paste systems, Cem. Concr. Res., 13, 319-324.

Bonacorrsi E., Merlino S. and Taylor H.F.W (2004) The crystal structure of jennite, $Ca_9Si_6O_{18}(OH)_6.8H_2O$, Cem. Concr. Res. 34, 1481-1488.

Bonaccorsi E., and Merlino S. (2005) The crystal structure of tobermorite 14A (Plombierite), a C-S-H phase, J. Amer. Ceram. Soc., 88(3), 505-512.

Cong X. and Kirkpatrick, R.J. (1996) ^{29}Si and ^{17}O NMR investigation of the structure of some crystalline calcium silicate hydrates, Adv. Cem. Based Matls., 3, 133-143.

Feldman R. F., Sereda P. J. and Ramachandran V. S (1964) A study of length changes of compacts of Portland cement on exposure to H_2O, Highway Research Record No 62, Highway Research Board, Washington, D.C.,106-118.

Feldman R.F (1968) Sorption and length-change scanning isotherms of methanol and water on hydrated Portland cement, Proc. V Int. Congr. Chem. Cem., Tokyo, Paper III-23, 53-56,

Feldman R. F (1972) Factors affecting the Young's modulus-porosity relation of hydrated Portland cement compacts, Cem. Concr. Res., 2(4), 375-386.

Feldman R. F. and Swenson E. G (1975) Volume change on first drying of hydrated Portland cement with and without admixtures, Cem. Concr. Res., 5(1), 25-35.

Gard J. A. and Taylor H. F. W (1976) Calcium silicate hydrate (II) ("C-S-H (II)"), Cem. Concr. Res., 6, 667-678.

Hara N. and Inoue N (1980) Formation of jennite from fumed silica, Cem. Concr. Res., 10, 677-682.

Komameni S., Roy D.M., Fyfe C.A. and Kennedy G.J. (1987), Naturally occurring 1.4nm tobermorite and synthetic jennite: Characterization by ^{27}Al and ^{29}Si MAS NMR spectroscopy and cation exchange properties, Cem. Concr. Res. 17, 891-895.

Powers T. C. and Brownyard T. L. (1948), Studies of the physical properties of hardened Portland cement paste: Part 2. Studies of water fixation, Bulletin 22, Portland Cement Association, USA, 249-468.

Ramachandran V. S., Feldman R. F. and Beaudoin J. J (1981) Chapter 2, Microstructure and strength development, Concrete Science, Heyden & Son Ltd., London, pp. 427.

Richardson I. G (2008) The calcium silicate hydrates, Cem. Concr. Res., 38(2), 137-158.

Roper H (1966) Dimensional change and water sorption studies of cement paste, Highway Research Board, Special Report 90, 74-83.

Sereda P.J. and Feldman R. F (1963) Compacts of powdered material as porous bodies for use in sorption studies, J. Appl. Chem., 13, 150-158.

Sereda P.J., Feldman R.F. and Swenson E.G (1966) Effect of sorbed water on some mechanical properties of hydrated Portland cement pastes and compacts, Highway Research Board, Special Report 90, 58-73.

Soroka I. and Sereda P.J (1968) The structure of cement- stone and use of compacts as structural models, Proc. 5th Int. Symp. on the Chem. of Cem., Vol. 3., Tokyo, 67-73.

Taylor H.F.W (1986) Proposed structure for Calcium Silicate Hydrate Gel, J. Amer. Ceram. Soc. 69, (6), 464-467.

Taylor H. F. W (1997) Chapter 5, Hydration of the calcium silicate phases, Cement Chemistry, Thomas Telford Publishing, London, pp. 459.

Thomas, Jefferey J., Jennings H. M. and Allen A.J (2010) Relationships between composition and density of tobermorite, jennite and nanoscale $CaO\text{-}SiO_2\text{-}H_2O$, J. Phys. Chem. C, 114, 7594-7601.

Viehland D., Yuan L.J., Xu Z., Cong X.-D. and Kirkpatrick R. J. (1997), Structural studies of jennite and 1.4nm tobermorite: Disordered layering along the[100] of jennite, J. Amer. Ceram. Soc., 80(12), 3021-3028.

Young J. F., Berger R.L. and Bentur A (1978) Shrinkage of tricalcium silicate pastes: Superposition of general mechanisms, Il Cemento, 75 (3), 391-398.

Yu P. and Kirkpatrick R.J (1999) Thermal dehydration of tobermorite and jennite, Concr. Sci. and Eng., 1, 185-191.

Figure Captions

Figure 1. XRD patterns for silicate minerals used in this study: (a) C-S-H (C/S = 0.80 and 1.20); (b) 1.4 nm tobermorite and (c) jennite

Figure 2. Schematic of Tuckerman extensometer used for length-change measurements. Information pertaining to the numbers is provided in the text.

Figure 3. Length-change versus mass-loss curves for 1.4nm tobermorite, jennite, C-S-H and hydrated Portland cement paste.

Figure 4. Changes in basal-spacing versus mass-loss for 1.4nm tobermorite, jennite, C-S-H and hydrated Portland cement paste.

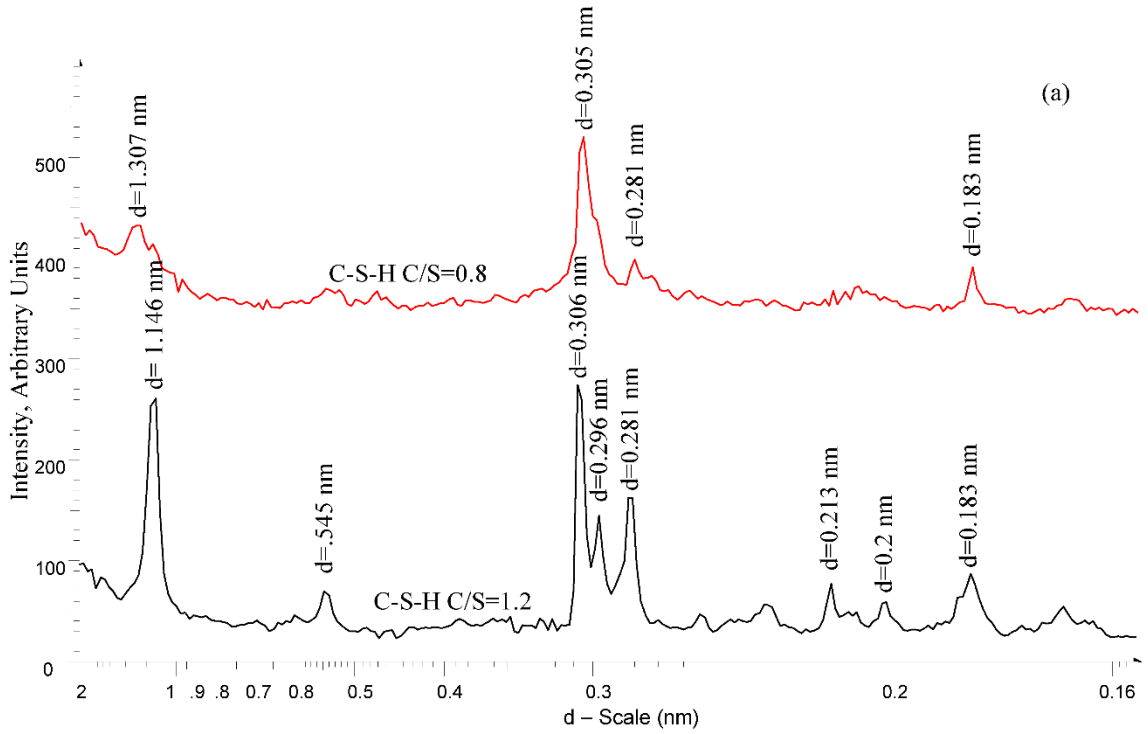

Figure 1. XRD patterns for silicate minerals used in this study: (a) C-S-H (C/S=0.80 and 1.20)

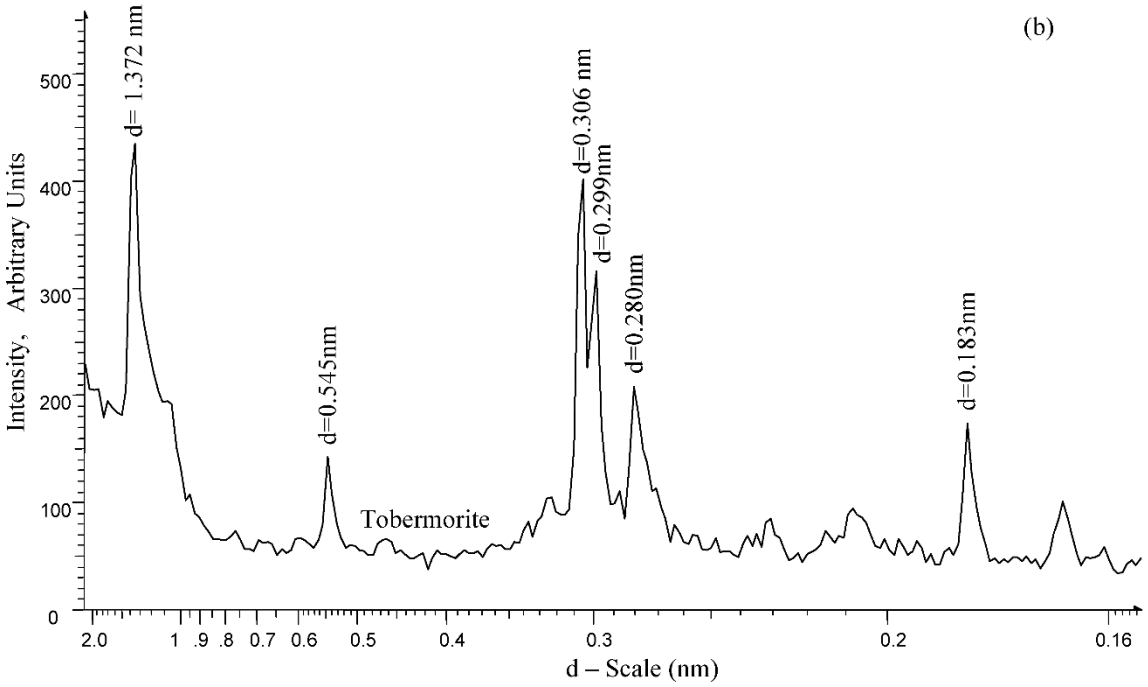

Figure 1. XRD patterns for silicate minerals used in this study: (b) 1.4 nm tobermorite

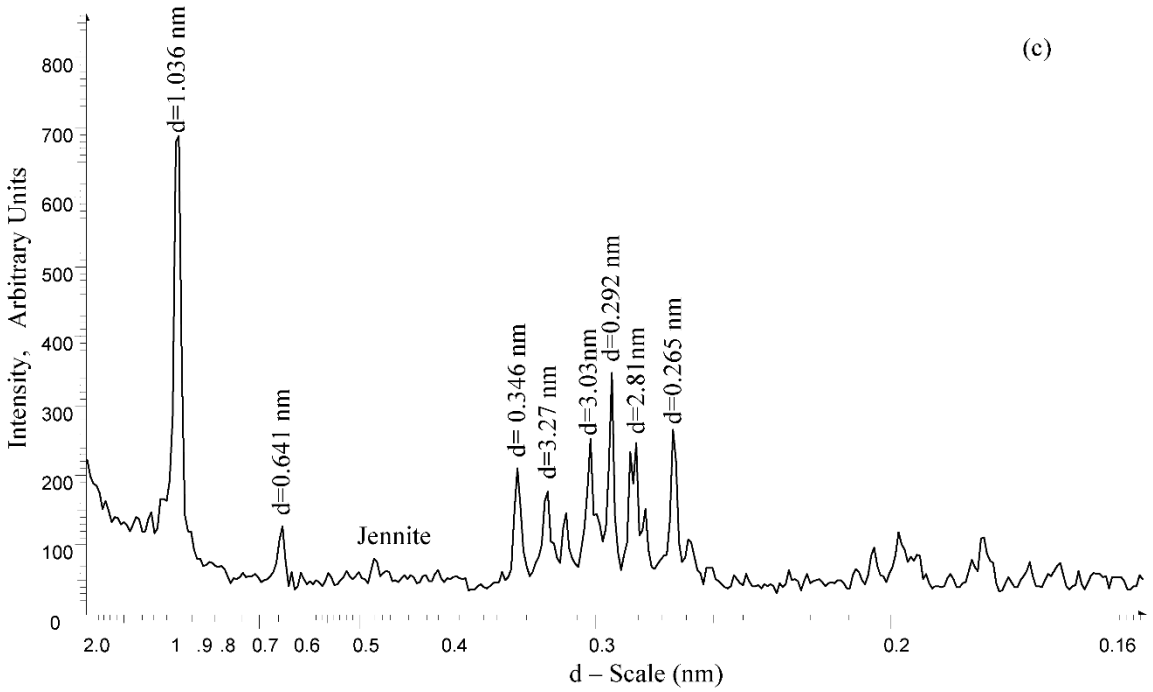

Figure 1. XRD patterns for silicate minerals used in this study: (c) jennite

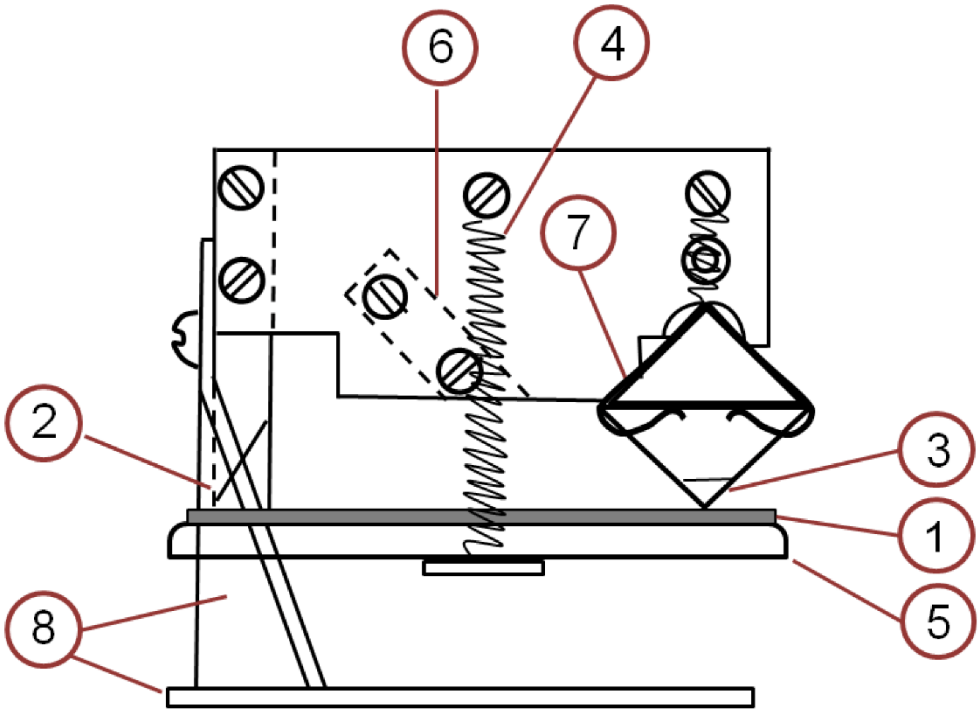

Figure 2. Schematic of Tuckerman extensometer used for length-change measurements. Information pertaining to the numbers is provided in the text.

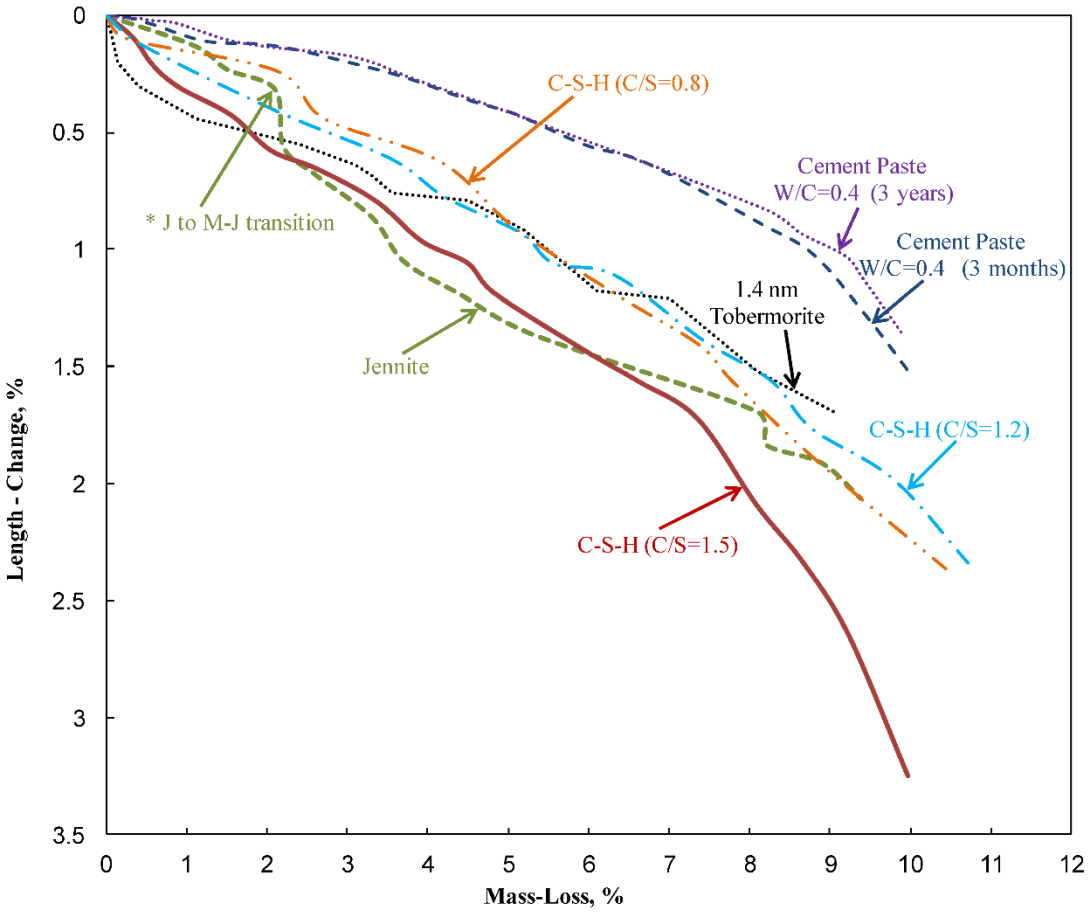

Figure 3. Length-change versus mass-loss curves for 1.4nm tobermorite, jennite, C-S-H and hydrated Portland cement paste.

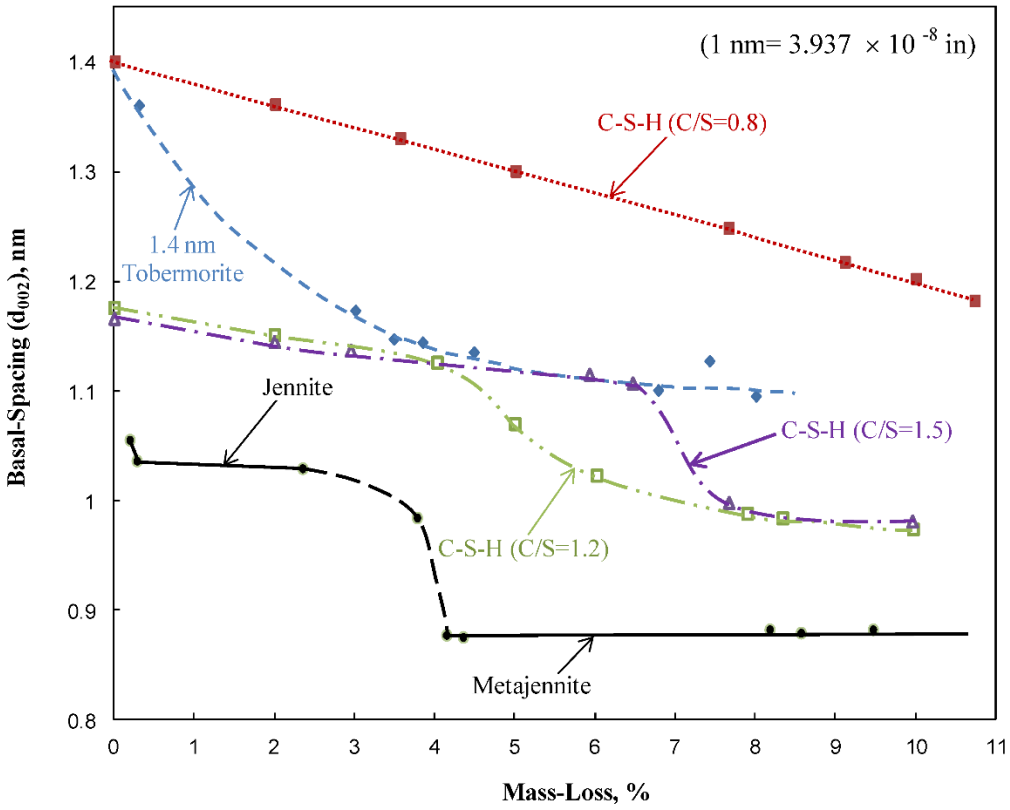

Figure 4. Changes in basal-spacing versus mass-loss for 1.4nm tobermorite, jennite, C-S-H and hydrated Portland cement paste.

9.4 Paper 6: Drying of Calcium-Silicate-Hydrates: Regeneration of Elastic Moduluus

The modulus of elasticity of all the layered calcium silicates investigated in this chapter generally decreases on drying from 11% RH due to the removal of adsorbed and interlayer water. Prolonged drying at temperatures up to 113^{o}C results in a 'regeneration' of the initial elastic modulus obtained at 11% RH. It is suggested that a possible 'regeneration' mechanism is associated with bond formation between interlayer Ca^{2+} and the silicate sheets as well as cross-linking. The 'regeneration' phenomenon observed here is consistent with the notions expressed for nanostructural models that are comprised of structural units based on 1.4 nm tobermorite and and jennite.

Drying of Calcium Silicate Hydrates:

Regeneration of Elastic Modulus

(Advances in Cement Research, DOI: 10.1680/adcr.14.00048)

P. Pourbeik[a], J. J. Beaudoin[a], R. Alizadeh[b] and L. Raki[a]

[a] *National Research Council Canada, Construction Portfolio, Ottawa, ON, Canada*

[b] *Giatec Scientific Inc., Ottawa, ON, Canada*

Abstract

Dynamic mechanical thermal analysis (DMTA) measurements for layered calcium silicate systems (1.4 nm tobermorite, jennite, synthetic C-S-H and hydrated Portland cement paste) are reported. Elastic modulus results were obtained for samples initially conditioned to 11% RH and dried during the DMTA test and for samples subjected to prolonged vacuum and thermal drying prior to a DMTA test. Decreases in elastic modulus relative to the 11% RH starting condition typically observed during a DMTA test were recovered subsequent to the prolonged thermal treatment. A possible 'regeneration' mechanism for the elastic modulus is discussed. The 'regeneration' occurs for all the calcium silicate systems studied. The results are consistent with the notions expressed for nanostructural models of C-S-H in cement paste that are comprised of structural units based on 1.4nm tobermorite and jennite.

Keywords: Regeneration, 1.4nm Tobermorite, Jennite, layered calcium-silicate-hydrates, nanostructure, Elastic Modulus

Introduction

Recent compositional models for the nanostructure of C-S-H in hydrated cement paste are comprised of structural units of 1.4 nm tobermorite and jennite (Richardson, 2004; Taylor, 1986). There is however a paucity of information regarding the engineering performance of these layered silicate minerals and other layered silicates of relevance to improved understanding of the mechanical properties of cement-based materials. Basic engineering parameters such as modulus of elasticity are moisture sensitive and drying path dependent (Sereda et al., 1966). Differences in elastic modulus values can be as large as 100% depending on the equilibrium state of water in the system. Mechanisms responsible for these differences may involve variations in the bonding environment between the layers of the silicates. A study was designed to assess the role of 'ageing' in layered silicates due to prolonged drying and its effects on changes in elastic modulus values. Previous work by Feldman has demonstrated the potential for regenerating the elastic properties of cement paste by controlling the egress and ingress of interlayer water (Feldman, 1972). This work focuses on regeneration of stiffness through variation of drying protocols.

Experimental

Materials

Four cementing systems were prepared: synthetic calcium-silicate-hydrate (C-S-H with C/S = 0.8); 1.4nm tobermorite; jennite and hydrated Portland cement paste (water/cement ratio = 0.40).

C-S-H: synthetic C-S-H was produced from the pozzolanic reaction between CaO and amorphous silica in excess water. Calcium oxide was obtained by calcining reagent grade calcium carbonate at 900 °C. Reactive silica (CAB-O-SIL, grade M-5 from Cabot Corporation, USA) was heated at 110 °C to remove any surface adsorbed water. Distilled water was de-aired and used for the reactions. All materials were kept sealed in N_2 purged bottles until they were used. Variation in C/S ratio was achieved by adjusting the stoichiometric amounts of the reactants. The reaction period was 6 months. The material was then filtered and dried under vacuum for 4 days at room temperature. The dried C-S-H was stored in nitrogen purged glass vials before the experiments. Characterization of these materials by X-ray diffraction (XRD) and thermal methods gave results directly comparable to C-S-H (I) as reported by Taylor (Taylor, 1997).

1.4nm tobermorite: the reactants (CaO and SiO_2) were prepared as described above. The C/S ratio was 0.9. The reactants were placed in a high density polyethylene bottle mixed in excess deionized water (water/solids = 11) and maintained at 80 °C using a heating wrap. The mixture was continuously agitated with a magnetic stirrer for a period of 4 months. The XRD spectrum and TGA curve were similar to those obtained by Yu and Kirkpatrick (Yu and Kirkpatrik, 1999).

Jennite: the reactants (CaO and SiO_2) were prepared as described above. The C/S ratio was 1.4. The reactants were placed in a high density polyethylene bottle mixed in excess deionized water (water/solids = 11) and maintained at 80 °C using a heating wrap. The mixture was continuously agitated with a magnetic stirrer for a period of 4 months. The XRD pattern was similar to that obtained by (Yu and Kirkpatrik, 1999; Gard and Taylor, 1976; Hara and Inoue, 1980). The TGA curve matched that published by (Yu and Kirkpatrik, 1999).

Portland Cement Paste: The Portland cement paste (made with Type I Portland cement) was prepared using a water/cement ratio of 0.40. Rectangular prisms (250 x 100 x 12mm) were cast. The samples were vibrated and stored in a moist curing room for 24 h. They were then demoulded and curing was continued for two months in a saturated lime solution. Thin slices (1 x 12 x 60 mm) were cut from the paste prism using an Isomet diamond saw.

Humidity Conditioning

Specimens for all four cementing systems were conditioned for several days at 11%RH in vacuum desiccators containing saturated lithium chloride solution. The powders were conditioned at 11%RH before compaction and for a few days after compaction. Theoretically there is a monolayer of water on the surfaces of the particles in addition to interlayer water at this humidity.

Preparation of Compacted Specimens

Solid rectangular prism samples for all the phase pure powdered materials were prepared by pressure compaction in steel moulds with a cross-section of 12.8 x 83 mm. The thickness of most of the prism samples was nominally 1mm but varied between the limits of 1-2mm.Numerous studies on the use and validity of compacts as models for hydrated cement systems have been published (Soroka and Sereda, 1968; Feldman. 1972; Sereda and Feldman, 1963; Beaudoin, 1983) .It has been shown that compacted specimens of powdered hydrated Portland cement have similar mechanical property-porosity relationships to that of

the original hardened paste of the same material (Soroka and Sereda, 1968). The porosity of compacted samples was determined using helium pycnometry or in the case of the phase pure minerals by calculation using published density values. The porosity of all the phase pure samples tested in this study was about 30%. The porosity of the cement paste sample was about 12%. The calculation is made knowing the apparent volume and the solid volume of the sample. Porosity is varied by controlling the compaction pressure.

Drying Protocols

The initial DMTA measurements for all the silicate systems were made at the 11% RH condition. The E' versus temperature curves that were obtained are referred to as the control curves. A second series of curves were obtained for specimens subjected to a prolonged drying regime prior to the DMTA tests. Drying took place in a glass cell.

The cell was made so that the sample could be subjected to high vacuum. Ground glass joints and valves were used in its construction to exclude CO_2. Heating tapes connected to a rheostat were wrapped around the cell to apply heat as required. A drying protocol consisting of 14 steps was utilized with mass-change measurements taking place after each step. The steps involved: vacuum at room temperature for periods varying from 18 hours to 3.75 days; heating under vacuum at 46 °C for periods varying from 1 day to 14 days; at 65°C for periods varying from 1 day to 6 days; at 70°C for 2 days; at 79°C for 2 to 6days; at 96°C for 1 to 5 days; at 100°C for 2 days; at 113°C for 2days. All specimens dried to a given step were dried through all the preceding steps before testing.

Thermogravimetric Analysis (TGA)

Thermogravimetric analysis experiments were performed using a TA Instruments SDT Q-600. Twenty five mg of the sample were heated from ambient temperature to 1000°C at a rate of 10°C/min.under a flow of nitrogen gas (10ml/min.). The derivative mass-loss (DTGA) was determined using Universal Analysis 2000 software.

Dynamic Mechanical Thermal Analysis (DMTA)

The dynamic thermal mechanical analysis (DMTA) method involves the application of an oscillating force to the sample and measurement of displacement (Menard, 1999). The elastic property of interest that was obtained by DMTA is referred to as the storage modulus (E'); it is analogous to the static modulus of elasticity. In a DMTA experiment there is usually a time lag between the applied force and the resulting displacement. The time lag can be quantified in terms of a phase angle between the load and the displacement due to their ideally sinusoidal nature. The DMTA analysis was conducted using a Rheometrics RSA II instrument on all samples in this investigation. The frequency range was 0.1 to 10.0 Hz. The curves were similar at all frequencies. Results are reported at a frequency level of 3.98Hz as the characteristics of the curves at this frequency are clear and distinct. The experiments involved heating the sample from 25°C to 300°C. E' versus temperature curves were constructed for each test specimen. Temperature was increased in increments of 2°C every 5 minutes. E' versus temperature curves were plotted. Each test took about 11h and 45min.to complete. Additional details are given in a previous publication. (Alizadeh et. al, 2011)

Results and Discussion

Several factors affect stiffness and strength of hydrated cement systems (Neville, 1963). These include extent of hydration, pore structure parameters and other microstructural and nanostructural descriptors. The latter are evident from observed increases in strength and stiffness with little or no apparent increases in the degree of hydration that are often referred to as 'ageing' effects (Mills, 1965). It has also been observed that stiffness or modulus of elasticity is not uniquely dependent on moisture content; stiffness, even in the dry state, is not unique (Sereda et. al, 1966; Feldman, 1972). For example, when the dry state has been obtained by 'd-drying' hydrated cement powders prior to compaction into solid bodies as opposed to compacting powders conditioned to 11%RH followed by 'd-drying' (i.e. drying to the vapor pressure of dry-ice at -78°C) there is a two fold increase in modulus of elasticity for the former. It was concluded that high compaction pressures can force the layers of 'd-dried' material closer together. This suggests the possibility that the significant increase in stiffness arises from bond formation at new sites between the C-S-H sheets. This will be discussed further later.

Current compositional models for the nanostructure of C-S-H are comprised of structural units of 1.4nm tobermorite and jennite. The engineering behavior and volume stability of these minerals are not well known. It is therefore of interest to explore factors responsible for performance variability. The factors controlling variation of stiffness and its 'regeneration' in cement systems are both of practical and fundamental interest.

The results reported here were obtained from experiments specifically designed to demonstrate the effect of degree and duration of drying on mechanical property 'regeneration' possibilities. The focus is directed to changes in stiffness or modulus of elasticity resulting from different drying treatments. The control state for all samples is 11%RH with no drying. The drying treatments (described earlier) consist of a continuous sequence beginning with vacuum at room temperature for various periods up to 72 hours to vacuum plus heat (46, 65, 70, 79, 96, 100, 108, and 113 °C) for periods varying from 24 to 72 hours at each temperature. DTGA curves for each of these drying steps (each step is in addition to the preceding steps) are shown in Figures 1 and 2 for 1.4nm tobermorite and jennite respectively.

A brief description of the DTGA curves in concert with earlier observations reported by Yu and Kirkpatrick is provided as follows (Yu and Kirkpatrick, 1999). The initial curve (Figure 1) for 1.4nm tobermorite has peaks at 50, 100 and 200 °C. The first two peaks are associated with the loss of interlayer water and the transition from the 1.4 nm form to the 1.2 nm form accounting for the loss of 4 moles of hydrate water. The peak at 200 °C is associated with the transformation from the 1.2 nm form to the 1.1nm form and the loss of two additional moles of hydrate water. There is also an inflection or change in slope at about 260 °C associated with the transformation to the 0.96 nm form and a further loss of two moles of hydrate water. All these peaks decrease in intensity with further drying and mass-loss as expected. The DTGA curves for jennite (Figure 2) all have peaks at 50, 125-130, 210 and 375 °C. The peak at 50 °C is due to removal of interlayer water. The peak at 125-130 °C is associated with the formation of metajennite and the loss of 4 water molecules. The peak at

about 225 °C is associated with the remnants of interlayer water. The peak at 375 °C is associated with transformation to a disordered phase. (Yu and Kirkpatrik, 1999)

A dynamic thermal mechanical analysis technique (DMTA) was used to determine the modulus of elasticity (storage modulus, E'). Figure 3 is a plot of E' versus temperature for 1.4nm tobermorite. The control sample (conditioned at 11%RH) experiences a rapid decrease in E' (18.5-14.5GPa) in the temperature range 30-50°C largely due to the loss of interlayer water (curve 1). A more detailed discussion will follow later. Values of E' obtained for the sample pre-heated up to 96 °C do not change significantly when the sample is reheated from ambient up to 96°C (curve 2). This occurs despite the continuous decreases in E' observed on heating the control samples from 25 to 300 °C during the DMTA test. The DMTA test involves heating in increments of 2 °C with a dwell time of 5 min. at each interval. This is relatively rapid compared to the lengthier dwell times (days) for the drying steps for the protocols used in this study. The 'ageing' processes occurring throughout the various drying steps appear to initiate a 'regeneration' of the modulus of elasticity. This is illustrated in Figure 3. Curve 1 as stated is for the reference sample that was conditioned to 11%RH. Curve 2 is for a tobermorite sample that had been dried through the drying-protocol up to and including 4 hours at 96 °C (6.1% mass loss). The initial modulus value was 'regenerated'. The abrupt decrease in E' values due to the 'rapid' heating in the DMTA test did not occur until about 100 °C. It is apparent that prolonged thermal drying introduces factors responsible for regenerating stiffness possibly including cross-linking of the silicate sheets.

A brief description of the thermal events affecting 1.4 nm tobermorite in the DMTA test and their effect on the E' value of the control sample should be useful in trying to understand the

'regeneration' mechanism. There is a decrease in E' over four distinct temperature ranges (Figure 3) involving changes in the slope as the temperature increases to about 130°C (i.e. 25-35°C; 35-60°C; 60-100°C; 100-130°C). The results for a sample having a porosity value of 30% were chosen for clarity as the peak and inflections of the curves in the figure are clear and distinct. The frequency level was 3.98 Hz. Peaks and inflections at other porosity levels occur in similar locations but vary in intensity level. The removal of adsorbed water occurs in the first temperature range possibly overlapping with the removal of interlayer water. The second range likely corresponds to further removal of interlayer water. Interlayer water (as discussed previously) can have a structural role in layered calcium silicate hydrate systems contributing to a stiffening effect (Sereda et. al; 1966). The decrease in E' results from the removal of both surface water and interlayer water as the temperature increases to about 60°C. Removal of a further amount of interlayer water and the conversion of 1.4nm tobermorite to the 1.2nm form occurs in the third temperature range (60-100°C). The conversion is accompanied by a significant density change (2.23 g/cm^3 to about 2.40 g/cm^3, (Thomas et. al, 2010)) resulting in an increase in porosity along with a loss of 4 moles of structural water (Yu and Kirkpatrik, 1999). The additional loss of interlayer water and increase in porosity are responsible for the continuing decrease in E' throughout this temperature range. There is a small inflection in E' curve as the temperature increases from 130 to 160 °C followed by a continuous decrease to 300C. There is a conversion from the 1.2nm tobermorite to the 1.1nm form in the temperature range, 130-200 °C and a transformation to the 0.96 nm form at about 260 °C. This is accompanied by loss of an additional 2 moles of water at 200 °C and a further 2 moles of water at about 260 °C as previously described. There is also an increase in density and porosity associated with these

conversions. A density of 2.48 g/cm^3 has been reported for the 1.1nm form (Thomas et. al; 2010). The 'regeneration' effect results in a delay of the rapid decrease in E' observed for the control. It now occurs at about 96 °C i.e. the temperature to which the sample was pre-heated. It appears that the sample can recover its previous elastic behavior. The magnitude of the rapid decrease in E' is about 6.5 GPa compared to 4.2 GPa for the control sample. Stiffness change due to removal of the first 4 moles of water and the transition to the 1.1nm form of tobermorite prior to testing is likely associated with the gradual decrease in the basal-spacing coupled with the possible interaction of Ca^{2+} with the silicate sheets. (Yu and Kirkpatrick, 1999) Further removal of water at temperatures above 96 °C appears to have a significant weakening effect on the tobermorite nanostructure. There is subsequently a very small increase in E' at 160 °C that is maintained to about 275 °C possibly associated with the transformation to the 1.1 form of tobermorite.

The 'regeneration' effect was also observed for hydrated Portland cement paste (Figure 4). The control curve for the paste (12% porosity) is qualitatively similar to that presented for 1.4 nm tobermorite exhibiting a continuous decrease in the E' value over the entire temperature range. The curve for the sample that was subjected to the complete drying protocol including heating at 113 °C for 48 hours (mass-loss ≈ 10.1%) clearly indicates that the initial E' value has been 'regenerated'. The decrease in E' on further heating in the DMTA test mimics that portion of the control curve at temperatures > 113 °C.

The regeneration effect following drying from 11%RH is primarily associated with changes to the 'solid' phase as no pore water is present at this humidity. Characteristics of the solid that affect stiffness or elasticity in cement paste would include degree of hydration, extent of

silicate polymerization, crystallinity, pore structure and possible variations in stacking of silicate sheets. It would be expected that a relatively low porosity level e.g. 12% would result in higher initial values of E' as would be predicted from the well-known porosity dependence of modulus of elasticity for cement pastes. The regeneration effect would still be readily observed at different porosity levels. It is suggested that in cement paste the regeneration effect is likely to be greater at low porosity values as the solid phase concentration is greater providing increased surface for facilitating ageing effects. Modulus of elasticity measurements on low water/cement ratio cement pastes by Mills as indicated previously support this view as the modulus increased with time following cessation of hydration to a greater extent than at high water/cement ratios or increased porosity (Mills, 1965).

A further example of the 'regeneration' effect is given in Figure 5 where two E' versus temperature curves are plotted for synthetic C-S-H (C/S = 0.8, porosity = 30%, mass-loss = 5.6%). The control curve (starting condition = 11%RH) has an initial E' value of about 11.5 GPa. There is a large decrease in E' at 50 °C (a relatively low temperature) to a value of 3.8 GPa due to the loss of adsorbed and interlayer water. The second curve was obtained for a sample that had been heated in steps up to 70 °C and held there for 48 hours. The 'regenerated' value of E' was 9.6 GPa which is 83% of the initial control value. This value is largely maintained until about 50 °C and rapidly decreases until a value of 2 GPa is reached at 100°C.

The delayed 'rapid' decrease in E' was qualitatively similar to that observed for the 1.4nm tobermorite samples. The magnitude of the decrease for the C-S-H however was about the same i.e. 7.5GPa. This approximate equivalence in magnitude of the rapid decrease in E'

may be due solely to removal of the interlayer water in the C-S-H as unlike tobermorite there are no phase changes. The 'regeneration' effect is also similar to that which occurs for tobermorite. The rapid decrease in E' results in a lower value (2GPa as opposed to 4GPa) as was the case for tobermorite with a very slight increase occurring as the temperature subsequently increases to 300 °C.

The nanostructure of jennite appears to be much more stable than the corresponding nanostructures of the silicate systems described above. The initial values of E' for the control samples and those dried by vacuum heating in steps up to 2.6% mass-loss show a 'regeneration' of E' values over the entire temperature range (see curves 1 and 2 in Figure 6).The dramatic decrease in slope at about 100 °C is due to the formation of metajennite (M-J). The loss of interlayer water up to that point brings the silicate sheets into closer proximity suggesting that there may be an 'ageing' effect on the application of vacuum and heat that contributes to increased stiffness. The sample heated at 79 °C for 72 hours is essentially M-J, (see curve 3, Figure 6). Curve 3 follows a parallel path to that portion of curves 1 and 2 attributed to the M-J thermal response up to 300 °C. Curve 3 lies between curves 1 and 2 at temperatures greater than 100 °C indicating that 'regeneration' of M-J stiffness also occurs after formation of M-J due to pre-heating. M-J formation and drying to 300 °C results in the loss of 6 water molecules accompanied by an increase in porosity as the density increases from 2.33 to 2.62 g/cm^3. Heating jennite up to 96 °C for 1 day results in a mass-loss of 7.4% (curve 4, Figure 6). The E' values for this heat treatment are not completely 'regenerated' and remain below those of M-J formed at 79 °C. The bonds holding the silicate sheets together appear to be weakened. It is apparent that there is a lack of potential with jennite to 'regenerate' the original stiffness level following conversion to metajennite. Regeneration of

stiffness prior to conversion to metajennite occurs (curve 1 in Figure 6). Regeneration of the stiffness of metajennite itself also occurs. (curve 3 in Figure 6).

A brief account of the thermal events affecting jennite in the DMTA test and their effect on the E' value of the control sample, as with 1.4nm tobermorite, should also be useful in trying to understand the 'regeneration' mechanism. There are 4 distinct temperature ranges in the E' versus temperature curve of the control sample in Figure 6 (25-35 °C, 35-85 °C, 85-175 °C, 175-300 °C). There is a gradual decrease in the value of E' between 25 and 35 °C largely due to the loss of adsorbed surface water. This is followed by a more rapid decrease in E' as the temperature increases to about 85 °C that is attributed primarily to the loss of interlayer water. It is clear that interlayer water has a structural role in the mechanical behavior of jennite. Metajennite forms in the third temperature range as the basal-spacing changes from 1.06nm to 0.86 nm. There is a loss of 4 water molecules from the structural unit and a large change in density from 2.33g/cm^2 to 2.62 g/cm^2 accompanied by an increase in porosity. The values of E' in this temperature range remain relatively constant suggesting that the new phase is more stable than jennite itself as it would otherwise be expected that increases in porosity would result in a reduction in stiffness. Further removal of interlayer water (about 2 moles) on heating to 300 °C results in a significant decrease in E' suggesting that the final 2 moles of water have a significant effect in maintaining the structural integrity of metajennite`. Metajennite is also transformed into a disordered phase above 250 °C (Yu and Kirkpatrik, 1999). This phase appears to contribute to the low stiffness values that are observed.

It is clear that the stiffness of metajennite is lower and characteristically different than that of jennite itself. Nevertheless both phases have the potential to regenerate stiffness following prolonged drying due to combined vacuum and thermal treatment.

Conclusions

1. Modulus of elasticity values of layered silicates conditioned to 11%RH generally decrease on drying in association with the removal of adsorbed and interlayer water.

2. Drying of layered silicates resulting from heating at the rate of about 0.4 °C/min. typical of a dynamic mechanical thermal analysis test (DMTA) generally results in a decrease in elastic modulus.

3. Prolonged drying (several days) under vacuum at variable temperatures up to 113 °C results in a 'regeneration' of the initial elastic modulus values obtained with the control samples conditioned at 11%RH.

4. The 'regeneration' phenomena associated with elastic modulus was observed for all the calcium silicate systems studied including 1.4nm tobermorite, jennite, C-S-H and hydrated Portland cement paste.

5. It is apparent that there is a lack of potential with jennite to 'regenerate' the original stiffness level following conversion to metajennite.

6. Regeneration of the original stiffness of jennite prior to conversion to metajennite can occur. Regeneration of the stiffness of metajennite itself also occurs.

7. The 'regeneration' phenomena observed for all the studied silicate systems is consistent with the notions expressed for nanostructural models that are comprised of structural units based on 1.4nm tobermorite and jennite.

8. It is suggested that a possible regeneration mechanism is associated with bond formation between interlayer Ca^{2+} and the silicate sheets as well as cross-linking.

References

Alizadeh R., Beaudoin J. J. and Raki L., Mechanical properties of calcium silicate hydrates, Matls. and Struct., 44, 13-28, 2011.

Beaudoin J.J., Comparison of mechanical properties of compacted calcium hydroxide and Portland cement paste systems, Cem. Concr. Res., 13, 319-324, 1983.

Feldman R. F., Factors affecting Young's modulus-porosity relation of hydrated Portland cement compacts, Cem. Concr. Res., 2, 375-386, 1972.

Gard J. A. and Taylor H. F. W., Calcium silicate hydrate (II) ("C-S-H(II)"), Cem. Concr. Res., 6, 667-678, 1976.

Hara N. and Inoue N., Formation of jennite from fumed silica, Cem. Concr. Res., 10, 677-682, 1980.

Menard K. P., Dynamic Mechanical Analysis-A Practical Introduction, CRC Press LLC, Boca Raton, pp. 208, 1999.

Mills R. H., The relationship between cube strength and non-evaporable water in cement pastes subjected to various curing regimes, Trans. South African Inst. Of Civ. Eng., 13-31, 1965.

Neville A. M., Properties of Concrete, John Wiley &Sons Inc., New York, pp.532, 1963.

Richardson I. G., Tobermorite/jennite- and tobermorite/calcium hydroxide-based models for the structure of C-S-H: applicability to hardened pastes of tricalcium silicate, Portland cement, and blends of Portland cement with blast-furnace slag, metakaolin, or silica fume, Cem. Concr. Res., 34, 1733-1777, 2004.

Sereda P.J. and Feldman R. F., Compacts of powdered material as porous bodies for use in sorption studies, J. Appl. Chem., 13, 150-158, 1963.

Sereda P.J., Feldman R.F. and Swenson E.G., Effect of sorbed water on some mechanical properties of hydrated Portland cement pastes and compacts, Highway Research Board, Special Report 90, 58-73, 1966.

Soroka I. and Sereda P.J., The structure of cement- stone and use of compacts as structural models, Proc. 5th Int. Symp. on the Chem. of Cem., Vol. 3., Tokyo, 67-73, 1968.

Taylor H. F. W., Chapter 5, Hydration of the calcium silicate phases, Cement Chemistry, Thomas Telford Publishing, London, pp 459, 1997.

Taylor H.F.W., Proposed structure for Calcium Silicate Hydrate Gel, J. Amer. Ceram. Soc. 69, (6), 464-467, 1986.

Thomas, Jefferey J., Jennings H. M. and Allen A.J., Relationships between composition and density of tobermorite, jennite and nanoscale $CaO\text{-}SiO_2\text{-}H_2O$, J. Phys. Chem. C, 114, 7594-7601, 2010.

Yu P. and Kirkpatrick R.J., Thermal dehydration of tobermorite and jennite, Concr. Sci. and Eng., 1, 185-191, 1999.

Figure Captions

Figure 1. The effect of vacuum and thermal drying on the derivative mass loss curve for 1.4nm tobermorite (T) equilibrated at 11% RH.

Figure 2. The effect of vacuum and thermal drying on the derivative mass loss curve for jennite (J) equilibrated at 11% RH.

Figure 3. DMTA curves for 1.4 nm tobermorite: curve 1 for control sample conditioned to 11%RH prior to testing; curve 2 for sample heated up to 96°C for 4 days prior to testing.

Figure 4. DMTA curves for hydrated Portland cement paste: curve 1 for control sample conditioned to 11%RH prior to testing; curve 2 for sample heated up to 113°C for 2 days prior to testing.

Figure 5. DMTA curves for C-S-H (C/S = 0.8): curve 1 for control sample conditioned to 11%RH prior to testing; curve 2 for sample heated up to 70C for 2 days prior to testing.

Figure 6. DMTA curves for jennite: curve 1 for control sample conditioned to 11%RH prior to testing; curve 2 for sample heated up to 79°C for 3 days prior to testing.

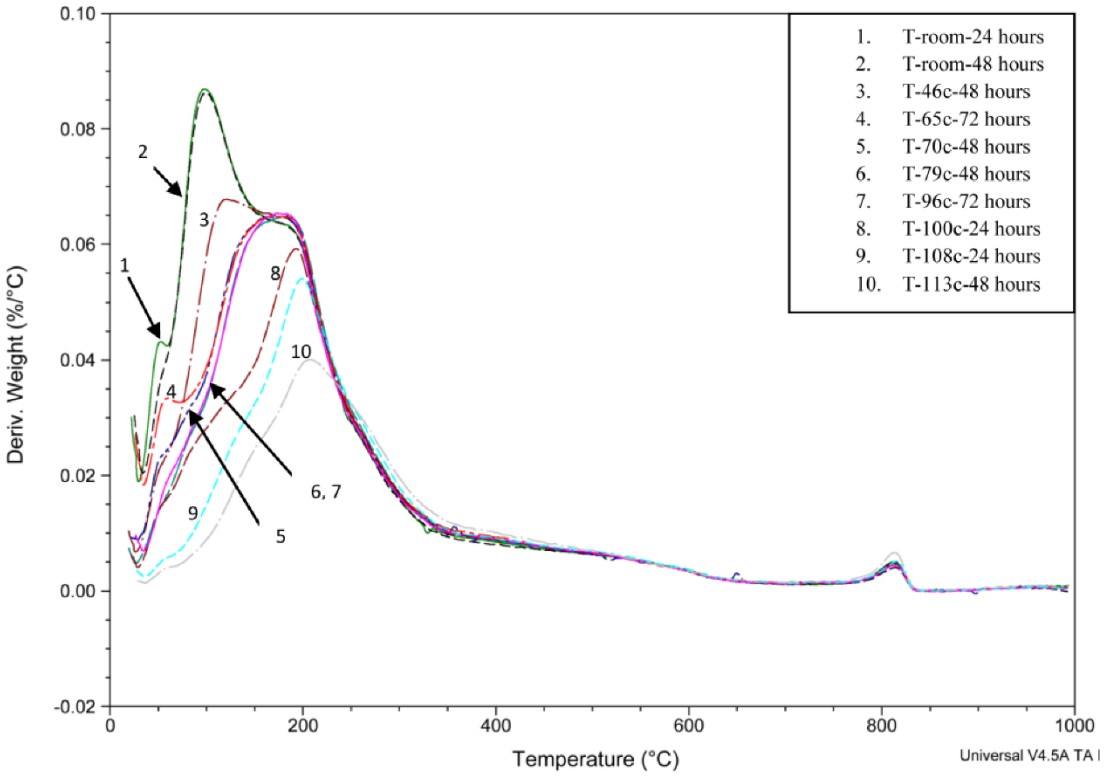

Figure 1. The effect of vacuum and thermal drying on the derivative mass-loss curve for 1.4nm tobermorite (T) equilibrated at 11% RH.

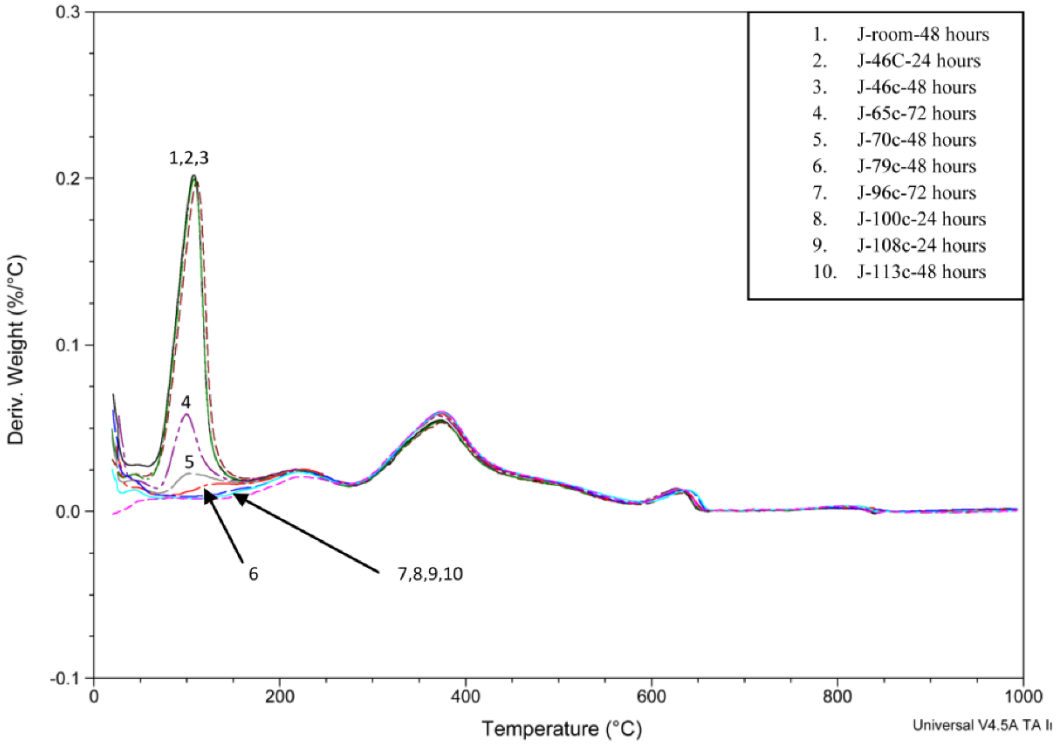

Figure 2. The effect of vacuum and thermal drying on the derivative mass-loss curve for jennite (J) equilibrated at 11% RH.

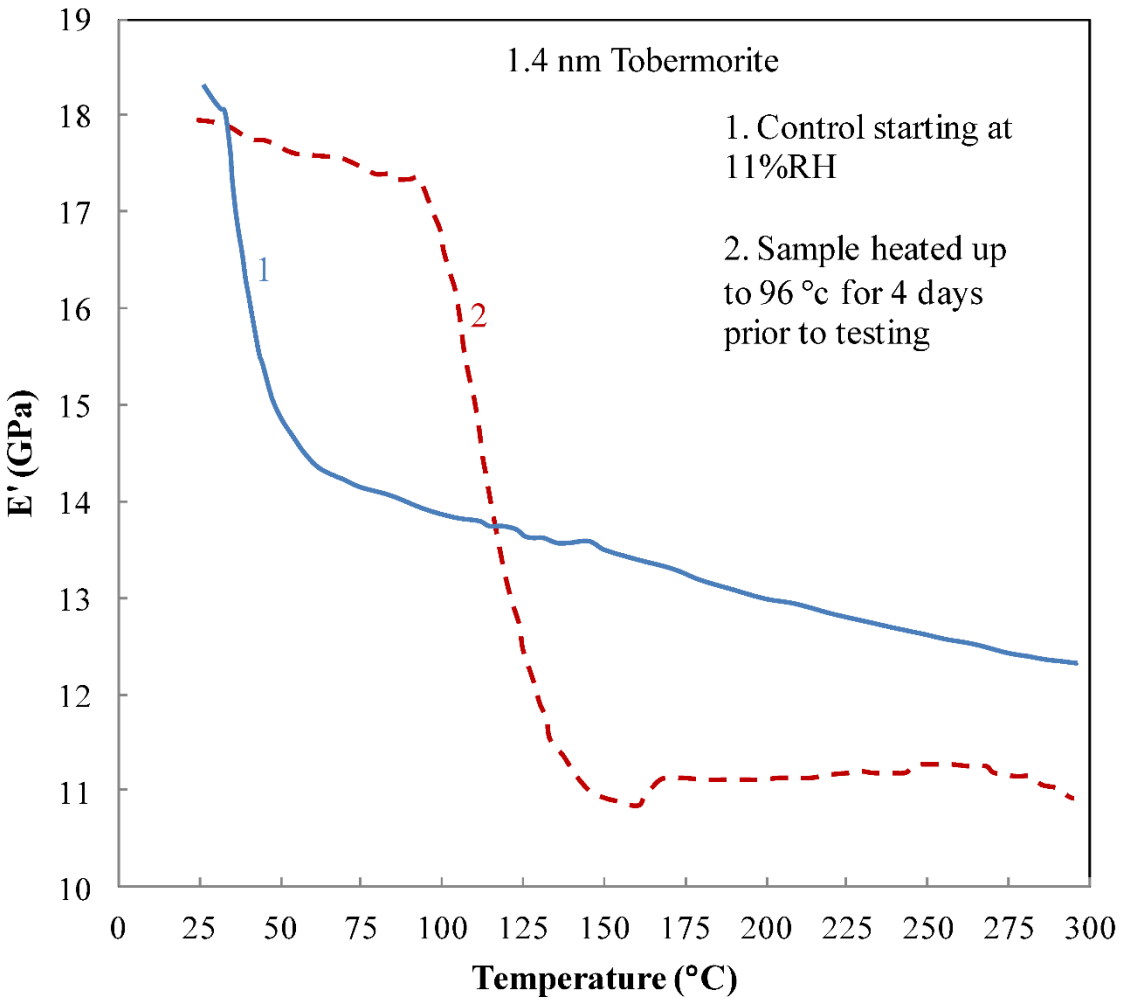

Figure 3. DMTA curves for 1.4 nm tobermorite: curve 1 for control sample conditioned to 11% RH prior to testing; curve 2 for sample heated up to 96°C for 4 days prior to testing.

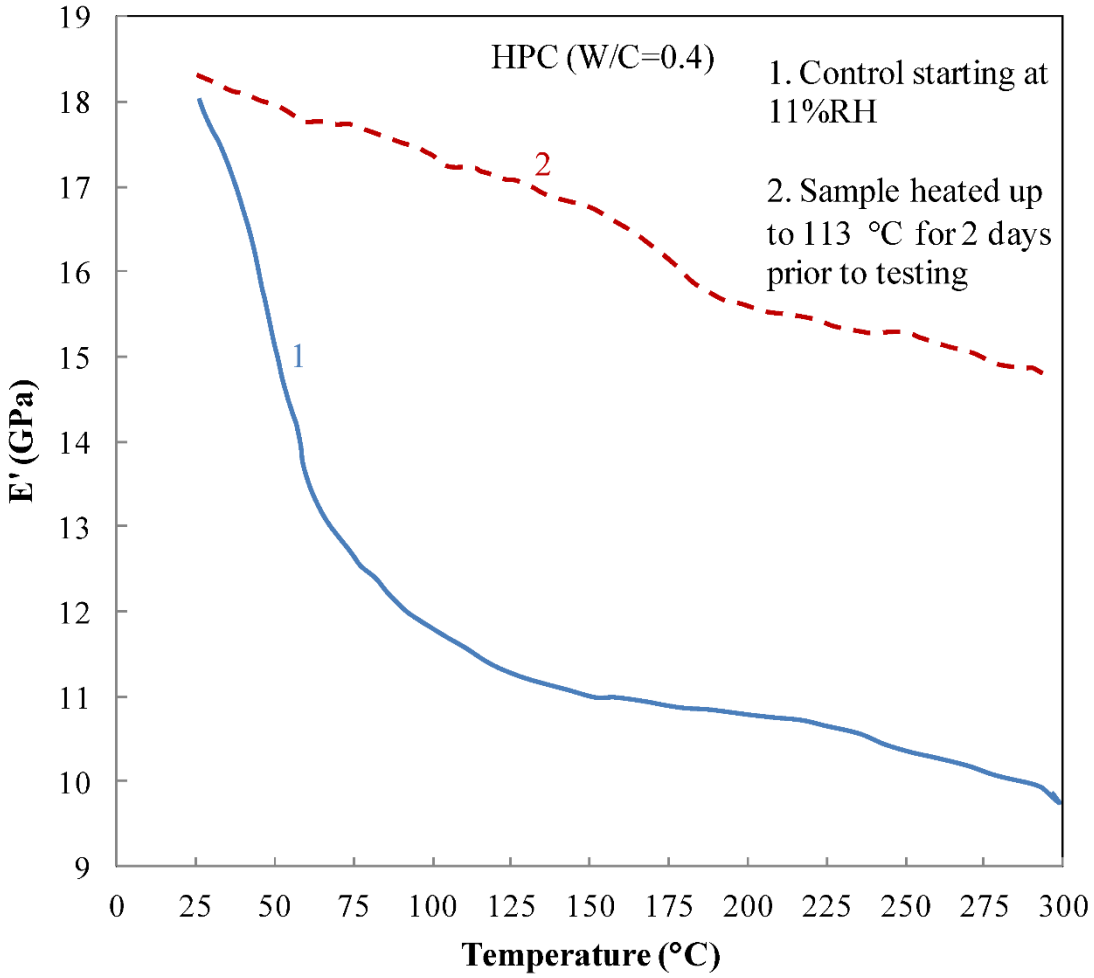

Figure 4. DMTA curves for hydrated Portland cement paste: curve 1 for control sample conditioned to 11% RH prior to testing; curve 2 for sample heated up to 113°C for 2 days prior to testing.

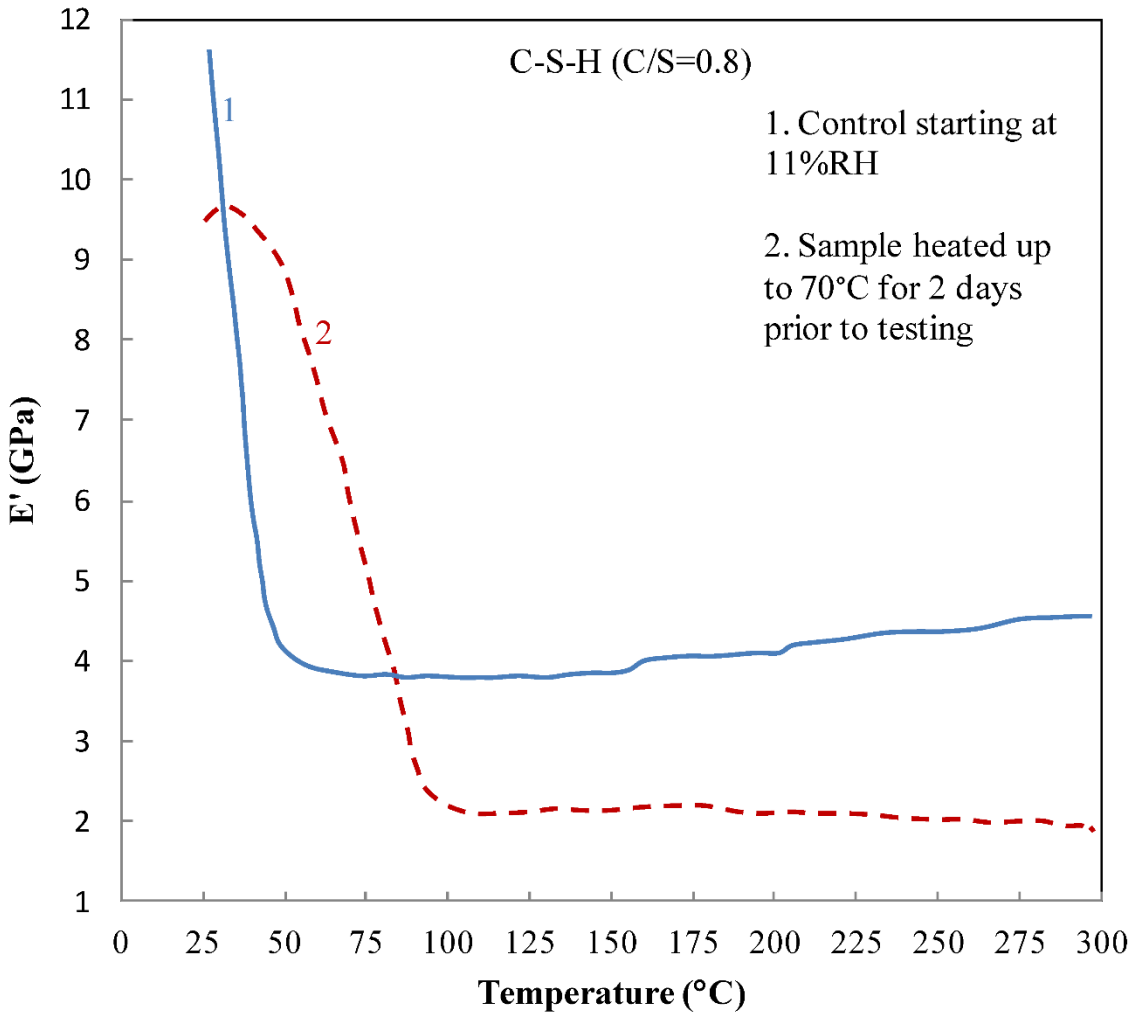

Figure 5. DMTA curves for C-S-H (C/S = 0.8): curve 1 for control sample conditioned to 11%RH prior to testing; curve 2 for sample heated up to 70C for 2 days prior to testing.

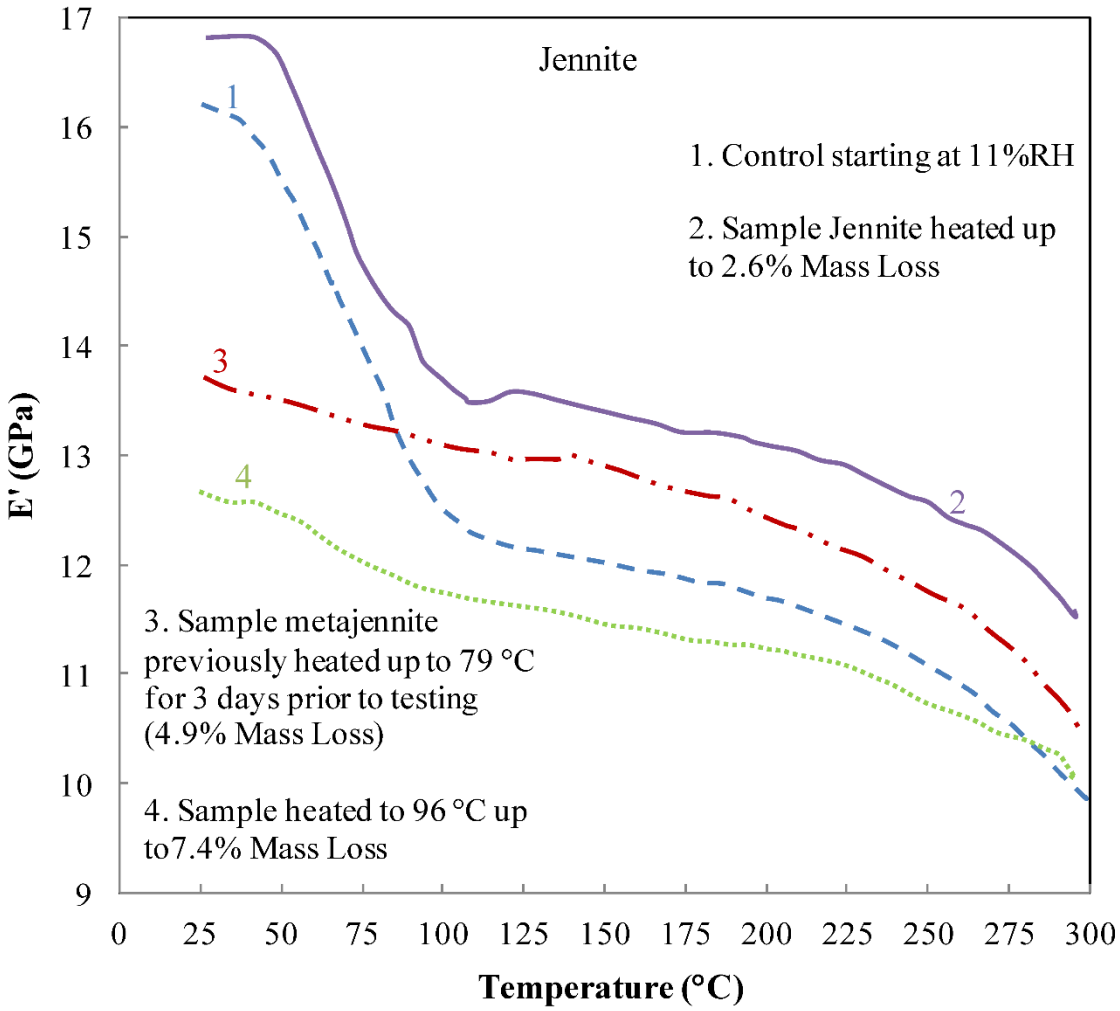

Figure 6. DMTA curves for jennite: curve 1 for control sample conditioned to 11% RH prior to testing; curve 2 for sample heated up to 79°C for 3 days prior to testing.

Chapter 10

Engineering Performance of 45 Year Old Hydrated Portland Cement

This chapter (Part 3 of the experimental program) is a continuation of the candidate's investigation into the correspondence between mechanical performance of layered calcium-silicate-hydrates and nanostructural characteristics/compositional features of these systems. Three papers (from Part 3 of the experimental program) addressing the effect of prolonged aging on the correspondence between engineering performance and the nanostructural character of C-S-H that forms from the cement-water reaction are presented in this chapter.

A unique opportunity to study the effect of the metamorphosis of C-S-H with age in hydrated Portland cement was provided to the candidate with the access to cement paste specimens (fabricated at the National Research Council, Canada) that were hydrated for a period of 45 years. These specimens had a wide range of water/cement ratios varying from 0.40 to 1.00. Prolonged hydration of cement has an effect on the C-S-H 'building-blocks' in cement paste i.e. the mean chain length (generally increasing) of the layered silicate phase, the number of defects or missing bridging silica tetrahedra, surface area and stacking of the silicate sheets. Changes to pore structure, creep and mechanical properties of C-S-H are linked to these nanostructural descriptors.

Experiments were designed to provide insight into the contribution of aging, related nanostructural changes and the role of interlayer water on the engineering performance of

cement-based materials. Properties of interest were determined using dynamic mechanical thermo-analysis and microindentation methods on both compacted hydrated cement powders and paste hydrated samples. These included storage modulus and tan∂ (internal friction) values in addition to creep, indentation modulus and hardness modulus determinations. Insight into creep mechanisms of layered silicates and the influence of interlayer water removal on related structural collapse processes are outcomes of this work.

The titles of the papers in this chapter are as follows:

Paper 7: Microindentation Creep of 45 Year Old Hydrated Portland Cement Paste, Advances in Cement Research, 25(5), 301-306, 2013.

Paper 8: Dynamic Mechanical Thermo-Analysis of Portland Cement Paste Hydrated for 45 Years, Materials and Structures, Accepted for Publication, 2014. DOI: 10.1617/S11527-014-0500-7

Paper 9: Creep of 45 Year old Cement Paste: the Role of Structural Water, Materials and Structures, Accepted for Publication, January 2015. DOI: 10.1617/s11527-015-0534-5

10.1 Introduction

The utility of the DMTA, microindentation and powder compaction methods for investigating the effect of prolonged aging on engineering performance is explored in the three papers presented in this chapter.

Microindentation methods were used to study the creep behavior of cement paste (w/c = 0.50, 0.80, 0.90 and 1.00) hydrated for 45 years. The results and the implications of the aging

process are reported in paper 7. Variation in creep behavior of young paste (hydrated 3days to 3 years) and old paste (hydrated 45 years) is discussed in terms of nanostructural differences.

Details of the aging process (as it relates to hydrated Portland cement paste) and its effects on the engineering parameters (storage modulus and tan∂ or internal friction) obtained from DMTA experiments are described in Paper 8. Age dependent nanostructural characteristics of C-S-H were shown to influence the mechanical behavior of cement paste. The use of specimens made from compacted powders of aged cement paste are particularly useful as they provide the versatility for fabricating samples with variable porosity by simply varying the compaction pressure. Comparison of engineering parameters for different matrix materials can then be made at equivalent porosities.

It is apparent that interlayer water in C-S-H has a structural role in engineering performance and particularly in the creep process. It is instructive to examine this role in the context of cement paste hydrated for 45 years. The correspondence between creep modulus versus mass-loss curves (from 11% RH) and tan∂ versus temperature curves for the pastes studied provided new insights as to the influence of interlayer water on the creep process. These are described in Paper 9.

10.2 Paper 7: Microindentation Creep of 45 Year Old Hydrated Portland Cement Paste

It is demonstrated in Paper 7 that microindentation methods can be successfully used to differentiate the creep behavior of Portland cement paste hydrated for times varying from short to extended periods. Nanostructural features of C-S-H e.g. degree of polymerization were shown to influence the creep rate of cement paste. C-S-H containing shorter silicate chain lengths was shown to be more susceptible to creep. Old cement pastes generally exhibit lower creep over a wide range of porosity values. The porosity dependence of the microindentation parameter, creep modulus, is discussed in the context of possible creep mechanisms.

Microindentation Creep of 45 year old Hydrated Portland Cement Paste

(Advances in Cement Research, 25(5), 301-306, 2013)

P. Pourbeik[a], R. Alizadeh[b], J. J. Beaudoin[a], D.-T. Nguyen[c] and L. Raki[a]

[a] *National Research Council Canada, Construction Portfolio, Ottawa, ON, Canada*

[b] *Giatec Scientific Inc., Ottawa, ON, Canada*

[c] *Department of Civil Engineering, University of Ottawa, Ottawa, ON, Canada*

Abstract

Microindentation methods were used to study the creep behavior of cement paste hydrated for 45 years. These 'old' pastes were prepared having a wide range of water/cement ratio varying from 0.50 to 1.00. The porosity dependence of the indentation parameters (creep modulus, indentation modulus and indentation hardness) was determined and discussed in the context of possible creep mechanisms. Microindentation creep was also determined for 3 year old cement paste and young paste hydrated for 3 and 7 days. Variation in creep behavior of the cement pastes for the 3 age groups is discussed in terms of nanostructural differences.

Keywords: Microindentation, 45 year old cement paste, creep, porosity, nanostructure

Introduction

The creep of concrete has been the subject of intensive research for decades (Neville, 1970). Modern concretes are expected to have specific properties for a particular application (Neville, 2006). This extends to specifications related to modulus of elasticity, dimensional stability or specific creep properties. Neville drew attention to the fact that some of the positive influences on strength lead to a sometimes undesirable increase in creep deformation (Neville, 2006). The 'active' component of concrete that is subject to creep is the cement paste binder. Despite much research creep mechanisms remain a subject of interest as differing views persist. The origins of creep in cement paste have recently been attributed to nanogranular behavior of the C-S-H and the sliding of 'globules' at points of contact (Vandamme et al. 2009). Other rsearchers attribute the viscoelastic nature of synthetic C-S-H to translation of the silicate sheets when subjected to sustained load and to the role of interlayer water (Alizadeh et al. 2010)

Nanoindentation methods have recently been used to assess the creep behavior of Portland cement paste (Vandamme et al. 2009). Deconvolution methods applied to frequency curves of, for example, the creep modulus parameter have been used to separate the contributions of the individual phases to creep of cement paste. There has been some criticism of this method concerning the possible interference of other hydrated cement phases in the zone of influence beneath the indenter (Trtik et al., 2009; Lura et al., 2011). Microindentation methods have been shown to be effective for determining creep behavior of monophasic cement hydrates eg. pure C-S-H preparations (Nguyen D-T et al., 2012). Microindentation is also suitable for determining the *average* 'composite' creep behavior of a cement paste 'composite' where no attempt is made to separate the influences of the various phases in the

composite. This is only possible at the nanoscale using nanoindentation methods (Trtik et al., 2009).

There is a paucity of information on the influence of prolonged periods of hydration on the creep behavior of hydrated cement paste. Characterization data for cement pastes and C_3S pastes hydrated for up to 30 years has been reported by a few researchers (Rodger SA et al., 1987; Taylor et al., 2007; Mohan K et al., 1982; Sarkar AK et al., 1972; Richardson IG et al., 1992). This includes application of ^{29}Si NMR, trimethylsilylation and other methods methods. The nanostructure of the pastes generally changes towards a greater degree of silicate polymerization and greater average chain length. Rodger et al. estimated the mean chain length for hydrated C_3S paste at about 2.64 units, 3.28 and 4.76 units at 14 days, 1 year and 26 years respectively (Rodger et al., 1987). Their 26 year old paste had a Ca/Si atom ratio of 1.75 ± 0.05 and the 3.5 year old paste had a value of 1.74 ± 0.13.The mean Ca/Si ratio of C-S-H in hardened C_3S pastes appeared to vary little with age (Taylor et al. 2007). Mohan and Taylor using trimethylsilylation methods, estimated about 40% dimer and 60% polymer in C_3S paste at 30 years. They hypothesized that polymerization of anions in the C-S-H might have been associated with reconstitution of particles and changes in microstructure and that changes in engineering properties might be directly associated with microstructural change. The effect of these changes on creep behavior has not been clearly established. The results of a study to assess the creep behavior of 45 year old cement paste using microindentation methods is reported in this paper.

Experimental

Materials

Cement pastes:

The 45 year old paste specimens were cast in glass cylinders with circular cross-section (25mm in diameter). The paste was prepared with water/cement ratios of 0.50, 0.80, 0.90 and 1.00. The cylinders were continuously rotated for 24h and the specimens were subsequently demolded and sheathed in a rubber membrane containing a few drops of lime saturated water. They were then stored in stoppered glass tubes for 45 years. Slices 1mm thick were then cut and ground into a fine powder for fabrication into compacted specimens. The use of compacted specimens provided an effective means for controlling the porosity. The cement used was a normal type I Portland cement. The oxide analysis for the cement (percentages are given in brackets) used was as follows: SiO_2 (20.72); Al_2O_3 (5.87); Fe_2O_3 (3.07); CaO (62.66); MgO (3.46);SO_3 (2.18). Ignition loss was 1.10 %; Insoluble residue was 0.24%. Free CaO was 0.24%. The Bogue compound composition was: C_3S (46.5%); C_2S (24.6%); C_3A (10.4%); C_4AF (9.3%). Blaine fineness was 3279 cm^2/g. The 'old' pastes were characterized using X-ray diffraction, TGA and ^{29}Si NMR methods.

The 3 year old paste (made with Type I Portland cement) was prepared using a water/cement ratio of 0.40. Rectangular prisms (250 x 100 x 12mm) were cast. The samples were vibrated and stored in a moist curing room for 24 h. They were then demoulded and curing was continued for 3 years in a saturated lime solution. Thin slices (1 x 12 x 60 mm) were cut from the paste prism using an Isomet diamond saw. Selected slices were also ground into a fine powder for fabrication into compacted specimens. The cement used was also a normal type I Portland cement. The oxide analysis for the cement (percentages given in brackets) used

was as follows: SiO_2 (19.80); Al_2O_3 (4.90); Fe_2O_3 (2.50); CaO (62.30); MgO (3.20); SO_3(3.20); Ignition loss was 2.80 %. Insoluble residue was 0.50%.Free CaO was 1.60%. The Blaine fineness was 4055 cm^2/g.

Young pastes (water/cement = 0.40) hydrated for short periods (e.g. 3 and 7 days) were prepared in a similar manner to the 3 year old paste. The cement used was the same as that used for the 3 year old paste.

Humidity Conditioning

Cement paste specimens for the three age groups were conditioned at 11%RH in vacuum desiccators containing saturated lithium chloride solution. The powders were conditioned for a few weeks at 11%RH before compaction and for several days after compaction. Theoretically there is a monolayer of water on the surfaces of the particles in addition to interlayer water at this humidity. There is virtually no pore water present. This position on the isotherm is used as a datum point for the testing as the results reflect more effectively the structural role of the solid (including interlayer water). Mechanical behavior at various equilibrium positions along the water isotherm would be expected to vary and is the subject of ongoing investigation.

Preparation of Compacted Specimens

Circular disc samples for all the powdered materials (from the three age groups) were prepared by pressure compaction in steel moulds with a cross-section of about 25 mm. The

thickness of most of the prism samples was nominally 1mm but varied between the limits of 1-2mm.The hydrated cement was ground to a mean particle size of 20-30 μm prior to compaction.Five different compaction pressures were used to fabricate the compacts: 111, 222, 333, 444 and 555 N/mm^2. Porosity values varied with water/cement ratio at each compaction pressure. For example, the range of porosity values (in %) at each pressure was 48-50; 34-40; 24-29; 19-22; 14-22 respectively. Numerous studies on the use and validity of compacts as models for hydrated cement systems have been published (Soroka et al., 1968; Feldman et al., 1972; Sereda et al., 1963; Beaudoin, 1983). It has been shown that compacted specimens of powdered hydrated Portland cement have similar mechanical property-porosity relationships to that of the original hardened paste of the same material (Feldman et al., 1972). Recent studies based on dynamic mechanical analysis (DMA) of various hydrated cement systems have demonstrated that irrespective of the age or extent of hydration the mechanical property-porosity dependence of compacted specimens are similar to those for paste hydrated specimens (Pourbeik et. al., 2012). The age-dependent differences are manifested in the relative position of the curve for each age category along the porosity axis. The age categories of interest in this current study are very young (3, 7 days), intermediate (3 years) and old (45 years). The mechanical property – porosity curves for the pastes and compacts representing each of these categories are displaced along the porosity axis. Earlier work (Sereda et. al., 1966) has demonstrated that the data constituting the mechanical property-porosity function is coincident for a range of water/cement ratios and degree of hydration. This curve was obtained for pastes hydrated up to 130 days. Taylor has argued that strength of calcium-silicate-hydrate systems, for example, is a function not only of porosity, but that it is dependent on the increasing proportion of coarse, dense , crystalline material (Taylor, 1977). Factors that may contribute to the latter descriptors are the amounts

of calcium hydroxide and unhydrated cement in the sample. A rationale for the porosity dependence of DMA parameters (e.g. storage modulus-porosity curves of cement paste specimens from the three age categories) based on the Taylor model has been presented elsewhere by the authors (Pourbeik et. al, 2012). It is apparent that there is no unique mechanical property-porosity curve for all cement pastes. Nevertheless in each age category a direct correspondence of the mechanical-property- porosity data for both compacted and paste hydrated specimens exists. Cement pastes contain a relatively large amount of C-S-H even at early ages. The degree of hydration is generally greater than 70% even after only a few days of hydration. Specimens hydrated for several months have a degree of hydration as high as 85% and those hydrated for 3 years have a degree of hydration > 90%.It is argued then that even though the 45 year old pastes are essentially completely hydrated (based on TGA evidence) all the pastes studied contain significant volume concentrations of C-S-H. This being the case it is argued that a significant contribution to any differences in mechanical properties of the pastes/compacts especially between age 3 and 45 years can be attributed to the nature of the C-S-H itself.

The use of specimens comprised of compacted powders of hydrated cement enables the variation of porosity while keeping the composition of the solid phase constant. This provides a useful means of assessing the significance of any changes to the solid phase microstructure on engineering performance. This technique was employed for assessing the creep behavior of three distinct age groups of hydrated cement paste including 3-7 days, 3 years and 45 years of hydration i.e. young, intermediate and prolonged periods of hydration.

The porosity of compacted paste samples was determined using helium pycnometry. The calculation is made knowing the apparent volume and the solid volume of the sample. Porosity is varied by controlling the compaction pressure.

Microindentation measurements

All the microindentation tests were performed using a CSM Instruments Instrumented Indentation Tester. The apparatus is housed in an environmental chamber. All tests were conducted at 11% RH on specimens equilibrated at 11%RH.Tests were conducted using a Berkovich indenter. The CSM microindentation instrument has a load range of 0.03 – 30 N with a resolution of 0.3 mN. The specimens were tested over a wide range of porosity values varying from about 10% to as high as 60%. There were approximately 25 indents on each sample at each porosity level for a total of approximately 125 indents for each material system. The results are considered to be representative of the cement paste composite as a whole. No phase separation procedures were attempted as these would require nanoindentation measurements and analysis.

The indentation depth was recorded as a function of time at the maximum load of 1000 mN for a 600s dwell period. The loading rate was 2000mN/min. The logarithmic creep was determined through curve fitting of the indentation-depth versus time curves during the 600s dwell time by the following equation:

$$\Delta h(t) = x_1 \ln (x_2 t + 1) + x_3 t + x_4$$

The creep modulus, C, is then calculated from: $C = P_{max}/ (2a_U x_1)$ where $a_U = [A_c/\pi]^{1/2}$. A_c is the projected area of contact between the indenter probe and the indenter surface. It is determined using the Oliver and Pharr method as a function of the maximum indentation

depth (18). The indentation modulus (M) and indentation hardness (H) were obtained from the software that uses the Oliver and Pharr method. $M = \pi^{1/2}S/ [2(A_c)^{1/2}]$ where $S = dP/dh |_{h = hmax}$ is the initial slope of the unloading branch of the P-h curve. P is the maximum indentation load. Indentation hardness (H) was estimated from the relation $H = P/A_c$.

Results and Discussion

Microindentation test results

Creep modulus versus porosity data for the young, intermediate and 'old' hydrated cement paste systems are plotted in Figure 1. The young and intermediate pastes have a water/cement ratio = 0.40. The curves for these systems (non-linear regression lines only are given for clarity) form lower bounds relative to the data sets for the 'old' pastes. A summary of the regression analysis for the curves in this figure is provided in Table 1. The distinction between the curves is evident.

The 'old' pastes were prepared at water/cement ratios of 0.50, 0.70, 0.80, 0.90 and 1.00. The degree of hydration is very high for the old pastes ranging from 95 to 99 % (based on TGA measurements not shown here). Creep modulus decreases as porosity increases for all systems. Examination of the data sets for the 'old' pastes shows that data for the paste with a water/cement ratio = 1.0 forms an upper bound. The data for water/cement ratios 0.80 and 0.90 form a lower bound. The relative position of the trend line for the creep modulus (or indentation hardness) data for the water/cement ratio = 0.50 preparation would not necessarily be expected to be sequential with the trend lines from the other water/cement ratio preparations. This is because at the relatively low water/cement ratio (i.e. 0.50) the pore

structure (especially after 45 years hydration) is highly discontinuous as the capillary pores are essentially completely filled. Analysis of the pore size distribution from the nitrogen adsorption isotherm supports this statement. The average chain length (determined from ^{29}Si NMR data obtained in the laboratory) for the water/cement ratio = 0.50 and 1.0 preparations i.e. 4.28 and 4.10 silicate units respectively are the highest. The chain length for the water/cement ratio = 0.80 and 0.90 are 4.02 and 3.78 units respectively. The nitrogen surface area values are however very similar for the water cement ratios 0.50, 0.70 and 1.00 being 44.5, 46.0 and 41.3 m^2/g but significantly higher for the water/cement ratio = 0.90 preparation i.e. 62.24 m^2/g. This preparation has both the lowest chain length and highest surface area. Surface area values are dependent on the accessibility of nitrogen to the surface. The 'stacking' of the layers during drying prior to a BET sorption experiment may be influenced by the spatial constraints imposed by the pore structure. This effect may be relaxed at the highest water/cement ratio as the 'stacking' of the layers may be more regular and impede the access of nitrogen to the surface. A limited amount of capillary porosity may still be present at water/cement ratio = 1.0 as indicated by analysis of the nitrogen sorption isotherm. There may be an optimum effect on surface area due to the 'stacking' effect that may account for the higher surface area at water/cement ratio = 0.90. Following consideration of the chain length and surface area information it is inferred that a higher chain length (and fewer surface defects) might be conducive to a higher creep modulus or lower creep rate. Conversely high surface area and low chain length (larger number of defects) might also be conducive to a lower creep modulus or a higher creep rate.

A comparison of the relative position of the curves for the three age groups is instructive. It was observed that it requires a lower porosity for the less hydrated solid phase (reference to

the younger pastes) to creep the same amount. Creep of cement paste is both nanostructure and porosity dependent. Creep of the same C-S-H binder would be expected to be less at low porosity. It is therefore inferred that the young C-S-H with the shorter silicate chains is more susceptible to creep in order to compensate for the low porosity. Alternatively the creep modulus is lower or creep is higher for the young paste when the porosity is constant i.e at a constant volume concentration of hydrated product. The lower chain length C-S-H in the young pastes contains more defects sites (positions of missing bridging silica tetrahedral. These positions are referred to here as active creep sites.

Creep modulus versus indentation hardness and indentation modulus data are plotted in Figures 2 and 3 respectively. The curves for the young and intermediate pastes (regression lines only are plotted for clarity) form an upper bound for the 'old' paste data sets. The 'old' cement paste data for water/cement ratio = 1.00 form an upper bound within this data set. The data for water/cement ratio = 0.80 forms a lower bound in Figures 2 and 3 with the exception of indentation hardness data above 600MPa (Figure 2). This would appear to be a consequence of relatively low porosity (i.e. < 20%). Very low porosity tends to minimize interfacial effects that may affect creep.

Young and intermediate age pastes tend to have a greater creep modulus value at a given value of indentation hardness or indentation modulus (Figures 2 and 3). These pastes also have, in general, lower indentation hardness or indentation modulus values at the same porosity with the exception of very low porosity values (e.g. <20%, Figure 4). Alternatively these pastes would have equivalent indentation hardness or modulus values (with respect to 'old' pastes) at lower values of porosity. This means (as stated above for arguments based on

the data in Figure 1) that it requires more of the solid material to provide an equivalent amount of 'creep-active' C-S-H.

Conclusions

1. Microindentation methods can be used to determine and differentiate the creep behavior of Portland cement paste hydrated for times varying from short to extended periods.

2. Microstructural features of C-S-H such as surface area, degree of polymerization and mean silicate chain length likely influence the creep rate of cement paste.

3. Cement paste systems containing C-S-H with shorter silicate chain lengths are more susceptible to creep. Defects at sites of missing bridging silica tetrahedra are considered as contributing to the magnitude of the creep.

4. Creep of old cement paste (hydrated 45 years) is nanostructure and porosity dependent. These pastes generally have a higher creep modulus or lower creep rate over a wide range of porosity, indentation modulus and indentation hardness values.

References

Alizadeh R, Beaudoin JJ and Raki L (2010) Viscoelastic nature of calcium silicate hydrate, Cement and Concrete Composites, 32: 369-376.

Beaudoin JJ (1983) Comparison of mechanical properties of compacted calcium hydroxide and Portland cement paste systems, Cement and Concrete Research, 13: 319-324.

Feldman RF (1972) Factors affecting the Young's modulus-porosity relation of hydrated Portland cement compacts, Cement and Concrete Research, 2(4): 375-386.

Lura P, Trtik P and Munch B (2011) Validity of recent approaches for statistical nanoindentation of cement pastes, Cement and Concrete Composites, 33: 457-465.

Mohan K and Taylor HFW (1982) A trimethylsilylation study of tricalcium silicate pastes, Cement and Concrete Research, 12: 25-31.

Neville AM (1970) Creep of concrete: plain, reinforced and prestressed, North Holland Pub. Co., pp. 622.

Neville AM (2006) Concrete: Neville's Insights and Issues, Thomas Telford, London, pp. 314.

Nguyen D-T, Alizadeh R, Beaudoin JJ, Pourbeik P and Raki L (2012) Microindentation creep of monophasic calcium-silicate-hydrates, submitted to Cement and Concrete Composites.

Oliver WC and Pharr GM (1992) An improved technique for determining hardness and elastic modulus using load and displacement sensing indentation experiments, Journal of Materials Research, 7: 1564-1583.

Pourbeik P., Beaudoin J.J., Alizadeh R. and Raki L., (2012) Mechanical property-porosity relationships of layered calcium silicate hydrate phases, Materials and Structures, DOI 10.1617/s11527-012-9990-3,

Richardson IG and Groves GW (1992) Models for the composition and structure of calcium silicate hydrate (C-S-H) gel in hardened tricalcium silicate pastes. Cement and Concrete Reserch, 22: 1001-1010.

Rodger SA, Groves GW, Clayden NJ and Dobson CM (1987) A study of tricalcium silicate hydration from very early to very late stages, Materials Research Society, Symposium Proceedings, Volume 85: 13-20.

Sarkar AK and Roy DM (1979) A new characterization technique for trimethylsilylated products of old cement pastes, Cement and Concrete Research, 9: 343-352.

Sereda PJ and Feldman RF (1963) Compacts of powdered material as porous bodies for use in sorption studies, Journal of Applied Chemistry, 13: 150-158.

Sereda PJ Feldman RF and Swenson EG (1966) Effect of absorbed water on some mechanical properties of hydrated Portland cement pastes and compacts, Highway Research Board, Special Report, 90: 58-73.

Soroka I and Sereda PJ (1968) The structure of cement- stone and use of compacts as structural models, Proceedings of 5th International Symposium on the Chemistry of Cement, 3: Tokyo, 67-73.

Taylor R, Richardson IG and Brydson RMD (2007) Nature of C-S-H in 20 year old neat ordinary Portland cement and 10% Portland cement-90% ground granulated blast furnace slag pastes, Advances in applied ceramics, Vol. 106 (6): 294-301.

Taylor H.F.W. (1977) Discussion of the paper, 'Microstructure and strength of hydrated cements' by R. F. Feldman and J. J. Beaudoin, Cem. Concr. Res. 7, 465-468.

Trtik P, Munch B and Lura P (2009) A critical examination of statistical nanoindentation on model materials and hardened cement pastes based on virtual experiments, Cement and Concrete Composites, 31: 705-714.

Vandamme M and F-J Ulm (2009) Nanogranular origin of creep, Proc. National Academy of Science (USA), 106 (26): 10552-10557.

Figure Captions

Figure 1. Creep modulus versus porosity for young, intermediate and 45 year old Portland cement paste.

Figure 2. Creep modulus versus indentation hardness for young, intermediate and 45 year old Portland cement paste.

Figure 3. Creep modulus versus indentation modulus for young, intermediate and 45 year old Portland cement paste.

Figure 4. Indentation hardness versus porosity for young, intermediate and 45 year old Portland cement paste.

Table Headings

Table 1. Non-linear Regression analysis of creep modulus-porosity data presented in Figure 1.

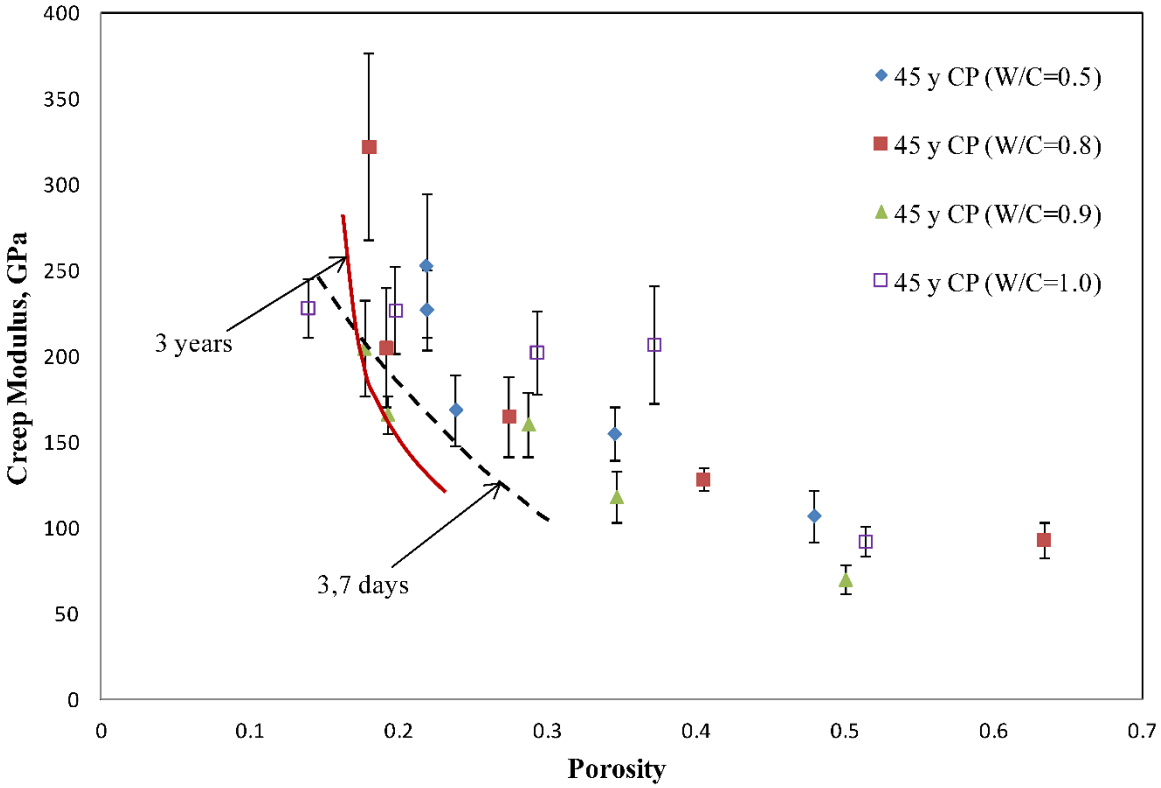

Figure 1. Creep modulus versus porosity for young, intermediate and 45 year old Portland cement paste.

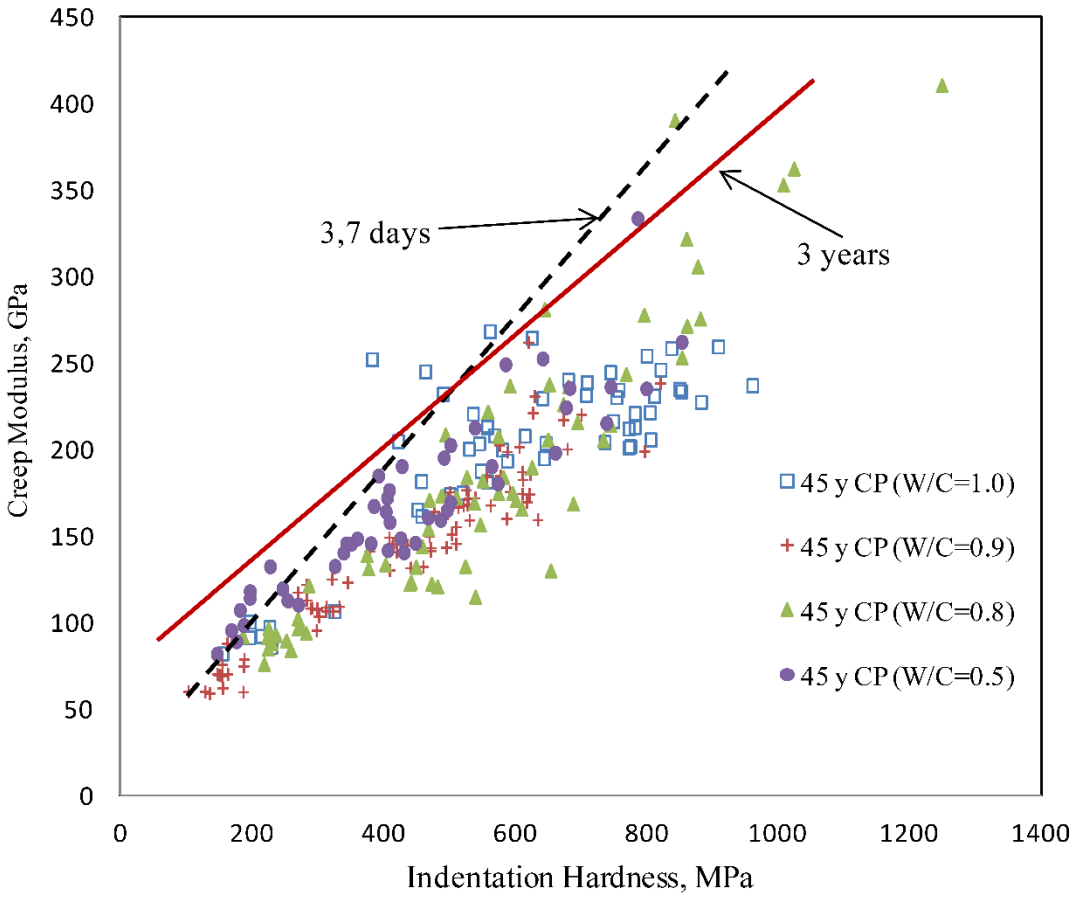

Figure 2. Creep modulus versus indentation hardness for young, intermediate and 45 year old Portland cement paste.

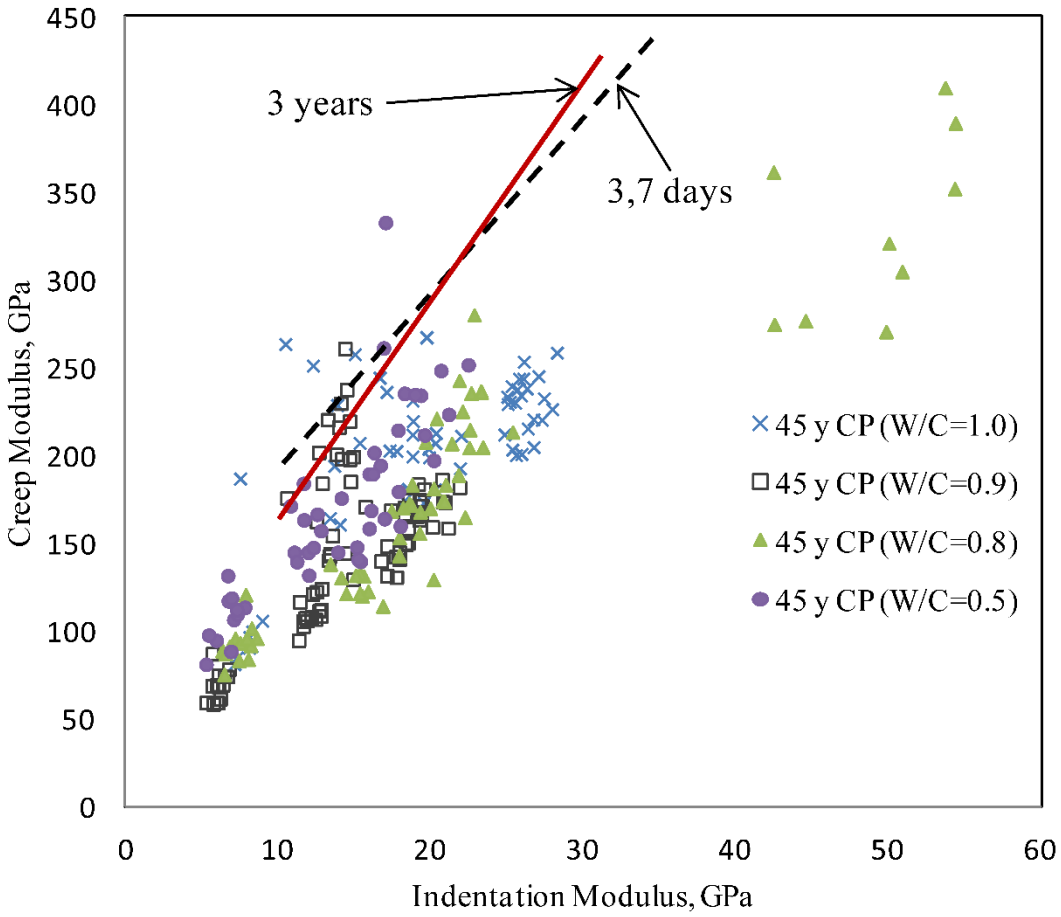

Figure 3. Creep modulus versus indentation modulus for young, intermediate and 45 year old Portland cement paste.

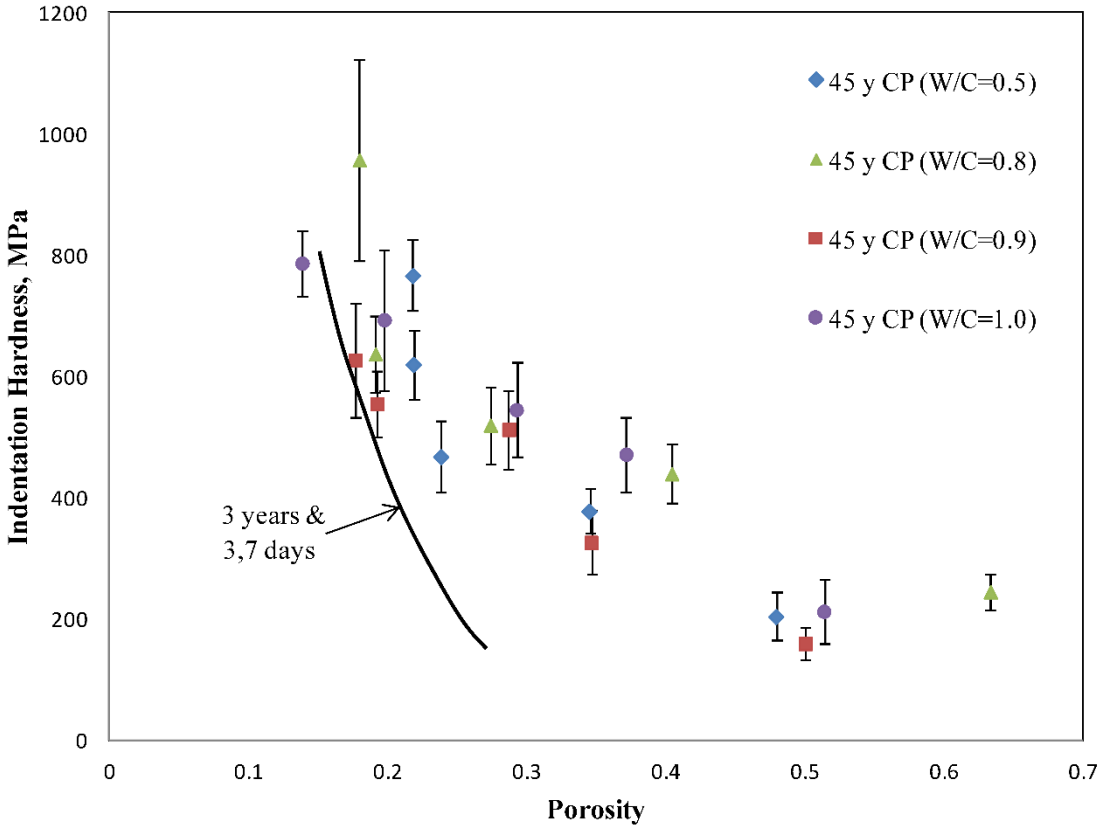

Figure 4. Indentation hardness versus porosity for young, intermediate and 45 year old Portland cement paste.

Table 1. Non-linear Regression analysis of creep modulus-porosity data presented in Figure 1.

Paste System	Regression Equation	Correlation Coefficient (R^2)
Old Pastes		
w/c=0.50	$y=1484.7x^2-1476.7x+475.89$	0.81
w/c=0.80	$y=1392.7x^2-1507.5x+492.37$	0.8
w/c=0.90	$y=64.36x^2-420.2x+263.12$	0.93
w/c=1.00	$y=-1366.6x^2+551.66x+173.06$	0.96
All w/c	$y=444.3x^2-695.5x+339.69$	0.7
Intermediate Paste	$y=98108x^2-40584x+4321.8$	
3 years		0.95
Young paste	$y=3459.7x^2-2940x+678.25$	
3,7 days		0.83

y= creep modulus; x= porosity,

Table 1. Non-linear Regression analysis of creep modulus-porosity data presented in Figure 1.

10.3 Paper 8: Dynamic Mechanical Thermo-Analysis of Portland Cement Paste Hydrated for 45 Years

DMTA methods were used to determine the effect of prolonged hydration of Portland cement on mechanical properties. Age dependent nanostructural characteristics of C-S-H were shown to influence the engineering behavior of cement paste.Specific differences are age dependent including degree of polymerization, silicate chain length and the extent of cross-linking of the silicate sheets. It was observed that it requires more C-S-H per unit volume in young paste to generate a similar amount of internal friction to that observed in mature paste. This is discussed in more detail in the paper. Additional evidence that compacts of hydrated cement paste are useful structural models for the investigation of engineering properties of cement-based materials using thermal methods was provided.

Dynamic Mechanical Thermo- Analysis of Portland Cement Paste Hydrated for 45 Years

(Materials and Structures, Accepted for Publication, 2014. DOI: 10.1617/S11527-014-0500-7)

P. Pourbeik[a], J. J. Beaudoin[a], R. Alizadeh[b] and L. Raki[a]

[a] *National Research Council Canada, Construction Portfolio, Ottawa, ON, Canada*
[b] *Giatec Scientific Inc., Ottawa, ON, Canada*

Abstract

The effect of prolonged hydration of Portland cement paste on engineering behavior was investigated using dynamic mechanical thermo-analysis (DMTA) methods. Specimens ranged in age from 3 days to 45 years. Compacts of hydrated cement powders and normally hydrated paste specimens were tested. Age dependent nanostructural characteristics of C-S-H were shown to influence the mechanical response of cement paste. Evidence was provided to support the use of compacts as structural models for hydrated cement paste. Details of ageing effects on the DMTA parameters (storage modulus and internal friction) as a function of temperature and porosity are reported.

Keywrods: Dynamic Mechanical Thermo-Analysis, Old Cement Paste, ageing effects, structural models, porosity

Introduction

There is a paucity of information on the influence of prolonged periods of hydration on the engineering behavior of hydrated cement paste. Characterization data for cement pastes and C_3S pastes hydrated for up to 30 years has been reported by a few researchers [1-5]. This includes application of 29Si NMR, trimethylsilylation and other analytical methods. The nanostructure of the pastes generally undergoes an 'ageing' process involving changes towards a greater degree of silicate polymerization and greater average chain length. The effect of these changes on engineering behavior has not been clearly established.

Repair and maintenance of concrete infrastructure is a global concern. Design of sustainable concrete structures requires an understanding of the engineering performance of the hydrated cement binder and its constituents. Effective forensic investigations are often only possible using synthesized powders of pure phases or cement binders particularly obtained from old structures. A useful thermal method of analysis to determine the engineering performance of these materials was utilized. The dynamic mechanical thermo-analysis (DMTA) method was first applied in cement science to detect low temperature phase changes by Radjy and coworkers [6-9]. The results of a study using DMTA methods to assess the engineering behavior of cement paste hydrated for periods ranging from 3 days to 45 years are reported in this paper.

Experimental

Materials

Cement pastes:

The 45 year old paste specimens were cast in glass cylinders with circular cross-section (25mm in diameter). The paste was prepared with water/cement ratios of 0.50, 0.70 and 1.00. The cylinders were continuously rotated for 24h and the specimens were subsequently demolded and sheathed in a rubber membrane containing a few drops of lime saturated water. They were then stored in stoppered glass tubes for 45 years. Slices 1mm thick were then cut and ground into a fine powder for fabrication into compacted specimens. The cement used was a normal type I Portland cement. The oxide analysis for the cement used was as follows: SiO_2 (20.72%); Al_2O_3 (5.87%); Fe_2O_3 (3.07%); CaO (62.66%); MgO (3.46%); SO_3 (2.18%). The following characteristics were also determined: Ignition Loss (1.10%); Insoluble Residue (0.24%); Free CaO (0.24%).The Bogue compound composition was: C_3S (46.5%); C_2S (24.6%); C_3A (10.4%); C_4AF (9.3%). The Blaine fineness was 3279 cm^2/g. The 'old' pastes were characterized using TGA, X-ray diffraction, and ^{29}Si NMR methods. In addition BET surface area and pore structure analysis using nitrogen sorption methods were conducted.

The geometry of the 45 year old samples (circular cross-section) was unsuitable for both DMTA and DMA tests. Compacted samples in the form of thin beams (1.0 x 12.8 x 60.0 mm were therefore fabricated from the powdered paste preparations. The use of compacted specimens was also strategic for comparison purposes as the 1.4nm tobermorite and jennite preparations were powders and test samples were in the form of compacted beams having

the same geometry. Hydrated cement paste specimens having the same geometry were also tested to further demonstrate the validity of the procedures used. Use of compacts as porous bodies for investigation in cement science is well documented. Their use is very convenient as it is possible to vary the porosity while keeping the composition of the solid phase constant. It should also be noted that the porosity of a compact consists of the porosity of the 'solid' phase (internal) and the porosity outside the 'solid' phase (external) referred to generally as 'capillary' porosity. It is therefore possible (at the same total porosity) for a lower water/cement ratio paste to have a greater volume of 'capillary' pores.

The degree of hydration was, as expected, very high for the 'old' pastes ranging from 95 to 99% (based on TGA measurements not shown here). The pore structure of the w/c = 0.50 paste is highly discontinuous (especially after 45 years of hydration) and the capillary pores are essentially filled with hydration products. Analysis of the pore size distribution data obtained from nitrogen adsorption isotherms supports this statement e.g. the total pore volume was 0.150 cc/g for w/c = 0.50 and 0.173 cc/g for w/c = 1.0. There was also a greater volume of smaller pores in the pore size range < 10nm for the lower w/c ratio preparation.

XRD analysis indicated the presence of primarily calcium hydroxide; the amount increased with water-cement ratio. Lower intensity peaks were also present for C-S-H. The CH content increased with water/cement ratio. A greater amount of CH generally forms in cement paste that contains a larger amount of capillary space as it provides more room for its deposition. Image analysis determinations by Diamond [10] for pastes with water cement ratio 0.30 and 0.45 show an increase of 2.6 mass % at 100 days. In addition evidence from TEM studies indicates that a small proportion of the CH in cement pastes is cryptocrystalline and intimately mixed with the C-S-H [11]. This occurs to a greater extent at lower water/cement

ratios. Chen et. al. provided evidence for CH/C-S-H nanocomposites in their coupled grid-indentation/SEM-EDX study of low water/cement ratio Portland cement pastes [12]. CH at the nanoscale is difficult to detect. It is argued that both capillary space availability and the existence of nanoscale CH influence the dependence of CH content on water/cement ratio. A small amount of ettringite was also detected.

The average silicate chain length (determined from 29Si NMR data analysis) ranged from 4.02 to 4.28 units. The BET nitrogen surface area values for the w/c = 0.50, 0.70 and 1.0 pastes are 44.5, 46.0 and 41.3 m2/g respectively.

The 3 day, 7 day, 2 month and 3 year old pastes (made with the same Type I Portland cement) was prepared using a water/cement ratio of 0.40. The oxide analysis for the cement used was as follows: SiO_2 (19.8%); Al_2O_3 (4.9%); Fe_2O_3 (2.5%); CaO (62.3%); MgO (3.2%); SO_3 (3.2%); ignition loss (2.8%); Ins. Res. (0.5%); free CaO (1.6%); Blaine fineness (4055 cm^2/g). Rectangular prisms (250 x 100 x 12mm) were cast. The samples were vibrated and stored in a moist curing room for 24 h. They were then demoulded and curing was continued for the specified period in a saturated lime solution. Thin slices (1 x 12 x 60 mm) were cut from the paste prism using an Isomet diamond saw. Selected slices were also ground into a fine powder for fabrication into compacted specimens. The silicate chain length of these pastes varied from 2.40 to 3.62 units as age varied from 3 days to 3 years. The BET surface area varied from 20.2 m^2/g to 38 m^2/g.

Humidity Conditioning

Cement paste specimens were conditioned for several days at 11% RH in vacuum desiccators containing saturated lithium chloride solution. The powders were conditioned for a few weeks at 11% RH before compaction and for several days after compaction. Theoretically there is a monolayer of water on the surfaces of the particles in addition to interlayer water at this humidity.

Preparation of Compacted Specimens

Solid rectangular prism samples for all the powdered materials were prepared by pressure compaction in steel moulds with a cross-section of 12.8 x 83 mm. The thickness of most of the prism samples was nominally 1mm but varied between the limits of 1-2 mm. Numerous studies on the use and validity of compacts as models for hydrated cement systems have been published [13-17]. It has been shown that compacted specimens of powdered hydrated Portland cement have similar mechanical property-porosity relationships to that of the original hardened paste of the same material [17]. The porosity of compacted paste samples was determined using helium pycnometry. The calculation is made knowing the apparent volume and the solid volume of the sample. Porosity is varied by controlling the compaction pressure.

Dynamic Mechanical Thermo-Analysis (DMTA)

The general dynamic mechanical analysis (DMA) method involves the application of an oscillating force to the sample and measurement of displacement [18]. The DMTA curves were obtained in the frequency range of 0.10Hz to 10Hz. The data reported in the paper was

obtained at frequencies of 3.98Hz. The curves were similar at all frequencies but changes were more pronounced at 3.98Hz. The elastic property obtained by DMA is referred to as the storage modulus (E'); it is analogous to the static modulus of elasticity. There is usually a time lag between the applied force and the resulting displacement. The time lag can be quantified in terms of a phase angle between the load and the displacement due to their ideally sinusoidal nature. The tangent of this angle (tan∂) represents the damping property of the material often referred to as internal friction. E' and tan∂ versus equilibrium mass-loss curves can be constructed for each test specimen with the starting condition being 11% RH. The oscillating character of the curves (e.g. decreases and increases in the E' values with mass-loss have been shown to be an effective means of determining the structural role of interlayer water in synthetic C-S-H and hydrated cement paste systems [19, 20].

Internal friction of the 'solid' phase is mainly related to the content of interlayer/structural water. It is dependent on the resistance to shear stress effects and the ability of the layers to translate relative to one another. Nevertheless it is suggested that large pores can contribute to increasing internal friction as they may facilitate the translation of silicate sheets. The implication is that large pores provide space and a lessening of the constraints on the sliding of silicate sheets with respect to each other as interlayer water is removed from the C-S-H structure. Higher values of internal friction in normally hydrated cement paste are generally associated with water/cement ratio. Several mechanisms are thought to influence the magnitude of internal friction in systems comprised essentially of layered calcium silicate hydrates. Samples conditioned at 11%RH contain essentially a monolayer of surface water and interlayer water. The latter has a structural role and its removal affects the potential translation of the silicate sheets relative to each other. Decreases in stiffness are associated

with the removal process and partial collapse of structure facilitating translation of the silicate sheets. Further removal of water can result in a more complete collapse of structure increasing the resistance to translation of sheets. This is likely associated with an increase in the degree of polymerization, crosslinking between sheets and interactions between interlayer calcium ions and the silicate sheets. A secondary effect is possibly related to water/cement ratio. The magnitude of internal friction is likely dependent on 'capillary' porosity as it generally increases with water/cement ratio. The DMTA analysis involves heating the sample at a constant rate during the experiment. It was conducted using a Rheometrics RSA II instrument on all samples in this investigation. The samples were heated from 25◦C to 300◦C. Temperature was increased in increments of 2◦C every 5 minutes. E' and tan∂ versus temperature curves were plotted. Each test took about 11h and 45min. to complete. It is apparent that the DMTA tests are much less tedious and time consuming to perform compared to DMA tests at room temperature that involve multiple measurements as dehydration occurs in equilibrium steps of water removal. The general characteristics of the E and tan∂ versus temperature DMTA curves mimic those of the E and tan∂ versus mass-loss DMA curves even though the latter are obtained under quasi-equilibrium conditions. The mass-loss due to removal of free water in the dynamic DMTA test is substantially but not totally complete at 100○C. A slower heating rate in the DTMA would not likely change the response very much especially as the DMTA curves already mimic those obtained with the room temperature DMA test.

The DMTA tests were conducted using a Rheometrics RSA II instrument on all samples in this investigation. The samples were heated from 25◦C to 300◦C. Temperature was increased in increments of 2◦C every 5 minutes. E' and tan∂ versus temperature curves were plotted.

These curves were shown to mimic the general oscillatory character of the equilibrium mass-loss curves i.e. the general pattern of the E'-mass-loss dependence [20].

Measures were taken to minimize carbonation. Specimens were stored in vacuum desiccators at 11% RH until the time of test. Transfer of the specimens to the chamber took less than 1 minute. The test chamber volume was relatively small (225cm^3) and sealed during the entire test period. Thermogravimetric analysis of selected specimens following the test indicated that carbonation was not significant. The surfaces of the samples were examined using both optical and scanning electron microscopy. There was no apparent evidence of microcracking. Previous DMA work on phase pure C-S-H using specimens with identical geometry indicated initial decreases in storage modulus followed by increases [19, 20]. This reversal in stiffness values would be unlikely to occur in the presence of any significant microcracking.

Results and Discussion

Previous investigations on the nanostructure of 20-30 year old hydrated C_3S pastes and Portland cement pastes indicate that there are significant differences in the nanostructure of the C-S-H phase on aging that may have an effect on engineering behavior [1]. These changes include increases in mean silicate chain length. The increase of polymerization of anions in the C-S-H may be associated with reconstitution of particles in the microstructure that affect mechanical performance [3]. The effect on engineering behavior of these reported changes have yet to be validated. The results of a dynamic mechanical thermo-analysis (DMTA) study of cement pastes hydrated for various periods ranging from 3 days to 45 years are reported.

A short section on the use of compacts as structural models precedes the discussion as they are an integral part of the experimental investigation.

Use of compacted powders as structural models

As previously stated the validity of compacts as structural models for hydrated cement systems has been discussed at length [13-17]. The 'total' porosity of compacted samples can be readily determined using helium pycnometry or in the case of the phase pure minerals by calculation using published density values. The calculation is made knowing the apparent volume and the solid volume of the sample. Porosity is varied by controlling the compaction pressure. The 'total' porosity of a compacted specimen includes the porosity of the 'solid-phase' of the powder itself plus the porosity external to the powder produced during the compaction process referred to here as 'capillary' porosity. The solid phase porosity in well hydrated systems is essentially 'gel' porosity. These distinctions are important if comparisons are made between compacted materials of equivalent 'total' porosity containing characteristically different solid phases i.e. solids prepared at different water/cement ratios. These comparisons will be made in this study. It is well known that the porosity of well hydrated cement paste is lower when the water cement ratio is lower. It is therefore noted however that if compacts of different water cement ratio pastes are produced with the same total porosity the paste prepared with the lower water/cement ratio solids will actually have a greater amount of 'capillary' porosity as previously stated. It would be expected then that a comparison (at the same 'total' porosity) of mechanical performance of compacted samples comprised of well hydrated porous 'solid-phase' particles of varying water-cement ratios would not have a classical water-cement ratio dependence.

DMTA- 45 year old cement paste

Tan∂ versus temperature

The tan∂-temperature curves (25-300°C) for the 45 year old compacted cement paste specimens (w/c = 0.50, 0.70 and 1.0) are plotted in Figure 1. The use of compacts enabled the manipulation of specimen porosity and formation of the beam specimens required for the DMTA tests. The selected curves were chosen to show the salient features of the mechanical response. There are some general characteristics common to all of the curves. These include an increase in internal friction reaching a maximum followed by a decrease in the temperature range 25°C to 110°C. A smaller second peak is sometimes observed in this temperature range. The increase in internal friction is attributed to the removal of surface and interlayer water. The decrease in tan∂ following the peak maxima is possibly due to cross-linking effects and the interaction of Ca^{2+} ions with the silicate sheets. Following the decrease to 110°C there is an increase in tan∂ for all the pastes. This increase extends from a value of 0.000 to 0.013 (at 225°C) for the w/c = 0.50 paste and exceeds the increases for all the other pastes. This seems at first to be counterintuitive as it would be expected that pastes with higher water/cement ratio and hence higher porosity would be conducive to generating higher internal friction. Plausibility of this result can however be demonstrated by comparison with the results for the w/c = 0.70 paste. The argument is as follows. These two paste systems have similar total porosity values (40.6 and 44.9%) and they are both nearly fully hydrated. The porosity of the 'solid phase' is less with the w/c = 0.50 preparation (water/cement ratio effect) meaning that the effective amount of 'capillary' porosity (as previously defined) is larger than is the case for the w/c = 0.70 preparation with approximately the same 'total'

porosity value. The larger value of internal friction in this temperature region for the w/c paste = 0.50 is associated with the larger amount of 'capillary' porosity. A similar result was obtained for the w/c = 0.50 paste (porosity = 43.6 %), the curve for which is not shown in Figure 1. In this case the value of tan∂ increased from 0.004 to 0.016 as the temperature increased from 110 to 200°C.

The tan∂ value in the temperature range 110-200 °C continues to increase for the w/c = 0.50 preparation but reaches a maximum at 150°C for the w/c = 0.70 paste that decays to a minimum at about 200°C. The shifting of the maximum to a lower temperature may also be a direct consequence of lower 'capillary' porosity for the higher w/c ratio compacts. There is also the consideration of the loss of compositional water in this temperature range. This could lead to the generation of a significant number of defects in the more porous 'solid phase' of the w/c = 0.70 paste contributing to the structural collapse of the C-S-H. The tan∂ decrease in this temperature range (160-200°C) is accompanied by an increase in stiffening (i.e. value of storage modulus, E') that will be discussed later. A decrease in the 'total' porosity of the w/c = 0.70 compact (to 36%, achieved by increasing the compaction pressure; the tan∂ versus temperature curve is not shown) illustrates the effect of reducing the capillary porosity in this temperature range. The value of tan∂ at the maximum is less (0.0040 compared to 0.0065). Further removal of constitutional water reduces the tan∂ value to 0.002 at 200°C which is similar at both porosity levels for the w/c = 0.70 compacts. The decrease in the tan∂ value after the maximum is reached is also significantly reduced for the 36% porosity sample. The constraints on translation of the C-S-H silicate sheets that result from the lower capillary porosity contribute to reduced internal friction.

The w/c = 1.0 paste has a 'total' porosity of 30.6%. The general characteristics of the tan∂ versus temperature curve are similar to those for the other water-cement ratios. The maximum value of tan∂ in the temperature range (150-250°C) is about 0.010. The maximum occurs at 200°C similar to the w/c = 0.50 compact specimens. The tan∂ value is greater than that for w/c = 0.70 but less than that for w/c = 0.50 despite the relatively low value of 'capillary' porosity. This apparent anomaly can be explained by the fact that the 'solid-phase' porosity of the w/c = 1.0 compact is the highest. The 'solid-phase' porosity in these compacts likely contributes significantly to the internal friction value and may be a more dominant factor in this case than the capillary porosity created during the compaction process. This illustrates the importance of the pore structure of the 'solid- phase' in old hydrated cement pastes on engineering behavior.

E' versus temperature

E' versus temperature curve for the 45 year old compacted cement paste specimens (w/c = 0.50, 0.70 and 1.0) are plotted in Figure 2. There is a rapid decrease in E' values as the temperature increases to 50-60°C. This is followed by a further continuous decrease to about 150°C. The decrease is attributed to the removal of surface and interlayer water as well as some constitutional water. A small increase to a maximum occurs on further heating at 200°C (w/c = 0.50, porosity = 40.5%; w/c = 0.70, porosity = 44.9%. There is also a very broad peak for the w/c = 1.0 specimen at 235°C. The maximum occurs earlier (at 150°C) for the w/c = 0.70 specimen when the porosity is reduced to 36% (curve not shown). The maxima in this temperature region can be attributed to ionic interactions between the silicate sheets and

possible cross-linking in addition to the removal of constitutional water and any remaining residual amounts of interlayer water.

The room temperature values of E' (GPa) are: 3.1 (w/c = 0.50; porosity = 40.5%); 6.6 (w/c = 0.70; porosity = 36%); 9.2 (w/c = 1.0; porosity = 30.6%). E' of the compacted specimens actually increases with w/c ratio at an equivalent total porosity level. As explained previously the 'solid-phase' in the compacted systems contains less porosity at the lower w/c ratio and therefore has a higher level of 'capillary' porosity. E', of course, would be expected to increase as the 'total' porosity decreases.

The reduction of elastic modulus is due to the loss of interlayer water and not microcracking as discussed in the previous section. Other silicates tested by the authors under similar conditions e.g. gyrolite (a layered calcium silicate) or porous vycor glass show no reduction in elastic modulus due to cross-linking in the case of gyrolite or the absence of interlayer water in porous glass.

Previous work by these authors on micro-indentation of 45 year old cement paste was performed at room temperature only [21]. Indentation hardness values are much higher for 45 year old pastes at the same total porosity than those for pastes hydrated up to 3 years when the porosity is greater than 20%.This finding is not inconsistent with the results presented in this paper.It was also concluded that creep of 45 year old paste is dependent on nanostructure and porosity. These pastes generally have a lower creep rate over a wide range of porosity, indentation modulus and indentation hardness values. It was also determined that cement paste systems containing C-S-H with shorter silicate chain lengths (i.e. younger pastes) are

more susceptible to creep. Defects at sites of missing bridging tetrahedra are considered as contributing to increases in the magnitude of creep.

Nano-indentation tests have not been performed on 45 year old paste. The results if available would be difficult to accurately interpret as there is substantial evidence that the C-S-H in hydrated cement paste is actually a C-S-H/CH nanocomposite [12]. Micro-indentation, in our view, provides a reasonable estimate of the properties of the C-S-H/CH microstructure. The results of Lura et. al. indicate that the homogenous C-S-H regions in cement paste are too small to cause independent and separated peaks in the elastic modulus plots [22]. They argue that spurious peaks in the frequency plots can be caused by the presence of other phases including unhydrated cement and calcium hydroxide.

DMTA- 3 year old cement paste

Tan∂ versus temperature

Tan∂ versus temperature curves for 3 year old normally hydrated paste and compacted paste specimens (w/c = 0.40; porosity = 15 and 18.6% respectively) are plotted in Figure 3(a). They have a similar character. The 'solid-phase' is identical in both cases. It is suggested that compacts (in a DMTA experiment) are useful models for paste hydrated systems as the curves for both preparations are qualitatively and quantitatively similar. Both paste and compact specimens have significant increases in the value of tan∂ as the temperature is increased from 25 to about 55°C reaching a maximum value of 0.0130-0.0135. This is followed by a decrease in internal friction (up to about 110°C) for reasons described in the previous section as adsorbed and interlayer water continue to be removed. Compacts of the

w/c = 0.40 paste prepared with higher porosity values (22.1 and 29.7%; not shown in Figure 3(a)) have values of tan∂ (internal friction) of 0.016 and 0.028 respectively. These are relatively high compared to the old paste compacts (described previously) prepared at w/c = 0.50 with 43% total porosity. This implies that factors associated with hydration period other than the amount of 'capillary' porosity may contribute to the generation of internal friction within the w/c = 0.40 paste. These may be related to descriptors of C-S-H nanostructure including average silicate chain length and degree of polymerization. There is also a small second peak observed at about 115-120°C possibly associated with removal of a small amount of remaining interlayer water. Further increases in temperature up to about 200°C show very little change in the value of tan∂. This follows from previous arguments as both the 'solid-phase' porosity and the 'capillary' porosity are sufficiently low to provide effective resistance to the translation of silicate sheets that acts as a source of internal friction.

E' versus temperature

The E' versus temperature curves for the normally hydrated paste specimen and the compacted paste specimen (w/c = 0.40, porosity = 15%) hydrated for 3 years has the same general character as all the curves for the 45 year old pastes, the primary difference being the initial magnitude of E' (i.e. 18GPa), Figure 3(b). The E' value is higher due to the lower 'total' porosity value. The curve for the compacted paste specimen (w/c = 0.40, porosity = 18.6%) follows the same general trend as the curve for the normally hydrated paste specimens. The initial E' value (i.e.10 GPa) is lower in accordance with the higher 'total' porosity value. It was suggested by Powers [23] that there is a limiting w/c ratio of about 0.36 below which complete hydration cannot occur due to volume constraint. The pore

structure of these pastes is highly discontinuous. The higher porosity value for the compacted specimen (w/c = 0.40) is likely to have a significant impact on E' values as the 'solid' phase is the same in both compact and hydrated paste specimens. The curves for the compacted specimens prepared at higher porosity values i.e. 22.1 and 29.7% are similar in character and have E' values of 5.7 and 4.0 GPa respectively. The E' curve reaches a minimum value at about 110°C and slowly increases in value thereafter. This was also observed for the 45 year old paste specimens at higher porosity values.

DMTA- 2month old cement paste

Tan∂ versus temperature

The tan∂ versus temperature curve for a cement paste hydrated for only two months (w/c = 0.40) has similar general features as the curve for the paste hydrated three years (Figure 3). The curve has a peak at about 70°C (tan∂ = 0.0075) and another peak at about 170°C (tan∂ = 0.009). The internal friction values appear to be high given the relatively low value of total porosity (16%). This can be explained as follows. Previous microindentation work by the authors demonstrated that to obtain an equivalent value of creep modulus for young cement paste (e.g. 2months hydration) with respect to the old cement paste (45 years) a lower value of total porosity is required [21]. The creep modulus versus porosity functions for young and very old pastes are in fact separate and distinct. This implies that it takes more C-S-H per unit volume in the young paste to produce the same amount of creep. The basic reason for this behavior is that the nanostructure (e.g. degree of polymerization) and viscoelastic nature of the C-S-H in the old paste is different as alluded to in the previous section. There is

therefore a natural tendency for equivalent values of internal friction to develop at lower porosity values in young paste.

E' versus temperature

The E' versus temperature curve for the paste (w/c = 0.40) hydrated for 2 months was similar in character to those for the more mature pastes i.e. there is a continuous decrease in E' values as temperature increases (Figure 4). There is however no indication of the presence of a peak in the vicinity of 200°C as was the case for the 45 year old pastes. It is suggested that this peak may be associated with higher degrees of silica polymerization that occur in more mature pastes.

DMTA- 3 and 7 day old cement paste

Tan∂ versus temperature

The tan∂ versus temperature curves for the 3 and 7 day old normally hydrated pastes (w/c = 0.40; porosity = 32.0 and 23.9% respectively) are qualitatively and quantitatively similar. The curve for the paste hydrated for 7 days is presented in Figure 5. The general character of the curve is also similar to the curves for the 45 year old pastes. This includes the peak in the temperature range 25 to 110°C attributed to the removal of surface and interlayer water and the peak at about 200°C influenced by the removal of hydrate water and possibly remnants of interlayer water. The increase in tan∂ from about 110°C to the peak at 200°C is about 0.006 or approximately 50% of the increase associated with the 45 year old paste. It appears that the generation of internal friction in the temperature range 110 to 300°C is strongly

influenced by the nanostructural characteristics of C-S-H that are age dependent e.g. the degree of polymerization, silicate chain-length and extent of cross-linking of the silicate sheets.

E' versus temperature

The E' versus temperature curves (not shown) for the 3 and 7 day old cement pastes are similar in character to the curve for the 2 month old paste including the absence of a peak at 200°C. There is a continuous decrease in E' values over the entire temperature range. The rationale for this decrease has been discussed in previous sections of this paper.

Conclusions

1. The ability to control the 'solid-phase' porosity and the 'capillary' porosity or porosity external to the 'solid-phase' in compacted specimens of hydrated cement systems provides a unique capability for study of the porosity effect on DMA parameters (e.g. internal friction (tan∂) and storage modulus (E')).

2. The general characteristics of the tan∂ and E' versus temperature curves for normally hydrated paste hydrated for periods of 3days to 3years and the curves for compacted specimens hydrated for periods of 3 days to 45 years are similar. Specific differences are related to nanostructural features of C-S-H that are age dependent including degree of polymerization, silicate chain length and the extent of cross-linking of silicate sheets.

3. The observed tan∂ increase in the temperature range 110-225°C is dependent on the amount of 'capillary' porosity in the compact. In a compacted system of 'equivalent' total porosity this varies inversely with water/cement ratio. Nanostructural changes in this temperature region likely result in the generation of defects possibly related to the removal of constitutional water.

4. The general overall decrease in storage modulus (E') with temperature for pastes and compacts (all ages) involves the removal surface and interlayer water as well as some constitutional water. Small increases in E' reaching a maximum in the vicinity of 200°C are attributed to ionic interaction with the silicate sheets and possible cross-linking.

5. The magnitude of all the room temperature storage modulus values for the compacted systems can be explained by the relative amounts of the 'solid-phase' porosity and the 'capillary' porosity when the 'total' porosity is constant.

6. Low values of both 'solid-phase' and 'capillary' porosity provide effective resistance to the translation of silicate sheets that acts as a source of internal friction.

7. There is a natural tendency for equivalent values of internal friction to develop at lower porosity values in young paste as compared to more mature pastes. This effect has been previously observed in studies of the viscoelastic nature of cement paste. It

apparently requires more C-S-H per unit volume in young paste to produce a similar effect. This relates to the nanostructural effects associated with aging alluded to in a preceding conclusion.

8. Compounds that are important constituents of hydrated cement often must be synthesized in powdered form prior to investigations of concrete durability. Sustainability studies involving these compounds require the preparation of solid bodies to facilitate the acquisition of relevant engineering data. In this context compacts of cement paste powders are useful structural models for investigating the engineering properties of cement-based materials using thermal methods.

References

1. S. A. Rodger, G. W. Groves, N. J. Clayden and C. M. Dobson, A study of tricalcium silicate hydration from very early to very late stages, Mat. Res. Soc. Symp. Proc., Vol 85, 13-20, 1987.
2. R. Taylor, I. G. Richardson and R. M. D. Brydson, Nature of C-S-H in 20 year old neat ordinary Portland cement and 10% Portland cement-90% ground granulated blast furnace slag pastes, Advances in applied ceramics, Vol. 106 (6), 294-301, 2007.
3. K. Mohan and H. F. W. Taylor, A trimethylsilylation study of tricalcium silicate pastes, Cem. Concr. Res., 12, 25-31, 1982.
4. A. K. Sarkar and D. M. Roy, A new characterization technique for trimethylsilylated products of old cement pastes, Cem. Concr. Res., 9, 343-352, 1979.
5. I. G. Richardson and G. W. Groves, Models for the composition and structure of calcium silicate hydrate (C-S-H) gel in hardened tricalcium silicate pastes. Cem.

Concr. Res. 22, 1001-1010, 1992.

6. F.Radjy and E. J. Sellevold, Internal friction peaks due to adsorbed and capillarywater in microporous substances, Nature Physical Science, 241, 133-135, 1973.
7. F.Radjy and C. W. Richards, Effect of curing and heat treatment history on The dynamic mechanical response and the pore structure of hardened cement paste, Cem. Concr. Res., 3, 7-21, 1973.
8. E. J. Sellevold and F. Radjy, Drying and resaturation effects on internal friction in hardened cement paste, J. Amer. Ceram. Soc., 59(5-6), 256-258, 1976.
9. F. Radjy, E. J. Sellevold and C. W.Richards, Effect of freezing on the dynamic Mechanical response of hardened cement paste down to -60°C, Cem. Concr. Res.,2, 697-715, 1972.
10. S.Diamond, Calcium hydroxide in cement paste and concrete-a microstructural appraisal, Materials Science of Concrete: Special Volume: Calcium Hydroxide in Concrete, American Ceramic Society, 37-38, 2001.
11. D. Viehland, J.-F.Li, L.-J.Yuan and Z.Xu, Microstructure of calcium silicate hydrate (C-S-H) gels in Portland cement paste: Short-range ordering, nanocrystallinity and local compositional order, J. Amer. Ceram. Soc., 79 (7), 1731-1744, 1996.
12. J.J.Chen, L. Sorelli, M.Vandamme, F.-J. Ulm and G. Chanvillard, Coupled grid-indentation/SEM-EDX study on low water/cement ratio Portland cement paste :evidence for C-S-H nanocomposites, J. Amer. Ceram. Soc., 93 (5), 1484-1493, 2010.

13. I. Soroka and P.J. Sereda, The structure of cement- stone and use of compacts as structural models, Proc. 5th Int. Symp. on the Chem. of Cem., Vol. 3., Tokyo, 67-73, 1968.
14. R. F. Feldman, Factors affecting the Young's modulus-porosity relation of hydrated Portland cement compacts, Cem. Concr. Res., 2(4), 375-386, 1972.
15. P. J. Sereda and R. F. Feldman, Compacts of powdered material as porous bodies for use in sorption studies, J. Appl. Chem., 13, 150-158, 1963.
16. J.J.Beaudoin, Comparison of mechanical properties of compacted calcium hydroxide and Portland cement paste systems, Cem. Concr. Res., 13, 319-324, 1983.
17. P.J.Sereda, R.F. Feldman. and E.G. Swenson, Effect of sorbed water on some mechanical properties of hydrated Portland cement pastes and compacts, Highway Research Board, Special Report 90, 58-73, 1966.
18. K. P. Menard, Dynami Mechanical Analysis-A Practical Introduction, CRC Press LLC, Boca Raton, pp. 208, 1999.
19. R. Alizadeh, J.J. Beaudoin and L. Raki, Mechanical properties of calcium silicate, Mater. and Struct., 44, 13-28, 2011.
20. R. Alizadeh, Nanostructure and engineering properties of basic and modified calcium-silicate-hydrate systems, PhD thesis, Department of Civil Engineering, University of Ottawa, pp. 231, 2009.
21. P. Pourbeik, R. Alizadeh, J. J. Beaudoin, D.-T. Nguyen and L. Raki, Microindentation creep of 45 year old hydrated Portland cement paste, Advances in Cement Research, Volume 25, Issue 5, October 2013, Pages 301-306, DOI: 10.1680/adcr.12.00058.

22. P. Lura, P.Trtik and B. Munch, Validity of recent approaches for statistical nanoindentation of cement pastes, Cem. Concr. Comp.,33,457-465,2011
23. T. C. Powers and T. L. Brownyard, Studies of the physical properties of hardened Portland cement paste. Part 3. Theoretical interpretation of adsorption data, Portland Cement Assoc., Bulletin 22, 469-548, 1948.

Figure Captions

Figure 1. Tan∂ versus temperature curves for compacts of 45 year old cement pastes compacts of (CP) prepared with similar 'total' porosity: w/c = 0.50, 0.70 and 1.00.

Figure 2. Storage modulus (E') versus temperature curves for 45 year old cement paste: w/c = 0.50, 0.70 and 1.00. Porosity values 'P' are indicated on the figure.

Figure 3. (a) Tan∂ versus temperature curves for normally hydrated cement paste and compacted cement paste specimens hydrated for 3 years: w/c = 0.40. Porosity values 'P' are indicated on the figure.

Figure 3. (b) Storage modulus (E') versus temperature curves for normally hydrated cement paste and compacted cement paste specimens hydrated for 3 years: w/c = 0.40. Porosity values, 'P' are indicated on the figure.

Figure 4. Tan∂ and E' versus temperature curves for normally hydrated cement paste specimens hydrated for 2 months: w/c = 0.40.

Figure 5. Tan∂ and E' versus temperature curves for normally hydrated cement paste specimens hydrated for 7 days: w/c = 0.40.

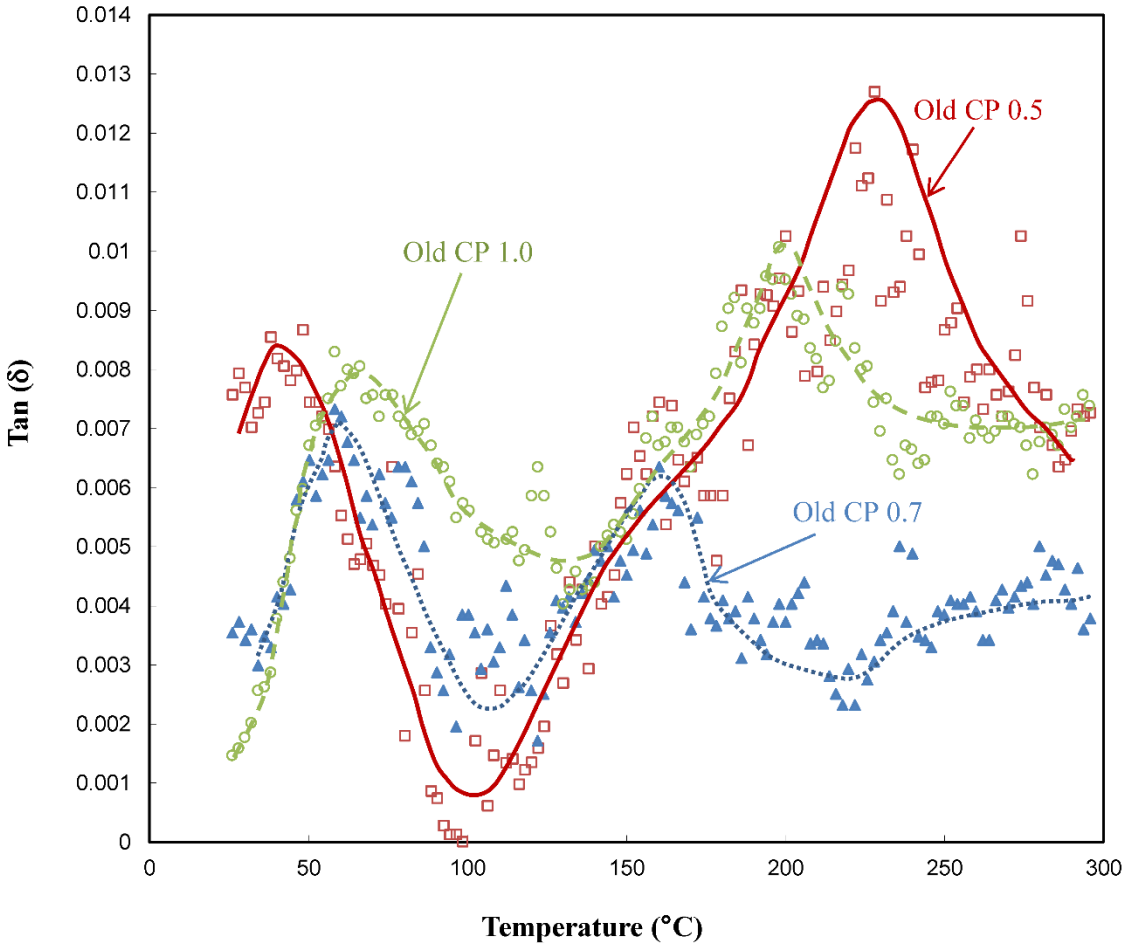

Figure 1. Tan∂ versus temperature curves for compacts of 45 year old cement pastes compacts of (CP) prepared with similar 'total' porosity: w/c = 0.50, 0.70 and 1.00.

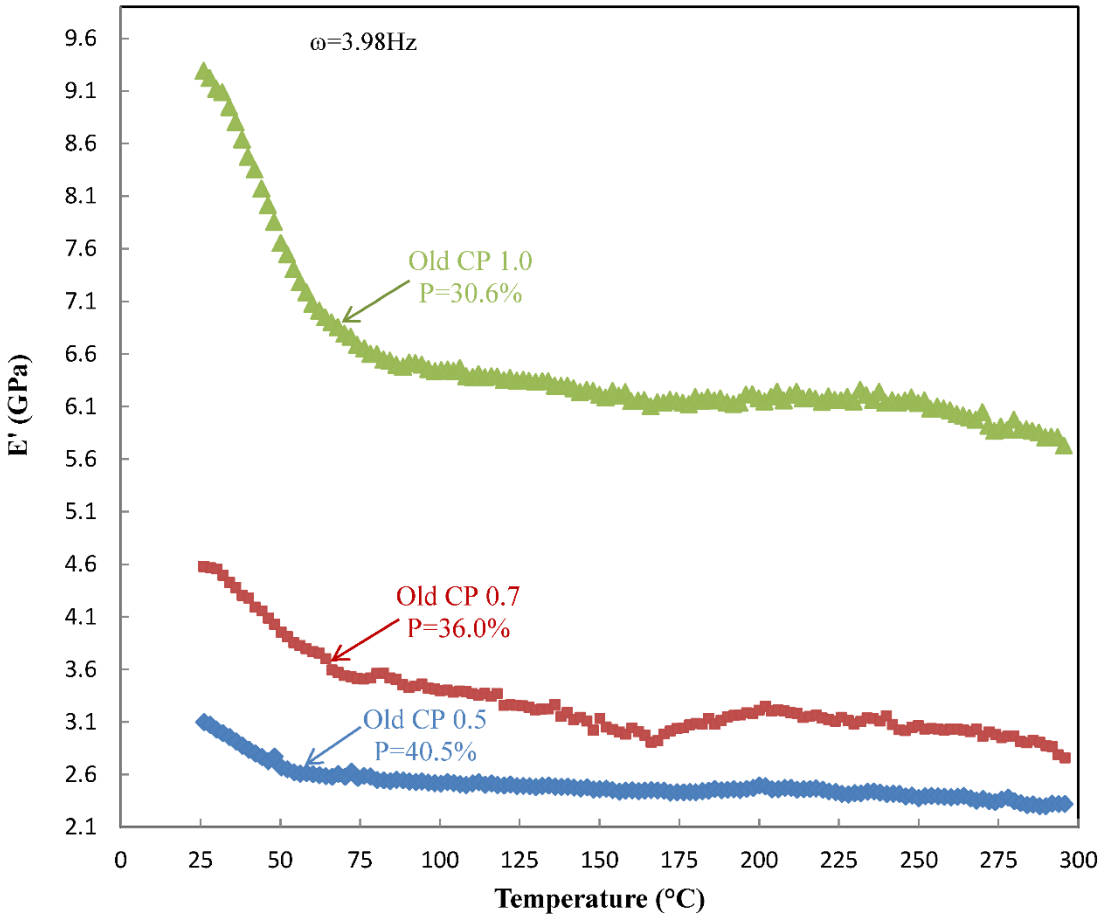

Figure 2. Storage modulus (E') versus temperature curves for 45 year old cement paste: w/c = 0.50, 0.70 and 1.00. Porosity values 'P' are indicated on the figure.

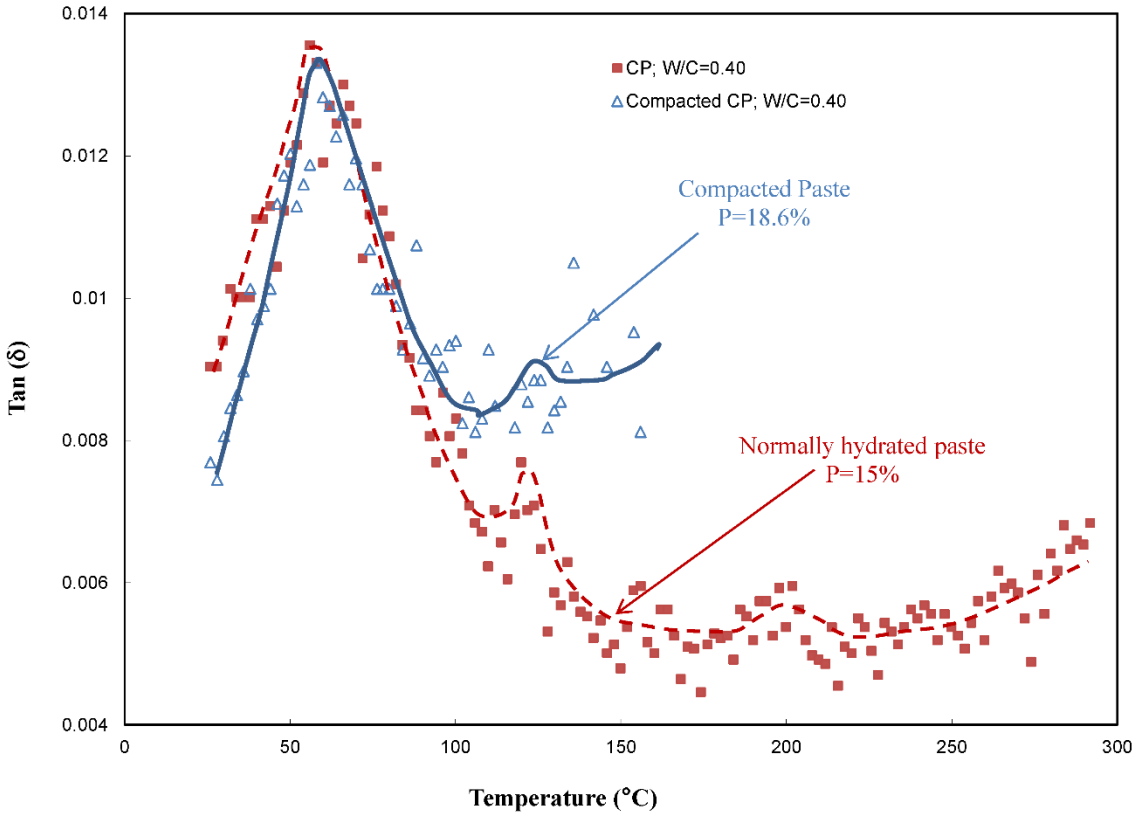

Figure 3. (a) Tan∂ versus temperature curves for normally hydrated cement paste and compacted cement paste specimens hydrated for 3 years: w/c = 0.40. Porosity values 'P' are indicated on the figure.

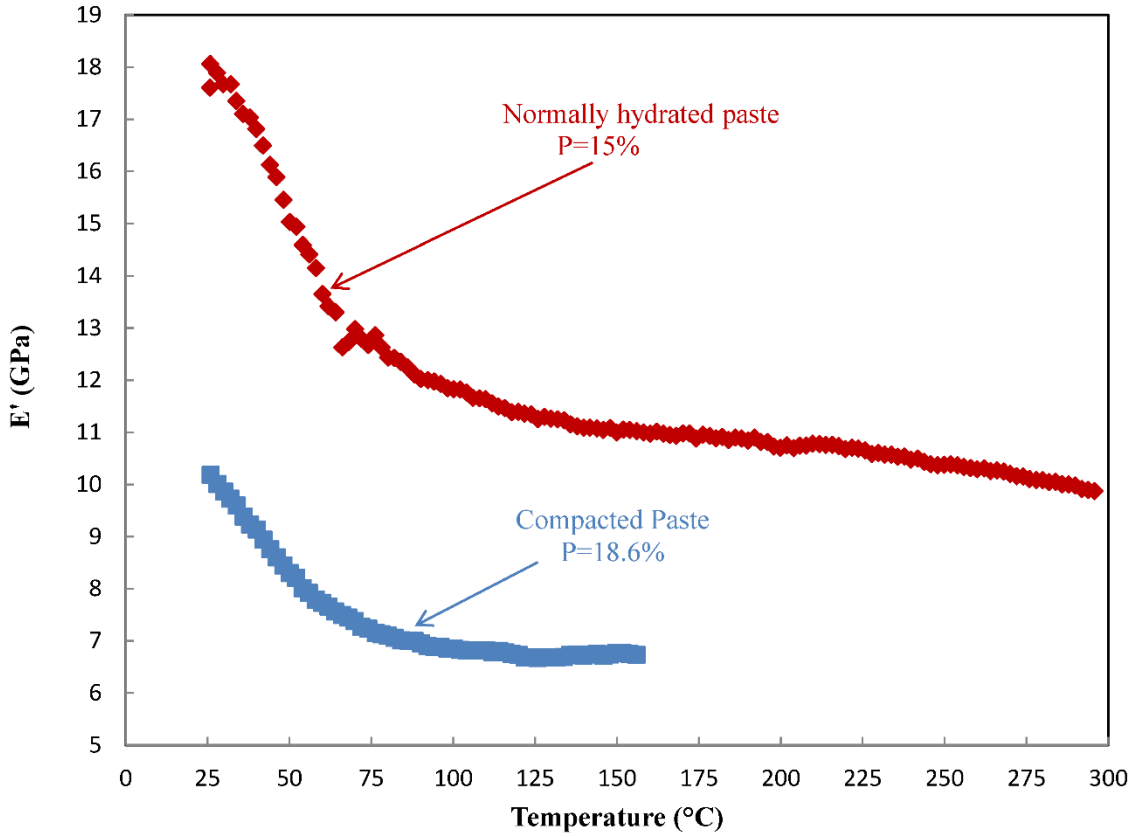

Figure 3. (b) Storage modulus (E') versus temperature curves for normally hydrated cement paste and compacted cement paste specimens hydrated for 3 years: w/c = 0.40. Porosity values, 'P' are indicated on the figure.

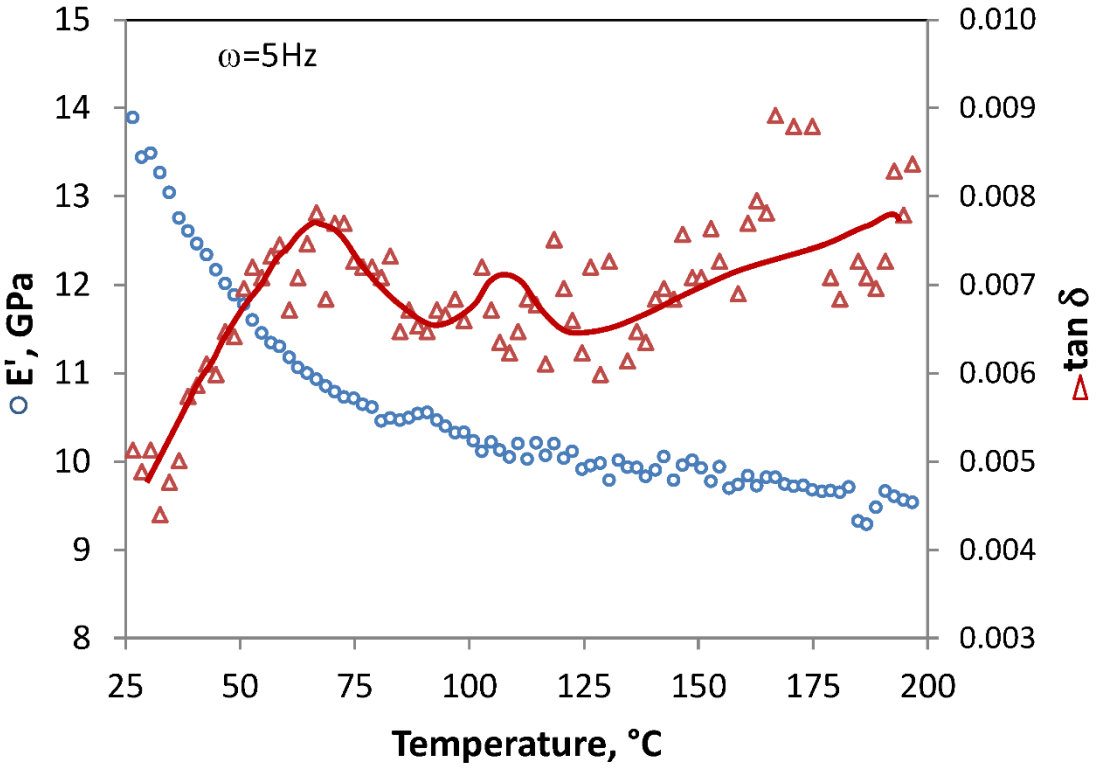

Figure 4. Tan∂ and E' versus temperature curves for normally hydrated cement paste specimens hydrated for 2 months: w/c = 0.40.

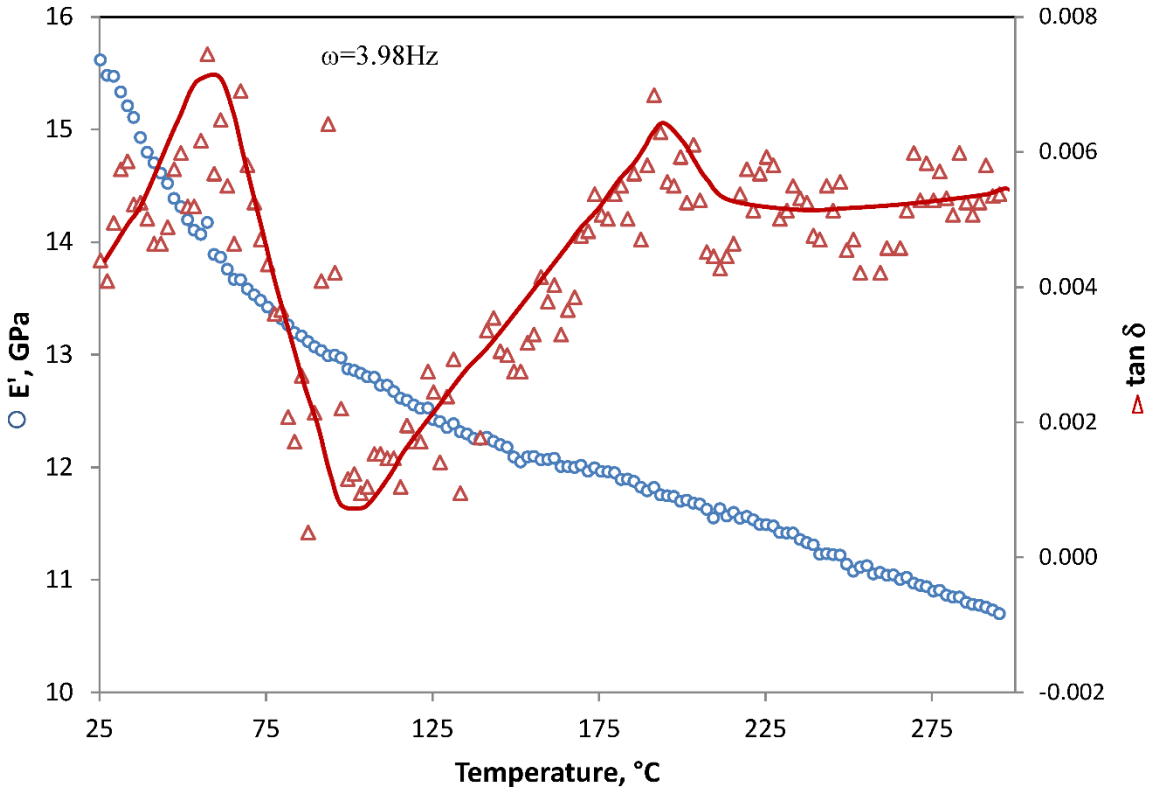

Figure 5. Tan∂ and E' versus temperature curves for normally hydrated cement paste specimens hydrated for 7 days: w/c = 0.40.

10.4 Paper 9: Creep of 45 Year Old Cement Paste-The Role of Structural Water

Data obtained from the complimentary use of microindentation and DMTA methods was shown to be useful in assessing the role of interlayer water in the creep of hydrated cement for both young and 45 year old cement paste. The microindentation experiments were performed at 11% RH and subsequently at incremental values of mass-loss. Mass-loss was typically obtained in equilibrium drying steps from the 11% RH condition. Internal friction or tan∂ versus temperature curves were obtained using DMTA. Maximum changes in the tan∂ with temperature (25 to 110^{o}C) curves were shown to correspond with minima in the creep modulus versus mass loss curves indicating a relationship between creep and internal friction. The analysis included an assessment of the influence of degree of hydration, capillary porosity, nanostructural parameters and the restraining effect of unhydrated cement particles (young paste) on the creep process. The contribution of interlayer was considered to be structural in nature.

Creep of 45 Year Old Cement Paste-The Role of Structural Water

(Materials and Structures, Accepted for Publication, January 2015. DOI: 10.1617/s11527-015-0534-5)

P. Pourbeik[a], J. J. Beaudoin[b], R. Alizadeh[b] and L. Raki[b]

[a]*National Research Council Canada, Construction Portfolio, Ottawa, ON, Canada*
[b]*Giatec Scientific Inc., Ottawa, ON, Canada*

Abstract

Microindentation creep and dynamic mechanical thermo-analysis (DMTA) measurements were carried out on compacted specimens of cement paste prepared at water/cement ratios of 1.00, 0.50 and 0.40 and hydrated for 45 years. Similar data was obtained for pastes prepared at w/c = 0.40 and hydrated only two months. Creep modulus-mass-loss curves were plotted for all the systems studied. These curves were used to emphasize salient differences between all the paste systems. The influence of degree of hydration, volume concentration of C-S-H, capillary porosity, C-S-H chain-length and the restraining effect of the unhydrated cement particles on creep are parameters that are used to provide a possible explanation for the observation that the creep of the old pastes is higher than creep of the young pastes. The structural role of water in the creep process at various stages of equilibrium drying from the 11% RH condition is discussed.

Keywrods: Dynamic Mechanical Thermo-Analysis, Old Cement Paste, ageing effects, structural models, creep modulus

Introduction

There is a paucity of creep data for old hydrated Portland cement-based materials. The first reported information appears to be data for the creep response of 50 year old concrete obtained by Nasser and Neville in 1964 [1]. They concluded that old concrete has the potential to exhibit a substantial amount of creep and speculated that the creep mechanism was similar for old and young concretes. They also argued that creep may be related to the amount of adsorbed water and that lower creep is possibly associated with a higher level of crystallinity at advanced ages. Several mechanisms for the creep of hydrated cement systems have been proposed. These were critically examined by Wittmann [2]. Feldman has suggested that the hydrated calcium silicate phase behaves as a layered material and that interlayer water has a significant influence on the creep response of cement paste [3]. Alizadeh et. al. in relaxation experiments with synthetic C-S-H (conducted at 11%-0% RH) demonstrated that the viscoelastic performance is dependent on the presence and amount of interlayer water [4]. He proposed that creep is a manifestation of gradual crystallization or aging in a poorly crystallized material accelerated by drying or stress. This view is compatible with that of Nasser and Neville and provides additional detail at the nanosructural level. It has been postulated that several mechanisms can simultaneously be operative during the creep process [5-10]. These include viscous flow, seepage, aging, intercrystalline slip and bond rupture. Nanostructural investigations have postulated that the origins of creep are associated with a particle-sliding mechanism [3, 11, 12].

The present study is focused on the microindentation-creep behavior of cement paste hydrated for 45 years with water/cement ratio varying from 0.40 to 1.00. The structural role

of water is investigated as creep modulus determinations are obtained at various mass-loss increments due to drying in steps from 11% RH to 0% RH. This data is supplemented by data obtained using a dynamic mechanical thermo-analysis (DMTA) method. The DMTA method was first introduced in cement science by Radjy and co-workers [13]. The method has also been used to detect phase transitions in layered calcium silicates [14]. In this study internal friction (tan∂) curves beginning from the 11% RH condition are generated; they mimic in a general sense many features of the creep modulus versus mass-loss curves. It is noted that at 11% RH no pore water is present. Hence contributions to creep due to meniscus effects in capillary pores do not occur. The results of this study lead to the proposal of a contributing creep mechanism for calcium silicate materials. Comparison is made with the creep modulus and DMTA behavior of a young cement paste hydrated for only two months. Inferences (based on internal friction determinations) regarding the creep recovery process in saturated cement paste (w/c = 0.35) have been reported by Sellevold and Sellevold and Richards [15, 16].

In summary the overall objective of this study is to assess the structural role of water on the creep of cement paste hydrated for extended periods. An attempt to determine differences in the creep behavior of young and very old cement paste was also made.

Experimental

Materials

Cement pastes: Preparation

The 45 year old paste specimens were cast in glass cylinders with circular cross-section (25mm in diameter). The paste was prepared with water/cement ratios of 0.40, 0.50, and 1.00.

The cylinders were continuously rotated for 24h and the specimens were subsequently demolded and sheathed in a rubber membrane containing a few drops of lime-saturated water. They were then stored in stoppered glass tubes for 45 years. Slices 1mm thick were cut and ground into a fine powder for fabrication into compacted specimens. The cement used was a normal type I Portland cement. The oxide analysis for the cement used was as follows: SiO_2 = 20.72%; Al_2O_3 = 5.87%; Fe_2O_3 = 3.07%; CaO = 62.66%; MgO = 3.46%; SO_3 = 2.18%. The Blaine fineness was 3279 cm^2/g. The Bogue compound composition was: C_3S = 46.5%; C_2S = 24.6%; C_3A = 10.4%; C_4AF = 9.3%.

The 2 month old paste (made with Type I Portland cement) was prepared using a water/cement ratio of 0.40. The composition of the cement used was: SiO_2 = 20.78%; Al_2O_3 = 6.20%; Fe_2O_3 = 2.22%; CaO = 64.83 %; MgO = 1.84%; SO_3 = 3.17%; Na_2O = 0.05%; K_2O = 0.40%. The Blaine fineness was 3000 cm^2/g. The Bogue compound composition was: C_3S = 51.4%; C_2S = 20.3%; C_3A = 12.7%; C_4AF = 6.7% Rectangular prisms (250 x 100 x 12mm) were cast. The samples were vibrated and stored in a moist curing room for 24 h. They were then de-molded and curing was continued for 2months in a saturated lime solution. Thin slices (1 x 12 x 60 mm) were cut from the paste prism using an Isomet diamond saw. Selected slices were also ground into a fine powder for fabrication into compacted specimens.

Cement pastes: Characterization

Some relevant data characterizing the pastes studied is provided in Table 1.

Table 1. Characterization Data of Pastes Studied

w/c	0.40	0.50	1.00	0.40
Age	45y	45y	45y	2mos
CH(%)*	4.05	4.36	5.12	3.75
α (%)**	98	99	95	77
CL (units)***	4.02	4.28	4.10	2.65
BET SA+ (m^2/g)	20.5	44.5	41.2	22.0

* CH- calcium hydroxide content.
** α- degree of hydration determined by TGA methods.
*** CL- silicate chain length determined by ^{29}Si NMR spectroscopy: $CL = 2(1 + Q^2/Q^1)$. Chemical shifts for Q^1, Q^2 and Q^3 in C-S-H are -79 to -80, -85 to -86 and near 96 ppm respectively. No Q^3 was observed.
\+ Surface areas were determined using the nitrogen sorption method. Calculations employed the BET analysis.

^{29}Si NMR spectra were obtained using a BrukerAvance 200 MHz instrument (magnetic field of 4.7 T and ^{29}Si Larmor frequency of 39.75 MHz) using a BL7 double resonance MAS probe and 7mm ZrO_2 spinners at the spinning speed of 5KHz. The spectra were acquired in a Bloch decay mode (^{29}Si π/2 pulse of 4μs) with a high power composite pulse proton decoupling at a delay of 60s between scans.

Simultaneous DSC-TGA experiments were performed using a TA Instruments SDT Q600 thermal analyzer. Specimens (about 50mg) were heated from room temperature to about 1000 $^{\circ}$C at a rate of 10°C/min.

X-ray diffraction patterns for the 45 year old pastes are qualitatively similar i.e. they exhibit the same number of peaks located at approximately the same d values. The peak intensities vary as would be expected from the analysis provided in Table 1. For example the water/cement ratio = 1.0 specimen contains the most CH. The presence of ettringite persists with peaks at d = 0.973, 0.561, 0.388, 0.277, 0.256 and 0.221 nm. CH peaks are prominent at d =0.490, 0.263 and 0.193 nm. A peak at d = 0.307nm may possibly be attributed to C-S-H.

A pore structure analysis of the 45 year old pastes was carried out using nitrogen sorption techniques (BET). The analysis was made on powdered samples. The results are tabulated in Table 2. The nitrogen sorption isotherms for the 45 year old paste (w/c = 0.40) and the 2 month old paste (w/c = 0.40) are very similar despite a significant difference in the degree of hydration. The similarities of the nitrogen isotherms of low and high water/cement ratio arise because access of the nitrogen molecule to the hydrated surfaces is dependent on the degree of stacking of the C-S-H sheets which in turn affects the level of crystallinity. Aging involves an increase in the degree of polymerization and layering of the silicate units. It is possible therefore that the nitrogen molecule can access a similar amount of surface in old and young pastes despite differences in the degree of hydration.

The pore network in pastes prepared at w/c = 0.40 is more discontinuous than that for pastes prepared with higher water/cement ratios. The discontinuity arises from the lack of space for the deposition of hydration products at the low water/cement ratio. Pore filling results in the blockage of pore connections in these systems more so than pastes prepared at high water/cement ratios. The porosity and the nitrogen surface area are also surprisingly similar. These similarities are likely a consequence of increased crystallinity (greater silicate chain length; see Table 1) resulting from the aging process. The similarities of the nitrogen isotherms of low and high water/cement ratio arise because access of the nitrogen molecule to the hydrated surfaces is dependent on the degree of stacking of the C-S-H sheets which in turn affects the level of crystallinity. Aging involves an increase in the degree of polymerization and layering of the silicate units [17]. It is possible therefore that the nitrogen molecule can access a similar amount of surface in old and young pastes despite differences in the degree of hydration.

Table 2. Pore Analysis of 45 year old cement pastes and a 2 mos paste

w/c	**0.40**	**0.50**	**1.00**	**0.40 (2 mos)**
pore volume (cc/g)	0.099	0.150	0.173	0.095
porosity (%)	23.8	40.6	41.5	24.2
pore radius (nm) (peak)	1.910	1.897	1.911	1.911
$dV(r)_{max}$ (m^3/nm/g x 10^{-3})	45.1	50.0	20.0	26.5

Humidity Conditioning

Cement paste specimens were conditioned for several days at 11%RH in vacuum desiccators containing saturated lithium chloride solution. The powders were conditioned at 11%RH

before compaction and for a few days after compaction. Theoretically there is a monolayer of water on the surfaces of the particles in addition to interlayer water at this humidity.

Preparation of Compacted Specimens

Circular disc samples for all the powdered materials were prepared (for microindentation tests) by pressure compaction in steel moulds with a cross-section of about 25 mm. The thickness of most of the prism samples was nominally 1mm but varied between the limits of 1-2mm. Numerous studies on the use and validity of compacts as models for hydrated cement systems have been published [18-22]. It has been shown that compacted specimens of powdered hydrated Portland cement have similar mechanical property-porosity relationships to that of the original hardened paste of the same material [22]. The porosity of compacted paste samples was determined using helium pycnometry. The calculation is made knowing the apparent volume and the solid volume of the sample. Porosity is varied by controlling the compaction pressure. Solid rectangular prism samples for the dynamic mechanical thermo-analysis (DMTA) determinations were prepared by pressure compaction in steel moulds with a cross-section of 12.8 x 83 mm. The thickness of most of the prism samples was nominally 1mm but varied between the limits of 1-2mm. The porosity of all the compacted specimens was nominally about 40%. This enabled comparisons to be made on the basis of approximately equivalent amounts of solid phase in any specimen.

Drying Protocols

The creep tests in this study (see next section) involved step by step drying on test samples initially conditioned to 11%RH. The removal of water was achieved by the application of vacuum or a combination of vacuum and heat in a special drying cell. Maximum care was taken in the sample treatment. The combination of vacuum and heat was applied over a lengthy drying period in order to avoid any physical damage to the samples. The initial mass-loss levels (expressed as a percentage of the mass of the sample at 11%RH) were obtained only through vacuum at room temperature. The temperature was gradually increased and only exceeded 50°C at mass-loss values above about 8%. Additional drying temperatures at higher mass-losses did not exceed 110 °C .The creep experiments involved the incremental removal of water from each sample prior to each test run.

Thermogravimetric analysis (TGA) was performed on samples before and after testing. The extent of carbonation was very small.

Microindentation Creep Measurements

All the microindentation creep tests were performed using a CSM Instruments Instrumented Indentation Tester. The apparatus is housed in an environmental chamber.

All tests were initially conducted at 11% RH on specimens equilibrated at 11%RH. Subsequently tests were conducted at lower moisture contents obtained by the incremental drying protocol described above. Drying agents were used to maintain low humidity levels in the environmental chamber. Samples were weighed before and after each test. A Berkovich indenter was used for all these tests. The CSM microindentation instrument has a load range

of 0.03 – 30 N with a resolution of 0.3 mN. The indentation depth was recorded as a function of time at the maximum load of 1000 mN for a 600s dwell period. The loading rate was 2000mN/min. The logarithmic creep was determined through curve fitting of the indentation-depth versus time curves during the 600s dwell time by the following equation proposed by Vandamme [23]:

$$\Delta h(t) = x_1 \ln (x_2 t + 1) + x_3 t + x_4$$

The creep modulus, C, is then calculated from: $C = P_{max}/ (2a_U x_1)$ where $a_U = [A_c/\pi]^{1/2}$. A_c is the projected area of contact between the indenter probe and the indenter surface. It is determined using the Oliver and Pharr method as a function of the maximum indentation depth [24]. Twenty five creep modulus determinations were made at each moisture content.

The average penetration depth (h_m) for P_{max} = 1N is dependent on the characteristics of the hydrated cement system e.g. degree of hydration and porosity level. In general h_m is approximately 10,000 nm or 10μm. The disturbed volume size is estimated to be approximately 2.09 x 10^3 μm^3 assuming the deformed zone is hemispherical.

The indenter tip calibration involves calculation of the contact area A_c utilizing a polynomial expressed as a function of penetration depth (h). The first term of the polynomial is A_c = 23.96 h^2. Calibrations are typically conducted with a fused quartz reference sample with known indentation characteristics. Calculations of contact area versus depth of penetration using only the first term of the polynomial (Berkovitch indenter) indicate that deviations from the reference are negligible especially if the depth of penetration is greater than 200nm. Therefore no further corrections to the calculations were made in this paper.

The creep modulus parameter was conceived by Vandamme [23]. He argued that the creep behavior reaches no asymptote over time and indentified the two functions that capture this behavior: a power function where the modulus is proportional to t^{α} and a logarithmic function where the modulus is proportional to ln (t/τ). The power function generally overestimates the creep deformation at large times. The logarithmic function is less accurate at early ages but more precise with respect to the long term creep behavior of concrete.

The 45 year old paste specimens in this study are essentially fully hydrated cements. As such they are more representative of microstructures for mature cement-based materials. Application of the logarithmic function in this case seems appropriate. Vandamme concluded that the observed logarithmic dependence of the time-dependent behavior could be explained by a rearrangement of the C-S-H particles. He further argued that creep may be due to a sliding of the C-S-H particles with respect to each other leading to a rearrangement of collections of C-S-H particles. A sliding mechanism of C-S-H layers has been previously proposed by Feldman [3] and Alizadeh [4]. The primary difference is that the latter authors include the effects of interlayer water ingress or egress on creep i.e. interlayer water is considered part of the solid C-S-H. The presence of structural water should have a major effect on the translation of the silicate sheets during the creep process as its removal affects the intrinsic properties of the solid itself.

The logarithmic function proposed by Vandamme was used to fit the overall creep data of calcium silicate hydrates obtained from his nanoindentation tests [23]. Vandamme established that the overall error was less than 1%. A similar finding was obtained for all the curves obtained in this study with the overall error being much less than 1%. Two examples for pure C-S-H materials are cited [25]: they are typical curves for C-S-H with C/S ratios =

0.80 and 1.20.The logarithmic expressions for the time dependent deformations ($\Delta h(t)$) as determined using the CSM Instruments regression analysis software are :$\Delta h(t)= 223.99 \ln (0.563t + 1) + 0.951t – 10.471$ for C/S = 0.80 and $\Delta h(t) = 150.13 \ln (0.956t + 1) – 0.003t - 8.419$ for C/S = 1.20. The standard error for the x_1 and x_2 parameters in the dominant first term are 0.466 and 0.001 (C/S = 0.80) and 0.420 and 0.027 (C/S = 1.20). The maximum load applied was 1004.52 mN and 1006.66 mN respectively. The goodness of fit was excellent and justified the use of the creep modulus based on a logarithmic assumption of the experimental creep curve.

A concern with the definition of creep modulus may be its lack of normalization and the effect of high indentation modulus values on its absolute value. The materials investigated are primarily calcium-silicate-hydrate phases and should not have a pronounced negative effect on the use of the creep modulus parameter for comparative purposes.

The calculation of $a_U$was made using a value for the contact area A_c obtained using the first term of the polynomial expressing A_c as a function of penetration depth. The divergence of A_c from a reference sample (as indicated earlier) is considered negligible especially at values of h > 200nm.

Dynamic Mechanical Analysis (DMA) – Internal Friction (Tan ∂) Measurements

The dynamic mechanical analysis (DMA) method involves the application of an oscillating force to the sample and measurement of displacement [26]. There is usually a time lag between the applied force and the resulting displacement. The time lag can be quantified in

terms of a phase angle between the load and the displacement due to their ideally sinusoidal nature.

The tangent of this angle (tan ∂) represents the damping property of the material often referred to as internal friction. The thermal dynamic mechanical thermoanalysis (DMTA) tests in this study were conducted using a Rheometrics RSA II instrument. The samples were heated from 25°C to 300°C. Temperature was increased in increments of 2°C every 5 minutes. Tan∂ versus temperature curves were plotted. Each test took about 11h and 45min. to complete. It is apparent that the DMTA tests are much less tedious and time consuming to perform compared to DMA tests at room temperature.

It has been demonstrated that DMA measurements on C-S-H systems that involved step by step drying of test samples before testing at room temperature are similar to those obtained in DMTA experiments where the samples are continuously heated from 25 to 300°C [17]. This implies that the curves generated by each test method generally contain a similar number of maxima and minima. The DMTA data set contains a large number of data points and is practically continuous. The DMA curve, as a result of the drying protocols, necessarily contains about 10 to 15 plot points. The spline then is a reasonable representative of the DMTA curve. Each DMTA test takes about 11h and 45 min to complete. The construction of each curve from DMA tests takes up to 2 weeks to complete. It is therefore practical and convenient to perform the DMTA test. It has been shown by Nguyen that indentation modulus versus mass-loss curves obtained from microindentation experiments are quantitatively and qualitatively similar to storage modulus versus mass-loss curves obtained from DMA experiments [27]. The latter curves are also similar to the DMTA curve. It is

therefore suggested that the creep modulus versus mass-loss spline is a real representation of the creep response.

It is also noted that the temperatures at which tan∂ peaks occur in DMTA tests for layered calcium silicates e.g.1.4 nm tobermorite correspond to well documented phase transitions suggesting that the 'averaging' approach to curve fitting provides real information for these silicates [14].

Tan ∂ versus temperature curves were constructed for each test specimen. Tests were conducted over a frequencyrange of 0.10 – 5 Hz. Results were similar at all frequencies. The curves plotted in the figures were obtained at 3.98 Hz as the peaks were more distinct. Additional details are given in a recent publication by the authors [14]. The character of the tan∂-temperature curves has been shown to mimic the tan∂ -mass-loss curves obtained by equilibrium drying in steps at room temperature. The number and shape of the observed peaks are similar.

Results and Discussion

Old Cement Pastes-Creep Modulus and DMTA Measurements

Creep modulus versus mass-loss and tan∂ versus temperature curves for the 45 year old pastes (w/c = 1.0 and 0.50) are plotted in Figures 1 and 2 respectively. Examination of the curves in Figures 1 and 2 indicates that the tan∂ curves are actually shifted relative to the creep modulus curves. The curves in Figure 1 show that the maxima for tan∂ correspond to minima in the creep modulus curve. There is an indication in Figure 2 that this is also the case although it is less clear.

Thus the correspondence of the creep modulus maxima with the tan∂ minima is interpreted as a connection between the lack of mobility of the silicate sheets and low creep. Structural collapse does of course lead to increased creep modulus and reduced tan∂.

The creep modulus curve in Figure 1(w/c = 1.0) exhibits peaks at about 1.50, 3.50, 6.00 and about 8.0% mass loss. The tan∂ versus temperature curve exhibits peaks at about 65, 120, 200 and about 275 °C. It is noted that the temperature scale does not directly correspond to the mass-loss scale. The tan∂ curve nevertheless, in a general sense, displays a similar oscillatory pattern to the pattern of the creep modulus curve. This has previously been observed by Nguyen et.al. for creep modulus and tan∂ mass-loss curves for synthetic C-S-H dried from the 11%RH condition [27]. The first two peaks in the creep modulus curve up to 3.50% mass-loss are associated with the loss of adsorbed and interlayer water.

The collapse of structure process (on removal of water) as detected by the time-dependent inflow of helium gas into the C-S-H structure was monitored previously by Alizadeh [17]. Details of the preparation of the C-S-H samples and the helium inflow technique are provided elsewhere [27, 28]. Briefly the C-S-H samples were prepared by the pozzolanic method using CaO and colloidal silica as the reactants. Hydration took place in excess water using a water solids ratio of about 10. Hydration occurred over a period of six months. The C/S ratio was controlled using stoichiometric amounts of the reactants. The helium inflow method monitors the inflow of helium gas at two atmospheres pressure into the C-S-H structure at 11%RH and other moisture contents obtained by incremental drying. Collapse of structure detected by

helium inflow has been observed to exhibit multi- stage behavior for highly polymerized C-S-H (low C/S ratio, C/S = 0.80), see Figure 3 [17]. This is compatible with the observation of the first two peaks in the creep modulus curve as the silicate chain lengths are significantly longer for old pastes (see Table 1). The third peak in the helium inflow curve at 6% mass-loss is associated with collapse of structure that typically occurs in younger paste containing shorter chain-length C-S-H and synthetic C-S-H having C/S ratios > 1.0. The helium inflow-mass-loss curves for the C-S-H (C/S=1.2) with shorter length typically exhibit a single peak at about 5-6% mass-loss indicative of a collapse of structure mechanism (see also Figure 3). This is also the case for younger pastes. The peak at 6% mass-loss (for C/S=0.80) occurs as a result of removing the remaining amounts of interlayer water.

It is apparent that the response of the nanostructure of C-S-H to both moisture-loss and applied stress is transient and non- uniform. The collapse of structure implies that the silicate sheets come into closer proximity. This process however varies along the length of the silicate chain as the stacking of the silicate sheets is irregular. The sheets in some regions come into the range where surface interactions inhibit their translation relative to one another. In other regions this is probably not the case. The net effect on the resultant mobility of the silicate sheets is to enhance creep. This nanostructural variability explains (at least in part) the connection between a slow creep process and the location or absence of the water molecules that have vacated interlayer space.

The tan∂ parameter is a descriptor of the internal friction developed during the removal of water and is closely tied to the creep process. The magnitude of creep is inversely related to the creep modulus. The increase in tan∂ exhibited by the first two peaks is also associated with the loss of adsorbed and interlayer water.

The initial loss of the interlayer water likely occurs at the ends of the layers. The ends of the layers come into closer proximity but translation is inhibited by the remaining water at various structural bridging sites along the length of the silicate chain. This latter phenomena accounts for stiffening and decreases in tan∂ due to further removal of water following the maximum. This is more pronounced in older pastes that have longer chains. Creep is associated with the ability of the silicate sheets to translate reflected by the generation of internal friction. The appearance of multiple peaks coincides with the incremental regeneration of internal friction due to the removal of interlayer water. Decreases in tan∂ values correspond to structural collapse processes that bring the C-S-H sheets closer together. These phenomena are compatible with cross-linking of the C-S-H sheets and interaction of the calcium ions with the silicate lamellae possibly through Si-O-Si or ≡SiO-Ca2+ linkages. Their action would tend to reduce internal friction and hence creep rate. Mass-losses above 6% have amplified structural significance as explained above. Some compositional water is likely to be lost at higher temperatures with a net effect of reducing creep rate.

Creep modulus versus mass-loss and tan∂ versus temperature curves for the 45 year old paste (w/c = 0.50) are plotted in Figure 2. The creep modulus reaches a maximum at about 2%

mass-loss and approaches a second maximum at about 7% mass-loss. The first peak in the creep modulus curve is associated with the loss of adsorbed and interlayer water. The second peak is associated with collapse of structure. There are fewer peaks in the creep modulus curve at this lower w/c ratio possibly due to pore structure considerations. The arguments associated with helium inflow into the structure as water is removed and their relevance to 'collapse' processes (discussed above) would appear to apply. The tan∂ versus temperature curve displays a similar character and pattern to the creep modulus-mass-loss curve. There are two peaks-one at about 50°C and the other at about 225°C. The increase in tan∂ exhibited by the first peak is also associated with the loss of adsorbed and interlayer water. The second peak is associated with structural collapse and the loss of some compositional water. The implications for creep are similar to those described above.

In summary the creep modulus increases with mass-loss over some ranges of mass-loss and also decreases with mass-loss over other ranges. This oscillatory behavior can be explained in 'structural' terms as follows. Mass-loss due to the removal of water in layered silicates e.g. C-S-H is an irreversible transient process. In essence the material is constantly changing in a 'structural' sense with each incremental change in moisture content as interlayer water is considered to be part of the solid [27]. Initially the removal of this water results in a decrease in the stiffness or elastic modulus of the system as the silicate layers come into closer proximity. Forces are activated that stiffen the system. These include an increase in the degree of polymerization, ionic-covalent interactions and possible cross-linking between the silicate chains as referred to above. During this process the removal of additional interlayer water continues and becomes sufficient to reinitiate a continuous decrease in

stiffness. It is noted that the layers are not perfectly aligned, contain defects and are 'kinked'. The oscillatory nature for changes in tan∂ with mass-loss is similarly affected by these processes except that minimum and maximum positions are reversed. It appears to be intuitive then that the creep modulus would change as the material changes and that it would be influenced by processes that affect the inherent ability of the basic particles-C-S-H layers to translate.

Young Cement Paste-Creep Modulus and DMTA Measurements

There are also fewer peaks in the creep modulus curves for the w/c = 0.40 preparations (compared to the w/c = 1.00 curve). Creep modulus-mass-loss curves for 'young' pastes and 'old' pastes are plotted in Figure 4. There are two peaks for the 'young' paste (at about 2 and 7 % mass-loss) and three peaks for the 'old' paste (at about 0.5, 6 and 7.5 % mass-loss) that were observed. The significance of the peaks with respect to the structural role of water would appear to be similar to that described above for the w/c = 0.50 pastes. The creep modulus is higher for the 'young' paste up to about 3.5% mass-loss and significantly higher at mass-loss values exceeding 5%. Creep is inversely related to creep modulus. Therefore, in general, creep is higher for the 'old' pastes.

Creep as is the case for shrinkage and strength is dependent on the volume concentration of the active component i.e. the hydrated cement phase. The 45 year old pastes are nearly completely hydrated and contain considerably more hydrated phase per unit volume than the young paste. It is arguable then that those pastes with a greater amount of C-S-H should exhibit a greater creep. This appears to be the case in this study (see Figure 4 where creep of

the young paste is lower for most of the mass-loss values). The higher degree of polymerization of the C-S-H phase in the old pastes means that the active component contains more structural defects (i.e. missing bridging tetrahedra in the silicate chains) which arguably would contribute to increased creep. The anhydrous phase undoubtedly contributes to a lower creep value for young paste as the intrinsic creep of the cement particles themselves is very low. The content of CH particles of the old pastes is however higher and would provide some volume change restraint. It would appear that all very old pastes creep more than young pastes. It would be counterintuitive if the porosity differences because of age were large enough to override the other effects. This is apparently not the case in this study.

Creep modulus versus mass-loss and tan∂ versus temperature curves for the 'young' paste, w/c = 0.40 are plotted in Figure 5. There is a large tan∂ peak at about 65°C with a shoulder at about 110 °C. The peak value of tan∂ is about 0.014 and is about twice the maximum value for the 'old' paste. Tan∂ decreases as temperature increases to about 135°C and then slowly increases up to 200°C when the measurements were terminated. The initial large peak is associated with the first creep modulus peak and the loss of adsorbed and interlayer water up to 4.5% mass-loss.

The maximum tan∂ values for the 'old' pastes are: 0.0010 (w/c = 1.00); 0.0075 (w/c = 0.50); 0.0090 (w/c = 0.40). The corresponding value for the 'young' w/c = 0.40 paste is, as stated previously, 0.014. The reduced creep rate for the 'young' paste despite the much higher value of internal friction (tan∂) is likely due to the much lower degree of hydration or lower volume

concentration of C-S-H (table 1), increased capillary porosity and the restraining effect of the unhydrated cement particles.

Porosity considerations-compacted paste systems

Specimens made from compacted powders of cement paste provide flexibility by allowing control over the composition of the 'solid' phase while varying the porosity. The solid phase consists of the porous particles of hydrated cement that are compacted under pressure. Compacts that are formed under applied pressure contain both the porosity within the solid phase referred to as internal and porosity external to the porous particles. The total porosity is the sum of the internal and external porosity. All the compact specimens were tested at the same total porosity. The compacts comprised of high w/c ratio paste-for a given total porosity- will have less capillary porosity external to the 'solid' phase as the solid particles contain more capillary pores than low w/c ratio preparations. It is suggested that the total capillary porosity governs the creep of the 'old' pastes (w/c 0.50 to 1.00). This explains the similar creep rate at the 11% RH or zero mass-loss condition (creep modulus of about 120 GPa, Figures 1 and 2). It is recalled that the total porosity of all the compacted specimens was nominally about 40%. The 'external' capillary porosity the magnitude of which (in compacted specimens) varies inversely with w/c ratio appears to have a greater effect on the generation of internal friction, The 'total' capillary porosity may be similar but the creep rate is significantly greater (particularly at 11% RH) for the 'old' paste at w/c = 0.40.The solid phase or internal capillary porosity or space would be completely filled with hydration product. Creep of pastes prepared at this w/c ratio may be governed by the external capillary porosity which is greater than it is for the higher w/c preparations. It is noteworthy that even

at the low w/c ratio of 0.40 the cement is nearly fully hydrated after 45 years. Generally low water /cement ratio pastes contain fewer connected pores that can facilitate mass-transfer of moisture to the surface of the sample. Apparently the kinetic barrier to hydration imposed by the lower degree of connectivity of the pore network is eventually overcome.

Creep Mechanisms

It is apparent that creep of hydrated cement paste following drying from the 11%RH condition is dependent on moisture content and specifically on the amount of interlayer water. This has been demonstrated in previous studies on synthetic C-S-H [29]. The apparent correspondence of creep modulus-mass-loss data and the generation of internal friction determined using dynamic mechanical thermo-analysis supports the view that a contributing mechanism to the creep process may involve the sliding or translation of silicate sheets relative to one another. This mechanism appears to be operative in both 'old' and 'young' pastes.

The reduced creep rate for the 'young' paste may be related to the much shorter silicate chain length (table 1.). The structural collapse due to interlayer water removal can take place more efficiently along the length of the chain possibly reducing the potential for creep deformations. Further the lower volume concentration of C-S-H product would necessarily reduce creep as the creep potential at humidities lower than 11%RH is dependent on the amount of water resident in the interlayer positions.

It may appear counterintuitive that creep of 'old' cement paste (w/c = 0.40) would be greater than creep of 'young' cement paste. One might expect older pastes to creep less as the overall

porosity is significantly lower at advanced ages. In the experiments with compacts reported here a comparison was made between well-hydrated material and material having a lower degree of hydration at the same porosity. This allowed a comparison of the properties of the properties of the 'solid' phase. Previous work by the authors enabled a comparison of microindentation parameters (Indentation Hardness and Indentation Modulus) on a porosity basis for 'old' and 'young' pastes [30].Values of these parameters were less for the 'old' paste than the 'young' paste at equal porosity (w/c = 0.40).

The creep modulus was also directly related to both these parameters. The indentation hardness values for 'young' and 'old' pastes (w/c = 0.40) were 322 and 217 MPa (at 11% RH) respectively. Corresponding values for indentation modulus were 5.80 and 1.45 GPa. A contribution factor to the lower values of the MI parameters for 'old' paste at the same porosity is likely the greater volume concentration of capillary or larger pores in the compacted samples as discussed previously.

Conclusions

1. Creep of both old and young paste at 11% relative humidity or less is dependent on the water content. Interlayer water appears to have a structural role in the creep process.

2. The tan∂ parameter obtained from thermal dynamic mechanical thermo-analysis is a descriptor of the internal friction developed during the removal of water and is closely tied to the creep process.

3. Creep of old high water/cement ratio pastes appear to have a more complex dependence on mass-loss due to drying from 11% relative humidity than pastes prepared at lower

water/cement ratios. This appears to be dependent, in part, on the chain length of the silicate phase.

4. The water/cement ratio of the old pastes affects the degree of structural collapse of the C-S-H. The collapse process is more irregular at high water/cement ratios as evidenced by multi-stage events during helium diffusion experiments.

5. The capillary porosity in compacted specimens of equal total porosity varies inversely with water/cement ratio as the capillary porosity in the solid phase decreases at lower water/cement ratios.

6. Creep of old cement paste at low water/cement ratio, e.g. w/c = 0.40, is greater. This appears to be a function of the amount of capillary porosity in a compacted specimen.

7. The reduced creep rate for the 'young' paste (w/c = 0.40) compared to the old paste at the same w/c ratio is likely due to the much lower degree of hydration or lower volume concentration of C-S-H, increased capillary porosity, shorter C-S-H chain length and the restraining effect of the unhydrated cement particles.

8. A contributing mechanism to the creep process in both young and old paste may involve the sliding or translation of silicate sheets relative to one another.

References

1. K.W. Nasser and A.M. Neville, Creep of old concrete at normal and elevated temperatures, ACI Journal, 97-103, 1967.

2. F.H. Wittmann, Creep and shrinkage mechanisms, Chapter 6 in Creep and Shrinkage in Concrete Structures, Eds. Z. P. Bazant and F.H. Wittmann, J. Wiley & Sons New York, 129-162, 1982.

3. R.F. Feldman, Mechanism of creep of hydrated Portland cement paste, Cem. Concr.Res. 2 (5), 521-540, 1972.

4. R. Alizadeh, J. J. Beaudoin and L. Raki, Viscoelastic nature of calcium silicate hydrate, Cem. Concr. Comp., 32, 369-376, 2010.

5. B.L. Meyers and F. O. Slate, Creep and creep recovery of plain concrete as influenced by moisture conditions and associated variables, Magazine of Concrete Research, 22(70), 37-41, 1970.

6. W. Ruetz, A hypothesis for the creep of hardened cement paste and the influence of simultaneous shrinkage, Proc. Int. Conf on the Structure of Concrete, London, Cement and Concrete Association, 365-387, 1968.

7. D. J. Hannant, The mechanism of creep in concrete, Materials and Structures, 1, 403-410, 1968.

8. I. Ali and C.E. Kesler, Mechanisms of creep, Symposium on Creep of Concrete, ACI Special Publication No. 9, 35-63, 1964.

9. Z. N. Cilosani, On the probable mechanism of the creep of concrete, Beton I Zhelezobeton, Moscow, No. 2, 75-78, 1964.

10. R.G. L'Hermite, Volume changes of concrete, Proc. Fourth Int. Symp. Chem. Cem., Vol. II, 659-694,Washington D.C., 1960.

11. R.F. Feldman and J.J. Beaudoin, Effect of applied stress on the helium inflow characteristics of hydrated Portland cement, Cem. Concr.Res., 13(4), 470-476, 1983.

12. M. Vandamme and F.-J. Ulm, Nanogranular origin of creep, Proc. Nat. Acad. Sci. (USA), 106 (26), 10552-10557, 2009.

13. F. Radjy, A thermodynamic study of the system hardened cement paste and water and its dynamic mechanical response as a function of temperature, PhD Thesis, Stanford University, pp. 349, 1968.

14. P. Pourbeik, J. J. Beaudoin, R. Alizadeh and L. Raki, Dynamical mechanical thermo-analysis of layered calcium silicate hydrates, Journal of Thermal Analysis and Calorimetry, 118(1), 1-14, 2014.

15. E. J. Sellevold, Low frequency internal friction and short-time creep of hardened cement paste: An experimental correlation, Hydraulic Cement Pastes: Their Structure and Properties, Proc. of a Conference, University of Sheffield, Cem. Concr.Assoc., 330-337, 1976.

16. E. J. Sellevold and C. W. Richards, Short-time creep transition for hardened cement paste, J. Amer. Ceram. Soc., 55(6), 284-289, 1972.

17. R. Alizadeh, Nanostructure and Engineering Properties of Basic and Modified Calcium-Silicate-Hydrate Systems, PhD thesis, University of Ottawa, pp. 231, 2009.

18. I. Soroka and P.J. Sereda, The structure of cement- stone and the use of compacts as structural models, Proc. 5th Int. Symp. on the Chem. of Cem., Vol. 3., Tokyo, 67-73, 1968.

19. R. F. Feldman, Factors affecting the Young's modulus-porosity relation of hydrated Portland cement compacts, Cem. Concr. Res., 2(4), 375-386, 1972.

20. P.J. Sereda and R. F. Feldman, Compacts of powdered material as porous bodies for use in sorption studies, J. Appl. Chem., 13, 150-158, 1963.

21. J.J. Beaudoin, Comparison of mechanical properties of compacted calcium hydroxide and Portland cement paste systems, Cem. Concr.Res., 13, 319-324, 1983.

22. P.J. Sereda, R.F. Feldman and E.G. Swenson, Effect of sorbed water on some mechanical properties of hydrated Portland cement pastes and compacts, Highway Research Board, Special Report 90, 58-73, 1966.

23. M. Vandamme, The nanogranular origin of concrete creep: A nanoindentation investigation of microstructure and fundamental properties of calcium-silicate-hydrates, PhD thesis, MIT, pp.366, 2008.

24. W. C. Oliver and G. M. Pharr, An improved technique for determining hardness and elastic modulus using load and displacement sensing indentation experiments, J. Mater.Res.7, 1564-1583, 1992.

25. D.-T. Nguyen, R. Alizadeh, J.J. Beaudoin, P. Pourbeik, and L. Raki, Microindentation creep of monophasic calcium-silicate-hydrates, Cem. Concr. Comp., 48, 118-126, 2014.

26. K. P. Menard, Dynamic Mechanical Analysis-A Practical Introduction, CRC Press LLC, Boca Raton, pp. 208, 1999.

27. D.-T. Nguyen, J. J. Beaudoin, R. Alizadeh and L. Raki, Creep of calcium- silicate-hydrates: A particle sliding mechanism, submitted to Materials and Structures, 2014. See also D.-T. Nguyen, Microindentation Creep of Calcium-Silicate-Hydrate and Secondary Hydrated Cement Systems, M.A.Sc. Thesis, University of Ottawa, pp. 142, 2014.

28. R.F. Feldman, The flow of helium into the interlayer spaces of hydrated Portland cement paste, Cem. Concr. Res., 1(3), 285-300, 1971.

29. D.-T. Nguyen, R. Alizadeh, J. J. Beaudoin and L. Raki, Assessment of the structural role of water on the creep of C-S-H, submitted to Advances in Cement Research, 2014.

30. P. Pourbeik, R. Alizadeh, J. J. Beaudoin, D.-T. Nguyen and L. Raki, Microindentation Creep of 45 Year Old Hydrated Portland Cement Paste, Advances in Cem. Res., 25(5), 301-306, 2013.

Figure Captions

Figure 1. Creep modulus versus mass-loss and tan∂ versus temperature for cement paste hydrated 45 years (w/c = 1.0). Error bars represent a variation of one standard deviation from the mean.

Figure 2. Creep modulus versus mass-loss and tan∂ versus temperature for cement paste hydrated 45 years (w/c = 0.5). Error bars represent a variation of one standard deviation from the mean.

Figure 3. Helium inflow at 40 hours versus mass-loss from the 11% RH condition for C-S-H samples (C/S = 0.8 and 1.2).

Figure 4. Creep modulus versus mass-loss curves for cement paste (w/c = 0.40) hydrated for 2 months (young) and 45 years (old). Error bars represent a variation of one standard deviation from the mean.

Figure 5. Creep modulus versus mass-loss and tan∂ versus temperature for cement paste hydrated for 2 months.

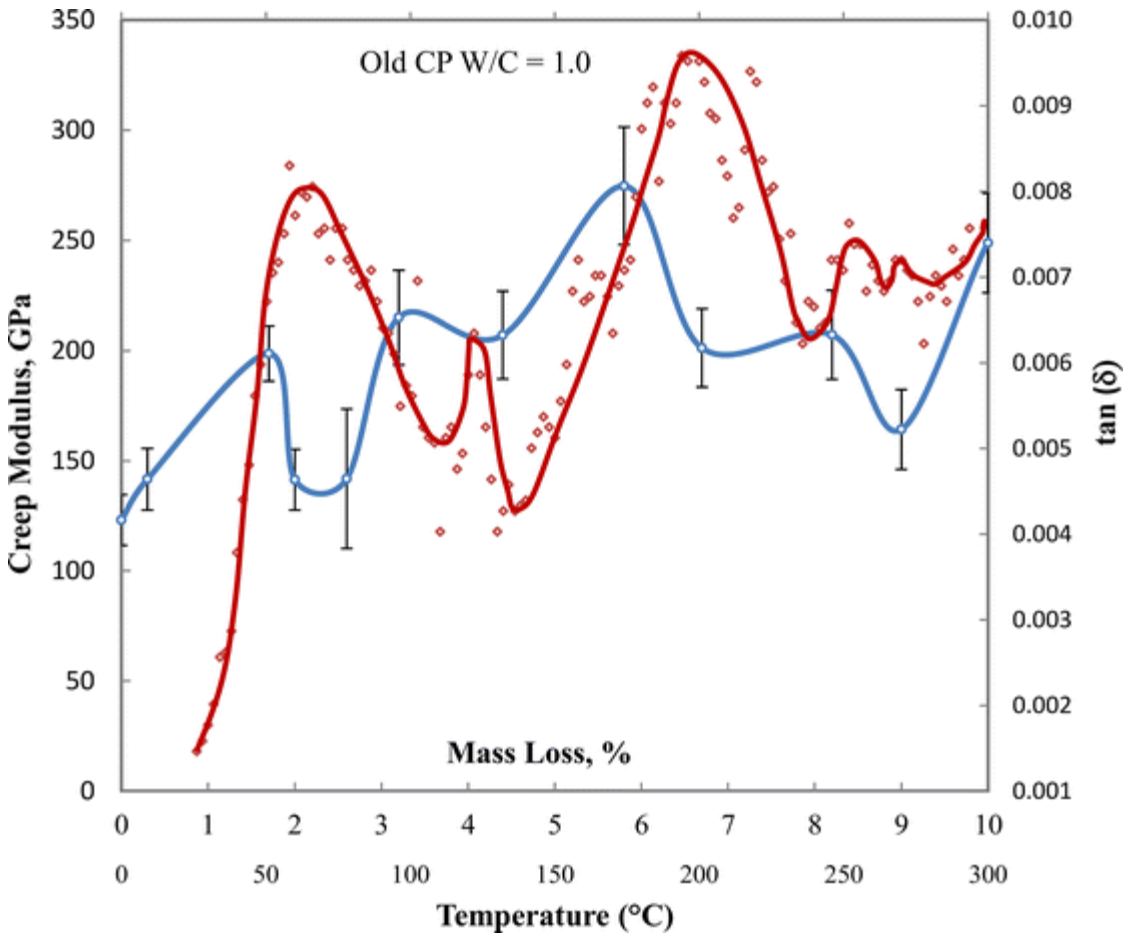

Figure 1. Creep modulus versus mass-loss and tan∂ versus temperature for cement paste hydrated 45 years (w/c = 1.0). Error bars represent a variation of one standard deviation from the mean.

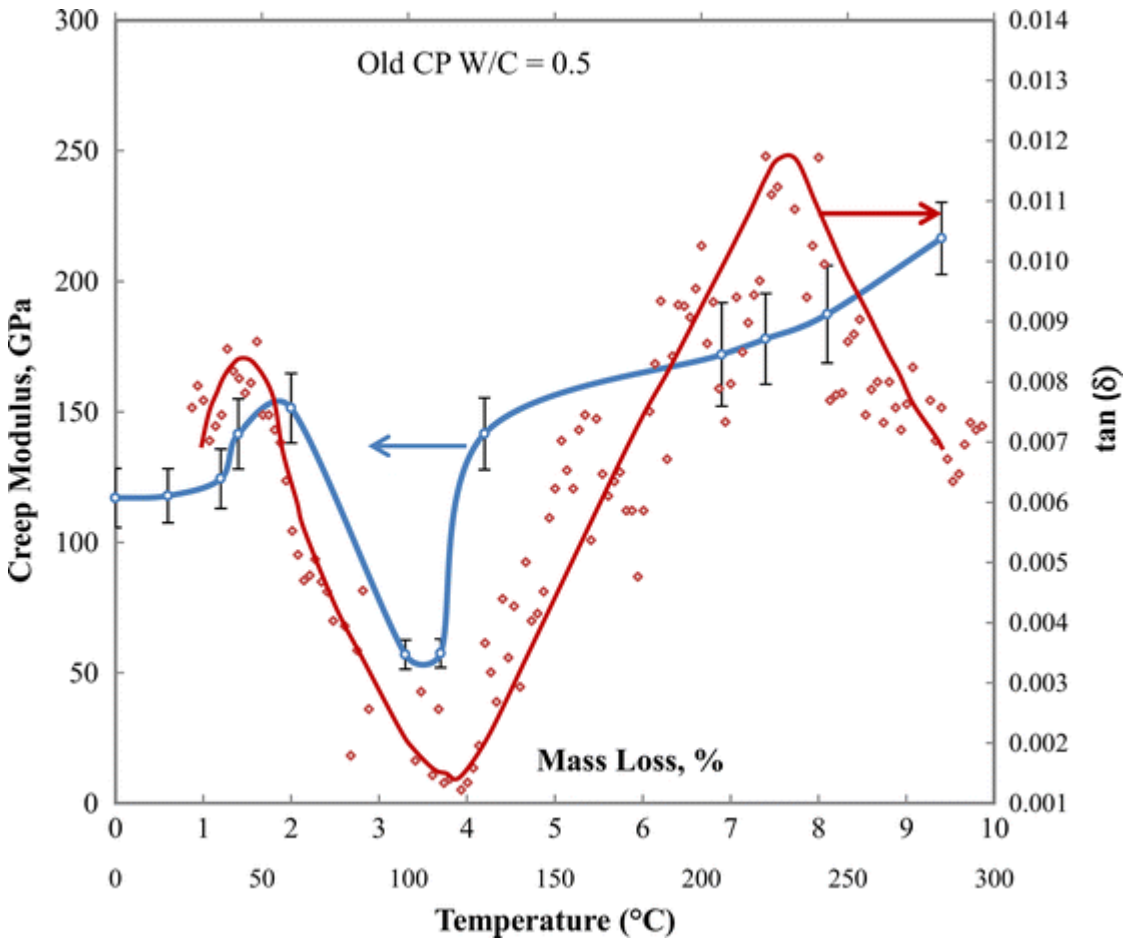

Figure 2. Creep modulus versus mass-loss and tan∂ versus temperature for cement paste hydrated 45 years (w/c = 0.5). Error bars represent a variation of one standard deviation from the mean.

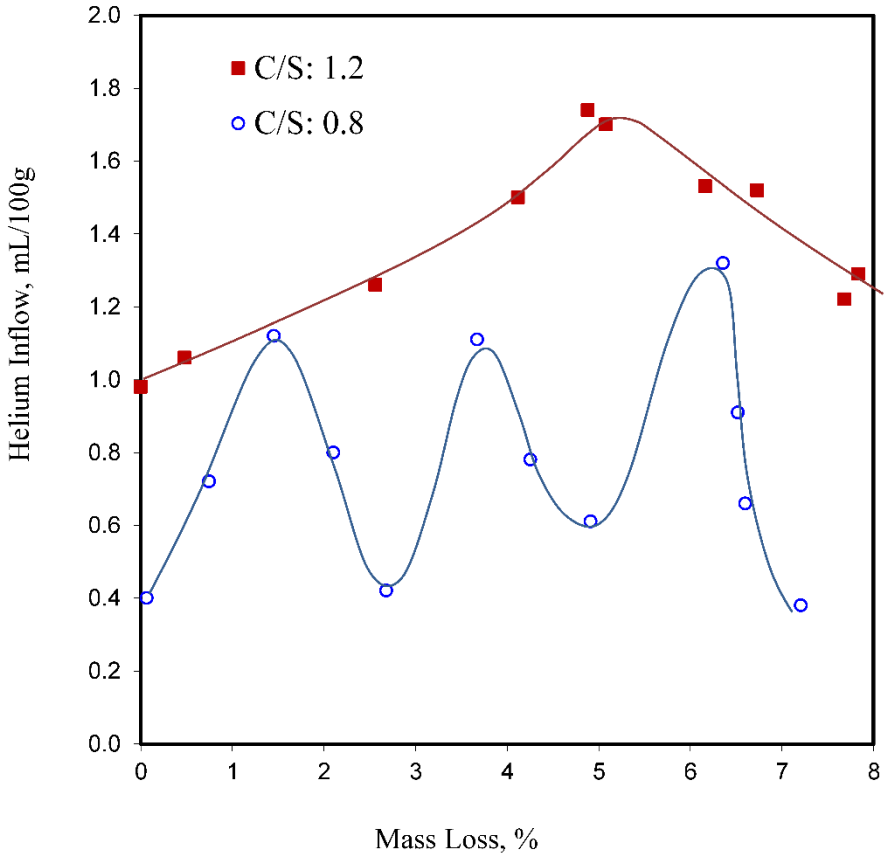

Figure 3. Helium inflow at 40 hours versus mass-loss from the 11% RH condition for C-S-H samples (C/S = 0.8 and 1.2).

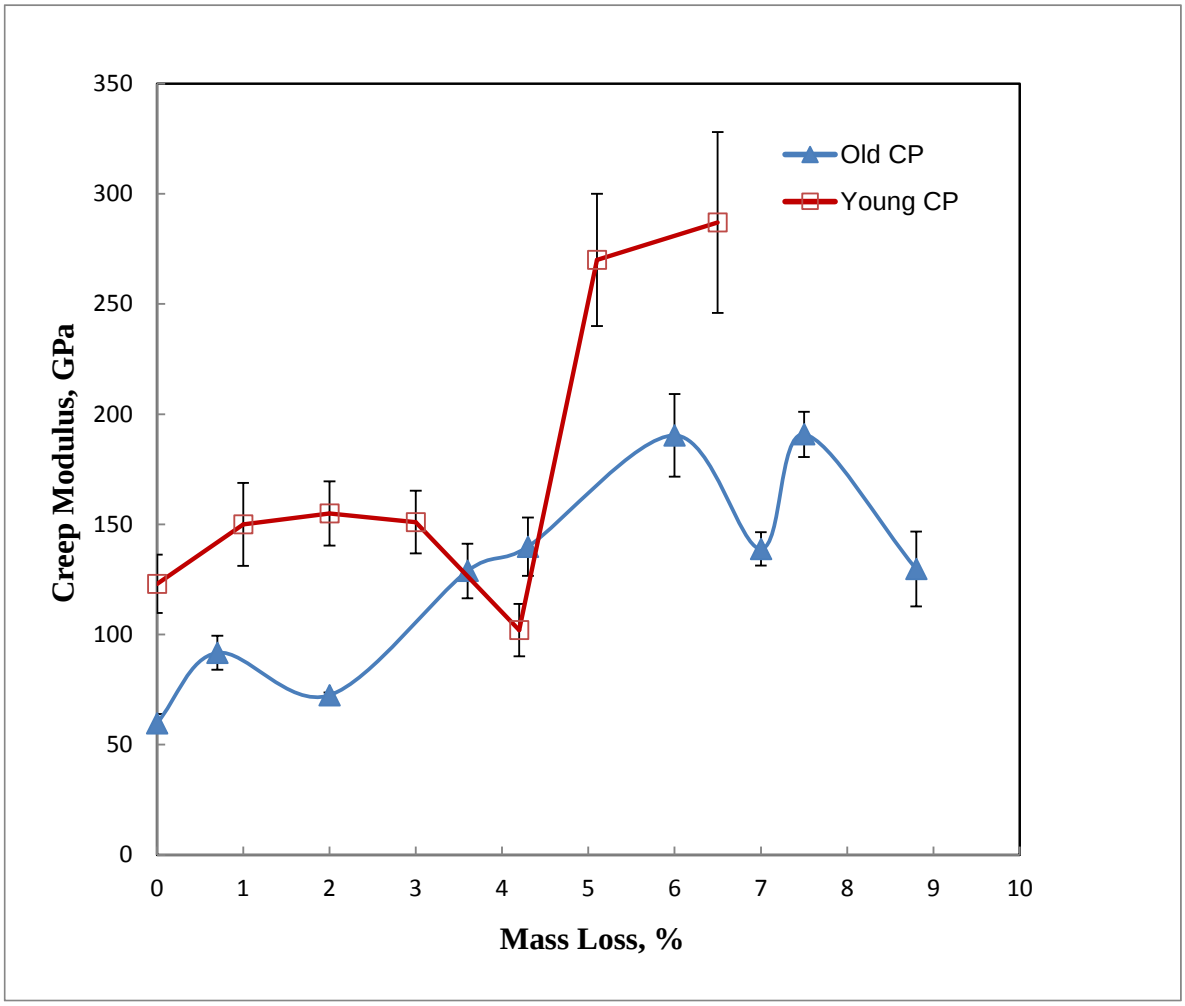

Figure 4. Creep modulus versus mass-loss curves for cement paste (w/c = 0.40) hydrated for 2 months (young) and 45 years (old). Error bars represent a variation of one standard deviation from the mean.

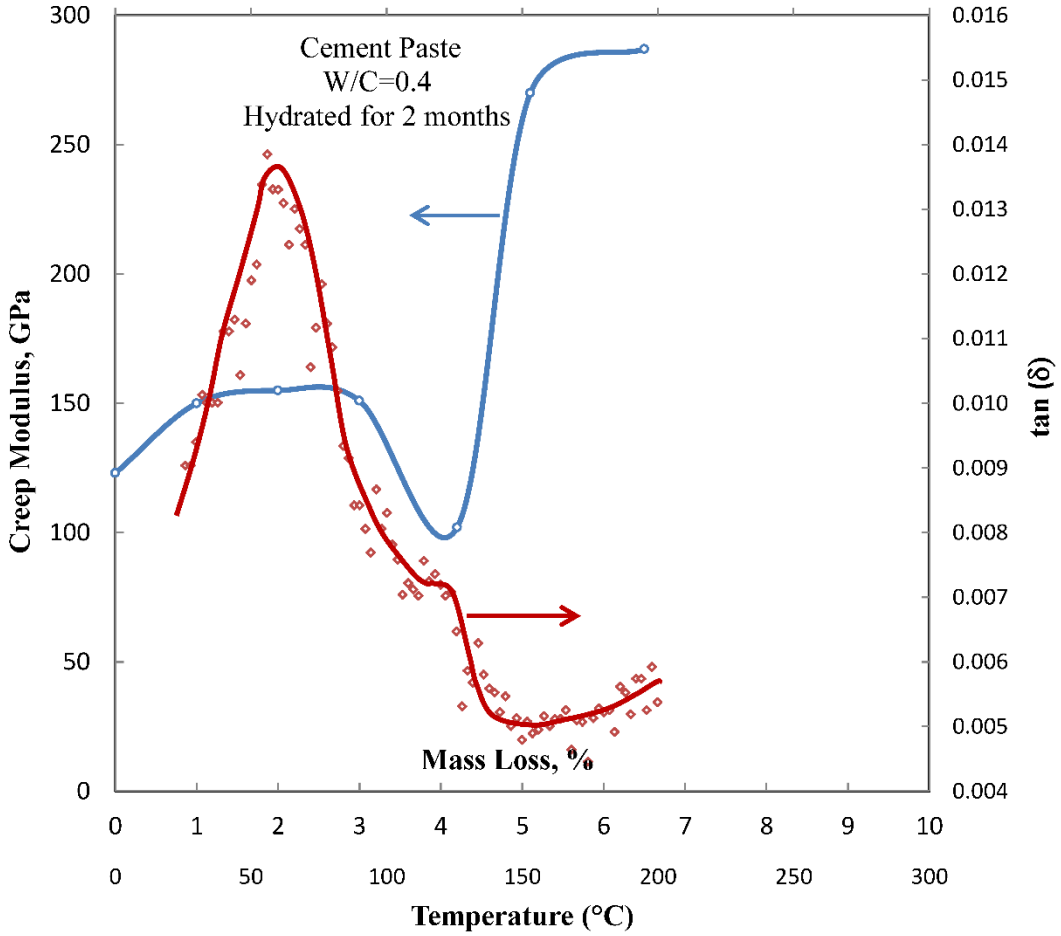

Figure 5. Creep modulus versus mass-loss and tan∂ versus temperature for cement paste hydrated for 2 months.

Chapter 11

Structural Factors Affecting the Engineering Behavior of Layered Calcium Silicate Hydrates

The research described in this chapter utilizes three new approaches to examine the structural role of water in the mechanical performance of C-S-H, 1.4 nm tobermorite and jennite. These involve the following: (1) correlation of microindentation parameters and their dependence on mass-loss with internal friction data obtained from dynamic mechanical thermo-analysis (2) a DMTA study of layered calcium silicate hydrates with varying degrees of cross-linking between their silicate sheets (3) manipulation of the drying history at humidities below 11% RH and the effect of applied stress in order to control the relative position of the silicate sheets and potentially the elastic behaviour of the layered silicates.

Three papers (from Part 4 of the experimental program) address the nanostructural issues associated with the interlayer environment including interactions involving interlayer water and cross-linking within the silicate structures as evidenced by Q^3 silica sites detected by ^{29}Si MAS NMR. Evidence will be presented that the incremental removal of interlayer water from 11% RH is intimately connected to the creep process. It is proposed that this involves movement of the layers into closer proximity accompanied by a translation of the silicate sheets relative to each other. The creep modulus-mass-loss characteristics for the pure silicate phases investigated are similar over a wide range of mass-loss supporting the view that both the chemical and physical aspects of the composition-based model are defensible and that

the removal of interlayer water has a pivotal role in the creep response of layered calcium-silicate hydrates. Further it is shown that the contribution of the interlayer water to the stiffness of the layered silicate materials is dependent on the extent of cross-linking between the silicate sheets. This was shown to vary with silicate species e.g. gyrolite versus C-S-H. It was also demonstrated that nanostructural changes associated with interlayer water mobility are likely a root cause of the path dependence of the sensitivity of elastic properties to moisture content and the nature of interparticle contact in hydrated cement systems. This sensitivity was demonstrated for the first time with C-S-H, tobermorite and jennite phases and employed six different pre-test sample conditioning protocols. The behavior of all the layered silicates investigated in this study is considered germane to the behavior of hydrated Portland cement paste.

The titles of the papers in this chapter are as follows:

Paper 10: Engineering Performance of Pure Calcium-Silicate-Hydrate Phases: The Structural Role of Interlayer Water, Submitted to Materials and Structures, 2014.

Paper 11: Structural Factors Affecting the Engineering Performance of Layered Calcium-Silicate Hydrates, (to be submitted), February, 2015.

Paper 12: The Non-Uniqueness of the Modulus of Elasticity of Layered Calcium-Silicate Hydrates with Respect to Water Sorption, to be submitted, February 2015.

11.1 Introduction

The utility of the DMA and the DMTA techniques for exploring several factors that influence the contribution of interlayer water to the structural integrity of C-S-H, tobermorite and jennite is demonstrated in the three papers presented in this chapter. These factors range from

the physico-chemical environment of the interlayer region to differences in the nature and structure of the species dependent silicate layers themselves. It is further demonstrated that the nature of the water sorption process in porous bodies comprised of layered silicates and its irreversible effects on the engineering behavior of these systems is consistent with mechanical performance observations of hydrated cement paste. These papers provide additional evidence in support of T and J composition-based models for C-S-H in hydrated Portland cement.

11.2 Paper 10: Engineering Performance of Pure Calcium-Silicate-Hydrate Phases: The Structural Role of Interlayer Water

This paper represents a systematic study of the microindentation (MI) parameters of C-S-H, 1.4 nm tobermorite and jennite and the influence of water removal from 11% RH to the dry state. This data has not been previously been available. Correlation of MI – mass-loss curves with tan∂ - temperature curves obtained from DMTA experiments enabled inferences to be made regarding the compatibility of the results with composition-based models for C-S-H in hydrated cements. The structural role of interlayer water is discussed in this context. It is suggested that the structural role of interlayer water is an integral part of creep, elastic deformation and failure processes associated with the engineering behavior of layered calcium-silicate-hydrates.

Engineering Performance of Pure Calcium-Silicate-Hydrate Phases: The Structural Role of Interlayer Water

(Submitted to Materials and Structures, 2014)

P. Pourbeik[a], J. J. Beaudoin[b], R. Alizadeh[b] and L. Raki[b]

[a] *National Research Council Canada, Construction Portfolio, Ottawa, ON, Canada*

[b] *Giatec Scientific Inc., Ottawa, ON, Canada*

Abstract

Results of a systematic study of the effect of the incremental removal of water from 11% RH to the dry state on the microindentation parameters of layered calcium-silicate-hydrates are reported. Creep modulus, indentation modulus and indentation hardness measurements on compacted specimens of C-S-H (C/S = 1.2), 1.4nm tobermorite (T) and jennite (J) were made. The values of these parameters were dependent on mass-loss i.e. on the removal of interlayer water. Correlation of these dependencies with tan∂ (internal friction) data obtained from dynamic mechanical thermos-analysis was made. The structural role of interlayer water is discussed in this context. Inferences regarding the compatibility of the results with composition-based models for C-S-H in hydrated cements are made.

Keywrods: Role of Interlayer Water, Calcium-Silicate-Hydrate, Jennite, Tobermorite, Creep, Dynamic Mechanical Thermo Analysis

Introduction

The state of water associated with the silicate phases in hydrated cement paste has been a moot point for several decades [1-6]. Considerations of the structure of the calcium-silicate-hydrate that forms in the paste have included colloidal particle-based models [1,3] and models based on layered calcium silicate systems [4-6]. The colloidal-based models are described as microporous solids containing capillary pores and 'gel' pores [1] or as globules that contain interlayer water in addition to 'gel' porosity [3]. Additional detail is provided in the discussion. Descriptors of the state of water that are often used in discussions of engineering performance are 'bulk' pore water, 'gel' pore water and surface adsorbed water. Engineering behavior and volume stability is considered to be influenced by these water types. Inerlayer water is not considered to have a major role. Models based on layered calcium-silicate-hydrates, however, do ascribe a structural role to interlayer water. More recent composition-based models for C-S-H in cement paste are comprised of structural elements of both 1.4nm tobermorite and jennite [7, 8]. These are layered silicate minerals; their structure has been recently resolved [9, 10].

This study was designed to investigate the effect of the incremental removal of interlayer water from synthetic C-S-H, 1.4nm tobermorite and jennite on their mechanical performance. It was expected that creep modulus, elastic modulus and hardness values for these systems would be dependent on the amount of interlayer water present. This in turn was expected to provide some insight as to the 'structural' nature of interlayer water in minerals that are key elements of composition-based models for the C-S-H in cement paste. The significance of using 11% RH as a datum point rests with the fact that at this humidity condition there is a

negligible amount of pore water present. The solids essentially contain only surface adsorbed water and interlayer water.

It has been shown by Sellevold [11] and Sellevold and Richards [12] that there is a correlation between low frequency internal friction obtained by dynamic mechanical analysis (DMA) methods and short–term creep of cement paste. Dynamic mechanical thermoanalysis (DMTA) methods were applied to the synthetic silicates in this study. The internal friction-temperature (mass-loss) dependence for each silicate mineral studied was correlated with the creep modulus-mass-loss characteristics. A comparison is also made between the indentation modulus and indentation hardness versus mass-loss dependencies of the three synthetic silicates investigated.

The characteristics of the microindentation parameter versus mass-loss dependencies of the silicate systems are used as a basis for discussion in support of a layered silicate model for C-S-H in hydrated cement paste. Evidence includes similarities in the concept of a structural role for interlayer water.

Experimental

Materials

Three calcium-silicate-hydrate systems were prepared: synthetic calcium-silicate-hydrate (C-S-H with C/S = 1.2); 1.4nm tobermorite; jennite.

C-S-H: synthetic C-S-H was produced from the pozzolanic reaction between CaO and amorphous silica in excess water. Calcium oxide was obtained by calcining reagent grade

calcium carbonate at 900°C. Reactive silica (CAB-O-SIL, grade M-5 from Cabot Corporation, USA) was heated at 110°C to remove any surface adsorbed water. Distilled water was de-aired and used for the reactions. All materials were kept sealed in N_2 purged bottles until they were used. The C/S ratio of 1.2 was achieved by utilizing the stoichiometric amounts of the reactants. The reaction period was 6 months. The material was then filtered and dried under vacuum for 4 days at room temperature. The dried C-S-H was stored in nitrogen purged glass vials before the experiments. Characterization of the C-S-H by X-ray diffraction (XRD) and thermal methods gave results directly comparable to C-S-H (I) as reported by Taylor [13]. The BET nitrogen surface area was $30 m^2/g$.

1.4nm tobermorite: the reactants (CaO and SiO_2) were prepared as described above. The C/S ratio was 0.9. The reactants were placed in a high density polyethylene bottle mixed in excess deionized water (water/solids = 11) and maintained at 80 °C using a heating wrap. The mixture was continuously agitated with a magnetic stirrer for a period of 4 months. The XRD spectrum and TGA curve were similar to those obtained by Yu and Kirkpatrick [14]. The BET nitrogen surface area was $58 m^2/g$.

Jennite: the reactants (CaO and SiO_2) were prepared as described above. The C/S ratio was 1.4. The reactants were placed in a high density polyethylene bottle mixed in excess deionized water (water/solids = 11) and maintained at 80 °C using a heating wrap. The mixture was continuously agitated with a magnetic stirrer for a period of 4 months. The XRD pattern was similar to that obtained by Yu and Kirkpatrick [14], Gard and Taylor [15] and Hara and Inoue [16]. The TGA curve matched that published by Yu and Kirkpatrick [14]. The BET nitrogen surface area was $32 m^2/g$.

Preparation of Compacted Specimens

Circular disc samples for all the powdered materials were prepared (for microindentation tests) by pressure compaction in steel moulds with a cross-section of about 25 mm. The thickness of most of the prism samples was approximately1mm.Numerous studies on the use and validity of compacts as models for hydrated cement systems have been published [17-19]. It has been shown that compacted specimens of powdered hydrated Portland cement have similar mechanical property-porosity relationships to that of the original hardened paste of the same material [17]. The porosity of the compacted mineral samples was determined using helium pycnometry. The calculation is made knowing the apparent volume and the solid volume of the sample. Porosity can be varied by controlling the compaction pressure. The porosity of all the compacted specimens in this study was nominally about 30%.

Solid rectangular prism samples for the dynamic mechanical thermoanalysis (DMTA) determinations were prepared by pressure compaction in steel moulds with a cross-section of 12.8 x 83 mm. The thickness of most of the prism samples was also 1mm but varied between the limits of 1-2mm. The thickness of each sample was measured to an accuracy of 0.1mm.The porosity of all the compacted specimens was nominally about 30%. This enabled comparisons to be made on the basis of approximately equivalent amounts of solid phase in any specimen.

Humidity Conditioning

Specimens for the three mineral systems were conditioned for 3 weeks at 11%RH in vacuum desiccators containing saturated lithium chloride solution. The powders were conditioned at

11%RH before compaction and for a few days after compaction. Theoretically there is a monolayer of water on the surfaces of the particles in addition to interlayer water at this humidity.

Microindentation measurements

All the microindentation tests were performed using a CSM Instruments Instrumented Indentation Tester. The apparatus is housed in an environmental chamber. All tests were conducted at 11% RH on specimens equilibrated at 11%RH.Tests were conducted using a Berkovich indenter. The CSM microindentation instrument has a load range of 0.03 – 30 N with a resolution of 0.3 mN. There were approximately 25 indents on each sample. The composition of the solid phase for monophasic systems remains constant. Pure materials do not require as many indents as multiphase materials as phase separation procedures involving the use of deconvolution methods are not necessary.

The indentation depth was recorded as a function of time at the maximum load of 1000 mN for a 600s dwell period. The loading rate was 2000mN/min. The logarithmic creep was determined through curve fitting of the indentation-depth versus time curves during the 600s dwell time by the following equation:

$$\Delta h(t) = x_1 \ln (x_2 t + 1) + x_3 t + x_4$$

The creep modulus, C, is then calculated from: $C = P_{max}/ (2a_U x_1)$ where $a_U = [A_c/\pi]^{1/2}$. A_c is the projected area of contact between the indenter probe and the indenter surface. It is determined using the Oliver and Pharr method as a function of the maximum indentation depth [20]. The indentation modulus (M) and indentation hardness (H) were obtained from

the software that uses the Oliver and Pharr method. $M = \pi^{1/2}S/ [2(A_c)^{1/2}]$ where $S = dP/dh |_{h = hmax}$ is the initial slope of the unloading branch of the P-h curve. P is the maximum indentation load. Indentation hardness (H) was estimated from the relation $H = P/A_c$.

Dynamic Mechanical Thermoanalysis (DMTA)

The DMTA analysis was conducted using a Rheometrics RSA II instrument on all samples in this investigation. Tests were conducted in the three point bending mode. Specimens were rectangular beams (12.8mm x 83mm x 1mm thick). A very low amplitude oscillation was applied on the brittle, thin samples in order to prevent any damage or micro-cracking. This was confirmed by microscopic analysis after the experiment. Moreover, no decrease was observed in the E' value when a trial specimen was repeatedly subjected to the same loading procedure. Samples were tested at a frequency of 0.10Hz at a maximum strain level of 0.01% and an initial static load of 20g in order to ensure a good contact between the upper fixture and the surface of the specimen throughout the dynamic loading process The induced stress was kept below 2MPa in order not to introduce any significant damage or micro-cracking to the sample. The original experiments were conducted in the frequency range from 0.10Hz to 10Hz. It was observed that the E' and tan∂-mass loss curves had similar features at all frequencies. They were more distinguishable, however, at 0.10Hz. Prior to conducting the experiments the calibration of the equipment was checked using standard weights and a steel bar.

The DMTA samples were heated from 25°C to 125°C. Temperature was increased in increments of 2°C every 5 minutes. E' and tan∂ versus temperature curves were plotted. Mass-loss occurred during the test due to temperature increases. Temperatures associated

with mass-loss or phase transition events for the mineral phases studied are well known and are referred to in the discussion of results.

Results and Discussion

The sensitivity of engineering parameters (e.g. creep, modulus of elasticity and compressive strength) to equilibrium moisture content in hydrated cement paste has been a key element of structural models of C-S-H since Powers described their origins in his colloidal model in terms of various states of water [1]. These states were governed by their location within the pore structure and as opposed to bulk water in relatively large capillary pores the descriptor, 'hindered' adsorbed water was applied to water in small 'gel' pores. It was argued that the mobility of this water under applied stress was at the seat of creep. It is more difficult to reconcile this concept with the observed stiffening of cement paste at higher humidity as it is uncertain as to what mechanism would be operative.

More recently Jennings has advanced a refined colloidal model of C-S-H the basic units of which are referred to as globules 4.2nm in width and nominally 50-60 nm in length [4]. Three categories of pores were defined as: intraglobular pores (IGP; ≤ 1nm); small gel pores (SGP; 1-3nm) and large gel pores (LGP; 3-12nm). Arguments were presented for the formation of low density C-S-H in the early stages of reaction and high density C-S-H at middle or later stages. The globules contain interlayer water, a monolayer of surface water and IGP space. Rearrangement of globules under stress associated with changes in LGP and SGP coupled with changes due to transport of 'hindered' water is central to predictions of the consequences

of irreversible changes that occur. It appears, however, that an important role or intrinsic value for the engineering performance of hydrated cement paste is not ascribed to the presence of interlayer water in the Jennings model.

The present investigation is concerned with the engineering performance of three pure layered calcium-silicate-phases: C-S-H (C/S = 1.20); 1.4nm tobermorite; jennite. The results of experiments with these systems will be described separately for creep modulus, indentation modulus and hardness modulus measurements in the following sections. It is emphasized that the experiments will be conducted over the humidity range of 11% RH to the 'dry' state. The state of the 'solid' phase at 11% RH is one where the only two types of water are a small amount of surface adsorbed water and a relatively large amount of interlayer water. It is clear that any change in mechanical performance of these layered systems upon the incremental removal of water will essentially be associated with the interlayer state. It is believed that this is the first data of this type to be reported for these minerals of significant importance to cement science in general and to constructs of composition-based models in particular. Data based on systematic studies of cement paste mechanical properties in the region 11%RH to the 'dry' state are not available.

Microindentation Creep Modulus Measurements

The creep modulus versus mass-loss curves (Figure 1) for C-S-H, 1.4nm tobermorite and jennite have similar trends up to about 7% mass-loss. At greater mass-loss values the creep modulus values rise steeply to over 300 GPa commensurate with the conversion of jennite to metajennite and a corresponding decrease in basal-spacing from 1.05nm to 0.87nm [13].

Hence the creep of metajennite (inversely proportional to creep modulus) is significantly lower than that of jennite.

The creep modulus at 11%RH is lowest for C-S-H (72 GPa) followed closely by the value for 1.4nm tobermorite (95MPa). The value for jennite is significantly higher (162 GPa). Creep at 11%RH is therefore in the following order: C-S-H > 1.4nm tobermorite > jennite. The greater basal-spacing for (T) as opposed to (J) would appear to be a factor for the difference in creep at 11%RH for these two minerals.

The initial change in creep modulus up to a 1%mass-loss is similar for (T) and (J) (i.e. a decrease of about 60 GPa) but actually increases slightly for C-S-H. The decrease is attributed to the removal of surface and interlayer water. The shorter silicate chain-length for C-S-H (as determined by ^{29}Si NMR [14]) does not appear to influence the initial creep to nearly the same extent. The increase in creep of (T) and (J) seems to be dependent on both chain-length and basal-spacing. Perhaps the slight decrease in creep of the C-S-H at 1% mass-loss level is a function of the short silicate chain-length arising from the missing bridging tetrahedra (especially with C/S > 1.0).

Creep modulus (inversely related to creep) generally increases (at 2% mass-loss) to a maximum value for all three silicates in the mass-loss region of 5 to 6%. The creep modulus values are quantitatively similar for all three systems in this mass-loss region. The decrease in creep up to this mass-loss is likely associated with loss of surface adsorbed water, interlayer water and the corresponding collapse of the layered structure. The latter may

involve interactions of interlayer Ca^{2+} with the silicate sheets and some possible cross-linking in the case of 1.4nm tobermorite and C-S-H based on ^{29}Si NMR evidence [21].

It is argued that further removal of water (up to 8% mass-loss) restores the creep potential of all three systems as the trends are similar. This will be discussed further in the following section. As stated previously the conversion of jennite to metajennite (above 8% mass-loss) reduces creep.

It is apparent that the incremental removal of water from the layered silicates studied is intimately connected to the creep process. Movement of the layers into closer proximity accompanied by a translation of the silicate sheets relative to each other is proposed.

Dynamic Mechanical Thermoanalysis

The work of Sellevold and Richards, cited in the introduction [11, 12] established a correlation between low frequency internal friction and short-term creep of cement paste. The results of companion dynamic mechanical thermoanalysis (DMTA) measurements in this study complement interpretation of the microindentation creep data. They also provide some insight as to the operative mechanism for creep deformation in the 11%RH to dry state region of the desorption isotherm. A plot of tan∂ (internal friction) versus temperature for the three pure phases investigated in this study is given in Figure 2. A brief description of the character of the curves in the figure follows:

(i) *1.4nm tobermorite*-there are three distinct peaks at about 35°C, 75°C and 100°C in the temperature range investigated. The first two peaks are attributed to the increase in internal

friction due to the removal of surface and interlayer water. Removal of water from the interlayer region can initially provide vacant space conducive to the translation of the silicate sheets and enhance creep effects as the internal restraint of the 'structural' water is removed. The decrease in tan∂ following the peak maxima is possibly due to cross-linking effects and the interaction of Ca^{2+} ions with the silicate sheets. The peak at 100˚C is likely associated with the conversion of 1.4nm tobermorite to the 1.2nm form [14]. The associated increases in density of the solid and porosity of the samples and any additional removal of interlayer water are likely contributors to the increase in internal friction. The increase in tan∂ beginning at about 110˚C is associated with the transformation of the 1.2nm form to the 1.1nm form.

Minima and maxima in the creep modulus values (Figure 1) up to a mass-loss of 5% can be explained by similar arguments as those in the preceding paragraph. The decrease in creep modulus (increase in creep) corresponds to the removal of up to 1.1% surface and interlayer water compatible with an increase in internal friction. A collapse of structure process corresponds to the subsequent increase in creep modulus (decrease in creep) and decrease in the internal friction value at mass-loss up to 3.5%. The small decrease in creep modulus at 4% and larger increase at 4.5% correspond to the second peak of the internal friction curve. The large decrease at higher mass-loss values is likely a result of the factors described above i.e. porosity, a phase transformation, solid density increase (2.23 g/cm^3 to 2.40g/cm^3) and porosity increase in addition to a further incremental removal of interlayer water.

(ii) *Jennite*- there are three distinct peaks (at 35 ˚C, 50˚C and 80˚C) in the temperature range studied. The rationale for the changes in internal friction in these temperature locations and

their relevance to the creep process are essentially similar to that for 1.4nm tobermorite. Two differences are the low probability of cross-linking (absence of a Q^3 signal in the ^{29}Si NMR spectra) and the transformation to metajennite in the temperature region above 85˚C. The latter results in an increase in internal friction accompanied by the following: a change in solid density from 2.33g/cm^3 to 2.62g/cm^3 and a loss of 4 water molecules from the interlayer regions. The collapse of silicate sheets in this region results in a significant increase in creep modulus or decrease in creep.

(iii) *C-S-H (C/S = 1.2)* - there are two distinct peaks (at 40˚C and 65˚C). The rationale for the changes in internal friction in these temperature locations and their relevance to the creep process are essentially similar to that for both 1.4nm tobermorite and jennite. The removal of interlayer water and concomitant interactions between the silicate sheets involving interlayer Ca^{2+} ions and possible cross-linking sites are integral to the creep process.

The initial 002 x-ray basal-spacing for C-S-H (C/S = 1.2 and 1.5) is similar (approximately 1.18 nm) [22]. Changes in the 002 x-ray basal-spacing versus mass-loss from 11% RH are also similar for both C/S ratios. They each undergo a significant decrease in basal-spacing at mass-losses between 5% and 7% to a value of about 1.00nm. Estimates of C/S ratio for C-S-H in hydrated Portland cement paste are in the range 1.5 to 1.8. It is suggested that the C-S-H used in this study mimics the behavior the C-S-H with C/S = 1.5. It is noted that the internal friction versus temperature curve for the C-S-H (C/S = 1.2) is positioned between the curves for 1.4nm tobermorite and jennite (Figure 2). This response is compatible with composition-based models for the C-S-H in cement paste as the latter are comprised of

structural elements of both tobermorite and jennite. The creep modulus–mass-loss characteristics for the three pure phases are similar in the mass-loss region between 2% and 7% (Figure 1). It is suggested therefore that both the chemical and physical aspects of the composition-based model are defensible. It is also readily apparent that the removal of interlayer water has a pivotal role in the creep response of layered calcium-silicate-hydrates.

Indentation Modulus Measurements

The modulus of elasticity (E) of cement paste has been shown by Sereda et. al. to be humidity dependent (see Figure 3) [17]. There is a large decrease in E on desorption from 11%RH to the dry state. Verbeck and Helmuth have also reported a large decrease in E on drying from the wet state [23]. They also observed partial recovery on re-wetting. Drying from 11%RH is significant as the water lost by the layered silicates in this study can be attributed to removal of interlayer water. Previous studies of cement paste systems have not focused on the incremental removal of water from 11%RH to the dry state. No data of this kind is available for tobermorite, jennite or synthetic C-S-H.

Indentation modulus versus mass-loss curves for the three systems studied are plotted in Figure 4. The three curves all exhibit an initial decrease in modulus up to about 1% mass-loss. The stiffening effect of the interlayer water is reduced as the space it occupied is vacated. This is followed by large increases in stiffness as the silicate sheets come into closer proximity and the basal-spacing decreases (see discussion in the previous section) in the mass-loss region between 1% and 7%. Oscillatory behavior in this region can be the result of this process combined with the further removal of interlayer water. The large increase in

the modulus value of jennite at mass-losses above about 8% are attributed to its transformation to metajennite. The latter has a significantly lower basal-spacing.

The indentation modulus of jennite and C-S-H are quantitatively similar except in the region of 5% to 6% mass-loss. This difference would in a general sense be somewhat compensated for with a binder system comprised of a mixture of tobermorite and jennite.

Indentation Hardness Measurements

Indentation hardness, modulus of elasticity and strength measurements of a variety of cement systems have been shown to correlate with each other through application of simple power laws [24]. It is argued that if interlayer water has a 'structural' role and is viewed as a component of the 'solid' phase the nature of its contribution to both stiffness and hardness due to drying from 11%RH to the 'dry' state would be similar. It follows that the general character of the indentation hardness versus mass-loss curves would mimic those of the indentation modulus-mass-loss curves. This is the case (see Figure 5). The rationale for the dependence of increases or decreases in indentation hardness on mass-loss is similar to that for indentation modulus (see previous discussion of indentation modulus and creep modulus data). Jennite appears to have a significantly lower initial value of hardness (compared to C-S-H or tobermorite) at 11%RH where the interlayer regions are filled with water. The main difference in the structure of jennite compared to tobermorite is the presence of OH groups linked to the calcium atoms present in the central region of the individual layers. This difference appears to be a contributing factor (weakening) to hardness up to about 2% mass-loss. Following this the structural collapse that brings the silicate sheets into closer proximity as a result of the removal of interlayer water appears to negate the differences. It is noted that

the curve for C-S-H is positioned between the curves for tobermorite and jennite in the mass-loss region between 2% and 6%. This response (as was the case for the creep modulus data) is compatible with composition-based models for the C-S-H in cement paste as the latter are comprised of structural elements of both tobermorite and jennite. The effect of the transformation of jennite to metajennite was also observed at mass-losses greater than 8%.

Conclusions

1. Microindentation parameters (e.g. creep modulus, indentation modulus and indentation hardness) of layered calcium-silicate-hydrates are dependent on the water content following drying from the 11% RH condition.

2. The oscillatory nature of the microindentation parameter-mass-loss curves (increases and decreases) of C-S-H, tobermorite and jennite is likely associated with the removal of interlayer water and collapse of structure processes involving interactions of Ca^{2+} ions and possible cross-linking of the silicate sheets.

3. The microindentation parameter-mass-loss curves generally mimic each other.

4. It is suggested that interlayer water present in the pure silicate phases studied has a structural role in determining the engineering performance of layered silicates.

5. It is apparent that the incremental removal of water from the layered silicates studied is intimately connected to the creep process.

6. Internal friction- temperature curves obtained using dynamic mechanical thermoanalysis (DMTA) compliment interpretation of the microindentation creep data.

7. Similarities in the character of the DMTA curves for the silicates studied and the position of the C-S-H curve between the other two curves suggests that this response is compatible

with expectations derived from composition-based models for the C-S-H in cement paste as the latter are comprised of structural elements of both tobermorite and jennite.

8. The data obtained for all the microindentation parameter dependencies on mass-loss from 11%RH for the pure phases studied support arguments for a tobermorite/jennite nanostructural model for C-S-H.

9. The structural role of interlayer water is an integral part of creep, elastic deformation and failure processes associated with the engineering behavior of layered calcium-silicate–hydrates.

References

1. T.C.Powers and T.L.Brownyard, Studies of the physical properties of hardened Portland cement paste: Part 2. Studies of water fixation, J. Amer. Concr. Inst., Proc. 43, 249-306, 1946.

2. R.F. Feldman, Sorption and length change scanning isotherms of methanol and water on hydrated Portland cement, Proc. Fifth Int. Symp. Chem. CemVol.III, 53-56, Tokyo, 1968.

3. H. M. Jennings, Refinements to colloidal model of C-S-H in cement: CM-II, Cem. Concr. Res., 38, 275-289, 2008.

4. M.Daimon, S. A. Abo-El-Enein, G.Hosaka, S. Goto and R.Kondo, Pore structure of calcium silicate hydrate in hydrated tricalcium silicate, J. Amer. Ceram. Soc., 60(3-4), 110-114, 1977.

5. R. F. Feldman and P. J. Sereda, A model for hydrated Portland cement as deduced from sorption-length change and mechanical properties, Materiaux et Constructions, 1(6), 509-520, 1968.

6. R.F.Feldman, Assessment of experimental evidence for models of hydrated Portland cement, Highway Res. Rec., No. 370, Hwy. Res. Board, 8-24, 1971.

7. H.F.W.Taylor, Proposed structure for Calcium Silicate Hydrate Gel, J. Amer. Ceram. Soc. 69, (6), 464-467, 1986.

8. I. G.Richardson, Tobermorite/jennite- and tobermorite/calcium hydroxide-based models for the structure of C-S-H: applicability to hardened pastes of tricalcium silicate, Portland cement, and blends of Portland cement with blast-furnace slag, metakaolin, or silica fume, Cem. Concr. Res., 34, 1733-1777, 2004.

9. Bonaccorsi E. and Merlino S., The crystal structure of tobermorite 14A (Plobierite), a C-S-H phase, J. Amer. Ceram. Soc., 88(3), 505-512, 2005.

10. Bonacorrsi E., Merlino S. and Taylor H.F.W., The crystal structure of jennite, $Ca_9Si_6O_{18}(OH)_6.8H_2O$, Cem. Concr. Res. 34, 1481-1488, 2004.

11. E. J. Sellevold, Low frequency internal friction and short-time creep of hardened cement paste: An experimental correlation, Hydraulic Cement Pastes: Their Structure and Properties, Proc. of a Conference, University of Sheffield, Cem. Concr. Assoc., 330-337, 1976.

12. E. J. Sellevold and C. W. Richards, Short-time creep transition for hardened cement paste, J. Amer. Ceram. Soc., 55(6), 284-289, 1972.

13. H. F. W.Taylor, Chapter 5, Hydration of the calcium silicate phases, Cement Chemistry, Thomas Telford Publishing, London, pp 459, 1997.

14. P.Yu and R.J.Kirkpatrick, Thermal dehydration of tobermorite and jennite, Concr. Sci. and Eng., 1, 185-191, 1999.

15. J. A. Gard and H. F. W.Taylor, Calcium silicate hydrate (II) ("C-S-H(II)"), Cem. Concr. Res., 6, 667-678, 1976.

16. N.Hara and N.Inoue, Formation of jennite from fumed silica, Cem. Concr. Res., 10, 677-682, 1980.

17. P.J. Sereda, R.F. Feldman and E.G. Swenson, Effect of sorbed water on some mechanical properties of hydrated Portland cement pastes and compacts, Highway Research Board, Special Report 90, 58-73, 1966.

18. I.Soroka and P.J.Sereda, The structure of cement- stone and use of compacts as structural models, Proc. 5th Int. Symp. on the Chem. of Cem., Vol. III, Tokyo, 67-73,1968.

19. P.J. Sereda and R. F.Feldman, Compacts of powdered material as porous bodies for use in sorption studies, J. Appl. Chem., 13, 150-158, 1963.

20. W. C. Oliver and G. M. Pharr, An improved technique for determining hardness and elastic modulus using load and displacement sensing indentation experiments, J. Mater.Res.7, 1564-1583, 1992.

21. R.Alizadeh, J. J. Beaudoin and L.Raki, Mechanical properties of calcium silicate hydrates, Matls. and Struct., 44, 13-28, 2011.

22. R. Alizadeh, Nanostructure and engineering properties of basic and modified calcium-silicate, hydrate systems, PhD thesis, University of Ottawa, pp.231, 2009.

23. G.J.Verbeck and R.H.Helmuth, Structures and physical properties of cement pastes, Proc. Fifth Int. Symp. Chem. Cem., Vol. III, 1-31, Tokyo, 1968.

24. R.F.Feldman and J.J.Beaudoin, A study of the mechanical properties of autoclaved calcium-silicate systems, Cem. Concr. Res., 5(2), 103-118, 1975.

Figure Captions

Figure 1. Creep modulus versus mass-loss curves following drying from 11%RH: C-S-H (C/S = 1.2); 1.4nm tobermorite; jennite

Figure 2. Dynamic mechanical thermoanalysis (DMTA) - tan∂ versus temperature curves for C-S-H (C/S = 1.2); 1.4nm tobermorite; jennite

Figure 3. Modulus of elasticity versus relative humidity for cement paste (w/c = 0.30); Ref [17].

Figure 4. Indentation modulus versus mass-loss curves following drying from 11%RH: C-S-H (C/S = 1.2); 1.4nm tobermorite; jennite

Figure 5. Indentation hardness versus mass-loss curves following drying from 11%RH: C-S-H (C/S = 1.2); 1.4nm tobermorite; jennite

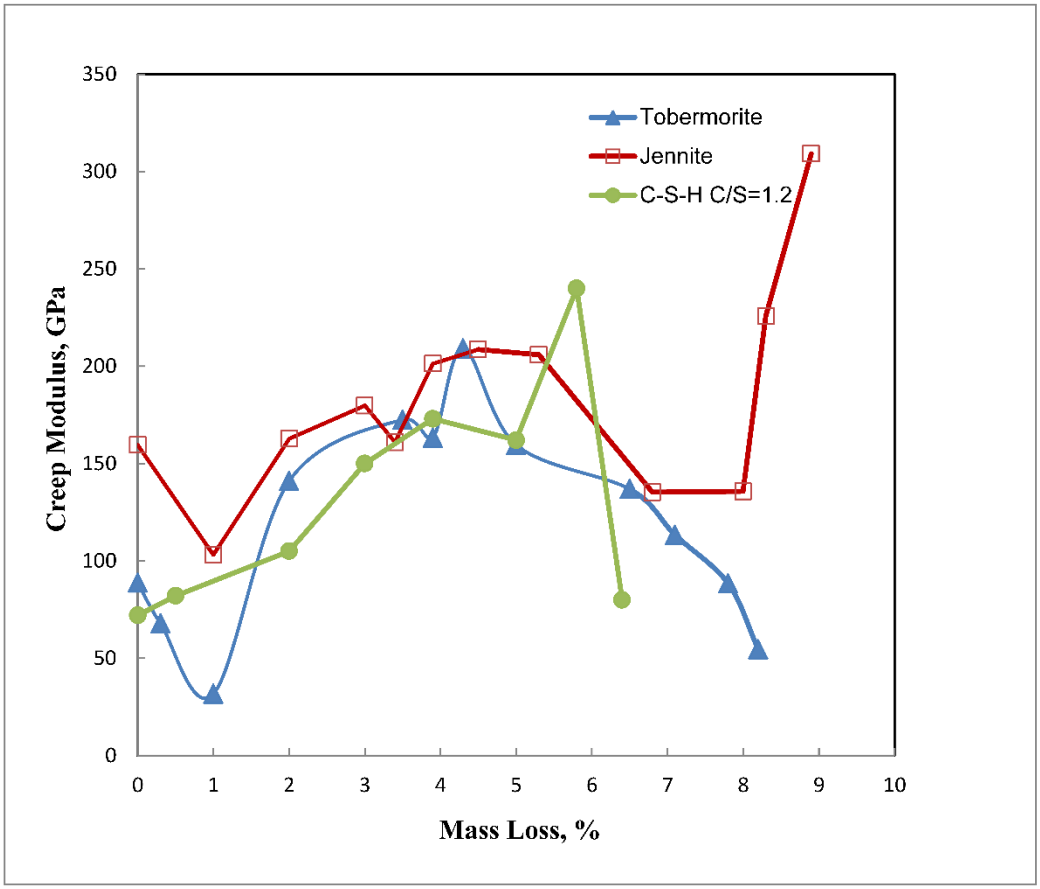

Figure 1. Creep modulus versus mass-loss curves following drying from 11%RH: C-S-H (C/S = 1.2); 1.4nm tobermorite; jennite

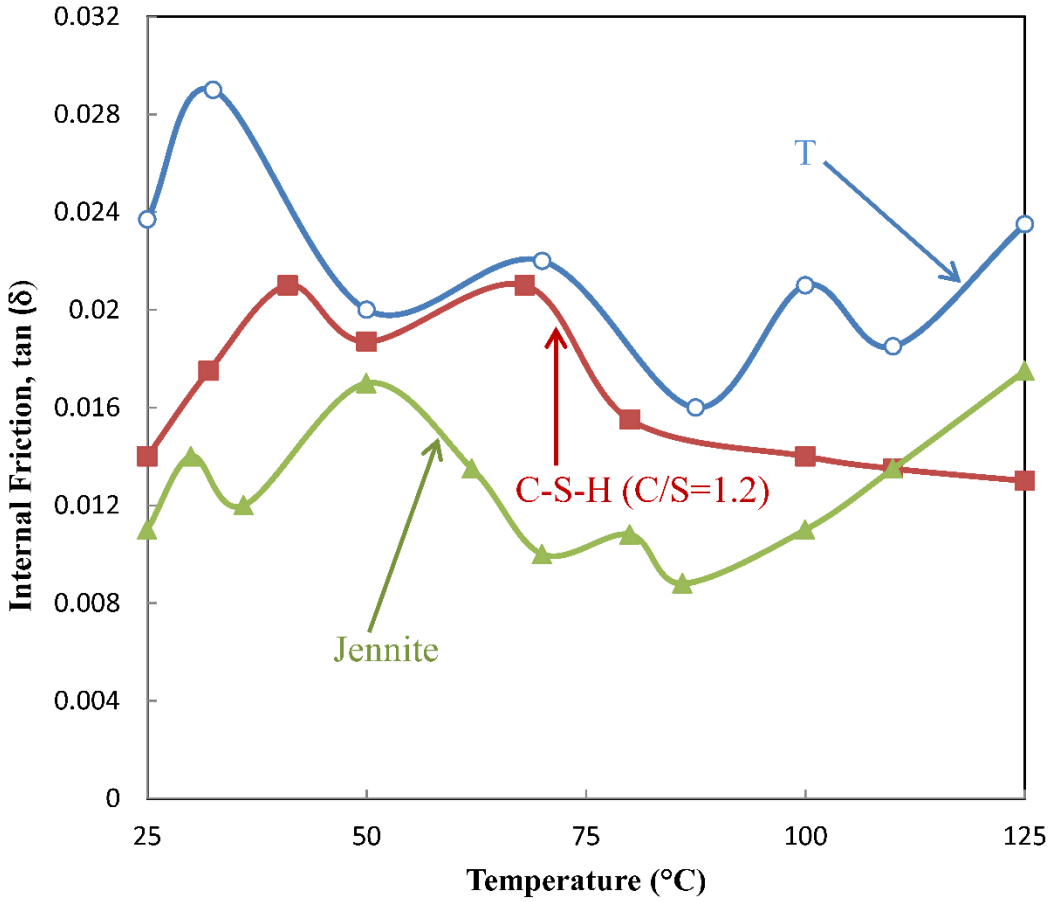

Figure 2. Dynamic mechanical thermoanalysis (DMTA) - tan∂ versus temperature curves for C-S-H (C/S = 1.2); 1.4nm tobermorite; jennite

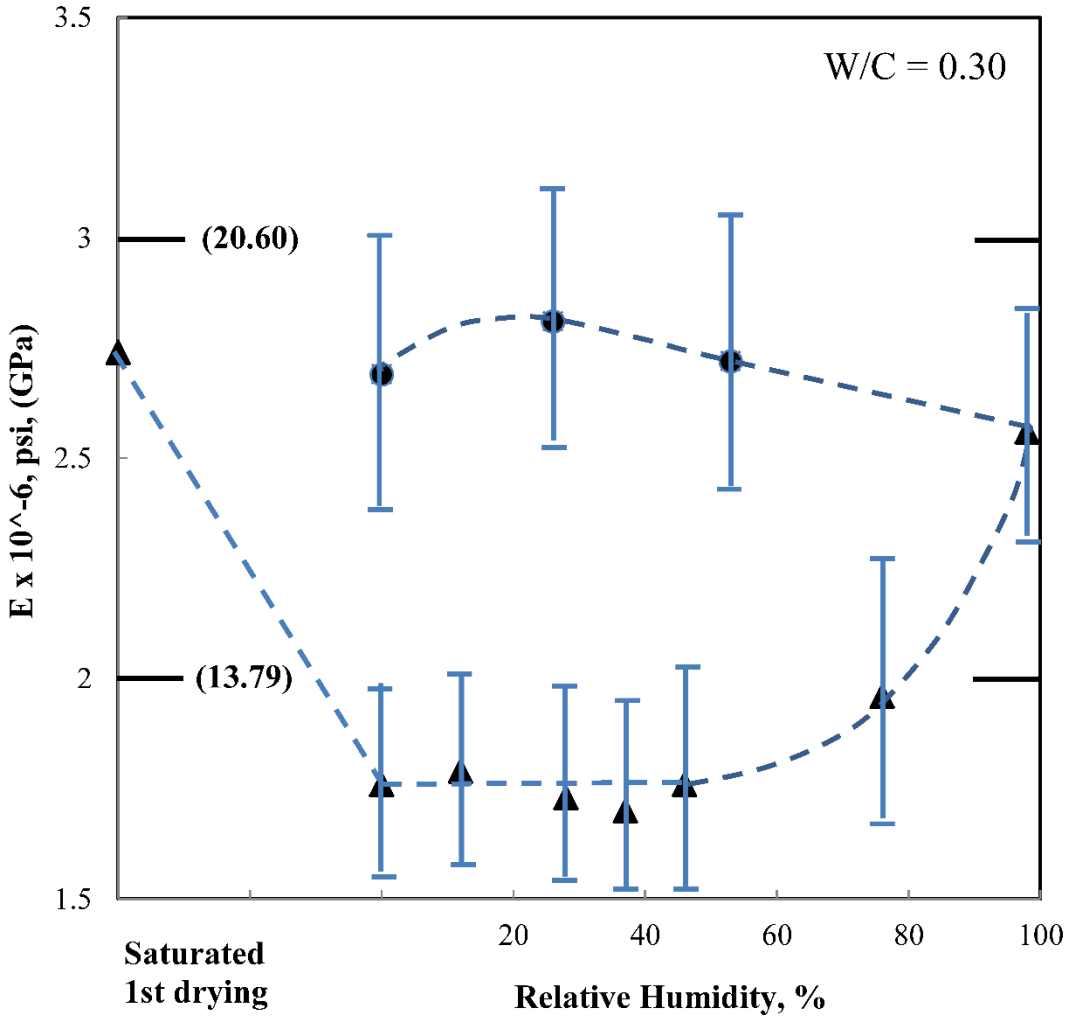

Figure 3. Modulus of elasticity versus relative humidity for cement paste (w/c = 0.30); Ref [17].

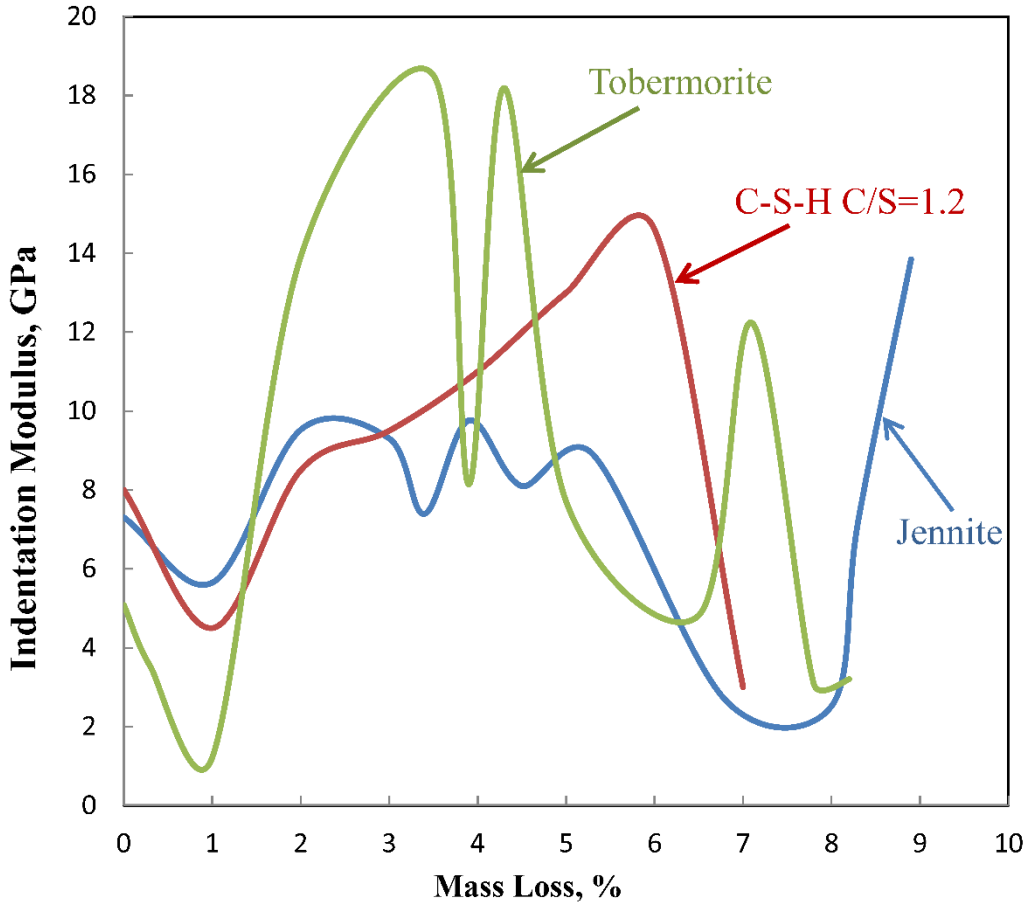

Figure 4. Indentation modulus versus mass-loss curves following drying from 11%RH: C-S-H (C/S = 1.2); 1.4nm tobermorite; jennite

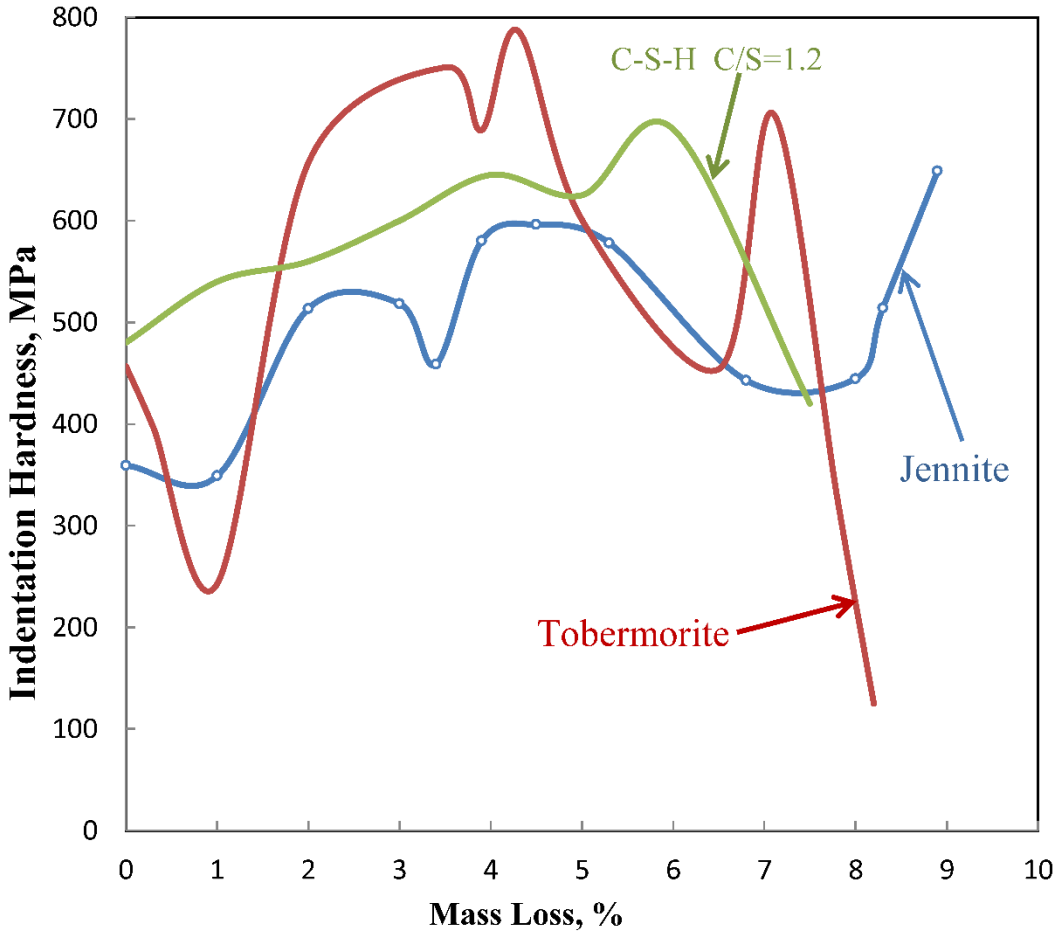

Figure 5. Indentation hardness versus mass-loss curves following drying from 11%RH: C-S-H (C/S = 1.2); 1.4nm tobermorite; jennite

11.3 Paper 11: Structural Factors Affecting the Engineering Performance of Layered Calcium Silicate Hydrates

A DMTA comparative study of 1.4nm tobermorite, jennite, gyrolite, xonotlite, hillebrandite, C-S-H (C/S = 1.5), hydrated Portland cement (w/c = 0.40) and porous Vycor glass was conducted. The pure calcium silicate phases represented layered silicate systems with variations in the degree of cross-linking as determined from the Q^3 peaks in the ^{29}Si NMR spectra e.g. gyrolite had strong Q^3 peaks whereas C-S-H had no Q^3 peaks. It is argued that the contribution of interlayer water to the stiffness of the layered silicate materials is dependendent on the extent of cross-linking between the silicate sheets. It is also suggested that the interlayer water has an attenuating effect on the bonds associated with cross-linking when they are subjected to shear stress. The systems that exhibit no cross-linking have greater flexibility and an increased tendency toward structural collapse. Removal of water from a microporous material e.g. Vycor glass does not appear to affect its structural integrity.

The Structural Role of Water in Layered Calcium Silicate Hydrates

P. Pourbeik, J. J. Beaudoin, L. Raki , R. Alizadeh

(To be submitted, February 2015)

Abstract

A dynamic mechanical thermo-analysis (DMTA) study of seven layered calcium silicate hydrate systems was conducted to elucidate the structural role of interlayer water on the engineering performance of these materials. The systems were: 1.4nm tobermorite; jennite gyrolite, xonotlite; hillebrandite; C-S-H (C/S = 1.5); hydrated Portland cement (w/c ratio = 0.40). In addition the DMTA behavior of Vycor glass (a microporous silicate) was determined. The structural response (i.e. change in the value of storage modulus (E') and internal friction (tan ∂)) on removal of water from the layered silicates during the test was evaluated. It is argued that the contribution of the interlayer water to the stiffness of the layered silicate materials is dependent on the extent of cross-linking between silicate sheets. It is also argued that interlayer water may have an attenuating effect on the bonds associated with cross-linking including Si-O-Si bonds when they are subjected to shear stress. A comparison of the DMTA results for the layered silicates studied with those for hydrated cement paste suggests that the C-S-H in the latter behaves as a layered silicate and that water has a structural role.

Introduction

Hydrated Portland cement is the primary binding phase in conventional cement-based construction materials including concrete. Calcium-silicate-hydrate (C-S-H) is the principal reaction product in the cement-water system. Several descriptors of engineering performance (e.g. strength and modulus of elasticity) are attributed to the behavior and characteristics of C-S-H. Numerous physico-chemical models for the structure of hydrated cement paste have been developed and discussed extensively in the literature for more than half a century [1-5]. Microstructural descriptions based on these models vary from colloidal in nature to layered-like structures [1, 2].

Water is also an important phase that affects the structural integrity and volume stability of these hydrates. The state of water and its location in the hydrate structure (gel-pore versus interlayer water) has been the subject of considerable debate [6].The authors argue that interlayer water has a major structural role in engineering performance and consider this water to be a constituent of the 'solid' C-S-H phase. Early evidence of the structural characteristics of interlayer water in hydrated cement paste was provided by the modulus of elasticity isotherms of Sereda et. al. [7]. The isotherms exhibited large primary and secondary hysteresis. The modulus was found to increase on adsorption by as much as 100% as the humidity increased from 50 to 100%.The increase was attributed to the stiffening effect of the water. Feldman also observed that the magnitude of the modulus was dependent on the stress level and its effect on the proximity of the silicate sheets in the 'dry-state' as deduced from experiments on compacted powders of hydrated cement [8]. Alizadeh et al conducted dynamic mechanical analysis (DMA) experiments on phase pure C-S-H. They observed

cyclic behaviour (decreases and increases) with respect to the storage modulus and its dependence on moisture loss from the 11% RH position [9].This behaviour was explained in terms of the structural role of interlayer water and the coupled effects of its loss on possible cross-linking and interactions of interlayer calcium ions with the silicate sheets.

The current study explores further the coupled behaviour of the structural aspects of interlayer water with the extent of cross-linking between the silicate layers. Dynamic mechanical thermo-analysis (DMTA) experiments (from 25^{o}C to 300^{o}C) using several layered silicate phases were performed. These included the high temperature phases gyrolite, xonotlite and impure hillebrandite containing 1.1 nm tobermorite. In addition the mechanical behaviour of phase pure C-S-H (C/S = 1.5), 1.4 nm tobermorite, jennite and well hydrated Portland cement paste (w/c=0.40) were investigated. These phases were chosen as they collectively have a wide variation in Q^1, Q^2 and/or Q^3 silica sites determined from ^{29}Si MAS NMR spectra. Silicates with Q^3 sites were of particular interest as they are indicators of cross-linking between the silicate sheets. Porous Vycor glass (a microporous silicate) was utilized as a reference material. Correlations were sought with the extent of changes in the DMTA parameters (E'-storage modulus and tan∂-internal friction) and the nature of the Si sites in the various silicate minerals initially conditioned at 11% RH as the temperature (and moisture-loss) increased.

The results of these experiments are reported in this paper. They are discussed in the context of the structural nature of interlayer water in layered silicates and hydrated Portland cement. Commentary on the relevance of the results as they pertain to both physico-chemical and composition-based models of Portland cement paste is given.

Experimental

Materials

Seven cementing systems were prepared: synthetic calcium-silicate-hydrate (C-S-H with C/S = 1.5)); 1.4nm tobermorite; jennite; gyrolite; xonotlite; hillebrandite and hydrated Portland cement paste (water/cement ratio = 0.40). In addition porous Vycor glass was used as a reference material.

C-S-H: synthetic C-S-H with C/S = 1.5 was produced from the pozzolanic reaction between CaO and amorphous silica in excess water. Calcium oxide was obtained by calcining reagent grade calcium carbonate at 900°C. Reactive silica (CAB-O-SIL, grade M-5 from Cabot Corporation, USA) was heated at 110°C to remove any surface adsorbed water. Distilled water was de-aired and used for the reactions. All materials were kept sealed in N_2 purged bottles until they were used. The reaction period was 6 months. The material was then filtered and dried under vacuum for 4 days at room temperature. The dried C-S-H was stored in nitrogen purged glass vials before the experiments. Characterization of these materials by X-ray diffraction (XRD) and thermal methods gave results directly comparable to C-S-H (I) as reported by Taylor [10].

1.4nm tobermorite: the reactants (CaO and SiO_2) were prepared as described above. The C/S ratio was 0.9. The reactants were placed in a high density polyethylene bottle mixed in excess deionized water (water/solids = 11) and maintained at 80 °C using a heating wrap. The mixture was continuously agitated with a magnetic stirrer for a period of 4 months. The XRD spectrum and TGA curve were similar to those obtained by Yu and Kirkpatrick [11].

Jennite: the reactants (CaO and SiO_2) were prepared as described above. The C/S ratio was 1.4. The reactants were placed in a high density polyethylene bottle mixed in excess deionized water (water/solids = 11) and maintained at 80 °C using a heating wrap. The mixture was continuously agitated with a magnetic stirrer for a period of 4 months. The XRD pattern was similar to that obtained by Yu and Kirkpatrick [11], Gard and Taylor [12] and Hara and Inoue [13]. The TGA curve matched that published by Yu and Kirkpatrick [11].

Gyrolite: The reactants (CaO and SiO_2) were prepared as described above. The C/S ratio was 0.66.The reactants were mixed in excess deionized water and hydrothermal synthesis was carried out in saturated steam at 216°C for 6 days. The XRD pattern was similar to that published by Heller and Taylor [14] and Siauciunis and Baltakys [15]. The ^{29}Si CP MAS NMR spectrum was similar to that published by Bell et. al. [16]. It was obtained at 5MHz with a magnetic field of 4.7T. Details are given in the discussion of results. The gyrolite product is considered to be relatively pure. The BET nitrogen surface area was 21.3 m^2/g.

Xonotlite: The reactants (CaO and SiO_2) were prepared as described above. The C/S ratio was 1.0. The reactants were mixed in excess deionized water and hydrothermal synthesis was carried out in saturated steam at 250°C for 6 days. The XRD pattern was similar to that published by Heller and Taylor [14] and Noma et. al. [17]. The ^{29}Si CP MAS NMR spectrum was similar to that published by Bell et. al. [16] and Noma et. al. [17]. It was obtained at 5MHz with a magnetic field of 4.7T. Details are given in the discussion of results. The xonotlite product is considered to be relatively pure. The BET nitrogen surface area was 49.2 m^2/g.

Hillebrandite: The reactants (CaO and SiO_2) were prepared as described above. The C/S ratio was 2.0. The reactants were mixed in excess deionized water and hydrothermal synthesis was carried out in saturated steam at 250°C for 4 days. The reaction product was not pure as it also contained some 1.1 nm tobermorite. This was confirmed by XRD analysis. Nevertheless it was considered useful to study the mechanical behavior of this mixed product given the objective to elucidate the structural role of water in layered silicates. The ^{29}Si CP MAS NMR spectrum exhibited a large Q^2 at -85.8 ppm as expected. It also had a small Q^1 peak. Details are given in the discussion of results. The hillebrandite will be designated hillebrandite* to indicate that it is not pure. The BET surface area was 28.1m^2/g.

Vycor Glass: This material is a microporous glass containing approximately 96% SiO_2. It has a porosity of about 28%.The internal surface area is about150 m^2/g. It has often been used as a surrogate reference material for studies of physico-chemical phenomena occurring in hydrated Portland cement paste [18].

Portland Cement Paste: The Portland cement paste (made with Type I Portland cement) was prepared using a water/cement ratio of 0.40. Rectangular prisms (250 x 100 x 12mm) were cast. The samples were vibrated and stored in a moist curing room for 24 h. They were then demoulded and curing was continued for two months in a saturated lime solution. Thin slices (1 x 12 x 60 mm) were cut from the paste prism using an Isomet diamond saw. Selected slices were also ground into a fine powder for fabrication into compacted specimens.

Humidity Conditioning

Specimens for all seven cementing systems were conditioned for 3 weeks at 11%RH in vacuum desiccators containing saturated lithium chloride solution. The powders were conditioned at 11%RH before compaction and for a few days after compaction. Theoretically there is a monolayer of water on the surfaces of the particles in addition to interlayer water at this humidity. The Vycor glass specimens were also conditioned at 11% RH for several weeks.

Preparation of Compacted Specimens

Solid rectangular prism samples for all the powdered materials (from the seven cementing systems) were prepared by pressure compaction in steel moulds with a cross-section of 12.8 x 83 mm. The thickness of most of the prism samples was approximately 1mm. The thickness of each sample was measured to 0.1mm.Numerous studies on the use and validity of compacts as models for hydrated cement systems have been published [7,19-21].It has been shown that compacted specimens of powdered hydrated Portland cement have similar mechanical property-porosity relationships to that of the original hardened paste of the same material [7]. The porosity of compacted samples was determined using helium pycnometry as well as by calculation using published density values for the phase pure minerals. The calculation is made knowing the apparent volume and the solid volume of the sample. Porosity is varied by controlling the compaction pressure.

Vycor Glass Specimens

Prisms of Vycor glass were cut from 1mm thick glass sheets. The prisms had a geometry similar to that of the compacted cement mineral systems.

Thermogravimetric Analysis (TGA)

TGA experiments were performed using a TA Instruments SDT Q-600. Twenty five mg of sample were heated from ambient temperature to 1000°C at a rate of 10°C/min under a flow of nitrogen gas (10 ml/min).

Dynamic Mechanical Analysis (DMA) and Dynamic Mechanical Thermal Analysis (DMTA)

Principles

The dynamic mechanical analysis (DMA) method involves the application of an oscillating force to the sample and measurement of displacement [22].The elastic property obtained by DMA is referred to as the storage modulus (E'); it is analogous to the static modulus of elasticity. There is usually a time lag between the applied force and the resulting displacement. The time lag can be quantified in terms of a phase angle between the load and the displacement due to their ideally sinusoidal nature. The tangent of this angle (tan∂) represents the damping property of the material often referred to as internal friction.

The DMTA test

The samples were heated from 25°C to 300°C. Temperature was increased in increments of 2°C every 5 minutes. E' and tan∂ versus temperature curves were plotted. Each test took

about 11h and 45min.to complete. It is apparent that the DMTA tests are much less tedious and time consuming to perform compared to DMA tests at room temperature conducted on samples where moisture is removed in equilibrium steps. Mass-loss occurred during the DMTA test due to temperature increases. Temperatures associated with mass-loss or phase transition events for the pastes or the silicate minerals studied are well known and are referred to in the following sections.

Apparatus

The DMTA analysis was conducted using a Rheometrics RSA II instrument on all samples in this investigation. Tests were conducted in the three point bending mode. Specimens were rectangular beams (12.8mm x 83mm x 1mm thick). A very low amplitude oscillation was applied on the brittle, thin samples in order to prevent any damage or micro-cracking. This was confirmed by microscopic analysis after the experiment. Moreover, no decrease was observed in the E' value when a trial specimen was repeatedly subjected to the same loading procedure. Samples were tested at a frequency of 0.10Hz at a maximum strain level of 0.01% and an initial static load of 20g in order to ensure a good contact between the upper fixture and the surface of the specimen throughout the dynamic loading process. The induced stress was kept below 2MPa in order not to introduce any significant damage or micro-cracking to the sample. The original experiments were conducted in the frequency range from 0.10Hz to 10Hz. It was observed that the E' and tan∂-mass loss curves had similar features at all frequencies. They were more distinguishable, however, at 0.10Hz. Prior to conducting the experiments the calibration of the equipment was checked using standard weights and a steel bar.

Results and Discussion.

An understanding of the variability of elastic properties of cement-based materials with moisture content is important for designers concerned with volume stability issues related to concrete sustainability. Dynamic mechanical thermoanalysis (DMTA) methods have been shown by the authors to be useful in studying the dehydration characteristics of layered silicates including the detection of phase transformations [23]. Changes to the storage modulus (E') and internal friction (tan∂) of these systems as a function of temperature can provide a link between engineering performance and nanostructural modification. This includes information relating the loss of surface, interlayer and constitutional water to engineering behavior. Evaluation of the latter included an assessment of E' and tan∂ versus temperature curves for the following layered silicates: gyrolite, xonotlite, impure hillebrandite containing 1.1 nm tobermorite, 1.4nm tobermorite, jennite, C-S-H (C/S = 1.5). In addition DMTA curves for hydrated Portland cement paste and porous Vycor glass were examined. Vycor glass contains primarily micropores and was used as a reference material. All samples were conditioned to 11% RH prior to the DMTA tests. There is no pore water in these samples as there is only a monolayer of surface water and interlayer water present at this humidity. The Vycor glass which is not a layered material contains no interlayer water. The following is a detailed account of this assessment.

E' versus temperature(25-100°C)

(i) gyrolite, xonotlite, 1.4nm tobermorite and Vycor glass

The E' values for both gyrolite, xonotlite, tobermorite and Vycor glass change very little in this temperature range (Figure 1(a)). There is a small decrease of about 0.5 GPa for gyrolite

and xonotlite, 1.5 GPa for tobermorite and nearly zero for Vycor glass. These values are relatively minor compared to the other layered silicate materials studied and reflects in this case the relatively minor contribution of the interlayer water to the overall stiffness of these 'high-temperature' silicates. This is a consequence of the inherent rigidity due to cross-linking of the silicate layers of these silicate systems (see description of NMR spectra) in the previous section.

The structurally robust layers of gyrolite were described by Mamedov and Belov [24] as being built of Ca octahedral layers with single layers of Si tetrahedra between which form eight and five-fold rings. Gard et.al. proposed a similar structure to reyerite consisting of Ca octahedral layers with single layers of interconnected Si tetrahedral between, which form six-fold rings [25]. Merlino [26] determined that gyrolite consisted of different layers: a centrosymmetric layer consisting of two types of six-membered silicate rings; a double tetrahedral silicate layer containing two types of six-membered rings; an octahedral calcium layer containing calcium octahedral combined by the edge; interlayer space containing Ca^{2+} and H_2O. Heller and Taylor [14] estimated that approximately three quarters of the total water is lost at 450°C with only a slight effect on the X-ray pattern. This was consistent with the author's X-ray analysis. The basal-spacing was maintained over the temperature range of the DMTA test. This suggests that the gyrolite structural framework was not disturbed during the removal of the interlayer water as the temperature increased.

The ^{29}Si CP MAS NMR spectrum for gyrolite (not shown) has several peaks representing Q^3 sites.It is similar to that reported by Bell et. al.[16].The spectrum has Q^3 peaks at- 99.2,-95.8,-93.4 and -91.4 ppm. The Q^2 peak at 85.8 ppm was considered by Bell et.al. to be a real feature

of the gyrolite structure. There also appears to be a small Q^1peak at 79.9 ppm in both cases. This was attributed by Bell to the possible occurrence of C-S-H in the sample.

The crystal structure of xonotlite includes chains of SiO_4 tetrahedra in a double 'dreierketten' arrangement where the chains are branched at every third SiO_4 tetrahedron [16].The CP NMR spectrum for xonotlite produced in this study was also similar to that obtained by Bell et.al. [16]. Peaks at -86.9 ppm and -97.7 ppm show the presence of chain Q^2 and bridging Q^3 groups respectively. The author's CP ^{24}Si MAS spectrum, like theirs, exhibits a peak at -79.8 ppm. This was associated with discontinuities in the chain structure balanced by the presence of OH groups and a local deficiency in calcium. Churakov and Mandaliev [27] reported that silica defects in Q^3 sites were found to be more abundant compared to Q^2 tetrahedra. The paired substitutions in the silicate double chain at neighbouring Q^3 sites are energetically more stable than isolated Q^3 defects. The defects in the silicate chains of xonotlite offer structural channels accessible for diffusion of ions and water. The defect sites are also potential candidates for incorporation of foreign ions in the xonotlite structure. The rigidity of the silicate chains is only slightly affected by the removal of interlayer water due to the stabilizing effect of cross-linking at the Q^3 sites. The effect is similar to that for gyrolite. The magnitude of the stiffness for gyrolite however is about 2.5 times higher as a resuit of numerous defects in the xonotlite structure. The porosity of the compacted specimens in this case was similar for both systems (i.e. approximately 30%).

The 1.4nm tobermorite layer is comprised of a central Ca-O polyhedral sheet sandwiched between the single Si-O tetrahedral chains. The silicate chains have a dreierketten structure

with two tetrahedra (pairing) pointing to the CaO sheet and one tetrahedron (bridging) pointing to the interlayer space. Ideally each bridging tetrahedron has one SiOH bond. There is a decrease in E' of 1.4nm tobermorite over 3 distinct temperature ranges involving changes in slope as the temperature increases to about 100^{o}C.The removal of adsorbed water and some interlayer water occurs in the first temperature range (25-35 ^{o}C). The second range (35-60 ^{o}C) likely corresponds to further removal of interlayer water. Removal of a further amount of interlayer water and the conversion of 1.4nm tobermorite to the 1.2nm form occurs in the third temperature range (60-100 ^{o}C). The conversion to the 1.1 form (130-200 ^{o}C) will be discussed later. The CP ^{29}Si MAS NMR spectra obtained by Bell et.al. [16] show resonances at -85.8 and – 96.1 ppm indicating the presence of chain middle groups, Q^2, and branching sites, Q^3. They suggested that some Si-O-Si bridges are present in the tobermorite structure and that there is a close similarity to the structure of xonotlite. The small decrease in E' on removal of interlayer water (similar to that for gyrolite and xonotlite) would appear to be significantly influenced by cross-linking between silicate sheets.

It is instructive to examine the E' curve for the Vycor glass. There is virtually no change in E' (initially about 10GPa) over the entire temperature range. Vycor glass contains a micropore system with an average pore diameter of about 5 nm. This high surface area material (about 150 m^2/g) contains only a monolayer of water at 11%RH. The rigidity of this system is apparently not affected by loss of this water as it would have a negligible structural contribution to its elastic response to stress.

(ii)C-S-H, Hillebrandite* and Jennite

These three silicate systems contain no Q^3 peaks in their ^{29}Si NMR spectra [16]. In this study the hillebrandite* product, although not pure (it contained a small amount of 1.1nm tobermorite detected by X-ray diffraction) had a ^{29}Si CP MAS NMR spectrum (obtained by the authors) that had a small Q^1 peak at – 79.2 ppm in addition to the predominate Q^2 peak at -85.2 ppm. The NMR spectrum for jennite contains essentially a large Q^2 peak [28]. The NMR spectrum for C-S-H (C/S = 1.5) has a Q^1/Q^2 ratio>1.0 indicative of a significant number of structural defects due to missing bridging tetrahedra.

The decrease in E' with temperature for these silicate materials ranges from approximately 2.2-2.5GPa (Figure 1(b)). This is 4-5 times larger than is the case for the layered silicates that exhibited cross-linking (Q^3 sites). The decrease essentially terminates at about 65 ºC for C-S-H and hillebrandite and the rate of the decrease is significantly reduced for jennite. The E' values remain relatively constant up to 100ºC.

It is clear that the more flexible silicate layers are affected to a greater extent by the loss of interlayer water. Conversely the latter provides structural rigidity to these layered silicates as the interlayer water can be considered as part of the 'solid' hydrate. The formation of metajennite at temperatures above 85ºC appears to have a small stiffening effect due to a reduction in basal-spacing (1.06 to 0.86nm) and an increase in density from 2.33 to 2.62 g/cm^3 counteracting any increase in porosity due to the latter.

E' versus temperature (100- 300 °C*)*

(i) gyrolite, xonotlite, 1.4nm tobermorite and Vycor glass

The E' value of gyrolite actually increases by about 1.5GPa (Figure 2(a)) in this temperature range. The mass-loss (from 11%RH) due to the removal of water increases by about 4% as determined by TGA analysis. The increase in E' despite virtually no change in the x-ray basal-spacing may be due to continued loss of interlayer water, interactions of interlayer calcium ions with the silicate sheets and stiffening effects resulting from possible variation in stacking due to moisture loss.

The E' value of xonotlite decreases by a very small amount. This reflects the rigidity of the silicate layers due to cross- linking despite the presence of a relatively high number of defects .The mass-loss in this temperature region is small (about 0.75%).

The E' value for 1.4nm tobermorite also decreases by a very small amount (about 0.40GPa). This behaviour is accompanied by conversion to the 1.1nm form (130-200^{o}C) and a transformation to the 9.6nm form (at about 260^{o}C). The gradual decrease in basal-spacing coupled with possible interaction of the interlayer calcium ions with the silicate sheets could account for this small decrease. Cross-linking of the silicate sheets undoubtedly contributes to the structural integrity of the layers.

The E' value of the Vycor glass remains essentially constant throughout the entire temperature range. The water present in the micropores evidently has little effect on the structural integrity of the porous body.

(ii)C-S-H, Hillebrandite* and Jennite

The DMTA results are presented in Figure 2(b).The C-S-H (C/S = 1.5) system exhibits a small increase in the E' value (0.40 GPa) followed by a small decrease (0.50 GPa) in the value of E'. The increase (shallow peak) is in the temperature range 150-200^{o}C. The hillebrandite* curve exhibits a larger maximum E' value (an increase of approximately 1.5 GPa) at about 210^{o}C. These increases are possibly associated with the loss of some chemically bound water.The TGA results of Yu and Kirkpatrick indicate that chemically bound water is continuously removed as 1.4nm tobermorite, jennite and C-S-H are heated from 100^{o}C to 1000^{o}C [11].

Tan∂ versus temperature(25-100°C)

(i) gyrolite, xonotlite, 1.4nm tobermorite and Vycor glass

The t*an∂* versus temperature curves for both gyrolite and xonotlite exhibit a continuous decrease in the t*an∂* values throughout this temperature region (Figure 3(a)). The magnitude of these changes is relatively large (0.025 for gyrolite and 0.015 for xonotlite). The nanostructure of the silicate layers for both of these minerals was described in detail in the previous section in which the E' results were discussed. It was noted that the extent of cross-linking was effective in maintaining the structural stiffness of these systems as interlayer water was removed. Removal of this water however also appears to increase the ability of the silicate layers comprising the nanostructure of these minerals to resist shear or translation of the silicate sheets relative to one another manifested as a decrease in internal friction. It is

suggested that the interlayer water may have an attenuating effect on the bonds associated with cross-linking including Si-O-Si bonds that are subjected to shear stresses.

The t*an∂* versus temperature curve for 1.4nm tobermorite (unlike the curves for gyrolite and xonotlite) exhibits three distinct peaks at about 35, 65 and 85ºC in this temperature range (Figure 3(a)). The first two peaks are associated with the removal of surface and interlayer water. This process results in an increase in internal friction as the silicate sheets come closer together. The decrease in t*an∂* following the peak maxima is possibly due to cross-linking effects and the interaction of Ca^{2+} ions with the silicate sheets. It is noted that in this system the extent of cross-linking as detected by the Q^3 silicon site in the ^{29}Si MAS NMR spectrum of Yu and Kirkpatrick [11] is significantly less than that for gyrolite and xonotlite. The second maximum arises due to the continued removal of interlayer water. The peak at 85ºC is likely associated with the conversion of 1.4nm tobermorite to the 1.2nm form. The corresponding increases in density and porosity and any additional removal of interlayer water are likely contributors to the increase in internal friction. The following decrease is again possibly due to ionic-covalent interactions between the sheets as the basal-spacing is reduced with further increments of interlayer water removal. The changes in internal friction of tobermorite (despite the small amount of cross-linking of the silicate chains) due to the removal of interlayer water are more akin to those of C-S-H. This will be discussed later.

The t*an∂* versus temperature curve for the porous vycor glass sample remained relatively constant in this temperature range. Removal of micropore and surface water from this system

apparently had no effect on the value of the internal friction. The ability of the porous glass to resist shear stresses was apparently not changed.

(ii)C-S-H, Hillebrandite* and Jennite

The t*an∂* versus temperature curve for C-S-H (C/S = 1.5) in this temperature range is shown in Figure 3(b). The curve exhibits a low temperature peaks at about 55^{o}C and a plateau between 65 and 85^{o}C. The occurrence of these two thermal events is due to the removal of interlayer water occurring with the continuous collapse of the silicate structure. The translation of silicate sheets relative to one another is facilitated by the removal of this structural water. The decrease in internal friction following the first peak is likely a result of cross-linking between the silicate layers (as the silicate sheets collapse into closer proximity) and a concomitant increase in the degree of polymerization. An increase in the interaction of calcium ions with the silicate sheets may contribute to this effect. The damping behavior of C-S-H may be reduced by bridging of the C-S-H and an increase in the number of strong bonds (either Si-O-Si or ≡ Si-O-Ca^{2+}).Subsequent increase in damping as more interlayer water is removed may be due to sliding of the silicate sheets as they come closer together. The decline after the second event or plateau is attributed to the remaining amount of interlayer water and possibly some constitutional water at higher mass-loss. It is emphasized that the C-S-H solid is constantly changing during the test and that the restraint on particle translation decreases the magnitude of internal friction.

It is noted that the ^{29}Si MAS NMR spectrum for the C-S-H system studied contains primarily Q^1 silicon sites as well as a lesser amount of Q^2 sites [29]. The C-S-H system studied therefore

contains a large number of defect sites i.e. missing bridging tetrahedra. It is noted that although the tobermorite spectrum (discussed in the previous section) exhibits mostly Q^2 sites with some Q^3 sites (indicative of some cross-linking) the t*an∂* versus temperature curves in this temperature range also exhibit cyclic behavior for the reasons cited above.

The hillebrandite* studied was impure and contained some crystalline 1.1nm tobermorite. The t*an∂* versus temperature curve in this temperature range was similar to that for gyrolite and xonotlite i.e. there was a continuous decrease in the t*an∂* value (Figure 3(b)). It is suggested that the tobermorite phase was able to constrain the translation of silicate sheets as interlayer water was removed from this composite system. Interlayer water apparently can attenuate the bonds in the solid phase that provide shear resistance.

The t*an∂* versus temperature curve for jennite contains three peaks (at 35, 50 and 75 ^oC) in this temperature region (Figure 3(b)). This is a similar pattern to that observed for the curves for C-S-H. The increase in t*an∂* from 25 to 35 ^oC is largely due to loss of surface adsorbed water and possibly some interlayer water. The increase from 35 to 50^oC is likely due to the removal of interlayer water. The decrease in t*an∂* from 50 to 75^oC may also be linked (as is the case for tobermorite) to the interactions of interlayer Ca^{2+} ions with the silicate sheets. There are no Q^3 signals observed in the ^{29}Si MAS NMR experiments unlike the case for tobermorite suggesting that any cross-linking of the silicate sheets may be minimal in the jennite system [11]. The small increase in t*an∂* leading to a maximum at 75^oC is possibly due to further removal of interlayer water and additional interaction of Ca^{2+} ions with the silicate sheets.

Tan∂ versus temperature (100- 300 °C)

(i) gyrolite, xonotlite, 1.4nm tobermorite and Vycor glass

The TGA determinations for gyrolite and xonotlite (Figure 4) indicate continued mass-loss in this temperature range due to dehydration and loss of compositional water. The mass-loss from the 11%RH condition was 3.80% for gyrolite and 1.45% for xonotlite. The t*an∂* versus temperature curves for gyrolite and xonotlite both exhibit peaks at about 220^{o}C (Figure 5(a)). There is an increase in internal friction beginning at about 125^{o}C until the peak maximum is reached followed by a continuous decrease up to 300^{o}C. This is attributed to loss of compositional water in this temperature range. The additional space created during dehydration facilitates translation of the silicate sheets and an increase in internal friction. The decrease in internal friction following the peak maximum is attributed to collapse of structure and a possible rearrangement of the stacking order of the silicate sheets.

The t*an∂* versus temperature curve for 1.4 nm tobermorite is distinctly different from the curves for gyrolite and xonotlite (Figure 5(a)). There is an increase in t*an∂* beginning at about 110^{o}C, reaching a maximum at 130^{o}C, and subsequently decreasing as the temperature increases to about 200^{o}C. The peak is associated with the transformation of 1.2nm tobermorite to the 1.1nm form. The increase in internal friction is apparently influenced by the increased porosity and removal of interlayer water in this temperature range. The decrease after the maximum may be due to additional cross linking and ionic-covalent interactions with the silicate sheets that may occur as the basal-spacing decreases. There is no dehydration peak at 220^{o}C as is the case for gyrolite and xonotlite. The latter minerals, as stated

previously, have strongly cross-linked silicate structures with virtually no basal-spacing change in the case of gyrolite.

The t*an∂* versus temperature curve for vycor glass undergoes very little change over the entire temperature range. Loss of micropore water from the glass has very little influence on the value of the internal friction.

(ii)C-S-H, Hillebrandite* and Jennite

The t*an∂* versus temperature curve for C-S-H (C/S = 1.5) is shown in Figure 5(b). A small increase in the value of t*an∂* occurs at about 150-175^{o}C possibly due to the loss of some chemically bound water. Coincidently there is also a peak at about 220^{o}C (as was the case for gyrolite and xonotlite) possibly due to the loss of constitutional water.

The curve for the impure hillebrandite* is similar to that for tobermorite and contains a peak at 130^{o}C that is likely associated with the phase transformation to the 1.1nm form of tobermorite as described in the previous section.

The jennite curve exhibits a large increase in t*an∂* between 100 and 145^{o}C associated with the formation of metajennite, the accompanying loss of 4 water molecules from the interlayer and a significant increase in density and porosity [11]. Further removal of 2 mol of water from metajennite in the temperature range 145 to 220^{o}C likely results in additional interactions involving interlayer Ca^{2+}.

Hydrated Portland Cement Paste

Details of the nanostructure of the C-S-H that comprises a major component of hydrated Portland cement have been the subject of considerable debate [6]. Cement paste has been described by some investigators as having the characteristics of a colloidal microporous gel [2,3]. Others consider cement paste to behave as a layered silicate material [1,4]. The DMTA evidence that follows would appear to support the latter.

The DMTA curves for hydrated Portland cement (w/c = 0.40) are presented in Figure 6. The features of these curves, in general, mimic those of the curves for synthetic C-S-H. There is an initial decrease in E' to about 65^{o}C followed by a more gradual decrease as the temperature is increased to about 200^{o}C. Tan∂ increases to a maximum at about 60^{o}C and then decrease4s to about 85^{o}C. This is followed by an inflection point at about 110^{o}C and subsequent decrease to 125^{o}C. Further heating results in a gradual (small) decrease.

The C-S-H in cement paste is nearly amorphous and incorporates in its structure elements such as aluminum. This may reduce the cross-linking potential and interaction of silicate sites in cement paste that contribute to an increase in stiffness of synthetic C-S-H [9]. Synthetic C-S-H (C/S = 1.5) displays only a small increase in stiffness following the large initial decrease. The E' versus temperature curve for this C/S ratio more closely approximates that for cement paste. The average C/S ratio in cement paste is about 1.7 [30].

The structural response (i.e. change in value of E' and tan∂) on removal of water from the layered silicates studied strongly suggests that the water removed has an integral structural

role in the stability of the material. Removal of micropore water from porous glass has virtually no effect on structural stability. It is suggested that these results support arguments that the C-S-H in hydrated cement, although highly disordered behaves as a layered material.

Summary and Conclusions.

It is argued that interlayer water has a structural role in all the silicate systems studied and contributes to the engineering performance of hydrated Portland cement-based materials. The magnitude of these contributions appears to be dependent on the structural stability of the silicate layers themselves. For example, the contribution to stiffness appears to be reduced significantly for silicate layers (specifically as it relates to gyrolite, xonotlite and 1.4 nm tobermorite) that are cross-linked as evidenced by Q^3 silicon sites in their ^{29}Si MAS NMR spectra. Cross-linking appears to have a stabilizing effect on potential changes to the rigidity of the system. Removal of water from silicates that contain only micropores does not appear to change the structural integrity of the material. The change in stiffness of the silicates with no cross-linking between their silicate sheets was significantly increased (i.e. about 4-5 times larger). The flexibility of silicate layers containing defects (i.e. missing bridging tetrahedra) is affected to a greater extent by the loss of interlayer water.

The ability of the silicate layers to resist shear (as evidenced by decreases in tan∂) is however significantly increased with the removal of interlayer water from strongly cross-linked silicates. Interlayer water may have an attenuating effect on the bonds associated with cross-linking including Si-O-Si bonds that are subjected to shear stresses. The systems that exhibit no cross-linking have greater flexibility and an increased tendency toward structural collapse.

This brings the silicate sheets into closer proximity and increases the tendency for the tan∂ curves to exhibit cyclic behavior i.e. increases and decreases in internal friction accompanying the removal of interlayer water. The removal of interlayer water is often transient as the collapse is irregular. Cyclic behavior of internal friction measurments can also result from phase changes and loss of constitutional water due to dehydration.

A first principles study by Shahsavari et. al. [31] of the interlayer interactions of tobermorite and jennite illustrated that layered materials are not necessarily soft in the interlayer direction. This is dependent on the interlayer distance and its effect on the relative magnitude of coulombic interlayer interactions and any shielding effects that interlayer ions and water molecules may have on the coulombic interactions. They concluded that water molecules in 1.4nm tobermorite and jennite have a structural role and are part of a Si(OH)-H_2O-Si(OH) bridge in the interlayer distance. These findings are compatible with the experimental studies reported here.

The changes in the engineering parameters of the silicate systems studied confirm that the interlayer water removed has a structural role in the performance of these materials. The similarity of these changes (particularly for silicates without cross-linked structures) with those for hydrated cement paste support the view that the C-S-H in hydrated cement paste behaves as a layered silicate. Removal of water from a microporous material e.g. Vycor glass does not appear to affect its structural integrity.

References

1. Feldman R. F., Sorption and length-change scanning isotherms of methanol and water on hydrated Portland cement, Vol. III, 53-56, 1968.

2. Powers T. C. and Brownyard T. L., Studies of the physical properties of hardened Portland cement paste-part 3: theoretical interpretation of adsorption data. J. Amer. Concr. Inst., 18(4), 469-504, 1946.

3. Jennings H. M., Refinements to colloid model of C-S-H in cement: CM-II. Cem. Concr. Res. 38, 275-289, 2008.

4. Daimon M., Abo-El-Enein S. A., Hosaka G., Goto S. and Kondo R., Pore structure of calcium silicate hydrate in hydrated tricalcium silicate, J. Amer. Ceram. Soc., 60(3-4), 110-114, 1977.

5. Richardson I.G. and Groves G.W., Models for the composition and structure of calcium silicate hydrate (C-S-H) gel in hardened tricalcium silicate pastes, Cem. Concr. Res., 22, 1001-1010, 1992.

6. Feldman R. F., Assessment of experimental evidence for models of hydrated Portland cement, Highway Res. Rec. No. 370, 8-24, 1971.

7. Sereda P.J., Feldman R.F. and Swenson E.G., Effect of sorbed water on some mechanical properties of hydrated Portland cement pastes and compacts, Proc. Symp. On Structure of Portland cement paste and concrete, Highway Research Board, Special Report 90, Washington D.C., 58-73, 1966.

8. Feldman R. F., Factors affecting the Young's modulus-porosity relation of hydrated Portland cement compacts, Cem. Concr. Res., 2(4), 375-386, 1972.

9. Alizadeh R., Beaudoin J. J. and Raki L., Mechanical properties of calcium silicate hydrates, Matls. and Struct., 44, 13-28, 2011.

10. Taylor H.F.W., Proposed structure for calcium silicate hydrate gel, J. Amer. Ceram. Soc, 69 (6) 464-467, 1986.

11. Yu P. and Kirkpatrick R. J., Thermal dehydration of tobermorite and jennite, Concr. Sci. Eng., 1, 185-191, 1999.

12. Gard J. A. and Taylor H. F. W., Calcium silicate hydrate (II) ("C-S-H(II)"), Cem. Concr. Res., 6, 667-678, 1976.

13. Hara N. and Inoue N., Formation of jennite from fumed silica, Cem. Concr. Res., 10, 677-682, 1980.

14. Heller L. and Taylor H.F.W., Crystallographic data for the calcium silicates, London, Her Majesty's Stationery Office, pp.79, 1956.

15. Siauciunas R.and Baltakys K., Formation of gyrolite during hydrothermal synthesis in the mixtures of CaO and amorphous SiO_2 or quartz, Cem. Concr. Res., 34, 2029-2036, 2004.

16. Bell G.M.M., Bensted J., Glasser F.P., Lachowski E.E., Roberts D.R. and Taylor M. J., Study of calcium silicate hydrates by solid state high resolution ^{29}Si nuclear magnetic resonance, Adv. Cem. Res., 3(9), 23-37, 1990.

17. Noma H., Adachi Y., Matsuda Y. and Yokoyama T., ^{29}Si and ^{1}H NMR of natural and synthetic xonotlite, Chem. Lett., 3, 219-220, 1998.

18. Feldman R. F., Length change-adsorption relations for the water-porous glass system to -40°C, Can. J. Chem. 48, 288-297, 1970.

19. Soroka I. and Sereda P.J., The structure of cement- stone and use of compacts as structural models, Proc. 5th Int. Symp. on the Chem. of Cem., Vol. 3., Tokyo, 67-73,1968.

20. Sereda P.J. and Feldman R. F., Compacts of powdered material as porous bodies for use in sorption studies, J. Appl. Chem., 13, 150-158, 1963.

21. Beaudoin J.J., Comparison of mechanical properties of compacted calcium hydroxide and Portland cement paste systems, Cem. Concr. Res., 13, 319-324, 1983.

22. Menard K. P., Dynamic Mechanical Analysis-A Practical Introduction, CRC Press LLC, Boca Raton, pp. 208, 1999.

23. Pourbeik P., Beaudoin J.J., Alizadeh R. and Raki L., Dynamic mechanical thermoanalysis of layered calcium silicate hydrates, J. Therm. Anal. Calorim., 118(1), 1-14, 2014.

24. Mamedov KH. S. and Belov N.V., the crystal chemistry of mica-like Ca-hydrosilicates: okenite, nekoite, truscottite, gyrolite, A new silica radical [Si_6O_{15}], Dokl. Akad. Nauk SSSR, 121, 720-723, 1958.

25. Gard J. A., Mitsuda T. and Taylor H.F.W., Some observations of Assarsson's Z-phase and its structural relations to gyrolite, truscottite and reyerite, Min. Mag. 40 (312), 325-332, 1975.

26. Merlino S., Gyrolite: its crystal structure and crystal chemistry, Mineralogical Magazine, 52, 377-387, 1988.

27. Churakov S.V. and Mandaliev P., Structure of the hydrogen bonds and silica defects in the tetrahedral double chain of xonotlite, Cem. Concr. Res., 38, 300-311, 2008.

28. Cong X. and Kirkpatrick R., ^{29}Si and ^{17}O NMR investigation of the structure of some crystalline calcium silicate hydrates, Adv. Cem. Bas. Mat., 3, 133-143, 1996.

29. Cong X. and Kirkpatrick R., ^{29}Si MAS NMR study of the structure of calcium silicate hydrate, Adv. Cem. Bas. Mat., 3, 144-156, 1996.

30. Taylor H.F.W., Nanostructure of C-S-H: current status, Adv. Cem. Bas. Mat., 1, 38-46, 1993.

31. Shahsavari R., Buehler M.J., Pellenq R. J.-M. and Ulm F.-J., First-principles study of elastic constants and interlayer interactions of complex hydrated oxides: case study of tobermorite and jennite, J. Amer. Ceram. Soc, 92(10), 2323-2330, 2009.

Figure Captions

Figure 1 (a). Storage modulus versus temperature (25-100°C): gyrolite, xonotlite,1.4 nm tobermorite and Vycor glass.

Figure 1 (b). Storage modulus versus temperature (25-100°C): C-S-H, hillebrandite* and jennite.

Figure 2 (a). Storage modulus versus temperature (100-300°C): gyrolite, xonotlite,1.4 nm tobermorite and Vycor glass.

Figure 2 (b). Storage modulus versus temperature (100-300°C): C-S-H, hillebrandite* and jennite.

Figure 3 (a). Tan∂ versus temperature (25-100°C): gyrolite, xonotlite,1.4 nm and Vycor glass.

Figure 3 (b). Tan∂ versus temperature (25-100°C): C-S-H, hillebrandite* and jennite.

Figure 4. TGA curves for gyrolite, hillebrandite* and xonotlite.

Figure 5 (a). Tan∂ versus temperature (100-300°C): gyrolite, xonotlite, 1.4 nm tobermorite and Vycor glass.

Figure 5 (b). Tan∂ versus temperature (100-300°C): C-S-H, hillebrandite* and jennite.

Figure 6. Storage modulus (E') and internal friction (tan∂) versus temperature: hydrated Portland cement paste (w/c = 0.40).

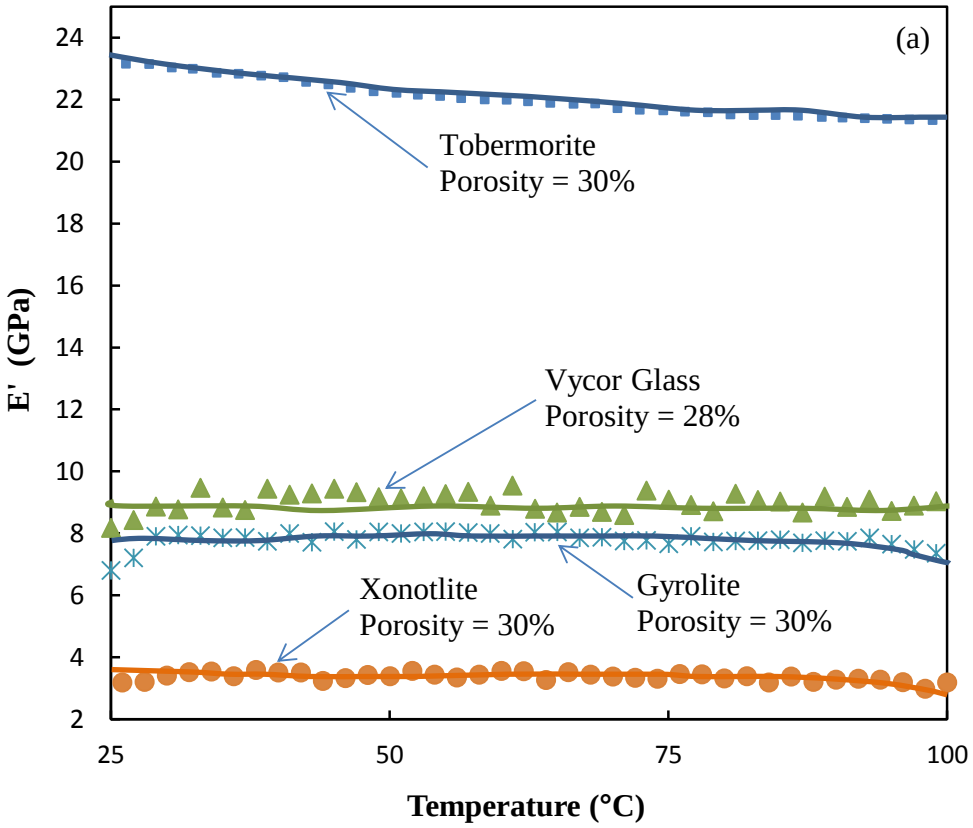

Figure 1 (a). Storage modulus versus temperature (25-100°C): gyrolite, xonotlite, 1.4 nm tobermorite and Vycor glass.

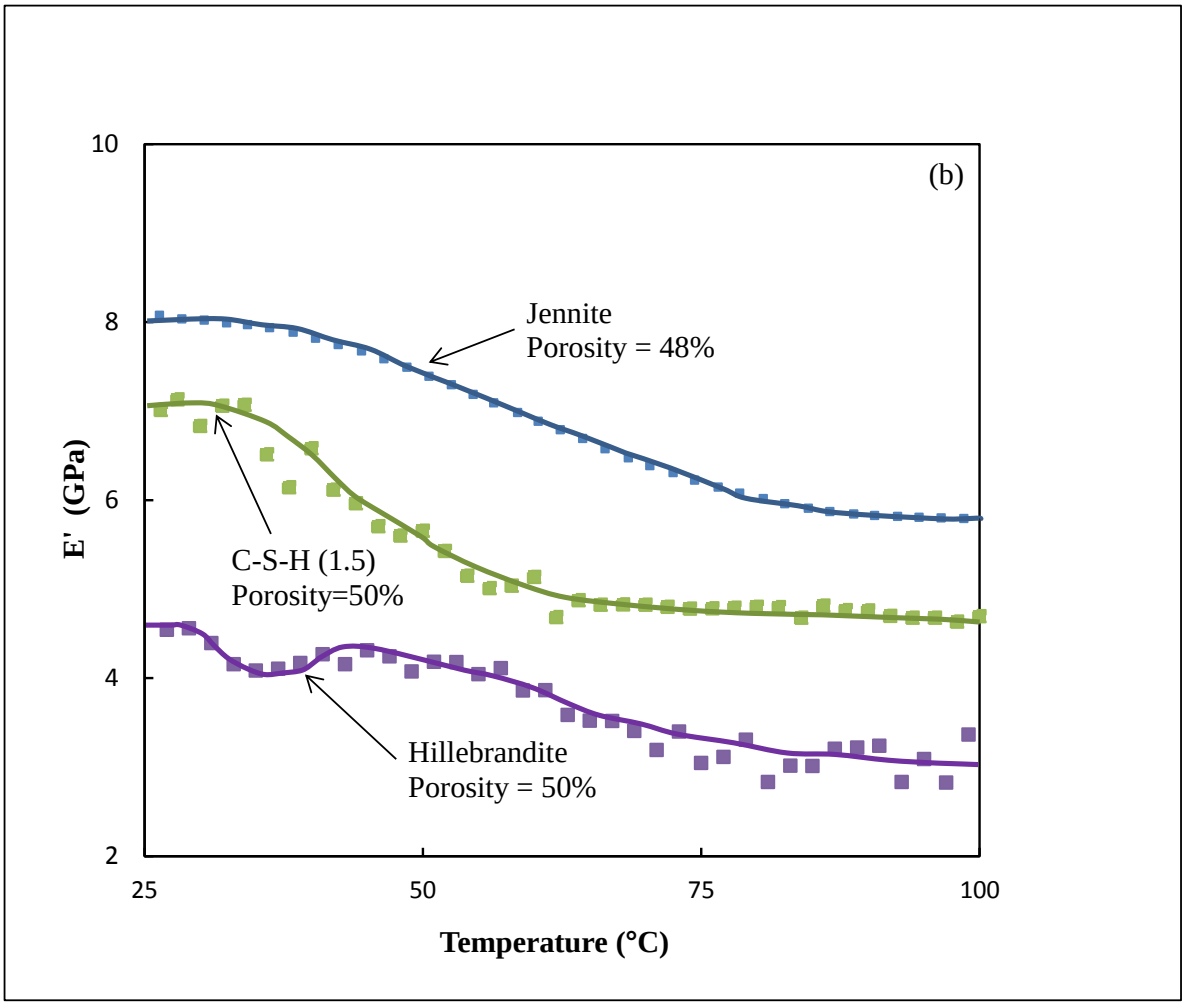

Figure 1 (b). Storage modulus versus temperature (25-100°C): C-S-H, hillebrandite* and jennite.

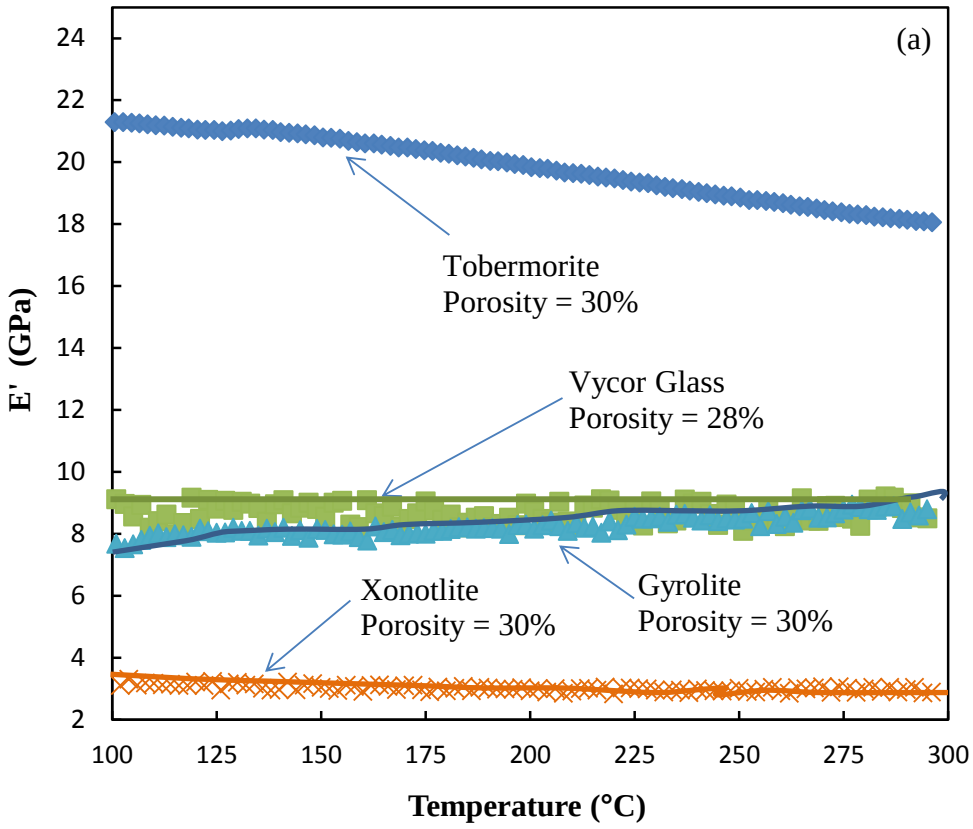

Figure 2 (a). Storage modulus versus temperature (100-300°C): gyrolite, xonotlite, 1.4 nm tobermorite and Vycor glass.

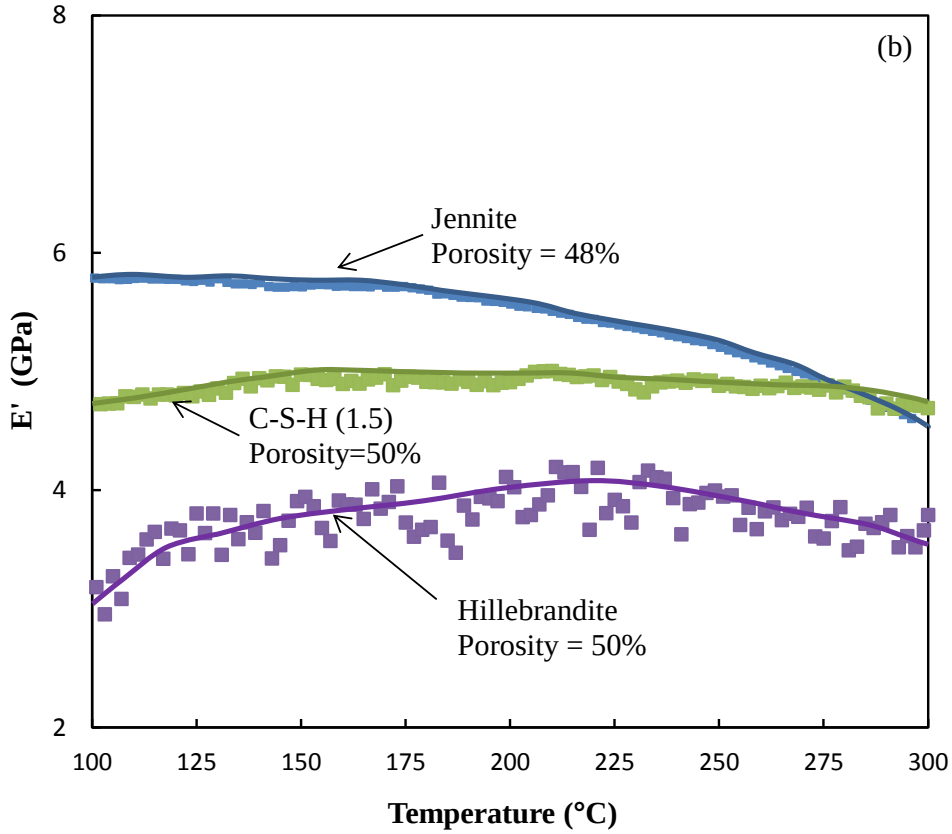

Figure 2 (b). Storage modulus versus temperature (100-300°C): C-S-H, hillebrandite* and jennite.

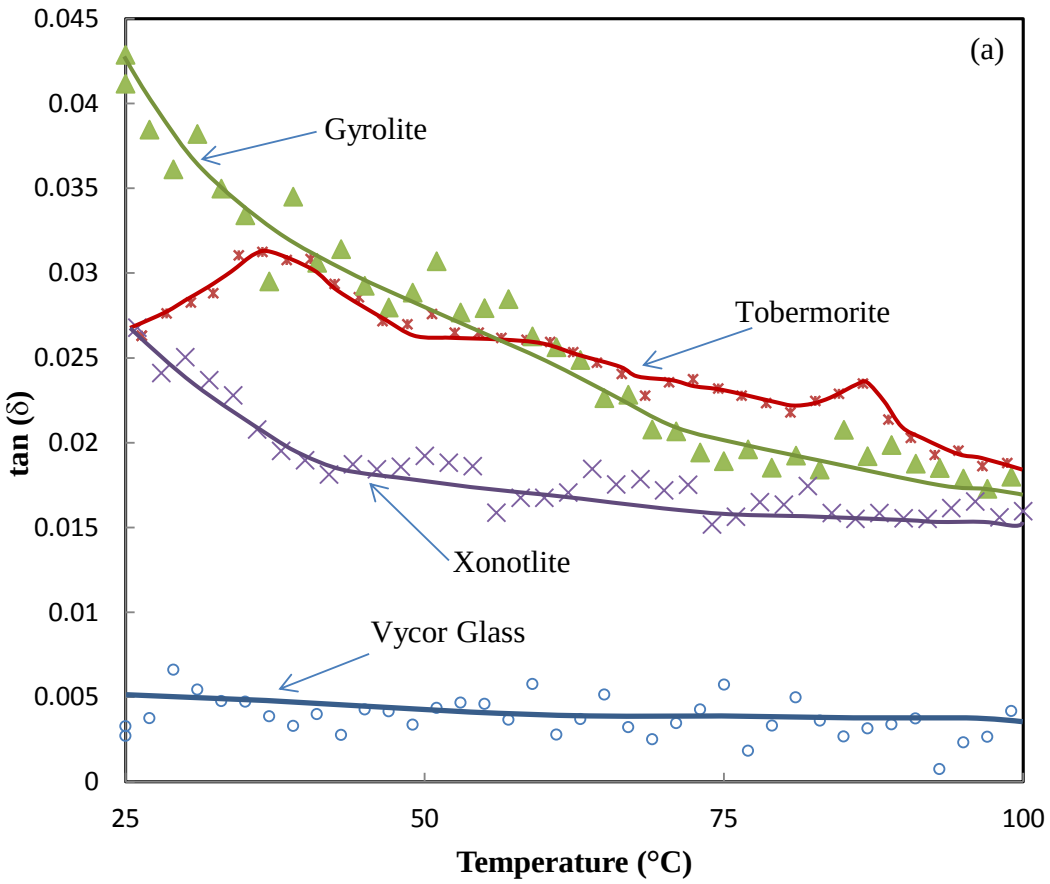

Figure 3 (a). Tan∂ versus temperature (25-100°C): gyrolite, xonotlite, 1.4 nm and Vycor glass.

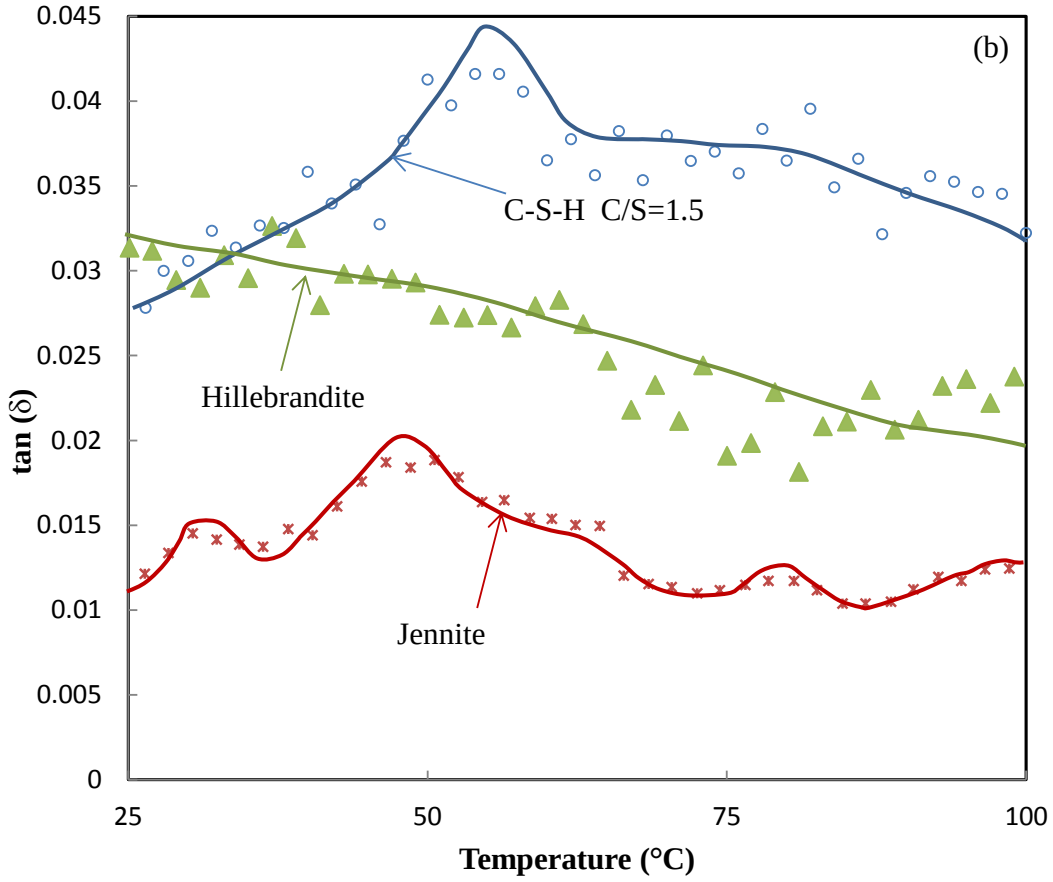

Figure 3 (b). Tan∂ versus temperature (25-100°C): C-S-H, hillebrandite* and jennite.

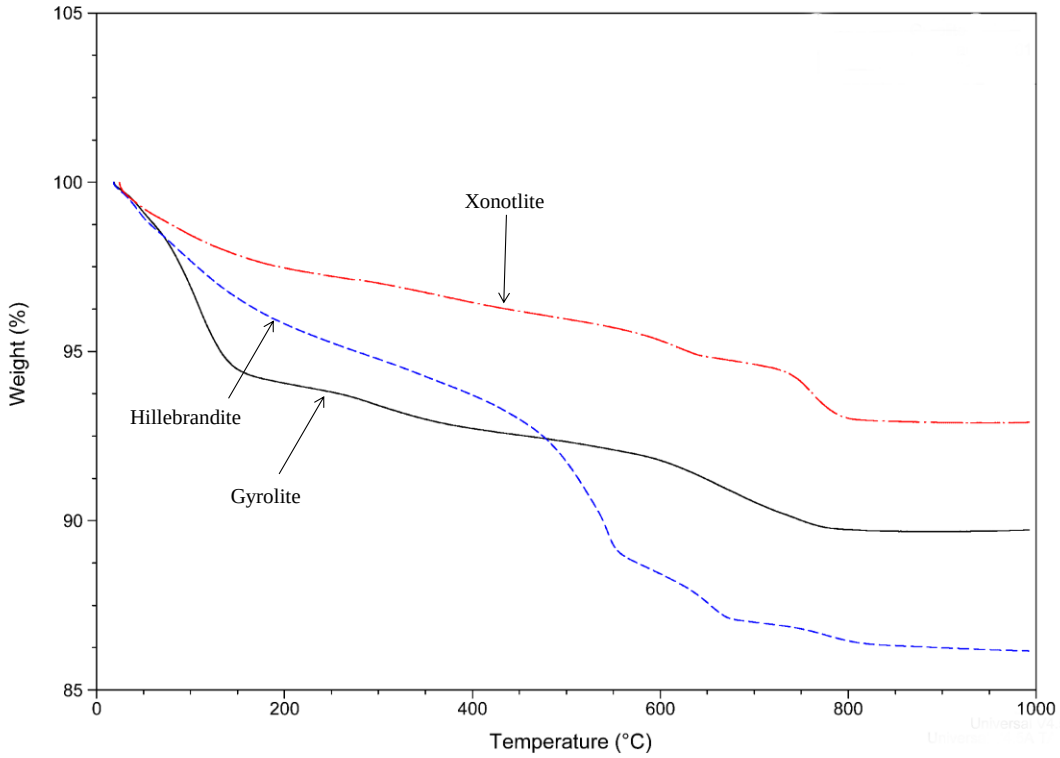

Figure 4. TGA curves for gyrolite, hillebrandite* and xonotlite.

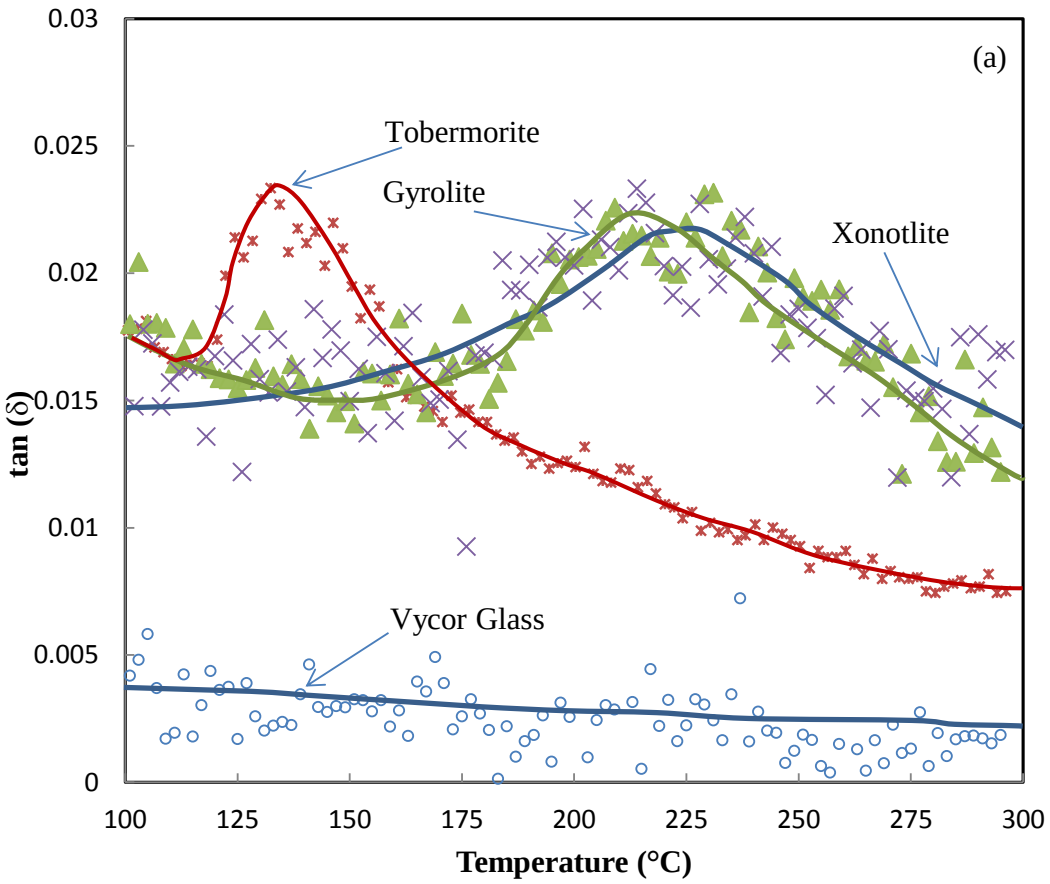

Figure 5 (a). Tan∂ versus temperature (100-300°C): gyrolite, xonotlite, 1.4 nm tobermorite and Vycor glass.

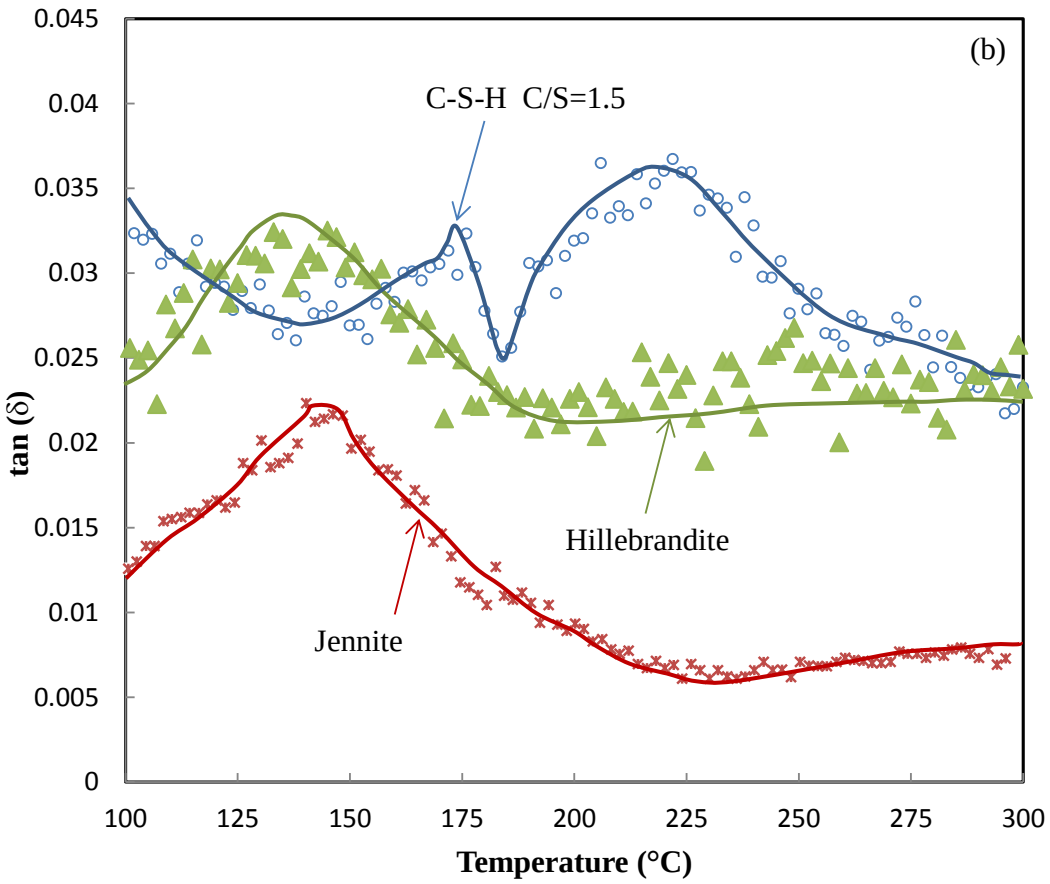

Figure 5 (b). Tan∂ versus temperature (100-300°C): C-S-H, hillebrandite* and jennite.

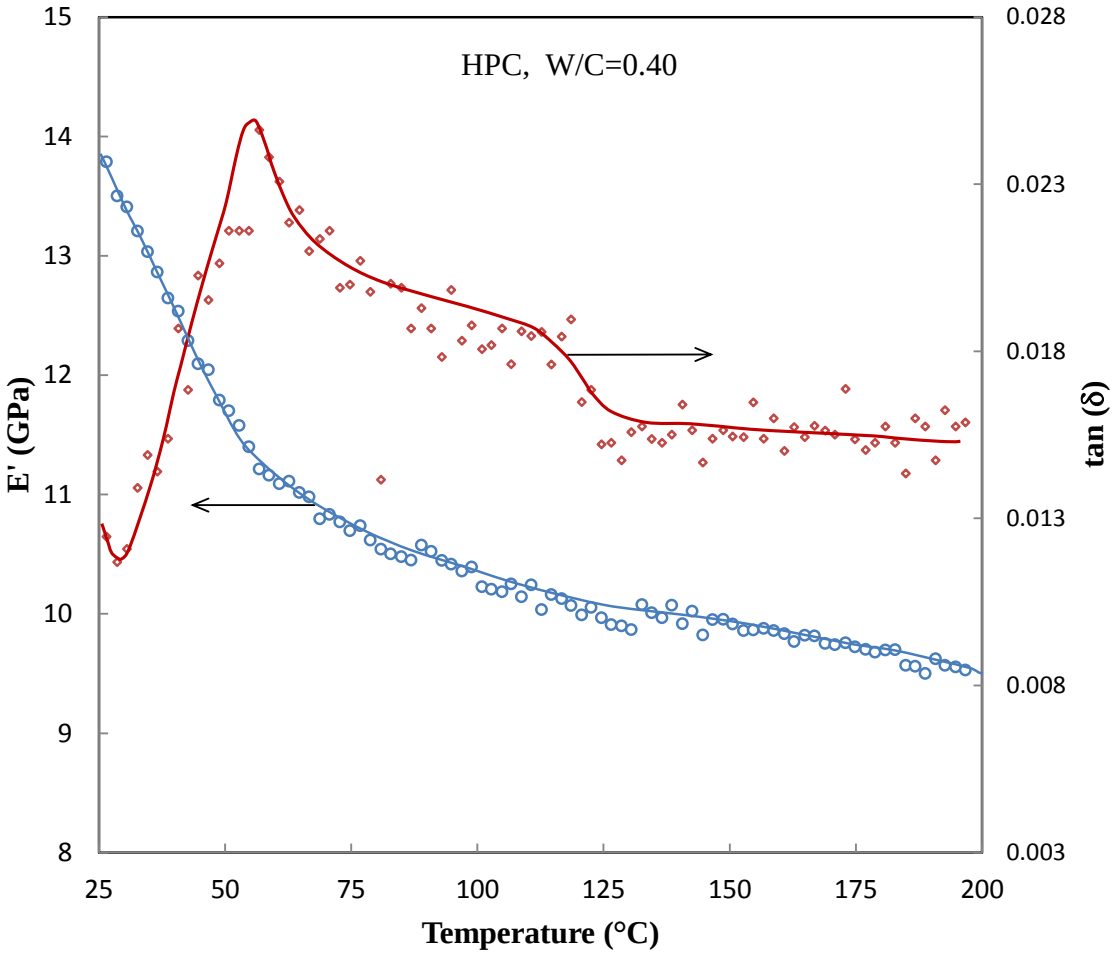

Figure 6. Storage modulus (E') and internal friction (tan∂) versus temperature: hydrated Portland cement paste (w/c = 0.40).

11.4 Paper 12: The Non-Uniqueness of the Modulus of Elasticity of Layered Calcium Silicate-Hydrates with Respect to Water Sorption

The DMA method was used to determine the modulus of elasticity of compacted powders of C-S-H, 1.4 nm tobermorite and jennite prepared using six different drying and fabrication methods. The non-uniqueness of the modulus of elasticity with respect to moisture content and the 'interlayer-environment' was demonstrated and discussed. The latter appears to be influenced by both the calcium-silicate-hydrate species and the effect of applied stress during the fabrication of compacted specimens. This appears to have a direct effect on the proximity of the layers and the probability of activating interactions within the 'interlayer-environment'. It is apparent that even the dry-state is not unique as the positioning of the layers relative to each other is dependent on the drying protocols. It appears that modelling the engineering behavior of hydrated Portland cement paste is complex and that behavioral aspects of all the layered silicates investigated in this study are germane.

The Non-Uniqueness of the Modulus of Elasticity of Layered Calcium-Silicate-Hydrates with Respect to Water Sorption

(to be submitted, February 2015)

P. Pourbeik, J. Beaudoin, R. Alizadeh and L. Raki

Abstract

The results of a study to examine the nanostructural factors that influence the modulus of elasticity of layered calcium-silicate-hydrates are reported. Compacted powders of C-S-H (C/S = 1.5), 1.4 nm tobermorite and jennite were prepared using six different drying and fabrication methods. Modulus of elasticity values were determined using the dynamic mechanical analysis (DMA) method. The non-uniqueness of the modulus of elasticity of the studied systems with respect to moisture and the 'interlayer-environment' is discussed. The ability of interlayer water to compensate (through its interaction with the silicate sheets) for the collapse of structure on drying differs for C-S-H, tobermorite and jennite. Behavior of all the layered silicates investigated in this study is considered germane to the behavior of hydrated Portland cement paste.

Introduction

The 'irreversible' nature of hydrated Portland cement with respect to its interaction with adsorbed and interlayer water has been well documented [1, 2]. This includes various types of isotherms with water as the adsorbate i.e. mass-change, length-change and mechanical property curves as functions of the partial pressure of water vapor. The isotherms generally display large primary and secondary hysteresis and the existence of scanning loops. Typical mass, length and modulus of elasticity water isotherms for cement paste are shown in Figure 1. The importance of this is seated in the observation that there is no unique moisture content at any given relative humidity and the concomitant implication that the solid hydrates are constantly changing their structure and properties. It is clear that the engineering behavior of cement-based materials is dependent on nanostructural changes (intrinsic to the C-S-H phase) which are themselves highly variable, path dependent (with respect to moisture) and influenced by applied stress [3, 4]. The fundamental reasons for this behavior are however not fully understood.

The mechanical properties of pure C-S-H phases have been studied intensively in recent years [5-9]. The storage modulus (E') obtained from DMA experiments, for example, has been shown to be dependent on both C/S ratio and to undergo significant change when the equilibrium moisture content is below 11% RH [5]. The oscillatory nature of the E' versus mass-loss curve can be explained in terms of nanostructural changes that occur when interlayer water is removed from the system. It is evident that decreases in E' can result from the absence of the 'stiffening' contribution of the interlayer water. Subsequent increases in E' actually occur on further removal of interlayer water. The mechanisms responsible for this

increase are of particular interest as they may provide a means of 'tailoring' engineering performance through control of the relative positioning of the calcium-silicate-hydrate sheets. Alizadeh et. al. attributed the increase in E' of C-S-H on drying to an increase in the degree of polymerization and possible cross-linking of the silicate chains [5,10]. Evidence for this was based on ^{29}Si NMR observations where there is an increase in the Q_2/Q_1 ratio and some indication of the presence of a Q_3 peak. There is also the possibility of strong 'surface-cation-surface' ionic-covalent interactions occurring as water is removed. Drying of the C-S-H produces more calcium containing ions that are dehydrated between the layers; these are likely to promote such ionic-covalent bonds that influence the elasticity of the C-S-H.

The authors have demonstrated the sensitivity of the C-S-H structure to water removal. They note that decreases in elastic modulus of C-S-H relative to 11% RH observed during a dynamic mechanical thermo-analysis (DMTA) test can be recovered subsequent to prolonged thermal treatment [11]. It was suggested that this 'regeneration' of stiffness was associated with bond formation between the interlayer Ca^{2+} and the silicate sheets as well as possible cross-linking.

It has also been observed that stiffness of hydrated Portland cement even in the dry-state is not unique [3]. For example drying cement powders prior to compaction into solid bodies as opposed to compacting powders conditioned to 11% RH followed by drying can result in a two-fold increase in modulus of elasticity for the former. It was concluded that high compaction pressures can force the layers of dried material closer together. This will be discussed in greater detail later as it is germane to this study.

It is suggested that the effect of stress and drying and how they affect the relative position of the silicate sheets varies with the type of layered silicate and the equilibrium state of the interlayer water present. A study was designed to assess the possibility of controlling the elastic behavior of layered silicates of interest in cement science (i.e. C-S-H, 1.4 nm tobermorite and jennite) through manipulation of their drying history at humidities below 11% RH. It was anticipated that interactions between the silicate sheets resulting from the experiments on the pure phases would vary but that an assessment of the ultimate potential of changing the 'interlayer-environment' to produce improved products might be possible. It was also hoped to obtain additional insight into the 'structural' nature of the silicate sheets themselves.

Experimental

Materials

Three calcium-silicate hydrate systems were prepared: C-S-H (C/S = 1.5); 1.4nm tobermorite; jennite.

C-S-H: synthetic C-S-H was produced from the pozzolanic reaction between CaO and amorphous silica in excess water. Calcium oxide was obtained by calcining reagent grade calcium carbonate at 900°C. Reactive silica (CAB-O-SIL, grade M-5 from Cabot Corporation, USA) was heated at 110°C to remove any surface adsorbed water. Distilled water was de-aired and used for the reactions. All materials were kept sealed in N_2 purged bottles until they were used. A C/S ratio = 1.5 was achieved by adjusting the stoichiometric amounts of the reactants. The reaction period was 6 months. The material was then filtered and dried under vacuum for 4 days at room temperature. The dried C-S-H was stored in

nitrogen purged glass vials before the experiments. Characterization of these materials by X-ray diffraction (XRD) and thermal methods gave results directly comparable to C-S-H (I) as reported by Taylor [12].

1.4nm tobermorite: the reactants (CaO and SiO_2) were prepared as follows. Calcium oxide was obtained by calcining reagent grade calcium carbonate at 900˚C. Reactive silica (CAB-O-SIL, grade M-5 from Cabot Corporation, USA) was heated at 110˚C to remove any surface adsorbed water. Distilled water was de-aired and used for the reactions. All materials were kept sealed in N_2 purged bottles until they were used. The C/S ratio was 0.9. The reactants were placed in a high density polyethylene bottle, mixed in excess deionized water (water/solids = 11) and maintained at 80 °C using a heating wrap. The mixture was continuously agitated with a magnetic stirrer for a period of 4 months. The XRD spectrum and TGA curve were similar to those obtained by Yu and Kirkpatrick [13].

Jennite: the reactants (CaO and SiO_2) were prepared as described above. The C/S ratio was 1.4. The reactants were placed in a high density polyethylene bottle mixed in excess deionized water (water/solids = 11) and maintained at 80 °C using a heating wrap. The mixture was continuously agitated with a magnetic stirrer for a period of 4 months. The XRD pattern was similar to that obtained by Yu and Kirkpatrick [13], Gard and Taylor [14] and Hara and Inoue [15]. The TGA curve matched that published by Yu and Kirkpatrick [13].

Fabrication of Compacted Specimens

Solid rectangular prism samples for all the phase pure powdered materials (from the three layered silicate systems) were prepared by pressure compaction in steel moulds with a cross-

section of 12.8 x 83 mm. The thickness of most of the prism samples was nominally 1mm but varied between the limits of 1-2mm.Numerous studies on the use and validity of compacts as models for hydrated cement systems have been published [16-18]. It has been shown that compacted specimens of powdered hydrated Portland cement have similar mechanical property-porosity relationships to that of the original hardened paste of the same material [4]. The porosity of compacted samples was determined using helium pycnometry or in the case of the phase pure minerals by calculation using published density values. *The porosity of all the phase pure samples tested in this study was about 30%.* The calculation is made knowing the apparent volume and the solid volume of the sample. Porosity is varied by controlling the compaction pressure.

Humidity Conditioning and Drying

Specimens of powders or compacts for the layered silicate systems were conditioned for several days at 11%RH in vacuum desiccators containing saturated lithium chloride solution. The powders were conditioned at 11%RH before compaction and for a few days after compaction. Theoretically there is a monolayer of water on the surfaces of the particles in addition to interlayer water at this humidity. Drying of powders or compacts was achieved in a vacuum vessel wrapped with a heating tape.

Preparation of Compacts for DMA Testing

The program comprised six pre-test sample treatments that were followed prior to the DMA experiments: (1) compaction of powders conditioned at 11% RH; (2) drying (3h at 100°C) of compacts prepared as in treatment (1); (3) compact from step (2) re-wet at 11% RH; (4)

compact formed from dried powder (3h at 100°C); (5) compact from (4) re-wet at 11% RH; (6) compact formed from re-wetted dried powder i.e. powder re-wet at 11% RH.

Dynamic Mechanical Analysis (DMA)

The dynamic mechanical analysis (DMA) method involves the application of an oscillating force to the sample and measurement of displacement [19].The elastic property of interest that was obtained by DMA is referred to as the storage modulus (E'); it is analogous to the static modulus of elasticity. In a DMA experiment there is usually a time lag between the applied force and the resulting displacement. The time lag can be quantified in terms of a phase angle between the load and the displacement due to their ideally sinusoidal nature. The DMA analysis was conducted using a Rheometrics RSA II instrument on all samples in this investigation. The frequency range was 0.1 to 10.0 Hz. Results are reported at a frequency level of 0.10Hz.

Results and Discussion

The structural sensitivity of interlayer water present in the C-S-H formed from the hydration of Portland cement and the concomitant bonding environment of the silicate sheets has a significant effect on the engineering behavior of cement paste [3] Removal of interlayer water can result in ionic-covalent interactions, cross-linking and increases in the degree of polymerization of the silicate chains. In this context a brief discussion of the effects of drying on the structural stability of C-S-H in cement paste is warranted. Feldman demonstrated using a vacuum electro-balance and thermal balance techniques that vacuum degassing cement paste (prepared conventionally at w/c = 0.50 and hydrated 1 year or using bottle-hydrated

cement hydrated 4 months at w/c = 5.0) at 85°C for 3h produced the same result for the non-evaporable water content as the conventional 'd-drying' procedure (i.e. drying to equilibrium at the vapor pressure of dry-ice at -79°C or 5 x 10^{-4} mm Hg) [1]. D-drying has been referred to as 'hard-drying' and was considered by Brunauer et. al to be a state where no interlayer water was able to penetrate between the silicate layers on adsorption.[2] The sorption isotherms of Feldman for *both* these drying conditions were virtually identical qualitatively and quantitatively. They exhibited large primary and secondary hysteresis independent of the drying method. The significance of these two states of drying is that both conditioned the samples for the same nanostructural response to sorption re. the entry and exit of interlayer water and associated changes to the solid. It has been shown by three of the authors that the collapse of structure processes on the drying (from 11% RH) of synthetic C-S-H are similar to those that occur in hydrated Portland cement paste [20] Large decreases in the x-ray basal-spacing of C-S-H are shown to occur at about 5% mass-loss when collapse of structure is detected by helium-inflow characteristics of both paste and C-S-H systems. This suggests that nanostructural responses to drying of both systems have similarities. It however leaves open the question as to whether the combination of applied stress and drying (for example during compaction of hydrated powders) can alter the engineering response of the system and if the response is dependent on the sequence of these stimuli. Are synthetic layered calcium-silicate-hydrates uniquely sensitive to applied stress at the nanostructural level in a manner that affects engineering characteristics?

These nanostructural changes associated with interlayer water mobility are likely a root cause of the path dependence of changes in elastic properties with moisture content and the nature of interparticle contact in hydrated cement systems. A brief description of these phenomena

is provided with reference to the salient features of the work of Feldman using compacts of hydrated cement powders [3]. This will be followed by a presentation of the results of this study which focus on the transient elastic properties (sensitive to the interlayer water environment) of other layered silicates including C-S-H (C/S = 1.5), 1.4nm tobermorite and jennite.

Hydrated Cement Compacts

The behavior of interlayer water as a solid bridge between the layers of the calcium-silicate-hydrate phase in Portland cement paste was demonstrated by Feldman in his experiments on hydrated Portland cement compacts [3]. The cement paste powders (water/cement = 5.0) were hydrated 28 days, passed through a 100 mesh sieve and conditioned at 32% RH for several days. Two sets of compacts were produced. One set involved drying the conditioned powders at 85°C prior to compaction at a pressure of 550 MPa. The other set were compacted at 32% RH prior to drying at 85°C. The modulus of elasticity was shown to be dependent on the drying and compaction history. Compaction of dry powders brings the silicate layers into closer proximity than is the case for compaction at 32% RH. The structural role of water is emphasized when the first set of specimens is rewetted and the modulus of elasticity remains constant. This is followed by a significant decrease in the modulus value on re-drying, similar to those of the second set of samples. This result is interpreted as the ability of water to reenter the interlayer positions on re-wetting even though the layers are closer together than normal. The water appears to compensate for the decrease in elastic modulus when the layers move apart. A second removal of interlayer water from the first set of samples restores the layers to the original position for the second set of compacted samples. A second re-wetting of the first set of compacts increased the elastic modulus to the original high value. It is apparent

that the path dependence of elastic modulus on drying history and compaction pressure can result in at least three configurations for the silicate layers: (1) separated layers with water molecules occupying the interlayer positions; these molecules have a structural role resulting in a high value for elastic modulus (2) partial collapse resulting from removal of water from between the layers; a reduction in elastic modulus of over 50% can occur (3) silicate layers pressed closer together than in the second configuration resulting in an elastic modulus similar to that in configuration one.

C-S-H Compacts - C/S = 1.5

The C-S-H compacts were subjected to six different test treatments prior to the determination of the elastic storage modulus using the Dynamic Mechanical Analysis (DMA) method. The storage modulus values (E') at 25 °C are initially of particular interest. The six treatments were as follows: (1) compacts conditioned to 11%RH (2) compacts conditioned to 11% RH and subsequently dried for 3h at 100 °C (3) compacts prepared according to treatment (2) and rewet at 11% RH (4) compacts prepared from powder dried for 3h at 100 °C (5) compacts prepared according to (4) and rewet at 11% RH (6) compacts formed from rewetted (11% RH) dried powder. The E' values for C-S-H are 7.2, 7.0, 5.9, 8.0, 9.0, and 5.0 GPa respectively. The relative magnitude of the E' values is rationalized as follows:

(i) water replaced by drying at 100°C brings the silicate sheets closer together compensating for any loss in E' due to the removal of interlayer water (7.2 vs. 7.0 GPa)

(ii) re-wetting at 11% RH partially separates the layers without penetration of much interlayer water resulting in a decrease in E' (5.9 GPa).

(iii) compacts formed from dried powder yield an increase of 14% in the value of E' as the layers are brought into closer proximity compared to the case when compaction occurs at 11% RH (8.0 GPa).

(iv) re-wetting dried powder at 11% RH slightly stiffens C-S-H (about 12%) compensating for the close proximity of the layers (9 GPa). Only a small amount of interlayer water has re-entered at this point.

(v) second-drying of the re-wetted (11% RH) compacts of the dried C-S-H powder results in a significant decrease in stiffness. This is similar to hydrated cement paste where second-drying results in a collapse of structure and decrease in E'. The layers appear to be in their original relaxed position unlike that position which occurs as a result of compacting dry powder.

1.4 nm tobermorite

The tobermorite compacts were subjected to the first five treatments prior to the determination of elastic storage modulus. The E' values were 10.0, 11.5, 8.5, 14.0 and 7.8 GPa respectively. The relative magnitude of the E' values is rationalized as follows:

(i) tobermorite also compensates for the loss of interlayer water on drying at 100 °C bringing the sheets closer together resulting in about a 15% increase in E' (10.0 vs. 11.5GPa).

(ii) re-wetting decreases the stiffness because the drying at 100°C limits the re-entry of interlayer water but the perturbations at the ends of the layers (involving some

expansion) causes the stiffness of the layers to readjust without the compensating effect of the interlayer water (E' decreases from 11.5-8.5 GPa).

(iii) compacts formed from dried powder resulted in an increase in E' of about 40% compared to compacts pressed at 11%RH and then dried as the silicate sheets come into closer proximity when the former preparation method is used (14.0 vs 11.5 GPa).

(iv) re-wetting (at 11%RH) a compact formed from dried powder results in a significant decrease in stiffness E' to 7.8GPa. The collapse of structure cannot be compensated for by re-entry of interlayer water despite the possible occurrence of perturbations at the ends of the layers.

jennite

The jennite compacts were subjected to the same six treatments as were the C-S-H compacts prior to determination of the storage modulus, E'. The E' values were 11.0, 8.0, 12.0, 9.5, 11.8 and 7.5 GPa respectively. The relative magnitude of the E' values is rationalized as follows:

(i) Drying jennite at 100°C (from 11%RH) results in significant decrease in E' (11.0-8.0GPa) due not only to loss of interlayer water but also to a phase change to meta-jennite.

(ii) Re-wetting of meta-jennite increases stiffness as much of the interlayer water re-enters the system (8.0-12.0GPa).

(iii) Compacts formed from dried powder (essentially meta-jennite) exhibit an 18% increase in E' (9.5 GPa from 8.0GPa) compared to compacts dried after

compaction at the 11% RH condition. It is argued that this is a result of the silicate sheets being brought into closer proximity through dry compaction.

(iv) Re-wetting the compacts of meta-jennite (at 11%RH) produced by dry-compaction re-generates the value of E' (9.5-11.8GPa) likely because interlayer water re-enters the meta-jennite relatively easily at this stress state.

(v) second-drying of re-wetted compacts results in a significant decrease in the value of E' as was the case for the C-S-H compacts (11.8-7.5GPa). This is a reflection of the structural role of interlayer water in meta-jennite and the reduced role of irreversible drying effects in this system.

Drying of a C-S-H compact prepared from powder conditioned to 11% RH is unlike a Portland cement paste compact as it does not experience any significant loss in stiffness on first-drying. The interlayer water residing in the C-S-H sheets during compaction does not appear to restrict the sheets from coming into sufficiently close proximity to compensate for a decrease in the value of E'. Re-wetting then partially separates the layers resulting in a decrease in stiffness. Compaction of dried powder brings the layers into even closer proximity yielding slightly higher stiffness than compaction at 11% RH. Compaction of re-wetted dried powder followed by second-drying results in a small increase followed by a significant decrease in stiffness suggesting that the layers may now be in a relaxed position. It appears then that drying has a more pronounced effect on the nanostructure of synthetic C-S-H as the internal stress generated enhances the interactions within the interlayer-environment.

Drying a tobermorite compact prepared from powder conditioned to 11% RH is also unlike a Portland cement paste compact as like C-S-H it does not experience any significant loss in stiffness on first drying at 100°C. Re-wetting tobermorite at 11% RH also has a similar effect to that for C-S-H i.e. a decrease in stiffness. The stiffness of compacts formed from dried powder compared to compacts dried after compacting at 11% RH increases for all three systems i.e. C-S-H, tobermorite and Portland cement paste suggesting that in all these cases dry compaction brings the silicate sheets closer together. Unlike C-S-H, however, re-wetting tobermorite results in a significant decrease in E'. In the latter case the collapse of structure does not appear to be compensated for by interlayer water.

Drying of jennite at 100°C is complicated by a phase change to metajennite. The formation of metajennite is accompanied by an x-ray basal-spacing change from 1.06 to 0.86 nm. There is also a loss of 4 water molecules from the structural unit and a large change in density from 2.33 to 2.62 g cm^{-2} that occurs with an increase in porosity [21]. The decrease in E' on drying at 100°C may be due to both the loss of interlayer water and the phase transition. It is difficult to separate the two effects. The significant increase in stiffness on the re-wetting of metajennite (at 11% RH) is analogous to what occurs in the re-wetted compacted cement paste system (dry powder) following second-drying or the increase in stiffness of cement paste compacts prepared from powders conditioned at 11% RH, dried and rewet. The decrease in stiffness on the second-drying has similarities to the behavior of cement paste and reflects the structural role of interlayer water.

Concluding Remarks

The modulus of elasticity or stiffness of calcium-silicate-hydrate systems is not uniquely dependent on their moisture content. It is a function of their nanostructure and the 'interlayer-environment' including the proximity of the silicate sheets relative to one another. Interactions involving Ca^{2+} cations and possible cross-linking sites are likely to influence engineering behavior. In turn the structural role of interlayer water is related to these factors. The 'interlayer-environment' appears to be influenced by both the calcium-silicate-hydrate species and the effect of applied stress on the proximity of the layers and the probability of activating the interactions described above. The preparation protocols for the compacted specimens in this study were designed to stimulate the 'interlayer-environment' of the silicates studied through the application of stress in both the 'dry-state' and in a moisture state where the silicate surfaces contained a monolayer of adsorbed water and interlayer water between the layers. It appears that drying at 100°C enhances the interactions within the 'interlayer-environment' of both C-S-H and tobermorite (initially at 11% RH) to a greater extent than hydrated Portland cement paste. The ability of interlayer water to compensate (through its interaction with the silicate sheets) for the collapse of structure on drying differs for C-S-H, tobermorite and jennite. Increases in stiffness associated with the re-wetting of jennite are analogous to what occurs on re-wetting dried hydrated Portland cement paste. It appears that modelling the engineering behavior of hydrated Portland cement paste is complex Behavioral aspects of all the layered silicates investigated in this study are germane to improve our understanding of the engineering behavior of layered silicates.

Figure captions:

Figure 1. Mass (A), Length Change (B) and Modulus of Elasticity (C) Isotherms of Hydrated Portland Cement Paste (W/C=0.50) [1, 2]

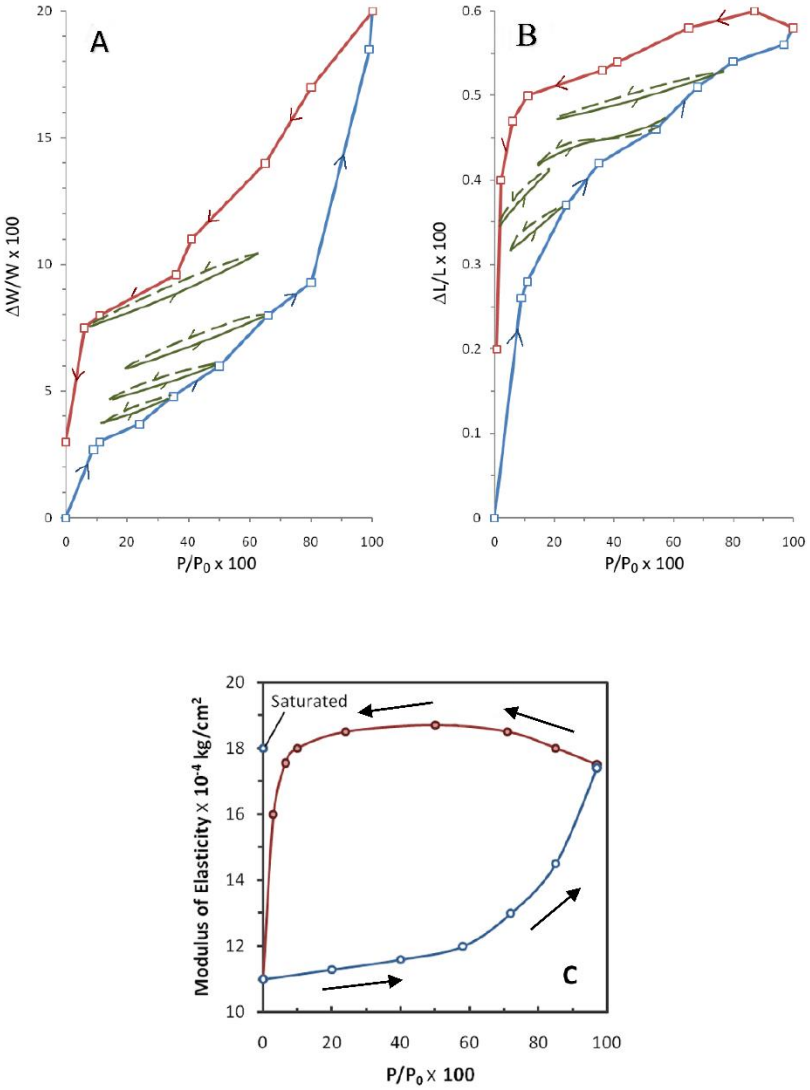

Figure 1. Mass (A), Length Change (B) and Modulus of Elasticity (C) Isotherms of Hydrated Portland Cement Paste (W/C=0.50) [1, 2]

References

1. Feldman R.F., Sorption and length-change scanning isotherms of methanol and water on hydrated Portland cement, Proc. Fifth Int. Symp. Chem. Cem., Tokyo, Part III, Vol. III, 53-66, 1968.

2. Feldman R. F., Assessment of experimental evidence for models of hydrated Portland cement, Highway Research Record No. 370, National Academy of Sciences, Washington D.C., 8-24, 1971.

3. Feldman R. F., Factors affecting Young's modulus-porosity relation of hydrated Portland cement compacts, Cem. Concr. Res., 2(4), 375-386, 1972.

4. Sereda P. J., Feldman R. F. and Swenson E. G., Effect of sorbed water on some mechanical properties of hydrated Portland cement pastes and compacts, Symp. On Structure of Portland Cement Paste and Concrete, Highway Research Board Special Report 90, National Academy of Sciences, Washington D.C., 58-73, 1966.

5. Alizadeh R., Beaudoin J. J. and Raki L., Mechanical properties of calcium silicate hydrates, Mater. and Struct., 44, 13-28, 2011.

6. Plassard C., Lesniewska E., Pochard I. and Nonat A., Investigation of the surface structure and elastic properties of calcium silicate hydrates at the nanoscale, Ultramicroscopy, 100, 331-338, 2004.

7. Constantinides G. and Ulm F.-J., The effect of two types of C-S-H on the elasticity of cement-based materials: results from nanoindentation and micromechanical modeling, Cem. Concr. Res., 34, 67-80, 2004.

8. Manzano H., Dolado J.S., Guerrero A. and Ayuela A., Mechanical properties of crystalline calcium-silicate-hydrates: comparison with cementitious C-S-H gels, Phys Status Sol A, 204(6), 1775-1780, 2007.

9. Manzano H., Dolado J.S. and Ayuela A., Elastic properties of the main species present in Portland cement pastes, Acta Mater, 57, 1666-1674, 2009.

10. Alizadeh R., Nanostructure and engineering properties of basic and modified calcium silicate hydrate systems, PhD thesis, Department of Civil Engineering, University of Ottawa, pp.231.

11. Pourbeik P., Beaudoin J. J., Alizadeh R. and Raki L., Drying of calcium-silicate hydrates: regeneration of elastic modulus, Advances in Cement Research, doi.org/10.1680/adcr.14.00048, 2014.

12. Taylor H.F.W., Hydration of calcium silicate phases, Cement Chemistry, Chapter 5, Thomas Telford Publishing, London, UK, 1997.

13. Yu P. and Kirkpatrick R. J., Thermal dehydration of tobermorite and jennite, Concr. Sci. and Eng., 1(3), 185-191, 1999.

14. Gard J. A. and Taylor H. F. W., Calcium silicate hydrate (II) (C-S-H (II)), Cem. Concr. Res., 6(5), 667-678, 1976.

15. Hara N. and Inoue N., Formation of jennite from fumed silica, Cem. Concr. Res., 10(5), 677-682, 1980.

16. Beaudoin J. J., Comparison of mechanical properties of compacted calcium hydroxide and Portland cement paste systems, Cem. Concr. Res., 13, 319-324, 1983.

17. Sereda P. J. and Feldman R. F., Compacts of powdered material as porous bodies for use in sorption studies, J. Appl. Chem., 13, 150-158, 1963.

18. Soroka I. and Sereda P. J., The structure of cement-stone and use of compacts as structural models, Fifth Int. Symp. Chem. Cem., Tokyo, Vol III, 67-73, 1968.

19. Menard K. P., Dynamic mechanical analysis-a practical introduction, CRC Press LLC, Boca Raton, pp. 208, 1999.

20. Alizadeh R., Beaudoin J. J. and Raki L., C-S-H(I)- A nanostructural model for the removal of water from hydrated cement paste, J. Amer. Ceram. Soc., 90(2), 670-672, 2007.

21. Thomas J. J., Jennings H. M. and Allen A. J., Relationships between composition and density of tobermorite, jennite and nanoscale $CaO\text{-}SiO_2\text{-}H_2O$, J. Phys. Chem. C, 114, 7594-7601, 2010.

Chapter 12

Summary and Future Work

12.1 Summary

The physico-chemical and physico-mechanical behaviour of hydrated cement systems e.g. cement paste and concrete are of paramount importance to practicing engineers and the construction industry in general. Concrete sustainability issues remain an integral concern of major infrastructure owners. Solutions to these problems are rooted in improved understanding of the interactions of calcium-silicate-hydrates (the primary binding phase) with aggressive environments at the nanostructural level.

Models for the nanostructure of C-S-H in hydrated cement paste have been advanced over the last several decades and generally fall into two categories-colloidal particle types or layered silicate types. These are discussed in detail in Chapter 4. Debate continues as to the most appropriate classification. Nevertheless the bulk of experimental evidence and support for a layered silicate model is very strong. Current composition-based models are essentially comprised of defect structures of 1.4 nm tobermorite and jennite. Prior to the work carried out in this thesis no mechanical property measurements of phase pure tobermorite and jennite were available. The global objective of this work as stated in Chapter 1 was to investigate the correspondence of the engineering performance of pure layered calcium-silicate-hydrates including tobermorite and jennite with that of hydrated Portland cement and pure C-S-H. An assessment of the compatability of the T-J models with actual determination of pure phase

mechanical characteristics would ostensibly provide additional evidence to confirm the applicability of these models. In this context the question of the structural attributes of interlayer water was addressed. The contribution of the 'interlayer-environment' to mechanical performance was also explored and found to be consistent with the tenets of the composition-based models.

The thesis was divided into four parts linked through the global objective. Each part was comprised of three research papers. Numerous analytical and characterization techniques were used throughout. Extensive use was made of Dynamic Mechanical Analysis (DMA), Dynamic Mechanical Thermo-Analysis (DMTA) and Microindentation Methods (MI). Mechanical property determinations were facilitated through the fabrication of specimens from compacted powders. Details of all the experimental techniques are provided in Chapter 5. A summary of the major findings/innovations are provided for each part in the following paragraphs.

Part 1.

This part focused on DMTA studies of 1.4 nm tobermorite, jennite and C-S-H with variable C/S ratio. This led to new applications of DMTA that identified its ability to detect phase transformations in layered silicates in addition to structural effects associated with the removal of interlayer water from 11% RH. Changes in storage modulus (E') and internal friction (tan∂) were monitored following the step-wise removal of interlayer water and found to be invaluable in assessing the concept of a T-J model for the C-S-H present in hydrated Portland cement. The DMTA method was also applied to determine differences in the engineering behaviour of paste hydrated for periods of 2 months and 3years and pastes

hydrated for prolonged periods up to 45 years. Results for the shorter hydration periods could be explained by application of a T/J dominant model. The behaviour of 45 year old paste conformed to a J-T/CH structural model with a minor amount of T. The DMTA method was also able to detect irreversible effects in mechanical performance associated with pre-heating T for prolonged periods at temperatures associated with phase transformations. Detection of thermal events associated with disordered phases that form at higher temperatures in the jennite system pre-heated to 175^{o}C was possible.

Part 2.

An innovative approach to the interpretation of mechanical property-porosity relationships for phase pure layered calcium-silicate-hydrates including 1.4 nm tobermorite, jennite and C-S-H is described. It incorporates Taylor's views on the influence of particle type, density and crystallinity. This analysis is compatible with the views expressed in Part 1 concerning T-J composition-based models for C-S-H present in hydrated Portland cement.

The contribution of adsorbed and interlayer water to shrinkage (drying below 11% RH) of all the layered calcium-silicate-hydrates in this investigation was carefully examined. Correlation of the results with changes in the x-ray basal spacing on drying provided additional evidence in support of T-J composition-based models for hydrated Portland cement.

Original experiments clearly demonstrated the ability of all the layered silicates in this study to 'regenerate' their elastic properties following prolonged thermal drying i.e. decreases in

elastic modulus can be recovered. The results are compatible with the previously expressed notions of T-J composition-based models.

Part 3.

The research described in this part focuses on the nanostructural characteristics and behaviour of cement paste that has been hydrated for 45years. In the experiments reported in Part 1 prolonged hydration was demonstrated to change the nanostructure (details provided in Chapter 10) and affect engineering behaviour. This study was considered complimentary to the work of both Parts 1 and 2 as it provided further insight into the relevance of the T-J composition-based models. The effect of a greater degree of silicate polymerization, longer silicate chains and fewer structural defects were expected to have demonstrably positive effects. The MI and DMTA methods were used extensively in this work. The DMTA parameters (E' and tan∂) were monitored and MI creep measurements were obtained. The role of structural water on the creep process was determined by direct correlation of the corresponding features of creep-mass-loss and tan∂-temperature curves as drying occurs from the 11% RH condition. The analysis included an assessment of the influence of degree of hydration, capillary porosity, nanostructural parameters and in the case of 'young' paste (studied for comparative purposes) the restraining effect of unhydrated cement particles. It is apparent that the continuous aging of layered C-S-H phases in hydrated Portland cement and their inherent thermodynamic instability are intrinsic characteristics of this material that can enhance sustainability if properly understood.

Part 4.

The contributions in this part of the thesis focus on structural factors that affect the engineering behaviour of layered calcium silicate hydrates including C-S-H, T and J. These include original experiments involving: the correlation of internal friction data with microindentation parameters and their dependence on mass-loss from 11% RH; an assessment of the effect of the structural rigidity of the silicate sheets themselves as determined by the extent of cross-linking in systems ranging from highly cross-linked gyrolite to C-S-H with no detectable cross-linking; control of the 'interlayer-environment' and extent of interaction between the silicate sheets through application of interparticle pressure and the path dependent generation of drying-wetting stress.

The systematic influence of water removal from 11% RH on creep of C-S-H, T and J was determined for the first time. The structural role of interlayer water is discussed in the context of compatability of the results with composition-based models for C-S-H in hydrated cements-a central theme throughout the thesis. It is argued that the structural role of interlayer water is an integral part of creep, elastic deformation and failure processes associated with the layered behaviour of layered calcium-silicate-hydrates.

An assessment of the extent of cross-linking (indicated by the relative strength of the Q^3 ^{29}Si MAS NMR sites) of the silicate sheets themselves on the DMTA engineering parameters was performed. The contribution of the interlayer water to the stiffness of the layered silicate materials was considered to be dependent on the extent of cross-linking between the silicate sheets; the latter varied with silicate species ranging from strong for gyrolite to absent for C-

S-H. It was also suggested that water has an attenuating effect on the bonds associated with cross-linking when they are subjected to shear stress.

The non-uniqueness of the modulus of elasticity with respect to moisture content and the 'interlayer-environment' was demonstrated and discussed. It was demonstrated that control of this environment is possible through the application of pressure and selective sorption-desorption cycles. It is apparent that even the 'dry-state' is not unique as relative positioning of the silicate layers is dependent on the drying protocols. It is apparent that behavioural aspects of all the layered silicates in this study are germane to the global objective of this thesis.

12.2 Recommendations for Future Work

Relatively few research papers have been published on the engineering properties and behaviour of phase pure calcium-silicate-hydrates. Despite this there is increasing recognition that additional fundamental work in this area is required to make advances that will result in 'knowledge-based' decisions that have a positive effect on sustainability of concrete infrastructure. Advances in experimental procedures have provided the opportunity to re-examine some of the controversial issues in cement and concrete science. A few relevant topics that merit detailed investigation in the future are suggested as follows**:**

- The C-S-H phase in hydrated Portland cement paste is generally a substituted form that contains some substituted alumina i.e. C-A-S-H. Future work would involve synthesis and characterization of pure C-A-S-H phases. These materials should provide the opportunity to investigate the effect of Al^{3+} substitution in C-S-H on

engineering performance. It is proposed that DMA, DMTA and MI experiments be carried out starting at 11%RH and engineering parameter(s) versus mass-loss curves be constructed to generate data that provides insight as to the influence of Al^{3+} substitution on mechanical behavior and the concomitant structural role of interlayer water.

- It has been demonstrated that the addition of C-S-H seeds to the C_3S-water system can accelerate hydration and alter the C/S ratio of the hydration product. This can be controlled by varying the properties of the seeds. It offers an elegant means of 'tailoring' the final C-S-H product for specific engineering applications. It is proposed to investigate the merits of studying C-S-H systems nucleated from 1.4nm tobermorite and jennite 'seeds'. It is also proposed to conduct similar experiments to those proposed for C-A-S-H materials.
- The water adsorption isotherm of layered silicates is highly irreversible exhibiting both primary and secondary hysteresis. It is suggested that a MI and DMTA study should be conducted on layered silicates over a region of the isotherm beyond 11% RH with drying and wetting along various scanning-loops. This should expand our knowledge base considering the irreversible effects of sorption phenomena on engineering performance.
- The degree of crystallinity of pure C-S-H varies with hydration time. It is proposed to study the influence of varying the degree of crystallinity of C-S-H on engineering properties of phase pure C-S-H with variable C/S ratio.

Appendix: Vita

Refereed Journal Papers:

1. P. Pourbeik, J. J. Beaudoin, R. Alizadeh and L. Raki, "Dynamic mechanical thermoanalysis of layered calcium silicate hydrates," *Journal of Thermal Analysis and Calorimetry*, 118 (1), pp. 1-14, 2014.
2. P. Pourbeik, J. J. Beaudoin, R. Alizadeh and L. Raki, "Correlation between dynamic mechanical thermo-analysis and composition-based models for C-S-H in hydrated portland cement paste, Materials and Structures, in-press, 2014.
3. P. Pourbeik, J. J. Beaudoin, R. Alizadeh and L. Raki, "Effect of Thermal Treatment of 1.4 nm Tobermorite and Jennite on Mechanical Performance, *Materials and Structures, To be Submitted*, February 2015.
4. P. Pourbeik, J. J. Beaudoin, R. Alizadeh and L. Raki, "Mechanical Property-Porosity Relationships of Layered Calcium Silicate Hydrate Phases", *Materials and Structures* 46(9), pp. 1489-1495, 2013.
5. P. Pourbeik, J. J. Beaudoin, R. Alizadeh and L. Raki, "Dimensional Stability of 1.4nm Tobermorite, Jennite and Other Layered Calcium-Silicate-Hydrates", *Advances in Cement Research* 26(1), pp. 1-9, 2014.
6. P. Pourbeik, J. J. Beaudoin, R. Alizadeh and L. Raki, "Drying of Calcium Silicate Hydrates: Regeneration of Elastic Modulus", *Advances in Cement Research*, Accepted for Publication, 2014, DOI: 10.1680/adcr.14.00048.
7. P. Pourbeik, J. J. Beaudoin, R. Alizadeh, D.-T. Nguyen and L. Raki, "Microindentation Creep of 45 Year Old Hydrated Portland Cement Paste", *Advances in Cement Research*, 25(5), pp. 301-306, 2013.
8. P. Pourbeik, J. J. Beaudoin, R. Alizadeh and L. Raki, "Dynamic Mechanical Thermo-Analysis of Portland Cement Paste Hydrated for 45 Years, *Materials and Structures*, Accepted for Publication, 2014. DOI: 10.1617/S11527-014-0500-7

9. P. Pourbeik, J. J. Beaudoin, R. Alizadeh and L. Raki, "Creep of 45 Year old Cement Paste- The Role of Structural Water, *Materials and Structures*, Accepted for Publication, January 2015. DOI: 10.1617/s11527-015-0534-5

10. P. Pourbeik, J. J. Beaudoin, R. Alizadeh and L. Raki, "Engineering Performance of Pure Calcium-Silicate-Hydrate Phases: The Structural Role of Interlayer Water, Submitted to *Materials and Structures*, 2014.

11. P. Pourbeik, J. J. Beaudoin, R. Alizadeh and L. Raki, "Structural Factors Affecting the Engineering Performance of Layered Calcium-Silicate Hydrates, *(to be submitted),* May, 2015.

12. P. Pourbeik, J. J. Beaudoin, R. Alizadeh and L. Raki, "The Non-Uniqueness of the Modulus of Elasticity of Layered Calcium-Silicate Hydrates with Respect to Water Sorption, (*to be submitted),* May 2015.

13. D.-T. Nguyen, R. Alizadeh, J. J. Beaudoin, P. Pourbeik, L. Raki "Microindentation creep of monophasic calcium-silicate-hydrates, *Cement and Concrete Composites*, 48, pp. 118-126, 2014.

Conference Presentations:

1. P. Pourbeik, J. J. Beaudoin, R. Alizadeh and L. Raki, "Dimensional stability of 1.4 nm tobermorite, jennite and other layered calcium silicate hydrates," *American Ceramic Society Meetings - 5th Advances in Cement-based Materials Symposium*, Tennessee Technological University, TN, USA, 2014. (Oral)
2. P. Pourbeik, J. J. Beaudoin, R. Alizadeh and L. Raki, "Microindentation Creep of 45 year old Hydrated Portland Cement Paste," *American Concrete Institute Fall Convention*, Toronto, Canada, 2012. (Oral)